

*BULLETIN OF THE*  
**RESEARCH LABORATORY FOR NUCLEAR REACTORS**

VOL. 35

2011



**RESEARCH LABORATORY FOR NUCLEAR REACTORS**  
**TOKYO INSTITUTE OF TECHNOLOGY**

BULLETIN OF THE RESEARCH LABORATORY FOR NUCLEAR REACTORS

*BULL. RES. LAB. NUCL. REACTOR, Vol.35, 2011*

CONTENTS

**Research Staffs** ..... 1

**I. Celebration of Professor Ninokata's 65th Birthday**

I.1 Nuclear Reactor Thermal Hydraulics Safety Analysis and Thoughts on FUKUSHIMA  
Hisashi NINOKATA ..... 3

**II. Research Reports**

**A. Energy Engineering**

A.1 Performance Test Results of a Supercritical CO<sub>2</sub> Compressor Used in a New Gas  
Turbine Generating System  
Masanori ARITOMI ..... 15

A.2 Experimental Study on Heat Transfer Characteristics of Vertical 5×5 Heated  
Rod Bundles around Critical Pressure with R-134a  
Noriyuki WATANABE and Masanori ARITOMI ..... 16

A.3 The Study of Velocimetry in High Temperature Flow  
Hiroshige KIKURA and Yasushi TAKEDA ..... 17

A.4 Basic Study of Velocity Profile Measurement by an Air-coupled Ultrasonic System  
Hiroshige KIKURA ..... 18

A.5 Proton-Beam-Transport Experiments through a Syringe Needle for the Development  
of a Cancer Therapy Using Proton-Induced X-rays  
Yoshiyuki OGURI and Jun HASEGAWA ..... 19

A.6 Innovative Nuclear Energy System using a Concept of Active Carbon Recycling  
Yukitaka KATO ..... 21

A.7 NIR Study on Hydration Reaction of Magnesium Oxide for Chemical Heat Storage  
Junichi RYU and Yukitaka KATO ..... 24

A.8 Development of Electron Cyclotron Emission Imaging System on LHD  
Shunji TSUJI-IIO ..... 25

A.9 Development of Fiber-Optic Diagnostic on Vacuum Vessel Current of QUEST  
Shunji TSUJI-IIO ..... 26

A.10 Stress Distribution in Helical Coils with Geodesic Windings Based on Virial Theorem  
Hiroaki TSUTSUI, Shunji TSUJI-IIO and Ryuichi SHIMADA ..... 27

A.11	Cold Arc-Jet Plasma Flowing along Weak Mirror or Cusp Magnetic Field Hiroshi AKATSUKA, Atsushi NEZU and Haruaki MATSUURA	30
A.12	Discussion on the Collisional Radiative Model Based on Ordinary Differential Equations Hiroshi AKATSUKA	32
<b>B. Mass Transmutation Engineering</b>		
B.1	Fabrication and Properties of Core-Shell Type SiC/SiO <sub>2</sub> Nanowires Formed by Low-Cost and Catalysis-Free Technique Toyohiko YANO, Wasana KHONGWONG and Katsumi YOSHIDA	33
B.2	Modeling and Material Design for Improvement of the Thermal Conductivity of Two-Dimensional SiC Fiber-Reinforced SiC Composites Katsumi YOSHIDA and Toyohiko YANO	36
B.3	Computational Analyses of <sup>238</sup> U Samples Irradiated in the Experimental Fast Reactor JOYO Tomooki SHIBA, Masaki SAITO and Hiroshi SAGARA*	38
B.4	Systematic Measurement of keV-Neutron Capture Cross Sections and Capture Gamma-Ray Spectra of Pd Isotopes Masayuki IGASHIRA, Kazushi TERADA and Tatsuya KATABUCHI	39
B.5	Separation of Am(III) from Eu(III) using Polymer gels Cross-Linked with TPEN Analogs Takeshi OGATA and Kenji TAKESHITA	41
B.6	Thermo-Responsive Extraction of Cadmium(II) Ion with Poly(TPEN-NIPA) Gel Yusuke INABA, Atsunori MORI and Kenji TAKESHITA	43
B.7	Nuclear Rare Metals, as “ <i>Kopernikanische Wendung</i> “ Masaki OZAWA and Tatsuya SUZUKI	46
B.8	Relativistic Density-Functional Study of the Alloying Behavior of Transition Metal into $\gamma$ -type Solid Uranium Jun ONOE, Masayoshi KURIHARA, Masaru HIRATA and Chikashi SUZUKI	50
B.9	Molecular Mechanisms of DNA Double-Strand Break Repair and Its Potentiality toward Cancer Radiotherapy Yoshihisa MATSUMOTO, Radhika Pankaj KAMDAR and Mukesh Kumar SHARMA	55
B.10	Local Structural Analyses of Molten Thorium Fluoride in Mono - and Divalent Cationic Fluorides Haruaki MATSUURA, Atsushi NEZU and Hiroshi AKATSUKA	57
B.11	Electrochemical Behaviour of Light Lanthanides in Molten Chlorides with Fluorides Haruaki MATSUURA, Atsushi NEZU and Hiroshi AKATSUKA	59

B.12	Nanospace Confinement Effects on Capillary Evaporation Phenomena of Water Takehiko TSUKAHARA .....	60
B.13	Application of Novel Ionic Liquids to the Extraction of Uranium(VI) from Nitric Acid Medium and a Study on the Chemical Form of the Uranyl Complexes Extracted Thomas James BELL and Yasuhisa IKEDA .....	61
B.14	Crystal Structure of $\text{UO}_2(\text{NO}_3)_2(\text{DMPU})_2$ (DMPU = ,3-dimethyl-3,4,5,6-tetrahydro-2(1H)-pyrimidinone) Tomoya SUZUKI, Takeshi KAWASAKI and Yasuhisa IKEDA .....	62
B.15	Flow Visualization in Centrifugal Extractor using Taylor-Couette Vortex Flow Hiroshige KIKURA and Kenji TAKESHITA .....	63
B.16	Numerical Analyses on Joule-Heated Glass Furnace for Disposal of High-Level Radioactive Waste Nobuyoshi TSUZUKI and Hiroshige KIKURA .....	64
<b>C. System and Safety Engineering</b>		
C.1	Study on Concept of Innovative Nuclear Reactors and Nuclear Safety Toru OBARA .....	65
C.2	Development of Methodology for Plutonium Categorization (IV) - Effect of Compression on Rossi-alpha- Yoshiki KIMURA, Masaki SAITO and Hiroshi SAGARA .....	66
C.3	Burn-up Characteristic of Am-fueled Space Reactor with Reflector Thickness Masanori NAKAMURA, Masaki SAITO and Hiroshi SAGARA .....	68
C.4	Effect of Inner Axial Blanket with Minor Actinides on Extension of Core Life-time of Large-scale Fast Breeder Reactor Erina HAMASE, Masaki SAITO, Hiroshi SAGARA and Chi Young HAN .....	69
C.5	Evaluation of Fukushima Dai-ichi Nuclear Power Plant Accident Kazumi KITAYAMA, Takao ISHIZUKA, Nobuyoshi TSUZUKI, Hiroshige KIKURA and Masanori ARITOMI .....	71
C.6	Legal Framework to Maintain Expertise in Nuclear Regulatory Body in Japan Tetsuo SAWADA and Toshio MORIMOTO .....	72
C.7	New Public Commons and Network of Nuclear Site Regions for the Post-Fukushima Accident Re-vitalization Tetsuo SAWADA .....	73
C.8	Conceptual Study of Liquid Lithium Target System for Boron Neutron Capture Therapy (BNCT) Minoru TAKAHASHI, Tooru KOBAYASHI, Shoji UCHIDA and Migguan ZHANG .....	75

C.9	Hydrodynamic Study on Flowing Liquid Water and Lithium Target for Boron Neutron Capture Therapy (BNCT) Minoru TAKAHASHI, Tooru KOBAYASHI, Masashi NAKATSUKA, Teddy ARDIANSYAH, Martine KULHANEK, Ales VOJACEK and Vaclav DOSTAL .....	77
<b>III. Co-operative Researches</b>		
III.1	Co-operative Researches within Tokyo Institute of Technology .....	79
III.2	Co-operative Researches with outside of Tokyo Institute of Technology .....	79
III.3	Themes Supported by Grants-in-Aid for Scientific Research of the Ministry of Education, Culture, Sports, Science and Technology .....	82
<b>IV. List of Publications</b> .....		<b>83</b>

**Research staffs of  
RESEARCH LABORATORY FOR NUCLEAR REACTORS,  
TOKYO INSTITUTE OF TECHNOLOGY**

**Director**

Masanori ARITOMI      Professor

**Energy Engineering Division**

Hisashi NINOKATA      Professor  
Masanori ARITOMI      Professor  
Masayuki IGASHIRA      Professor  
Hiroshi AKATSUKA      Associate Professor  
Minoru TAKAHASHI      Associate Professor  
Yukitaka KATO      Associate Professor  
Takatoshi TAKEMOTO      Visiting Associate Professor  
Tetsuo SAWADA      Assistant Professor  
Junichi RYU      Assistant Professor  
Noriyuki WATANABE      Assistant Professor

**System and Safety Engineering Division**

Ryuichi SHIMADA      Professor  
Masaki SAITO      Professor  
Yasuhisa IKEDA      Professor  
Yoshihiro YAMANE      Visiting Professor  
Fumiaki KAWAKAMI      Visiting Professor  
Shunji IIO      Associate Professor  
Toru OBARA      Associate Professor  
Hiroshige KIKURA      Associate Professor  
Hiroaki TSUTSUI      Assistant Professor  
Chi Young HAN      Assistant Professor  
Etsuko KOIZUMI      Assistant Professor

**Mass Transmutation Engineering Division**

Toyohiko YANO      Professor  
Kenji TAKESHITA      Professor  
Yoshiyuki OGURI      Professor  
Noriyosu HAYASHIZAKI      Associate Professor  
Yoshihisa MATSUMOTO      Associate Professor  
Jun ONOE      Associate Professor  
Tatsuya SUZUKI      Associate Professor  
Eiichi ASANO      Visiting Associate Professor  
Katsumi YOSHIDA      Assistant Professor  
Masao NOMURA      Assistant Professor  
Tatsuya KATABUCHI      Assistant Professor  
Haruaki MATSUURA      Assistant Professor  
Masayuki HARADA      Assistant Professor  
Takehiko TSUKAHARA      Assistant Professor  
Jun NISHIYAMA      Assistant Professor

**International Nuclear Research Cooperation Center**

Masaki OZAWA      Professor

**Technical Staffs**

Mitsuo MATSUZAKI      Senior Technical Specialist  
Atsushi NEZU      Senior Technical Specialist  
Hitoshi FUKUDA      Senior Technical Specialist  
Masamitsu IMAI      Senior Technical Specialist  
Ken-ichi TOSAKA      Senior Technical Specialist  
Kazuo TAKEZAWA      Senior Technical Specialist

## I.1 Nuclear Reactor Thermal Hydraulics Safety Analysis and Thoughts on FUKUSHIMA

Hisashi NINOKATA

### INTRODUCTION

I was given an honorable opportunity to contribute to the Bulletin as I finally reached the age 65 years old of "happy retirement." It should have been a happy retirement, if it were not for the accident that took place on the site of Fukushima Daiichi Nuclear Power Station operated by the Tokyo Electric Power Company (Tepeco) as a result of the 3.11 gigantic tsunami attacks.

When I was told to write this article, I thought it would be appropriate to make a recollection of my R&D work of the last 18 years in the Research Laboratory for Nuclear Reactors. However, at the same time when I started writing this several months ago, there was something that hindered me from starting with it while I found myself always thinking of the accident. This thought has never left me day and night from the beginning of the accident. Consequently I decided I should begin with my own evaluation of the accident.

Therefore, the first part of this article is to show my thoughts on the accident. It is cited from a summary of my lecture talk in Indonesia, in the beginning of the last December, 2011. This talk was based on my previous lecture and seminar talks including those delivered at MIT, June 16, at the ANS Annual Meeting in Hollywood, Florida, June 28, at NURETH-13 in Toronto, September 27, and others. The content is based on the open and latest information available to date in Japan. It may contain some erroneous or uncertain information. I tried to minimize it to my best capability. Also I tried to eliminate any critical issues or opinions that may jeopardize some people who were involved in.

The latter half of this article will be excerpts of my recent R&D activities related to the safety-by-design for sodium cooled fast reactors and light water reactors, thermal hydraulics analysis focusing on the simulation-based technology, in particular subchannel analysis and computational fluid dynamics.

### I. FUKUKUSHIMA DAIICHI NUCLEAR POWER STATION ACCIDENT

**Earthquake and Tsunami:** First of all, let me start with the deepest sympathy for all those affected by the tragic chain of events, especially the nuclear accident at Fukushima Daiichi Nuclear Power Station (1F NPS), following the devastating earthquake and tsunami that struck Tohoku region of Japan, March 11, 2011.

When the earthquake took place, I happened to be in Mito, 100 km to the north of Tokyo, 100 km to the south of the 1F NPS. The shake in Mito city was of Shindo-6, a

seismic intensity of 6 on the Japanese scale, which disabled me from standing upright without holding something firm and stable. It lasted long, I did not remember how long but I felt as if it lasted eternal. Richter scale of the East Japan Earthquake was over 9, followed by the gigantic tsunami that engulfed almost 20,000 lives. So devastating.

**Defense-in-Depth Principle and Deterministic vs Probabilistic Approach:** I could not believe that the 1F NPS was so vulnerable against Tsunami. It was pointed out clearly that the NPS was not provided with the defense-in-depth for the unforeseen natural phenomena, i.e., gigantic tsunami in this case, that exceeded the worst scenario. Why it was not provided? Partly because the safety regulation system in Japan has assumed the deterministic approach to approve NPS safety design. The plant is designed to be protected against the worst accidents that could be conceived. This category of accidents is called "design-basis-accident." DBAs are not likely to occur but assumed to occur 100%, just an assumption, and should be accommodated. Therefore the public are fully protected with more than sufficient safety systems against these kinds of accidents.

How about the accidents with extremely low occurrence probability, i.e., negligibly small but with a huge magnitude of disasters once it happened? Japanese utilities have been asked to take care of these beyond design-basis-accidents. If the utilities trust the authority and do not feel it mandatory to provide countermeasures against BDBAs, there would be no defense in depth beyond the threshold. My point here once again is that a lack of this defense-in-depth layer was the direct cause of the nuclear disaster in the 1F NPS accident. Countermeasures for flooding were poor, those for station black out and loss of DC powers were none because in Japan the power lines are so reliable and all electronic and electric devices are of high quality and, hence, less concerns about the SBO than in other countries. The regulatory guide says you don't have to prepare for SBO. Also the ultimate heat sink was assumed only at the ocean. No diversity was considered in providing additional heat sinks and the methods to transport heat from inside the primary containment vessel (PCV).

Here I would like to emphasize that the defense-in-depth for the unforeseen events is the response capabilities to overcome a disaster that exceeded all worst-case scenarios. Particular safety systems, i.e., hardware, are not installed for the beyond design basis accidents by definition but the accident management procedures. "How safe" depends on the worst scenario and on how we define it. However, no matter how the worst scenario had been defined at the 1F NPS, the tsunami was real that exceeded

the design basis tsunami height 5.7 m by about 10 meters. Nothing could be done to avoid the disaster if people were not prepared. It is true that all Tepco people in the 1F NPS did their best in the total blackout and did almost everything that was to be done. It is true that a total amount of radioactive release was surprisingly low in consideration of the magnitude of the accident and should be attributed to and thanks to their efforts. Nevertheless if defense-in-depth layers had been provided for the tsunami of unforeseen scales, I am pretty much sure that the consequence of the accident should have been of much smaller magnitude. There should be no such if's. The lessons should be reflected onto the introduction of more risk-informed regulation system. It is imperative to practice more probability based regulation as soon as possible.

### **Fukushima Daiichi NPS Accident – After 9**

**Months Later:** As of today November 2011, No.1 to No. 3 BWR units of the 1F NPS look stable and are close to cold shutdown state. On the one hand, it is still necessary to inject water into the reactor pressure vessel since the fuels are still emitting decay heat although its amount is sufficiently low, approximately 0.05% of the rated power, and would not create any critical problems in the sense of thermal hydraulics. On the other, these radioactive materials are not confined in a containment system that is supposed to be restored or re-defined. The reactor pressure vessels of all the units lost their integrity as a result of possible melt through of the molten core materials. Amounts of the molten core materials that fell onto the pedestal concrete floor would be different for reactor to reactor. See Figs. 1 and 2. Even so, the melt-through could have been still acceptable theoretically, should the containment function be fully maintained anyhow and the isolation ----- acceptable because the public would suffer no radiological consequences.

The tragedy was due to the fact that all three units lost the integrity of their PCVs of type Mark-I, the failure in containing radioactive fission products released during the core heat up, meltdown and relocation processes. Those corium materials are now immersed in the water inside or outside RPV, stably cooled, thus most of the fission products have been fixed in the corium, deposited on the structure surface and/or in the water. No large scale release of these radioactive materials is anticipated without any explosive mechanisms. However, we are nuclear engineers. We are well aware that there is always a risk anywhere. Our responsibility is to reduce the risk no matter how small it is and to let people know that we are making everlasting efforts in keeping them away from the risk.

The amount of water to inject is that of a make up for the evaporation plus leakage from the RPV. Then, as of July to August, far more than 100,000 tons of highly contaminated water was estimated to have flown out of the RPV/primary boundary, and then out of the PCV, and stayed in their reactor buildings as well as the turbine buildings. The contaminated water, also from the spent fuel pools, was occupying a large portion of the basement spaces. Another troublesome source is the underground

water stream. It is estimated to be flowing into the basements at a rate of 200 to 500 tons/day (estimated).

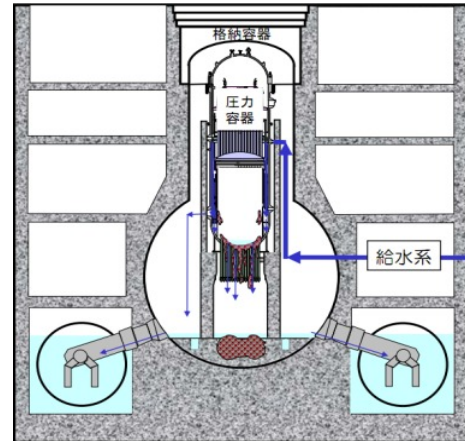


Fig. 1 The likely states of 1F1  
(by World Nuclear News, December 1, 2011)

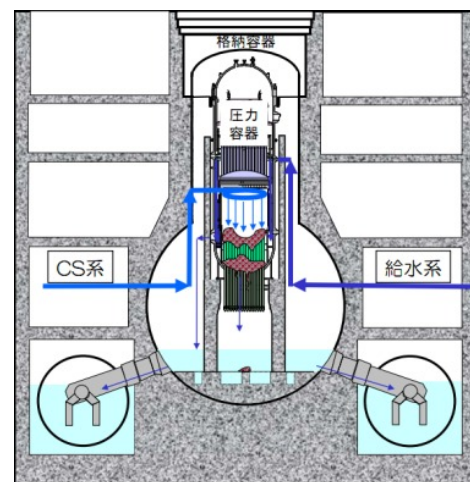


Fig. 2 The likely states of 1F2 and 1F3  
(by World Nuclear News, December 1, 2011)

Early this summer, a large chemical plant consisting of multi-step water treatment systems was introduced on the site. The basement water has been and is being extracted, decontaminated, separated from oil components, purified to a degree of potable water and re-circulated through approx. 4km long pipe lines into the RPVs to cool the core fuel materials. As a consequence, a semi-closed cooling circuit has been established implying much less increase in the amount of contaminated water. However, unless the underground water stream is stopped, the flooding in the basements won't stop and will continue to challenge all the water processing and storage capabilities.

The water temperatures are well below the saturation temperature, i.e., below 100°C but only at the measurement locations. Thus there remain uncertainties in exactly which temperatures are being measured although all units look stable.

However always with a risk of leakage to the environment from the system and long recirculation lines and with the failure in containment, it is questionable to make a statement that the reactor system is or will be under the cold-shutdown mode soon. The cold shutdown is a terminology for the intact NPS.

#### **Core Exposure and Meltdown of the Unit No. 1:**

The above are a consequence of the failure in removing the decay heat generated in all three units since the gigantic tsunami washed away all the engineered safety systems including the emergency Diesel Generators in place and caused station blackout (SBO) around 3:40PM, one hour after the M9 quake. SBO has disabled every decay heat removal capability except for the Isolation Condensers installed in the old unit No. 1.

Unfortunately the IC was not functioning long enough for some erratic reasons that are still not clarified yet. In the case of unit No.1, with the IC not operating after Tsunami until 18:18, it was reasonable to assume the safety relief valves (SRVs) were functioning to prevent the RPV pressure from exceeding about 8 MPa. Every time the SRVs opened, quite large an amount of high pressure vapor was released into the suppression chamber (S/C). All the SRVs on the 1F units are made by Okano Valve Co and are supposed to be highly reliable. It is hard to believe they malfunctioned during the course of accident.

This resulted in a rapid loss of coolant in the RPV and the water level was estimated to reach the top of active fuel (TAF) region within about 2 hours at most. This was estimated by a simple heat balance calculation and has been validated by the post simulation results provided by many organizations such as Tepco, NISA-JNES and Institute of Applied Energy, etc. In this early phase of accident, around 5 to 6 pm of 3.11, absolutely no information was available on what was going on at the 1F NPS. Post investigation by the government has revealed that the station master did not share the information that the IC was not functioning after tsunami. In confusion, or with no communication tools available except for one PHS channel which died soon, there is no way to find out whether the on-site command and control system worked out or not. Also it is another important point to make here that due to the loss of DC power, almost all plant data were not obtained (This is the situation where the accident management should be practiced). When they found the water level measurement was recovered, I speculate that they might have made a fatal error. They trusted the water level reading that indicated higher than the TAF while at that moment the water level was much lower and the core melt was about to take place or taking place. Many actions were taken based on this misreading. However any criticism should be avoided because everything said here is based on the speculation.

After reaching the TAF, the water level went down rapidly to the bottom of the core to uncover the whole core. Then fuels were cooled by steam, vapor and then by super heated vapor. At this timing, the uncovered reactor core of the unit No. 1 started its disintegration, partly by oxidation

of the Zircalloy cladding, with weakened structural strength, with the added heat and in the presence of hydrogen generated as a result of the chemical reactions. In fact, after the water level got lower than the TAF, there was no point of return and all physical and chemical reactions worked in a way to enhance disintegration of the core. Without sufficient heat removals from the core, cladding and fuel liquidus state was formed and eventually the elevated temperatures reached the fuel melting temperature. These sequences were considered to be irreversible, one-way and non-stop to the core melt. The core melt took place in a few hours after the whole core exposure. This observation should be justified and evidenced by the very high radiation level of 288mSv/h in the reactor building already at 21: 50. Why so fast? The answer is clear because the only emergency cooling device, IC, was not operated for many hours that have never been clearly explained why by Tepco yet.

Anything could be said if we were allowed to say based on "if". Nevertheless if we were allowed, I would dare to say, the 1F1 core might have survived without the core meltdown if the IC was kept operating without being stopped manually before the tsunami, if the RPV wall survived the thermal shock due to rapid temperature decreases, if the IC tank was always filled with water by fire engine pumps, and if the IC valves were fixed open after the reactor pressure was lower than the specified level at which the IC wouldn't function. An important factor to note here is that the ultimate heat sink (atmosphere) was always available there. It is very sad to say there are so many "if's" in this case.

#### **Core Exposure and Meltdown of the Unit No.2 and No.3:**

As for the unit No. 2 and No.3, the emergency cooling system RCIC (Reactor Core Isolation Cooling) was provided instead of the IC. RCIC consists of the high pressure turbine that is specially designed to stand low quality vapor coming from the RPV and that rotates the pump to transport available water from the service water tanks and/or condensate storage tanks to the core. Differing from the IC, the RCIC can inject more water than the evaporation and can compensate the loss of coolant but does not remove the decay heat to the ultimate heat sink. Operation of RCIC of the Unit No.2 lasted 72 hours, which was much longer than the battery life of about 10 hours. At first I thought someone in the plant volunteered the battery management and on-off maneuver had made it possible. However this was not likely according to the latest Tepco hearing. It seems that the RCIC line valve did not close when it should have and as a consequence the RCIC kept working as long as 3 days.

DC power was available for No. 3 unit since the batteries escaped being soaked by the sea water. Therefore the RCIC was operating as long as battery was alive but stopped when it died. Then the high pressure activated the HPCI (High Pressure Coolant Injection) that uses also the RPV high pressure vapor to operate the turbine of a 7 times larger capacity than the RCIC turbine. RCIC stopped in 20 hours and HPCI in 14 hours.

Once the RCIC and HPCI stopped, the event timelines followed mostly those for the unit No.1. Depressurized evaporation with the SRV opening, followed by the rapid reduction of water level, core exposures, hydrogen production and radioactive materials release from the core fuels, and core meltdown-melt-through, and a large scale radiological release in a few hours.

PCVs of unit No.2 and No.3 were isolated and with the isolation valves on the S/C to RHR (Residual Heat Removal system) line being closed there were no connected flow lines to the ultimate heat sink. Without any heat sink available, i.e., in the absence of RHR functions, the PCV pressure started increasing once the RCIC stopped. The events sequence is the subsequent automatic SRV opening due to overpressure in the RPV, followed by the depressurization of the RPV with the high pressure and high temperature vapor being released into the S/C water. This resulted in the rapid reduction of the water level in the RPV. Then, it was inevitable to lose the PCV depressurization capability at the wet-well (or Suppression Chamber) as the S/C water temperature becomes high and saturated; the S/C water does not condensate the vapor any longer. As a consequence, the PCV was over-pressurized by a mixture of vapor and hydrogen. The only method for these 2 units to survive the core meltdown was supposed to depressurize and release the heat by opening the PCV vent valves of either the wet vent or dry vent line.

At that time I considered that PCV flooding, recommended in PWR accident management, was an only way to save the RPV in the very early phase of the accident. However, no action was taken possibly due to no electricity and/or mobile generators/pumps available in time. I suspected that station managers and operators were aware that the flooding was not possible for seismic and practical reasons and I had to agree with them if it was their thinking.

**PCV Venting Issues:** If the venting was mandatory to protect the PCV, there should be no hesitation. If the venting was required to prevent core melt and to protect RPV, it was a very tough decision for the NPS operators to make. Our AESJ (Atomic Energy Society of Japan) Special Committee on the 1F NPS accident asserts that all the existing NPS should be equipped with filtered vent system so that the ventilation could be carried out as required.

In the 1F NPS, the PCV vent was not carried out timely, not in time. There were many reasons reported for this. Hydrogen explosions damaged not only the alternative water make-up injection lines but the vent lines in place. This is one of the multi-unit drawbacks. The high radiation levels prevented the operators to make access to the vent line valves. Also operators' familiarity with the Air Operated vent valves was not sufficient, according to media reports. In general, the delayed venting was most responsible for the PCV failures and there is no question about this. Issues are why the venting was delayed and this question will be answered sooner or later by the government investigation.

**Summary:** With the PCV isolated and without any decay heat removals and transport capabilities to outside the PCV (Loss of Ultimate Heat Sink), the cores of the three units have started to melt and eventually melt down to the bottom of the RPV. The timing of the core melt has depended on the termination of IC for Unit 1 and of RCIC for Unit 2, and RCIC and HPCI for the Unit 3. In alternative words, the timing was dictated by the amount of water available inside the suppression chamber (S/C) or the wet well of the PCV. The core melt is a rapid process and took place before the midnight of 3.11 at 1F1, and within a few days for 1F3 and 1F2. The venting and following alternative make-up water injection (borated) were made too late and hydrogen explosions followed the PCV ventilation.

**What Should Have Been Done in the Initial Phase of the Accident: Very Personal View:** Since the beginning of the accident, in particular in the first week, I have been thinking what could have been done to avoid the core meltdown and to save the nuclear reactors after the loss of ultimate heat sink was found to be inevitable. Still I have no definite answers yet. With regard to the 1F1 it is easy to say that it could have been saved if the IC was kept operating but this must be based on many assumptions. So many if's for the 1F1 would make a thin line of escape not realistic. What I could say right now is, it was extremely difficult and was almost impossible to avoid the core meltdown under the situation.

The only thin line of success to survive the event sequence from SBO, loss of DC power, without ultimate heat sink barely is seen. At least the following three actions must be carried out before the water level reached the top of active fuel (TAF):

- 1) *depressurization,*
- 2) *immediate water make-up,* and
- 3) *heat removals out of PCV (S/C).*

Those actions were required immediately after the IC and RCIC/HPCI lost their functions. To be honest, it is easy to say anything more than 6 months after the accident but almost impossible to put into practice under such a chaotic condition.

In Japan, however, new countermeasures have been already provided against large tsunami to all the NPS although on a temporary basis. More importantly we are prepared for the next tsunami coming. This makes the safety level of the current NPS in Japan much higher and more reasonable than before. We will never repeat the same mistake.

**After Fukushima** Nuclear energy is faced with challenges by the Fukushima Daiichi accident. Of course nuclear safety must be enhanced in a balanced way with other challenges such as radioactive waste management, economics, and non-proliferation. We recognize, nevertheless, the heightened importance of plant safety with lessons learned from the accident is the key to the nuclear deployment all over the world. It is more so if we understood that there would be no other energy sources

that can replace nuclear without intolerable cost increases or without damaging the environment. We must assure the people for the safe operation of nuclear plants fostering safety culture. In view of the global nature of these nuclear issues, it is imperative that we professionals play an important role to unveil the true causes and understand more about the accident and to enhance disclosure of the information. Exchange of ideas and critical information and encouragement of cross-fertilization of research and development efforts are of vital importance among not only in Japan but all nuclear countries.

(From *International Forum on Nuclear Power organized by the Hasanuddin University, Makassar, Indonesia, December 6, 2011*)

## II. NUCLEAR REACTOR SAFETY BY DESIGN

### II.1 Safety by Design

The first line of defense in the currently considered next generation reactors is to eliminate event initiators that could potentially lead to core damage. This concept could be implemented through the *safety-by-design*<sup>TM</sup> approach [1], which could be simply described as design the plant in such a way as to eliminate accidents from occurring, rather than coping with their consequences. Use of the *safety-by-design*<sup>TM</sup> as a defense in-depth barrier corresponds to enhancement of and strengthening the first barrier, i.e., a quantification of the well-known precepts of sound design, construction and operation. If it is not possible to eliminate certain accidents altogether by the “safety-by-design”, then the design inherently reduces their consequences and/or decreases their probability of occurring. This step could be achieved by practicing PSA and risk-informed design.

In the future, in relevance to the safety design of new advanced nuclear reactors, it would be necessary to consider the whole spectrum of possible accidents, not just the selected design or beyond design basis accidents. In this case, the accidents to be evaluated are selected due to certain criteria in relevance to a resultant core damage frequency and their consequence. And this is quite a challenging endeavor, but still manageable hopefully because a number of accidents could be eliminated in “safety-by-design” approach and, most importantly, because of the great improvements over the last decade in analytical and *computational methods*.

### II.2 Next Generation Nuclear Reactor: Sodium-cooled Fast Reactor

One of our research and development efforts has been directed toward the progress in the simulation-based technology and its application to design an ultimate but realizable sodium-cooled fast breeder reactor (SFR) system and providing much higher confidence in the public than current Liquid Metal cooled Fast Breeder Reactor (LMFBR) design.

The core is to be designed such that it is equipped with self-controllability with enhanced passive and inherent safety features where the *safety-by-design* is

embodied by eliminating the potentials of positive reactivity feedbacks in case of accidents.

**Why sodium?** Among many conceivable choices, the coolant should be sodium because of its excellent compatibility with structure materials, being used under the low pressure condition and with excellent heat transfer characteristics. These advantages should be emphasized. We should understand that the advantages overcome its drawback, i.e., its chemical potential. Sodium fire is not violent and of low energy phenomena. H<sub>2</sub> production due to the sodium-H<sub>2</sub>O reaction can be under control even if a H<sub>2</sub> explosion took place because of the intermediate (or secondary) heat transport circuits inserted between the primary sodium circuit and the steam generators. Reality is, the drawback has been overemphasized and SFRs are not in a good position even among some nuclear thermal-hydraulics (TH) professionals. This is a sad situation. The risk analysis would clearly show that SFRs render much lower core damage frequency than LWRs that are operated under the extremely high-pressure condition and the corrosive environment.

Our main concern is how the risk concept is understood by the public.

**Self-Controllability of SFR** Future fast reactors would be required to have inherent and passive safety characteristics against anticipated transients without scram (ATWS) and to render no fear against core disruptive accidents, even if they are extremely unlikely at the preset knowledge. For instance, in case of unprotected loss of flow (ULOF), transient over power (UTOP) and loss of heat sink (ULOHS) accidents, the reactor power during the transients should stay below a level corresponding to the core temperatures at which sodium boiling and fuel melting are assumed to take place. We call this specific safety characteristic as “*self-controllability*.” In order to evaluate the self-controllability, we have developed a general method, in which we employ self-controllability limit lines to judge whether a reactor can maintain the core integrity under the ULOF, UTOP and ULOHS conditions. [2]

Self-controllability limit line shows a relationship between the coolant effective reactivity  $\rho_{eff,cool}$  and fuel effective reactivity  $\rho_{eff,fuel}$  under such extreme conditions as sodium boiling or fuel melting initiation. The former effective reactivity is defined as a sum of the reactivity variations due to the coolant temperature difference  $\Delta T_C(z,0)$  from the core inlet and the latter as the one due to the fuel temperature difference  $\Delta T_F(z,0)$  from the coolant temperature at the axial elevation  $z$  and under steady-state operating conditions:

$$\rho_{eff,cool} \equiv \int K_C(z) \Delta T_C(z,0) dz \quad \text{and} \quad (1)$$

$$\rho_{eff,fuel} \equiv \int K_F(z) \Delta T_F(z,0) dz \quad (2)$$

where  $K_C$  and  $K_F$  are defined as:

$K_c(z) = K_{Dop}(z) + K_{Fexp}(z) + K_{Clad}(z) + K_{Na}(z) + K_{SAexp}(z)$ , and

$K_F(z) = K_{Dop}(z) + K_{Fexp}(z)$ .

In Eqs. (1)-(2),  $K$ 's are the reactivity coefficients; and the subscripts Dop, Fexp, clad, Na and SAexp are the Doppler, fuel expansion, cladding, sodium and subassembly expansion, respectively.

If a combination of  $\rho_{eff,cool}$  and  $\rho_{eff,fuel}$  obtained for a specific fast reactor is located below the limit lines for those ATWS's, we can judge that the reactor does not suffer from coolant boiling and fuel melting. However, in the process of deriving these limit lines, we must carry out a number of time-consuming transient calculations using a transient system analysis code. The objective of the study is to obtain the self-controllability limit lines with simple analytical expressions.

In pursuit of the objective, we introduce the following assumptions: (I) the extreme conditions are part of the quasi-steady responses under ULOF, UTOP and ULOHS conditions; (II) the total reactivity is zero under the extreme conditions; and (III) the power transient can be approximated by a simple exponential function in case of ULOF and the reactor power is well reduced to a decay power level in case of a ULOHS extreme state. Focusing on the extreme conditions, we consider the balance of feedback reactivities and core temperature distributions with the assumptions. Based on these considerations, we analytically derive self-controllability limit lines, instead of using a system transient analysis code. In summary the self-controllability region can be expressed as:

$$\begin{aligned} \rho_{tot}(t_{max}) &> \int K_F(z) [\Delta T_F(z, t_{max}) - \Delta T_F(z, 0)] dz \\ &+ \int K_c(z) [\Delta T_c(z, t_{max}) - \Delta T_c(z, 0)] dz \\ &+ \int K_c(z) [T_{c,in}(t_{max}) - T_{c,in}(0)] dz + \rho_{ext} \end{aligned} \quad (3)$$

where  $t_{max}$  is the timing of the onset of either coolant boiling or fuel melting. It is noted that the third integral term on the right-hand-side is the contribution of the inlet coolant temperature change in the case of ULOHS, which is zero in case of ULOF and UTOP.

Self-controllability limit lines under the ULOF, UTOP and ULOHS conditions are shown in Fig. 3 in terms of  $\rho_{eff,cool}$  and  $\rho_{eff,fuel}$ . There, good comparisons are made for ULOHS between analytical model and the results calculated by a system transient analysis code ARGO for the MOX- and metal-fueled cores. In general, the ULOHS line always stays above the ULOF line. This suggests that the ULOHS does not have to be considered in evaluating the self-controllability capabilities of fast reactors against ATWS but the ULOF and UTOP.

We consider that the above simple analytical method allows us to evaluate the self-controllability of any fast reactor core without carrying out a number of time-consuming system transient calculations for typical ULOF, UTOP and ULOHS accidents. Also the method provides us

with clear physical insights into the complicated feedback mechanisms related to the nuclear and thermohydraulics coupling phenomena.

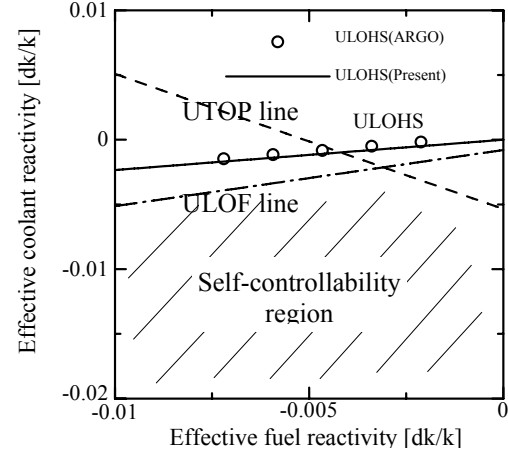


Fig. 3 Self-controllability lines for ULOF, UTOP and ULOHS

**Aluminum-Metal Fueled Fast Reactor Cores** An inherent safety fast reactor core has been proposed by Yokoyama, et al., [3] with ternary aluminum alloy (U-Pu-Al) fuels for large commercial reactors. Its high thermal conductivity will provide a favorable performance during reactor transients as illustrated by Ishizu, et al [4]. The proposed core has an inherent safety characteristics against ATWS events including both ULOF and UTOP events where we can make the burn-up reactivity less than 1\$ and the sodium void reactivity negative at the same time. An example of the core consists of short inner and tall outer core surrounded by radial blanket and bottom axial blanket regions as reported in the previous issue of this bulletin. Here, we have assumed a 4 year cycle length which corresponds to common fuel structure life time due to neutron fluence. The minimization of the reactivity swing has been pursued by mixing minor actinides to the fuel. Fundamental study was carried by Yokoyama, et al [3] out on the void reactivity of various fuel cores including metal-, nitride and MOX cores and inter-comparisons are being made.

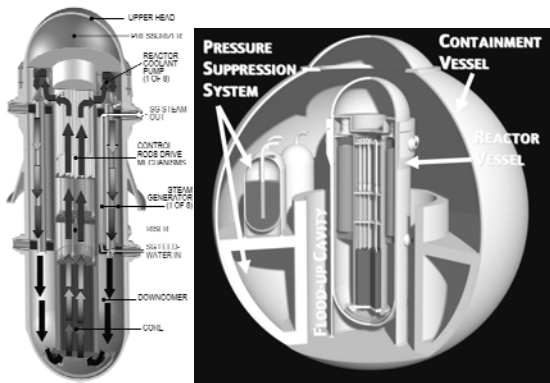
### II.3 Near-Term Deployment: IPSR

Should LMFBR be assumed to be in the next generation nuclear reactor, the near term deployment in particular in the countries with limited grid system would be achieved by installing Small-Medium Reactors (SMRs). Integrated Primary System Reactor (IPSR) would be the best candidate and is pursued in the international framework of the IRIS consortium, where IRIS is "International Reactor, Innovative and Secure." [1] Application of safety-by-design is the backbone of the IRIS design philosophy and combined with the PRA-guided design modifications. This has been carried out as "risk-informed-design" [5], continued into the framework of seismic margin analysis and extended to the studies with the seismic isolation system being implemented in the IRIS plant.

**PRA-Based Seismic Margin Analysis** IRIS is an advanced, modular, medium power (~335 MWe) PWR categorized in the Integrated Primary System Reactor (Fig. 4). Its compact, spherical, steel containment is able to withstand a higher ultimate pressure than a large cylindrical containment in a typical loop PWR. This positively impacts safety response in hypothetical accidents, while its small size enables a small footprint, reducing the overall construction cost.

The success of the IRIS Safety-by-Design™ and PRA-guided design is due to the effective interactions between IRIS Design team and IRIS PRA team (Fig. 5).

The IRIS development started with the lead of Westinghouse Electric Co, USA in 1999 and has since made a continuous progress, notably in the areas of improved safety and design simplification, as well as in novel engineering approaches. Such progress has been made possible by the IRIS international consortium, leading the IRIS development, which relied not only on world top-experts from industry but also on the academia and students [6], effectively integrating their talent and work into the IRIS design development. I have been a member of the IRIS university consortium since the beginning of its history. Our contributions include thermal hydraulics design proposals of future high-burnup core options, putting the PRA-based risk-informed design into practice, and the current SMA work.



(a) IRIS primary system (b) IRIS containment layout

Fig. 4 IRIS Integral Layout

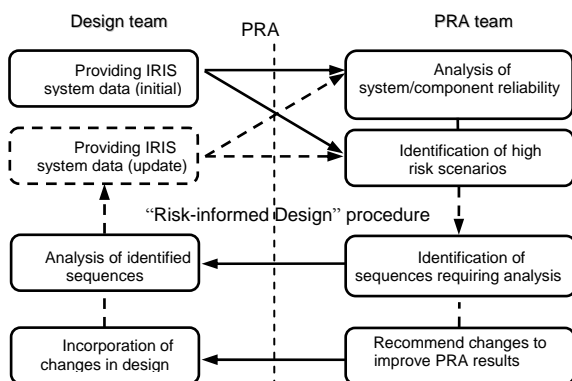


Fig. 5 IRIS Design and PRA Team Interactions

**PRA and SMA for IRIS** The application of the PRA guided design concept to internal events at power resulted in a very encouraging reduction of the IRIS Core Damage Frequency (CDF) in the range of lower  $10^{-8}/RY$  [5]. This brought to light such an external event as earthquake as principal contributors to the overall plant CDF. A seismic PRA is therefore needed to be developed. The development of a complete seismic PRA for a plant still in its design phase is a challenging work that also requires some update and modification in the seismic PRA techniques, especially under the point of view of the uncertainty reduction.

Within the framework of the IRIS risk-informed design, a preliminary PRA-Based Seismic Margins Assessment (SMA) has been continued to assess the ability of the IRIS Standard Design to respond to seismic events. This would complete a first step toward the development of a complete IRIS seismic PRA. In the SMA model, seismic initiating event trees and system fault trees was developed starting from the event and system fault trees conceived for the internal events at-power PRA. They were reviewed to identify the types of events that might be expected to occur as a consequence of the seismic event and screened according to general assumptions such as the “one fails, all fail”. In a PRA-Based SMA High Confidence of Low Probability of Failure (HCLPF) acceleration values are calculated for important accident sequences and for the plant as a whole. The HCLPF values are those seismic acceleration values for which there is a 95% confidence that the probability of failure for the specified sequence (or component) is less than 5%. This is the main result of an SMA; no probabilistic results in term of CDF are then expected. A detail of the results has been reported in Kumagai [7].

### III. CFD and SUBCHANNEL ANALYSIS

The essential of the simulation-based design approach consists of computational and experimental approaches. In spite of the recent progresses in Computational Fluid Dynamics (CFD), however, it is underlined that CFDs are given credits for a tiny fraction of the design and safety evaluation processes in nuclear industries and authorities unfortunately. There experimental evidences are always requested. This is not because the CFD is not reliable but the nuclear reactor design requires well-established and well-proven technology with the sufficient expertise accumulated in the past. Therefore, the full use of CFD in the simulation-based design procedure would be a challenge in the future nuclear reactor development.

In fact, when thermal hydraulics in actual nuclear fuel pin subassemblies is concerned, especially when fuel pins are wire-wrapped, the use of CFD is limited as turbulence models are required. Instead, subchannel analysis has been most commonly used with appropriate wire-spacer modeling for design purposes (Distributed Resistance Model by Ninokata, Efthimiadis and Todreas, 1987 [8]).

### III. 1 Low Reynolds Number Turbulent Flows and Tight-Lattice Configuration

As long-life core concepts with passive safety features including natural circulation decay heat removal options are considered for a candidate of the next generation nuclear reactors, tight lattice fuel pin subassembly design with the triangular pin array configuration (Fig. 6) attracts attention of thermal hydraulics communities. This configuration is often used in advanced nuclear reactors including high conversion light water reactors and sodium-cooled fast reactors. With lower pin pitch to diameter ratio  $P/D$ , i.e., less coolant volume fraction in the core, less neutron moderation assures harder neutron energy spectrum leading to more neutron population in the core and to a possibility of higher conversion of  $^{238}\text{U}$  to  $^{239}\text{Pu}$ . For example, in the Japanese prototype sodium cooled fast breeder reactor Monju with 280 MW electricity output (JAEA website [9]), 169 wire-wrapped fuel pins are encased in a hexagonal duct tube.  $P/D$  is 1.21 with  $P = 7.9$  mm and  $D = 6.5$  mm, which is much tighter than 1.3~1.4 of conventional light water reactors. Sodium flows in this core fuel subassembly at about 6.8 m/s ( $\text{Re} \sim 7.5 \times 10^4$ ) on an average. Also an inherently safe, small sodium-cooled fast reactor, 4S (Super-Safe, Small and Simple; see Toshiba, 2007-2008[10]) with 10MW electricity output, employs even tighter  $P/D = 1.08$  with  $P = 15.1$  mm and  $D = 14.0$  mm with grid spacers.

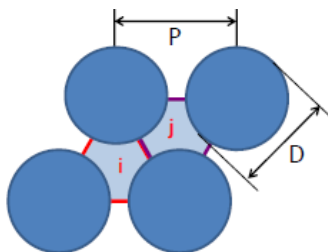


Fig. 6 Triangular pin array configuration:  $P$  is the pin pitch and  $D$  the pin diameter;  $i$  and  $j$  are the subchannel number

Flows in fuel pin subassemblies (or in any inhomogeneous channel geometry) are characterized, in general, by divergence cross flow and turbulent mixing. In the sodium-cooled fast reactor development, a large thermal hydraulics database has been constructed for fuel subassemblies of relatively high  $P/D$  and under highly turbulent flow conditions. In the case of tight lattice bundles where coolant flows at relatively low mass flow rates, however, very few experiments have been carried out. Therefore, no experimental data are available with respect to detailed velocity and temperature distributions inside fuel subassemblies or in the subchannel geometry configuration under low  $\text{Re}$  turbulent flow conditions. There, the flows of interest are characterized by unsteady and irregular flows which give something of the appearance of randomness; strong vorticity; stirring and diffusion of heat; dissipation of energy by momentum exchange. As the decay heat further decreases, natural

circulation mass flow rate would approach an extremely low range. Without much experimental information, it is a big challenge to apply CFD to these flows and obtain any physical insights out of it.

In the fully developed turbulent flows in a fuel pin sub-assembly without spacer effects, there are a couple of interesting phenomena that were hardly captured in the past by the Reynolds-Averaged Navier-Stokes (RANS) equations approach with isotropic  $k-\epsilon$  turbulence models but found theoretically or experimentally. They include

- i) turbulence-driven secondary flows in subchannels;
- ii) local transition between laminar and turbulent flows near a narrow gap between two adjacent fuel pins in particular in the case of tight lattice fuel pin subassemblies; and
- iii) the global pulsations leading to the coolant mixing between the two subchannels,

all these phenomena being connected to the anisotropy of turbulence. It is noted that the secondary flow effects play an important role in the local laminar-turbulent transition and global pulsation. Also these particular phenomena have been considered to be less dominant for fuel subassemblies of high  $P/D$  and at high  $\text{Re}$  because the turbulence would be more isotropic. However, as  $P/D$  and/or  $\text{Re}$  is reduced, these phenomena become conspicuous but the mechanisms have not been fully understood.

### III. 2 Computational Fluid Dynamics (CFD)

The simulation-based design approach consists of computational and experimental approaches of simulation. Nuclear reactor design requires well-established and well-proven technology with the expertise accumulated in the past. Therefore, it is indeed our challenge to make the CFD's fraction larger in the simulation-based design approach. The approach of Reynolds Averaged Navier-Stokes (RANS) is very useful but only when mechanisms of the phenomena are well known and understood. While experiments provide the information, however, CFD including LES, DNS and Direct Simulation Monte Carlo (DSMC), can provide us more detailed information for better understanding the phenomena that are observed in the experiment. *With the well understood phenomena and their modeling*, large scale mock up experiments could be replaced partially by CFD, and this would be one of our immediate targets of the simulation-based design approach [11].

**DNS/LES of Turbulent Sodium Flows** A major objective of our research is to establish a computational simulation-based design and safety approach in nuclear engineering, in particular in the area of nuclear fuel pin subassembly thermal hydraulics, design and safety. Emphasis is placed on the delineation, in-depth understanding and modeling of the complex turbulent flow structure inside nuclear fuel pin subassemblies characterized by non-homogeneous and anisotropic turbulence.

Applications of Direct Numerical Simulation (DNS) of turbulence and Large Eddy Simulation (LES) techniques

are fully employed being aimed at providing higher quality of computational data that should be equivalent to or more detailed information than those provided by experimentation. Also the computational results will be used for engineering modeling as well as the basis on which design data base is constructed.

Most calculations were carried out using the SPARKLE-DNS code [12], [13] on the Earth Simulator, one of the high-end computers in the world several years ago, for the eccentric annulus channel flows to confirm the eddy migration behaviors in the non-uniform flow channels, flow pulsation and flow stabilization [14], and then establish turbulence flow data base that should be useful for engineering applications, in particular in connection to the turbulent flows in tight lattice nuclear fuel pin subassemblies [15]. The targeted phenomena included the local laminarization and global pulsation phenomena. Our calculations have clearly delineated coherent structures and anisotropy conditions in the narrow gap which are all responsible for the local laminarization and the flow pulsation phenomena.

### III. 3 Remarks on the Mechanistic Modeling

In the late 90's, I have been involved in the advanced subchannel analysis code development project. Two phase flow is described by the two-fluid three-field representation. The product of the project was represented by the NASCA code for predicting Boiling Transition in BWR rod bundles [16]. The following is an important point to make for code developers as well as modelers.

In the averaging procedure to derive subchannel analysis conservation system equations, constitutive equations will appear that are representing the influences of local phenomena. The local phenomena of much smaller length- and time-scale, that may give significant influences onto the global behaviors of fluids, cannot be explicitly described by the macroscopic and time-averaged independent variables, i.e., unknowns in the subchannel analysis equations. Therefore the basic processes that are described with local and instantaneous variables should be converted into the fewer elementary processes. Then, the elementary processes are to be correlated with the macroscopic and time-averaged variables while maintains the framework focusing on geometrical parameters. This step is exactly the same process as for the friction factor derivation in a pressure drop correlation and interfaces the subchannel analysis with experimental data or CFD, in particular with DNS/LES.

As an example: we still need practical improvement in the cross-flow model such as divergence cross-flow, turbulent mixing and void drift. In the following, for single-phase turbulent flows in rod bundles, I would like to focus on the global details of flow pulsation phenomena in a tight lattice rod bundles. The phenomena have been pointed out to be responsible for the inter-subchannel fluid and energy exchanges. Nonetheless details of the mechanisms of GFP have never been clarified by CFD until Merzari successfully carried out the DNS/LES [13] and then by URANS based on the DNS/LES results.

### III.4 Global Flow Pulsations

Phenomena of interest are the secondary flows in subchannels, local laminar-turbulent transitions and global flow pulsation. All these phenomena have long been my most attracted research and development topics and with the Earth Simulator, have finally been resolved.

In particular the global flow pulsation phenomena have been a difficult subject until the high-end computers have been made available. Axial coolant flow inside a tightly packed pin subassembly presents complex behaviors; experimental analysis had clearly shown that when reducing the pitch-to-diameter ratio ( $P/D$ ) the turbulence field in pin subassemblies deviates significantly from that in a circular tube. Moreover for extremely tight configurations, the existence of large-scale periodic flow oscillations has been shown, which is responsible for the high inter-subchannel heat and momentum exchanges ([17] Moeller, 1991). Complete understanding of these oscillations has still to be achieved; the evidence shown up to this point in Lexmond and Van der Haagen [18] (2005) suggests that the oscillations are connected to interactions between eddy structures of turbulent flows in adjacent subchannels.

The substantial failure of traditional steady state RANS modeling in the simulation of tight fuel bundles is not surprising. Beside turbulence itself, the actual flow field in a fuel pin subassembly is neither steady nor stable, and presents long-term, large scale coherent patterns. The contribution of these structures cannot be taken into account by a steady-state simulation, unless specific ad-hoc models are introduced in the momentum equations. An ad-hoc model would lack generality, and would be geometry dependent; i.e., it is considered that the model would not work on both triangular arrays and quadratic arrays of pins at the same time.

First success in predicting the phenomena was reported by Baglietto and Ninokata ([19] 2005, [20] 2006) with a modified anisotropic  $k-\epsilon$  model in the CFD-code STAR-CD 3.26. We solved the boundary layer and for this the grid strategy includes: the first near wall mesh has been kept at a value of  $y^+=1$ ; in the wall layer, wall-normal cells have been used; and the sensitivity to the grid sizes has been tested out for steady state calculations. A total of more than 600,000 meshes have been used and the CFL condition has been kept below 0.2. A periodic boundary condition is imposed at the bottom and top of the flow channel (Fig. 7).

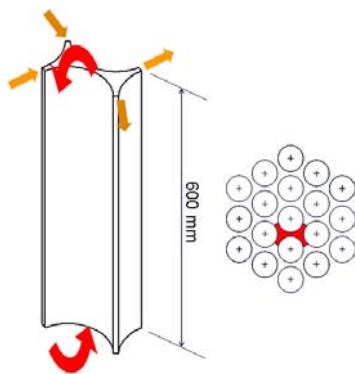


Fig. 7 Geometry and boundary conditions for an infinite array rod bundle

Results from the modified anisotropic  $k-\epsilon$  model (Baglietto, et al. 2004) have shown good agreement with the experimental data of Krauss and Meyer [21] (1998) including the wall shear stress, Reynolds stresses and stream-wise velocity distributions as reported in Merzari, Ninokata and Baglietto [22] (2008). A snapshot of the shape of the cross-flow velocity oscillations across the narrow gap is shown in Fig. 8. They are present also on the periodic boundaries giving place to a truly three-dimensional pulsation, confirming the assumption of this oscillation to be strongly correlated spatially in the entire subassembly. Figure 9 shows several instantaneous cross flow distributions in one subchannel at different elevations where thick arrows indicate the major cross flow directions. Typically, for an air flow  $Re = 38,750$  ( $\sim 20$  m/s in the main stream direction) in a tight lattice bundle of  $P/D = 1.06$  ( $D = 14$  cm) and the hydraulic diameter = 3.35 cm, the amplitude of the oscillation is 2 m/s with the wave-length of 19 cm and the peak frequency of 95.8 Hz. The shape of power spectra of the oscillation in the central gap is similar to the one provided by Krauss and Meyer [21]. With the axial velocity averaged in the gap ( $w_{gap} = 16.9$  m/s), the Strouhal number:

$$S_r = \frac{fD}{w_{gap}}$$

is 0.8, while in the experiment it is 0.93.

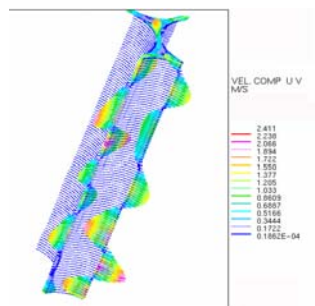


Fig. 8 Flow oscillation between subchannels and cross flow velocity components shown from different angles predicted by the URANS method

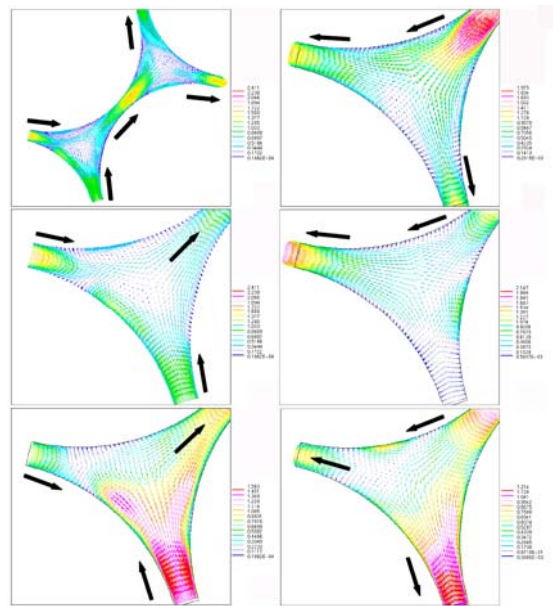


Fig. 9 Oscillations and distributions of transverse flow components in one subchannel at different elevations predicted by the URANS method; thick arrows indicate the major flow directions

### III.5 Subchannel Analysis Turbulent mixing [15]

The subchannel analysis is commonly used in nuclear reactor thermal hydraulics design and safety evaluations. Because subchannel analysis codes solve a set of the time- and volume-averaged Navier-Stokes and energy equations, they include numerous constitutive equations that are resultant from the volume- and area-integration procedures. Among them the fluid mixing between subchannels is one of the important phenomena that require modeling.

The coolant mixing could be explained in general by several transport mechanisms, e.g., convection by divergence cross-flow, turbulent and molecular diffusion, and other macroscopic flow processes including the global flow pulsation. Although the mixing has attracted much attention of thermal hydraulics community for nearly half a century, it has been well known that the single-phase turbulent mixing model often underestimates the mixing and cannot explain fully the phenomena taking place even in the high  $Re$  number flow regime. Lack of modeling of the flow pulsation has been pointed out to be one of the reasons for this underestimation as discussed in Krauss and Meyer [21]. In fact, in the narrow gap region, strong, large scale flow pulsations are simulated by CFD in the preceding sections for a wide range of geometrical and hydraulics parameters. The mixing should be certainly enhanced by the global pulsation. The process is important for high  $Pr$  fluids, in particular  $H_2O$ ; so would be even for low  $Pr$  fluids such as sodium.

The general form of energy mixing between two subchannels  $i$  and  $j$  is formulated as a sum of turbulent mixing and conduction as described by Ramm, Johannsen and Todreas [23] (1974):

$$W_{ij}^{*H} = \mu s_{ij} \left[ \frac{1}{\Delta x_{ij}^L \text{Pr}} + \frac{\varepsilon^H}{\Delta x_{ij}^T \nu} \right],$$

where  $W_{ij}^{*H}$  is defined as the energy flux per unit length due to turbulent and molecular effects;  $\mu$  is the viscosity;  $s_{ij}$  the gap width;  $\Delta x_{ij}^L$  and  $\Delta x_{ij}^T$  are the subchannel laminar and turbulent mixing lengths, respectively; Pr Prandtl number;  $\nu$  the kinematic viscosity; and  $\varepsilon^H$  is the eddy diffusivity of energy.

To see the influence of the cross-flow pulsation, we take a simple two subchannel i-j system without heating, where hot and cold sodium is flowing in and mixes between two subchannels at  $Re = 50,000$  with the temperature of  $400^\circ\text{C}$  and  $500^\circ\text{C}$  at the inlet of subchannels i and j, respectively. The hydraulic diameter is 5 mm, the gap width 2 mm and the channel length is 1 m.

Simple heat balance calculation is made with the turbulent and molecular diffusions. Figure 10(a) shows a result of sodium temperature distributions along the two subchannels. Note that axial heat conduction is neglected and the material properties are constant for simplicity. In this case, the exit temperatures reach  $438^\circ\text{C}$  and  $462^\circ\text{C}$  of subchannels i and j, respectively. Figure 10(b) implies that the molecular effect is no longer dominant for sodium flow at  $Re > 50,000$ . The ratio of transverse mass flux to the main flow mass flux (mixing Stanton number)

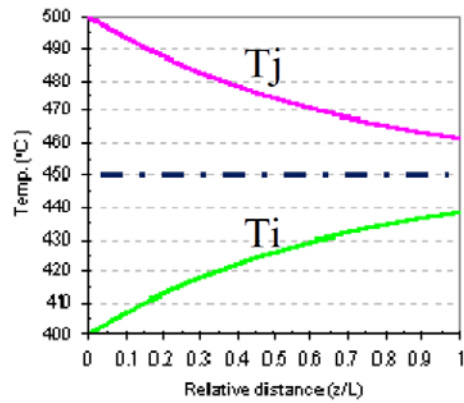
$$M_{ij} = \frac{w'_{ij}}{s_{ij} G_i}$$

decreases from 0.1 at  $Re = 1,000$  to 0.01 at  $Re=10,000$  and is minimum at  $Re \sim 50,000$ .

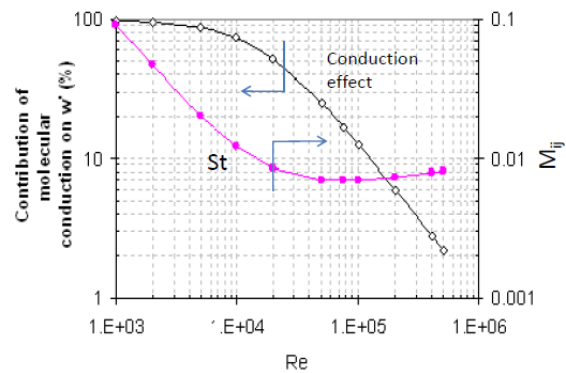
Now we apply the cross-flow pulsation at the subchannel boundary:

$$u(z, t) = u_0 \sin 2\pi \left( \frac{z}{\lambda} - \frac{t}{T} \right) \quad (6)$$

where  $u(z, t)$  is the pulsating cross flow component with the amplitude  $u_0$ ,  $\lambda$  the traveling wave length and  $T$  is the period of the oscillation. In this attempt to calculate temperature distributions without turbulent mixing and heat conduction, the amplitude of crossflow pulsation is assumed to be 5% of the main flow velocity. This would be considered reasonable in reference to the CFD simulation results. Figure 11 shows the time-averaged temperature distributions along the subchannel i and j where the asymptotic temperatures at the outlet are calculated to be  $455^\circ\text{C}$  and  $445^\circ\text{C}$ . The rate of mixing is sensitive to the amplitude  $u_0$  while the frequency and wave length do not give influences onto the time averaged temperature distributions. In comparison with Fig. 10 (a), it is obvious that the coolant mixing is enhanced by the cross-flow pulsation, i.e., the temperature difference at the outlet between two subchannels is  $10^\circ\text{C}$  in this case while  $24^\circ\text{C}$  with the turbulent and molecular effects.



(a)  $T_j$  and  $T_i$  at  $Re=50,000$



(b) Diffusion effects at various Re

Fig. 10 (a) Temperature distribution along the flow subchannels i and j due to turbulent mixing and heat conduction; (b) contribution of molecular diffusion and mixing Stanton number  $M_{ij}$ .

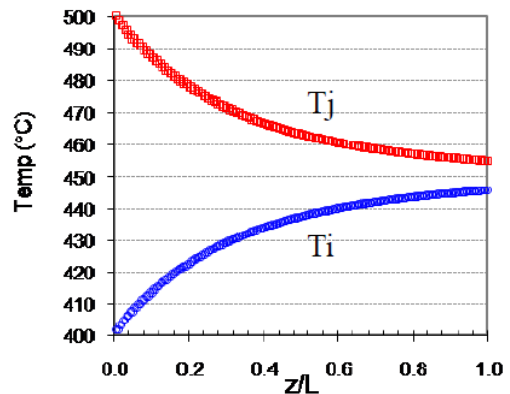


Fig. 11 Temperature distribution along the flow subchannels i and j due to cross-flow pulsation

**Concluding Remarks on Subchannel Analysis** It is well understood that simulating a whole bundle by DNS is not possible, while it could be done by LES on high-end computers available. As a result LES would be most promising among all CFD approaches in the near future when one wishes to carry out thermal hydraulics design of the nuclear fuel subassemblies solely by numerical simulation without expensive mockup tests. DNS would be in a position to provide LES and RANS with essential information of equal to or even higher quality than experiment but for an extremely small portion of a bundle with assumptions of infinite array, periodic boundary conditions, relatively low Re number single-phase and fully developed flows.

Spatial resolution of the subchannel analysis is of course low limited by the sizes of subchannel control volumes. The method, however, has been established and put into practice since 1960's. Instead of associating with the detail and complexity in the turbulent transport processes, the constitutive equations could be those of phenomenological modeling. It does not require refined flow modeling. As long as the models are backed up by experiment and/or DNS/LES, the subchannel analysis would be still useful and reliable until LES takes its place gradually and eventually.

## ACKNOWLEDGEMENT

My sincere thanks go to all of my colleagues and students in the Nuclear Engineering Department and RLNR as well as so many wonderful friends in Japan and all over the world, all who have made my life as a professor so exciting and productive. Thanks and Grazie.

## REFERENCES

- [1] M. D. Carelli, L. E. Conway, et al, The Design and Safety Features of the IRIS Reactor, *Nucl. Eng. Design* **230**, pp. 151-167 (2004)
- [2] H. Ninokata, et al.: On self-controllability and self-terminability of fast reactors; *Progress in Nucl. Energy*, vol. **32**, No. 3/4, pp. 737-744, (1998)
- [3] T. Yokoyama, M. Tokiwai, H. Endo and H. Ninokata, "Optimization of Aluminum-Metal Fueled Fast Reactor Cores for Inherent Safety," *Trans. Am. Nucl. Soc.* **93**, 671 (2005).
- [4] T. Ishizu, h. Endo, m. Tokiwai, T. Yokoyama and H. Ninokata, "Study of Self-Controllability and Self-Terminability of the Core Loaded with High Thermal Conductivity Fuels," COE-INES-1, (Tokyo, Japan) Paper 91 (2004).
- [5] Y. Mizuno, H. Ninokata and D. J. Finnicum, Risk-informed design of IRIS using a level-1 probabilistic risk assessment from its conceptual design phase, *Reliability Engineering and System Safety*, **87** (2005) 201-209
- [6] M.D. Carelli, B. Petrović, M. Ricotti, N. E. Todreas, N. Čavlina, F. Oriolo and H. Ninokata, Role of University Research in the Development of IRIS, *Proc. International Youth Nuclear Congress (IYCN-2006)*, Sweden, June, 2006.
- [7] Y. Kumagai, H. Ninokata and D. Finnicum, PRA-based SMA: the first tool toward a risk-informed approach to the seismic design of the IRIS, *J Nuclear Science and Technology*, Vol. **44**, No. 10, 1268-1274, 2007.
- [8] H. Ninokata, A. Efthimiadis and N.E. Todreas, Distributed resistance modeling of wire-wrapped rod bundles, *Nucl Eng Des*, **104**, 93 – 102 (1987)
- [9] <http://www.jaea.go.jp/04/monju/EnglishSite/index.en.html>
- [10] Toshiba (Slide Presentations), 2007-2008. 4S Reactor - Super-Safe, Small and Simple - Meetings with NRC Pre-Application Review, **ML072950025**, October 22, 2007; **ML080600037**, February 21, 2008; **ML081400095**, May 21, 2008; **ML082190834**, August 8, 2008. All available on the USNRC Website
- [11] H. Ninokata and E. Merzari, Computational Fluid Dynamics and simulation-based-design approach for tight lattice nuclear fuel pin subassemblies, Keynote lecture, KN#6, *12<sup>th</sup> Topical Meeting on Nuclear Reactor Thermal Hydraulics (NURETH-12)*, Pittsburgh, USA, October 1-5, 2007
- [12] T. Misawa, I. Maekawa and H. Ninokata, Calculation of Heat Transfer Coefficients on a Flat Plate by Pseudo Direct Numerical Simulation of Turbulence, *Journal of Nuclear Science and Technology*, Vol. **40**, No 10, pp 703 ~ 707 (2003)
- [13] E. Merzari, Dr-Eng Thesis, Tokyo Institute of Technology, September, 2008.
- [14] E. Merzari and H. Ninokata, Development of an LES Methodology for Complex Geometries, F00123, *12<sup>th</sup> Topical Meeting on Nuclear Reactor Thermal Hydraulics (NURETH-12)*, Pittsburgh, USA, October 1-5, 2007.
- [15] H. Ninokata, E. Merzari and A. Khakim, "Analysis of low Reynolds number turbulent flow phenomena in nuclear fuel pin subassemblies of tight lattice configuration", *Nuclear Engineering and Design*, **239** (2009) 855-866.
- [16] H. Ninokata, T. Anegawa, M. Aritomi, T. Hara<sup>2</sup>, H. Kamo, S. Kusuno, K. Mishima, S. Morooka, K. Nishida, M. Sadatomi, A. Sou, Y. Yabushita, Y. Yamamoto, Development of the NASCA code for predicting transient BT phenomena in BWR rod bundles, OECD/CSNI Workshop on Advanced Thermal-Hydraulic and Neutronic Codes Application Barcelona, Spain, April 10-13, 2000.
- [17] S.V. Moeller, On phenomena of turbulent flow through rod bundles, *Experimental Thermal and Fluid Science*, **4**, 25-35 (1991).
- [18] M. Lexmond, T. Van der Haagen, Visualization of the vortex street and characterization of the cross flow in the gap between two subchannels, (paper:122)11<sup>th</sup> NURETH (2005).
- [19] E. Baglietto and H. Ninokata, A turbulence model study for simulating tight lattice rod bundles, *Nucl Eng Des*, **235**, 773-784 (2005).
- [20] E. Baglietto, H. Ninokata, T. Misawa, CFD and DNS Methodologies Development for Fuel Bundle Simulations, *Nuclear Engineering and Design*, 236, 1503-1510 (2006).
- [21] T. Krauss and L. Meyer, Experimental investigation of turbulent transport of momentum and energy in a heated rod bundle, *Nucl Eng Des*, **18**, 185-206 (1998).
- [22] E. Merzari, H. Ninokata and E. Baglietto, "Numerical Simulation of the Flow in Tight-Lattice Rod-Bundles", *Nuclear Engineering and Design*, **238**, pp.1703-1719 (2008)
- [23] H. Ramm, K. Johannsen and N.E. Todreas, Single phase transport with bare-rod arrays at laminar, transition, and turbulent flow conditions, *Nucl. Eng. Des.*, **30**, 186-204 (1974).



# A.1 Performance Test Results of a Supercritical CO<sub>2</sub> Compressor Used in a New Gas Turbine Generating System

Masanori ARITOMI

Supercritical carbon dioxide (S-CO<sub>2</sub>) gas turbines can generate power at high cyclethermal efficiency, even at modest temperatures of 500-550°C, because of themarkedly reduced compressor work near the critical point.furthermore, the reaction between Na and CO<sub>2</sub> is milder than that between H<sub>2</sub>O and Na. A more reliable and economically advantageous power generation system could be achieved by coupling with a sodium-cooled fast reactor. At Tokyo Institute of Technology, numerous development projects have been conducted for development of this system in cooperation with JAEA. Supercritical CO<sub>2</sub> compressor performance test results were obtained as described herein. Maximum design conditions of the supercritical CO<sub>2</sub> test apparatus are 11 MPa pressure, 150°C temperature, a 6 kg/s flow rate, and a rotation rate of 24,000 rpm. Different compressor design points are examined using impellers of three kinds. Then test data were obtained under steady-state conditions. The pressure ratio (compressor outlet pressure/inlet pressure) was obtained with the function of compressor rotation speed and the fluid flow rate. The data, reported herein for the first time, cover a broad region from sub-critical to supercritical pressures. No unstable phenomenon was observed in the area where the CO<sub>2</sub> properties change sharply.Results show that enthalpy rise needed to achieve the same pressure ratio near the critical point is smaller than in a sub-critical condition. Compressor test data were calculated using three-dimensional CFD code (CFX). Data of the pressure ratio vs.flow rate agreed with those implied by the fundamental compressor theory. A sodium-cooled fast reactor supercritical CO<sub>2</sub> gas turbine system is presented in Fig. 1. In a typical design, a reactor’s thermal power, a turbine inlet pressure and an inlet temperature are respectively, 600 MW, 20 MPa, and 527°C.

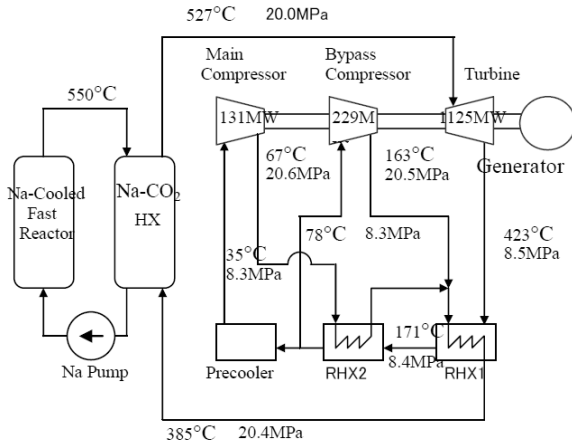


Fig.1 Cycle design using supercritical CO<sub>2</sub>

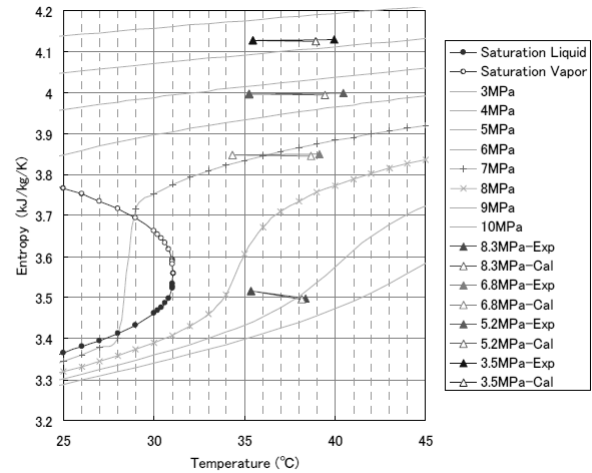


Fig.2 Test nad calculation results with temperature vs. entropy

Experimental and calculated results are presented in this Fig. 24 with four different pressure cases. A supercritical CO<sub>2</sub> compressor used near the critical point is a key component of sodium-cooled fast reactor supercritical CO<sub>2</sub> gas turbine systems. A supercritical CO<sub>2</sub> test apparatus with a small centrifugal compressor test model was constructed and tests data were obtained and the digital measured values are reported. The data were also evaluated using CFD code CFX.

1. Experimental data were obtained for a broad range from the sub-critical to the supercritical region using three different impellers. No unstable phenomenon was observed for the region with sharply changing CO<sub>2</sub> properties.
2. The compressor pressure ratio for the rotation rate is expressed as a parabolic equation under a constant pressure loss coefficient and compressor inlet fluid condition. The loci show arc lines for a constant rotating speed. Compressor characteristics are coincident with the fundamental compressor theory, even if the compressor is operating in the vicinity of the critical point.
3. Entropy, enthalpy, density, and specific heat change near the compressor rated operating condition are very sensitive to the temperature change. The accuracy of the measured temperature is important for compressor performance evaluation in the vicinity of the CO<sub>2</sub> critical point.

### Reference

[1]Masanori ARITOMI, Takao ISHIZUKA, Yasushi MUTO and Nobuyuki TSUZUKI: Performance Test Results of the Supercritical CO<sub>2</sub> Compressor for a New Gas Turbine Generating System; 18th International Conference on Nuclear Engineering (ICONE18), ICONE18-29371, Xi’an, China(2010).

## A.2 Experimental Study on Heat Transfer Characteristics of Vertical $5 \times 5$ Heated Rod Bundles around Critical Pressure with R-134a

Noriyuki WATANABE and Masanori ARITOMI

Recently, the supercritical water reactor (SCWR) has been promising as one of the next-generation light water reactors (LWRs) in terms of high thermal efficiency, effective use of plutonium, simplification of plant systems, and economical competitiveness in comparison with conventional LWRs.

From the standpoint of thermal hydraulics, as boiling phenomena do not exist any longer above the critical pressure, it is not necessary to be concerned about several thermal problems (boiling transition, CHF, DNB, etc.) in the rated operation condition of the SCWR. However, if the system pressure rapidly decreases from supercritical to subcritical due to abnormal-pressure transient accidents such as loss-of-coolant accidents (LOCA), the above thermal problems cannot be avoided.

To establish the SCWR as one of the next-generation commercial reactors, it is required to clarify the fundamental heat transfer characteristics in the vicinity of the critical point (especially around critical pressure) because the behavior of the thermal equilibrium qualities just before the critical pressure shows quite different tendencies according to the input thermal condition. Hence, the objective of this paper is to investigate the heat transfer characteristics around the critical pressure in the rod bundle geometry related to the SCWR's core. Specifically, the behaviors of the heating surface temperatures of each of the rods were experimentally investigated under transient pressure conditions, where the pressure constantly decreases in the vicinity of the critical point from supercritical to subcritical or constantly increases from subcritical to supercritical under constant inlet thermal conditions. This experimental approach nearly simulates the conditions of the abnormal-pressure transient accidents (LOCA) and the sliding-pressure start-up scheme during a start-up stage. In the present study, the experiment was performed using a forced circulation loop with  $5 \times 5$  heated rod bundles cooled by R-134a (see Fig. 1 and Fig. 2).

Representative behaviors of averaged heating surface temperatures with respect to each of the subchannels under transient pressure conditions, where the pressure constantly decreases from supercritical to subcritical or constantly increases from subcritical to supercritical under constant inlet thermal conditions, are shown in Fig. 3. As the pressure approaches the critical pressure, a DNB type or a dryout type of CHF was induced, and then the post-CHF was kept until the vicinity of the critical pressure. Under the supercritical pressure, the post-CHF disappeared due to the extinction of boiling phenomena, but the heat transfer

deterioration was induced in a certain pressure range. In the depressurizing process, the heating surface temperatures followed the trajectory of temperature behaviors as in the pressurizing process except for the quenching point. The quenching point from the post-CHF moved to the lower pressure side than the pressure as for the CHF in the pressurizing process. This phenomenon was considered as the hysteresis phenomenon frequently observed in pool boiling curve characteristics.

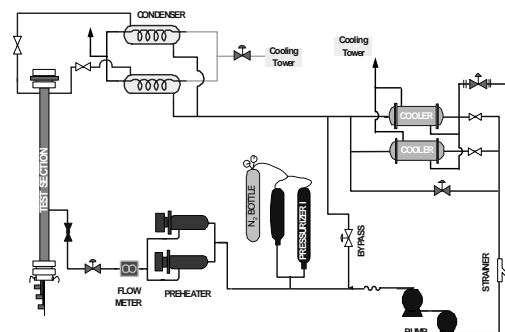


Fig. 1 Schematic diagram of experimental apparatus

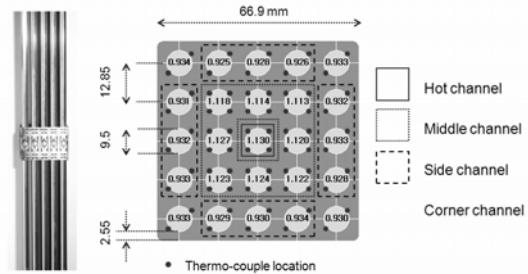


Fig. 2 Details of  $5 \times 5$  heated rod bundles test section

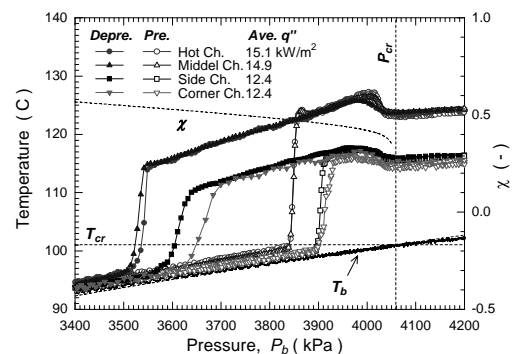


Fig. 3 Averaged heating surface temperatures at each subchannel during pressurizing and depressurizing processes around critical pressure ( $G=150\text{kg/m}^2$ ,  $T_{in}=90\text{C}$ )

### Reference

- [1] Noriyuki Watanabe, Se-Young Chun, Masanori Aritomi and Hiroshige KIKURA, *J. Nucl. And Sci.* **48**(1), 135-144(2011).

### A.3 The Study of Velocimetry in High Temperature Flow

Hiroshige KIKURA, Yasushi TAKEDA

A flow velocity measurement method in high-temperature fluid is needed in controlling and monitoring the plant in the field of atomic energy. High-temperature flow includes feed-water flow and boiling water flow in nuclear plant, liquid metal flow in fast breeder reactor, and so on. Above all, a molten glass flow in a vitrification melter of high-level radioactive wastes is one of the difficult flows. For keeping vitrification melters in stable operation, we focus on the subsidence of the platinum group metals and other substance contained in high-level radioactive wastes.

However, there are a lot of difficulties applying conventional technics such as Hot-wire anemometer, laser Doppler anemometry (LDA), and image flow visualization (PIV, PTV), because of the opaque and the large radiation. Moreover, the radiation technic that uses X-ray, gamma ray, and neutron ray, etc. is unsuitable for a general-purpose measurement because of a lot of difficulties and the restrictions of the radiation treatment. In this severe environment, ultrasonic technic is one of the applicable methods. Due to its propagation property, ultrasound technic is known as nondestructive evaluation of materials. Therefore, measurement can be made from the outside of a container, pipe etc. Ultrasonic velocity profiler monitor (UVP) has been developed to measure a velocity profile. This UVP can obtain velocity profile analyzing ultrasonic signals. During its calculation, a sound velocity is needed.

We obtained sound velocities of molten glass, and built UVP algorithm from scratch. Fig. 1 illustrates experimental apparatus constructed in this study.

Fig. 2 shows measured temperature dependency of a certain borosilicate glass. Because its difference is within plus-minus 5% at this temperature condition, we conclude that the ultrasound measurement can be applied for this kind of molten glass. So, we conclude that the sound velocity is almost constant from ten hundred degrees to twelve hundred degrees.

Finally, to evaluate the accuracy of this UVP system, the speed of moving buffer-rod was measured. Fig. 3 shows the obtained relation between actual velocities and measured velocities from 0.5 mm/s to 18 mm/s. The dot is the measured data and the slope of the solid line is 1. As velocities are calculated using FFT in this method, a measurable velocity is limited by many parameter. A lower limit of this condition is indicated by dashed line. As a result, the error of measured velocity within 4% when a value remained in measurable velocity.

#### References

[1] T. Ihara and H. Kikura : Ultrasound Characteristics in High-temperature Fluid, *JSME Fluids Engineering Conference 2010*, Yonezawa, Japan (2010-10), pp.527, in Japanese.

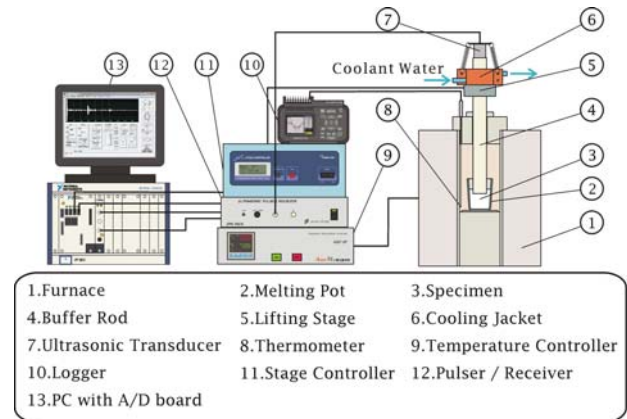


Fig. 1 Experimental apparatus

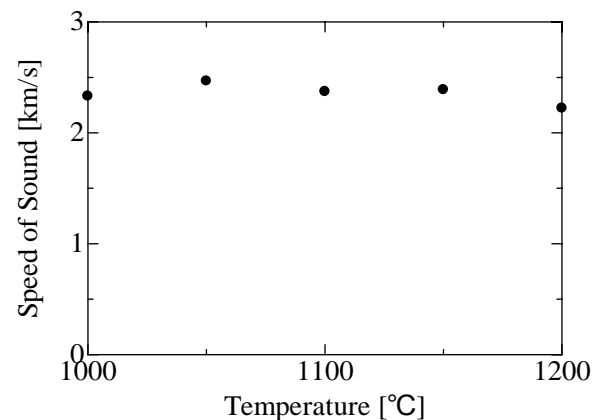


Fig. 2 Temperature dependency of sound velocity

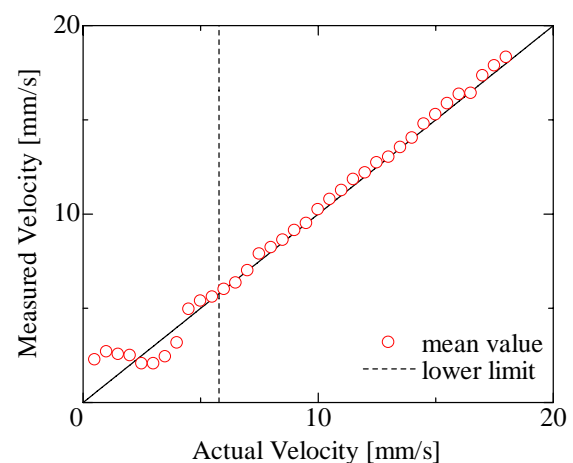


Fig. 3 Accuracy of measured velocity

[2] T. Ihara, H. Kikura, Y. Takeda, E. Ochi and A. Inagaki : Ultrasound Characteristics in High-Temperature Fluid, *The 8th ASME-JSME Thermal Engineering Joint Conference, Hawaii, USA (2011-3)*, CD-ROM Paper No. AJTEC2011-44243.

## A.4 Basic Study of Velocity Profile Measurement by an Air-Coupled Ultrasonic System

Hiroshige KIKURA

Velocity measurements using ultrasonic waves have attracted much attention in the engineering fields. Ultrasonic velocity profile monitor (UVP) especially has been a focus of attention because of its many diagnostic advantages. The major advantage is that UVP can obtain instantaneous velocity distributions on the beam line by measuring Doppler shift frequency of echo signals. Pulse repetition method is the processing of signals in UVP. Furthermore, UVP is easy to apply to existing pipes because UVP performs non-contact measurements. However, UVP is applicable to liquid flow. UVP is difficult to apply to air flow. In order to measure air flow by ultrasonic waves, a new ultrasonic probe for air-coupled ultrasonic measurement is manufactured and a new data processing program has been developed using a graphical-based Integrated Development Environment (IDE). In this study, for the purpose of applying UVP to air flow, air-coupled ultrasonic velocity profile system is built by improving the sensor and signal processing.

This system, shown in Fig.1, consists of a sensor, an external amplifier, a pulser/receiver, a digitizer, and an arithmetic processing unit. The sensor is controlled by the pulser/receiver. The pulser outputs signals and sensor transmits ultrasonic waves. Waves are reflected by tracer particles in air flow. The sensor receives waves and transduces echo signals. Received signals are filtered in the amplifier. The filter is band pass filter (BPF) that passes a certain band, and removing noise from signals. Signals are amplified in the receiver and converted to digital signals in the digitizer. Digital signals are processed in the arithmetic processing unit and the velocity profile of the flow is calculated from these echo signals. Conventional ultrasonic sensors have a problem that ultrasonic waves reflect at the surface of the sensor in the air and ultrasonic transmittance is less than 0.01%. Accordingly, a new air probe is manufactured. The probe has a matching layer between the surface of the probe and the air. Ultrasonic transmittance is improved by this layer.

Figure 2 shows the block diagram of a signal processing software. There are two routines, the routine of recording data and that of calculating velocity. These two routines run in parallel and processing time is shortened. The routine of calculating velocity is provided with two velocity profile methods. Ultrasound Time-Domain Correlation method (UTDC) and pulse repetition method are available as calculation methods of velocity profiles. UVP is difficult to apply UVP to the measurement of air flow. One of the problems is that the speed of sound in air is one fourth of that in water. Pulse repetition needs to transmit and receive ultrasonic pulses repeatedly. Then recording time is four times in air as long as that in water. However, in UTDC, the velocity profile is obtained by two

transmissions of ultrasonic pulses. The measurement time is shortened. Air flow is faster than water flow in general. Tracer particles cross ultrasonic beams in a relatively short time in air, compared with in water. UTDC can obtain the velocity by two echo signals and UTDC is effective for the measurement of air flow.

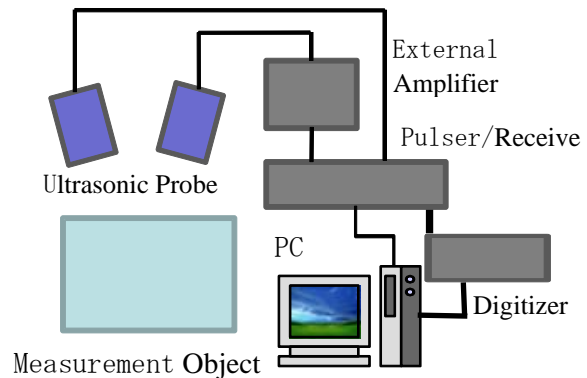


Fig.1 Measurement Hardware

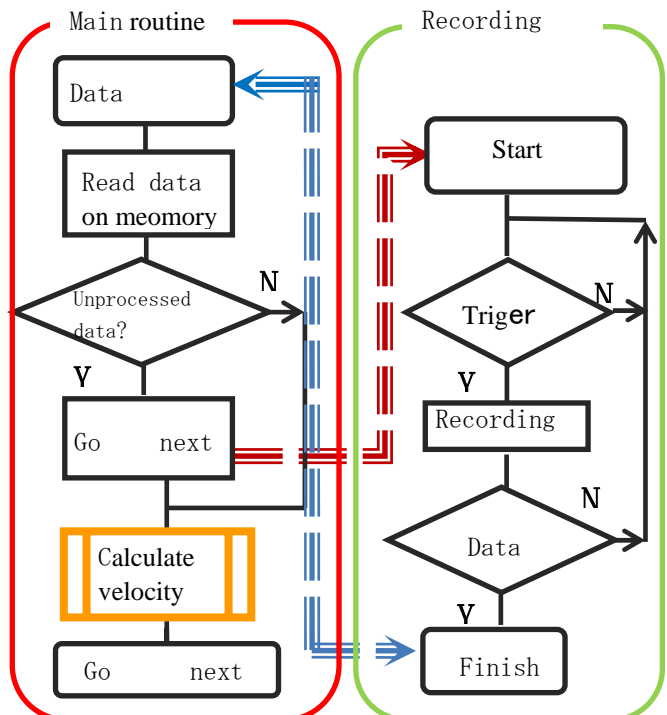


Fig.2 Block diagram of software

### References

- [1] K Tanaka, H Kikura, Basic study of air propagation ultrasonic velocity profile method, *IEICE Technical Report*, **110**, 107-112 (2011).
- [2] H Murakawa, H Kikura, M Aritomi, Trial Measurement on Two-phase Flow using a Multi-wave Ultrasonic Velocity Profile Method : 3rd Report: Measurement of Slug Flow and Visualization using High-speed Camera, *Symposium of PES*, **12**, 109-110, (2007).

## A.5 Proton-Beam-Transport Experiments through a Syringe Needle for the Development of a Cancer Therapy Using Proton-Induced X-rays

Yoshiyuki OGURI and Jun HASEGAWA

### 1. Introduction

Brachytherapy[1] has widely been utilized for many kinds of tumors such as prostate and cervical cancer, and significant therapeutic performances have been reported so far. However, this method poses a potential risk of lost source accidents, since many small radioactive sources (“seeds”) are used. Also, special care must be taken to avoid inadvertent exposure to surgical personnel during the seed implantation.

In order to overcome these problems, an accelerator-based ON/OFF-switchable radiation source illustrated in Fig.1 is applicable. A syringe needle is inserted into a tumor deep inside the patient’s body. A proton beam is transported through the needle to a small heavy-metal target at the end. Characteristic X-rays with energies of  $\approx 20\text{-}30$  keV emitted from the target are used for irradiation of the cancer. Such low-energy monochromatic X-rays are suitable for brachytherapy, because the dose must be precisely delivered to a well-defined small tissue volume. By choosing the target atomic number, we can change the X-ray energy. Moreover, the X-ray dose rate can be optimized by adjusting the incident beam current.

The success of the above method depends strongly on the intensity of the proton beam on the target at the needle end. In this short note, we report preliminary experimental results on the measurement of transport efficiency of a proton beam through a narrow syringe needle.

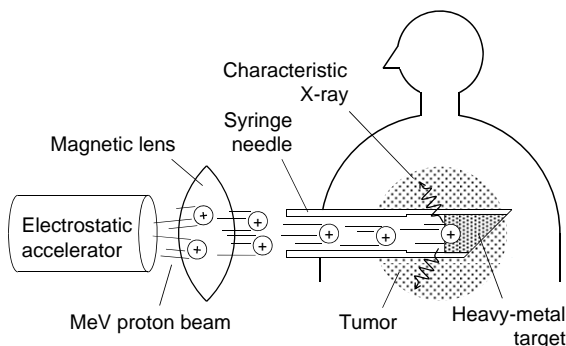


Fig. 1: Cancer treatment by proton-induced X-rays using a syringe needle

### 2. Experimental method

Figure 2 shows the experimental setup at the tandem electrostatic accelerator facility at RLNR, Tokyo Tech. We used a commercially available stainless-steel syringe

needle for research use (Hamilton 91022). The outer diameter, inner diameter, and the length of the needle are 0.7 mm, 0.4 mm, and 50 mm, respectively. The needle was fixed to a movable holder for proton microprobe experiments based on glass capillaries[2]. This holder can also be used as a Faraday cup to estimate the beam current injected into the needle. In front of the holder, a rectangular beam slit ( $2\text{ mm}\times 2\text{ mm}$ ) was placed in order to define the beam size. The alignment of the needle was performed by moving this holder by a pair of remote control actuators. The beam intensity at the exit of the needle was measured by another Faraday cup as a function of the needle tilt angle with respect to the beam axis. 2.5-MeV protons were used as projectiles. The beam was carefully focused and aligned using quadrupole magnets and beam steering magnets. A picture of the setup in a vacuum chamber is shown in Fig. 3.

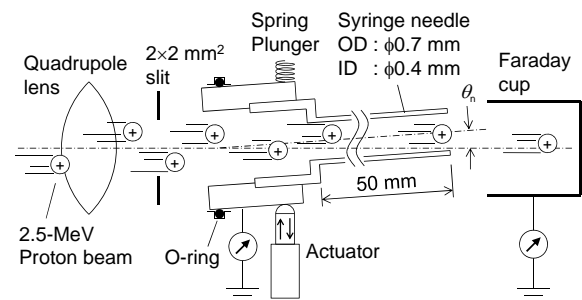


Fig. 2: Schematic of the beam transport experiment

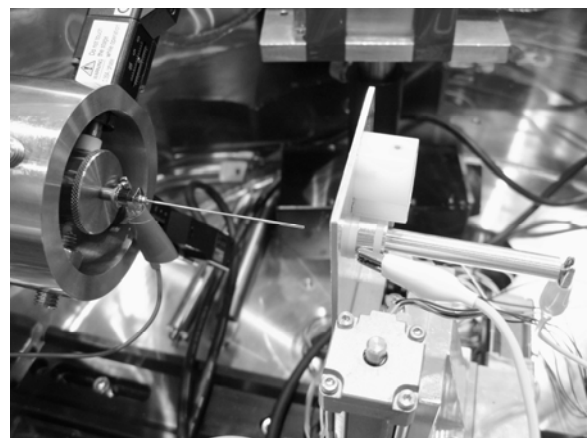


Fig. 3: Setup in the vacuum chamber

### 3. Results and discussion

After optimization of the parameters of the beam-optics devices in front of the syringe needle, the proton beam current behind the  $2 \times 2 \text{ mm}^2$  slit was 30 nA. From this value, if the beam in front of the slit is homogeneous, the intensity of the beam entering the needle can be estimated to be

$$I_{\text{in}} = \left\{ \frac{\pi(0.4/2)^2}{2 \times 2} \right\} \times 30 \text{ nA} = 0.9 \text{ nA}.$$

Figure 4 shows the measured beam current at the exit of the needle as a function of the needle tilt angle. The width of the peak in the figure is  $\approx 10 \text{ mrad}$ , which is roughly equal to the angle defined by the inner diameter and the length of the needle. As in the figure, the peak intensity is 0.7 nA. This result shows that the maximum beam transmission efficiency reached  $\approx 80\%$  of the expected value. The residual beam loss could be explained by the fact that the needle was not perfectly straight, and the trajectories of incident protons were not completely parallel with each other.

In this experiment, we could not see the beam focusing effect which was observed for glass capillary optics[3,4]. This could be due partially to the surface roughness of the inner wall of the syringe needle used in this experiment.

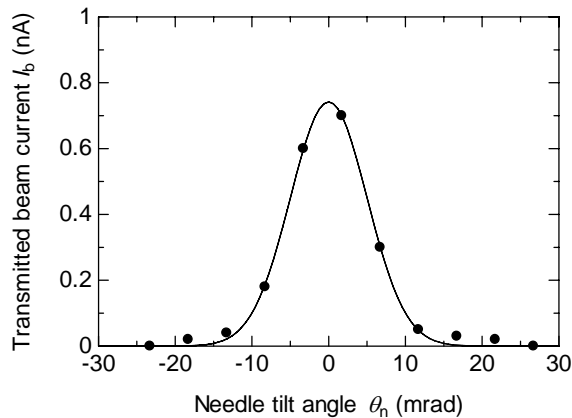


Fig. 4: measured beam current at the exit of the needle as a function of the needle tilt angle.

### 4. Conclusions

By means of the remote control precise alignment technique and careful optimization of the beam optics components, we have succeeded in transporting the 2.5-MeV proton beam through the narrow syringe needle. The beam loss during the transport was only  $\approx 20\%$ .

Nevertheless, further improvement of the beam intensity is needed, if we employ this method for practical cancer treatment as an alternative to the conventional brachytherapy. A preliminary X-ray production test is planned using a syringe needle with a small silver ( $Z = 47$ ,  $E_{K\alpha} = 22.1 \text{ keV}$ ,  $E_{K\beta} = 24.9 \text{ keV}$ ) target at the end.

### Acknowledgement

This work was supported by Grant-in-Aid for Challenging Exploratory Research, No. 21650126, Japan Society for the Promotion of Science (JSPS).

### References

- [1] A. Gerbaulet, R. Pötter, J-J. Mazeron, H. Meertens and E. van Limbergen, "The GEC ESTRO handbook of brachytherapy", Leuven, Belgium, ACCO (2005).
- [2] J. Hasegawa, S. Shiba, H. Fukuda and Y. Oguri, *Nucl. Instrum. Meth. B* **266** (2008) 2125.
- [3] J. Hasegawa, S. Jaiyen, C. Polee, N. Chankow and Y. Oguri, *J. Appl. Phys.* **110** (2011) 044913.
- [4] S. Jaiyen, N. Chankow, J. Hasegawa and Y. Oguri, submitted to *Nucl. Instrum. Meth. B*.

## A.6 Innovative Nuclear Energy System using a Concept of Active Carbon Recycling

Yukitaka KATO

### Introduction

Energy security is critical to the industrial and economic development of a society. Rapid changes and instability in the market prices of primary energy sources will lead to economic confusion in any age. This study discusses the establishment of energy security from the standpoint of carbon recycling. Carbon is the most important energy medium for the manufacturing industry and in the daily life of a human being, making carbon security essential for a sustainable society. In Japan, the supply of fossil fuels depends almost entirely on imports. The enthalpy of imported fossil fuels is 82% ( $18.9 \times 10^{18}$  J) of the total enthalpy of primary fuels used in Japan (Ministry of Economy). 17% of fossil fuels are converted into plastics, while the rest is consumed solely for heat generation. Japan undertook the obligation of adhering to the Kyoto Protocol, which came into effect in 2005, and will therefore need to drastically reduce its carbon dioxide ( $\text{CO}_2$ ) emissions. However, any limits imposed on  $\text{CO}_2$  emissions will directly restrict the use of carbon resources, which will, in turn, severely affect the manufacturing and service industries. The simultaneous establishment of carbon security and lower  $\text{CO}_2$  emissions is thus an important subject for the development of a modern society.

Here, a new energy system in which carbon is reused cyclically is discussed to reduce the emission of carbon dioxide into atmosphere from industrial processes. A carbon recycling system already exists in nature. In this paper, the concept of the Active Carbon Recycling Energy System, ACRES, is discussed. In ACRES,  $\text{CO}_2$  is converted artificially into hydrocarbons by using a primary energy source that has no  $\text{CO}_2$  emissions, allowing the hydrocarbons to be re-used cyclically as energy carrying media. ACRES recycles carbon and transforms energy without  $\text{CO}_2$  emission. Carbon monoxide ( $\text{CO}$ ) was the first candidate of the recycling medium in ACRES. Electrolysis of  $\text{CO}_2$  reduction for  $\text{CO}$  regeneration utilizing power from nuclear reactor was introduced for ACRES process. The feasibility of ACRES under proposed conditions was discussed thermodynamically.

### 2 Structure of ACRES

The structure of ACRES shown in Fig. 1 consists of three elemental processes of carbon material usage,  $\text{CO}_2$  recovery and separation, and carbon material regeneration. In the usage process, carbon materials can be used as both a heat source and a material.  $\text{CO}_2$  generated from carbon material consumption is recovered by physical and chemical sorptions. Recovered  $\text{CO}_2$  in a sorption material

is separated thermally from the sorption material by a heat input. This process produces highly concentrated  $\text{CO}_2$ . Recovered  $\text{CO}_2$  is regenerated into carbon material in the regeneration process. The regeneration process is endothermic and requires an energy input.

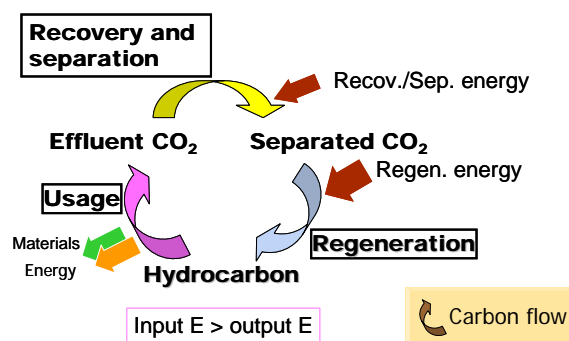


Fig. 1 Structure of the concept of ACRES

If the carbon recycling system can be established thermally and kinetically, it is expected that the system is diffused easily into conventional industries. A natural carbon recycle energy system already exists in the plant kingdom and is an ideal recycling system. However, the potential amount of bio-mass recycled by this system is not sufficient to meet the demands of a modern society. In particular, the domestic bio-mass potential in Japan is less than 10% of the total domestic energy demand (Kameyama and Kato, 2005). The natural recycling system is not sufficient to meet the energy demands in Japan. Therefore, an artificial active recycling system for carbon, viz., ACRES, is proposed in this study.

In ACRES, the total energy input at recovery and separation ( $E_S$ ), and regeneration ( $E_R$ ) should be larger than the energy output of the usage process ( $E_U$ ).

$$E_S + E_R > E_U \quad (1)$$

ACRES is an energy consumption process; hence, a discussion of the energy balance of the system is required for the feasibility evaluation of the system.

### 3 Enthalpy evaluation of ACRES

Practical hydrocarbons are examined those availability in ACRES by an enthalpy balance evaluation.

#### 3.1 Availability of recycling media for ACRES

Selection of recycling carbon material in ACRES is

the first key point. The recycling material is required to have high-quality as energy media and high-affinity with conventional energy consumption process. Exergy of the material is the criteria of energy density. Exergy of material is shown as ratio between Gibb's free energy ( $\Delta G$  [kJ/mol]) and reaction enthalpy ( $\Delta H$  [kJ/mol]). Fig. 2 shows ratios of some carbon materials having high values (High heating Value (HHV) base). Electricity has 100% of the ratio. Values of these carbon materials have higher than one of hydrogen of 82%. Carbon monoxide and carbon have similar values with electricity. These materials have higher values than hydrogen. When flow type reactor is better for an ACRES process, gas medium is suitable in the process. It was concluded that CO was the best gas material as the recycling carbon material, because CO has higher energy quality and density than hydrogen, and high-affinity to conventional energy consumption system such as iron-making and chemical processes.

On the other hand, carbon, C, is also good material for ACRES, because, C had higher energy quality and density in comparison with other carbon materials and is easily stored and transferred in solid phase, and crucial fuel for a blast furnace in conventional iron-making process. However, CO was discussed mainly in this study because of relatively ease to be produced by reduction of  $\text{CO}_2$ .

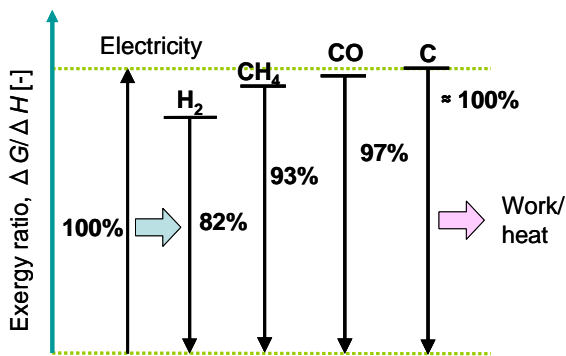
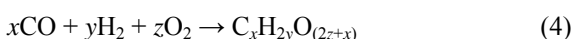
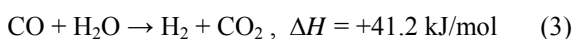
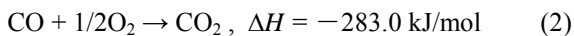


Fig. 2 Exergy ratios for recycling energy media candidate

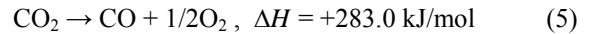
### 3.2 ACRES based on CO

#### (1) Enthalpy analysis of ACRES based on CO

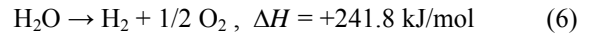
CO has a higher energy density than  $\text{H}_2$ . CO is a popular energy material in conventional chemical, steel, and other manufacturing industries. Therefore, ACRES for CO is evaluated. In the usage process of CO, the oxidation of CO (Eq. (2)) for the heat output and the shift reaction of CO for  $\text{H}_2$  production (Eq. (3)) is available. CO can be also converted into polymeric materials by polymerization (Eq. (4)).



CO is regenerative from  $\text{CO}_2$  by electrolysis (Eq. (5)).



A two-step reaction of hydrogen production by water electrolysis and reduction of  $\text{CO}_2$  with the hydrogen (Eqs. (6) and (7)) is a practical process for CO regeneration.



Required enthalpies per one molecule of methane for the processes of usage and regeneration are depicted by the lower-heating value (LHV) as following. Thermodynamic property values of reactions in the following were calculated on the basis of LHV because these reactions generally proceed at a sufficiently high temperature of more than  $100^\circ\text{C}$ . The enthalpy balance of ACRES for CO in LHV is shown in Fig. 3.

The regeneration process is assumed to use hydrogen for CO regeneration by the two-step reaction given in Eqs. (6) and (7).

Production of  $\text{H}_2$  (1 mol) requires an enthalpy of 242 kJ/mol-CO. Reduction of  $\text{CO}_2$  into CO with  $\text{H}_2$  is an endothermic reaction and requires a heat input of 41 kJ/mol-CO. Because CO has a higher energy density than  $\text{H}_2$ , CO is one of the most popular media in chemical processes.

CO is a considerably acceptable medium for conventional chemical and manufacturing industries. Hence, it is expected that CO is the most appropriate candidate for a regenerative medium in ACRES.

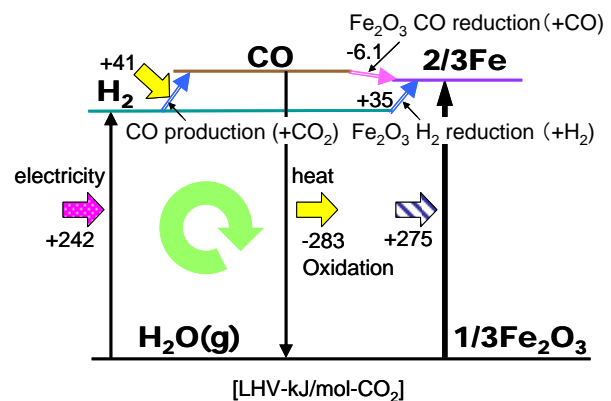


Fig. 3 Enthalpy balance of CO recycling system

#### 3.3 $\text{CO}_2$ electrolysis for CO regeneration in ACRES

Efficient regeneration of CO is a key technology for ACRES based on CO. The feasibility of the regeneration methods of CO is evaluated.  $\text{CO}_2$  electrolysis is one method of CO regeneration. Solid-oxide electrolysis cell (SOEC) in which a reverse operation of a solid-oxide fuel cell (SOFC) proceeds has a possibility for the electrolysis (Jensen, 2007). SOEC has been discussed for the

production of a syngas, which is a mixture of H<sub>2</sub> and CO generated from H<sub>2</sub>O and CO<sub>2</sub>. Temperature dependencies of enthalpy and Gibb's free energy changes, Δ*H<sub>i</sub>* [kJ/mol] and Δ*G<sub>i</sub>* [kJ/mol], of Eq. (5) for the electrolysis of CO<sub>2</sub> and Eq. (6) for H<sub>2</sub>O were calculated by a reaction equations module of HSC Chemistry (Ver. 6.12), Outotec. Electromotive forces, *V<sub>i</sub>* [V], for Eqs. (5) and (6) were derived from Eq. (14).

$$V_i = \frac{-\Delta G_i}{n_i F}, F = 9.65 \times 10^4 \text{ C/mol} \quad (8)$$

*n<sub>i</sub>* is the mole number of migrated electrons in a reaction. Δ*G<sub>i</sub>* corresponds to the electrical energy for electrolysis. Electricity consumption ratio for electrolysis, η<sub>el-*i*</sub>, is defined as follows:

$$\eta_{el-i} = \Delta G_i / \Delta H_i \quad (9)$$

Both *V<sub>i</sub>* and η<sub>el-*i*</sub> of Eqs. (5) and (6) are shown in Fig. 4. At higher temperatures, η<sub>el-CO</sub> and η<sub>el-H<sub>2</sub></sub> decreases. This implies that electrical energy consumption of CO<sub>2</sub> electrolysis becomes lower at a higher temperature like H<sub>2</sub>O. *V<sub>CO</sub>* becomes smaller than *V<sub>H<sub>2</sub></sub>* at a temperature higher than 820°C. This implies that higher-temperature CO<sub>2</sub> electrolysis has a smaller demand for electrolysis than the H<sub>2</sub>O electrolysis.

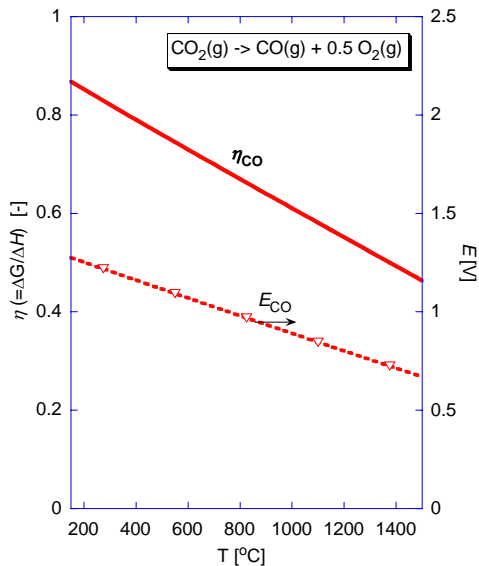


Fig. 4 Temperature dependency on enthalpy ratio for CO<sub>2</sub> electrolysis into CO

**Conclusions**

For an establishment of a practical ACRES, appropriate selections of a recycling hydrocarbon medium and a primary energy source for the system drive were important. CO was the most suitable as the recycle medium in ACRES because CO had a higher energy density and affinity than H<sub>2</sub> to

chemical processes in conventional manufacturing industries. HTGR was a candidate of a primary energy source of ACRES. CO<sub>2</sub> electrolysis at a high temperature had a higher efficiency than low temperature electrolysis. ACRES with CO driven by the heat output from HTGR was the most applicable combination. ACRES was expected to be a candidate of energy systems for the establishment of carbon supply security in a modern society.

**References**

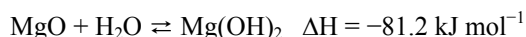
Ministry of Economy: Energy balance of Japan in 2004, *The White Paper for Energy in 2006 FY*, METI, Tokyo, Japan (2006).  
 H. Kameyama and Y. Kato ed., *HONEBUTO Energy Road Map (Honebuto no Energy Road Map)*, Kagaku-Kogyo-Sha, Tokyo, Japan (2005).  
 S. H. Jensen, P. H. Larsen, M. Mogensen: *Int. J. Hydrogen Energy*, **32** (2007) 3253.

## A.7 NIR Study on Hydration Reaction of Magnesium Oxide for Chemical Heat Storage

Junichi RYU and Yukitaka KATO

### Introduction

The heat storage technologies of waste heat from industrial processes and co-generation systems will contribute to “Energy Saving”. Especially, chemical heat storage technology is very interesting in view of their heat storage capacity. In recent years, the technologies of chemical heat pump and chemical heat storage are widely studied for the reduction of energy consumption and CO<sub>2</sub> emission. Chemical heat pump system with the reaction between magnesium oxide (MgO) and water vapor has been reported by our group. [1]



In this system, thermal energy above 350°C is required for practical heat storage operation. Recently, chemically modified magnesium hydroxide – metal salt added magnesium hydroxide, and magnesium containing mixed hydroxide – were proposed as new type material for chemical heat storage by our group. These materials can store thermal energy around 280 °C. [2,3] The heat storage density of these materials are higher than authentic magnesium hydroxide under 280°C of heat storage condition. However, reaction mechanism of these materials is not clear. Understanding of reaction mechanism is important task to develop a new material. In this work, hydration mechanism of LiCl added MgO as heat output operation was studied by NIR (near infrared) spectroscopy. [4]

### Experimental

LiCl added MgO was observed by calcination of LiCl added Mg(OH)<sub>2</sub> at 400°C under Ar flow. The reaction gas mixture of H<sub>2</sub>O and Ar was supplied into the quartz reactor for 80 min at 110°C for *in situ* measurement of the NIR spectra.

### Results

The changes in NIR absorption spectra for the hydration process of 6.8wt% LiCl/Mg(OH)<sub>2</sub> are shown in Figure 1. The Mg(OH)<sub>2</sub> peak and shoulder peak assigned to H<sub>2</sub>O were observed after 40 min of hydration. It is very difficult to distinguish these peaks (first overtone of Mg(OH)<sub>2</sub> and combination of H<sub>2</sub>O) because these peaks are too close each other. Therefore, this spectrum should be analysed by deconvoluting it into some components. The deconvoluted spectrum of 6.8wt% LiCl/MgO taken 40min after the beginning of the hydration operation is shown in Figure 2. The spectrum was deconvoluted into four components: 1) the Mg(OH)<sub>2</sub> first overtone, 2) isolated adsorbed water, 3) water cluster, and 4) crystallization water in LiCl, respectively.

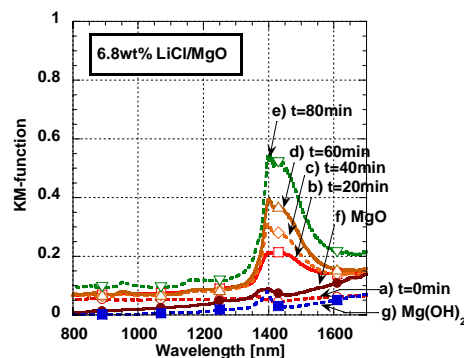


Figure 1 NIR spectra of 6.8wt% LiCl/MgO with hydration operation at 110 °C.

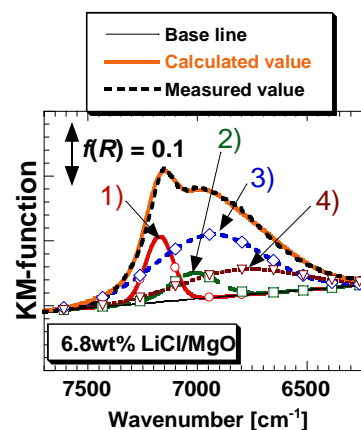


Figure 2 Deconvoluted NIR spectrum of 6.8wt% LiCl/MgO 40 min after hydration.

To understand the reaction mechanism of gas/solid reaction such as MgO and H<sub>2</sub>O, NIR measurement is useful analytical method.

### References

1. Y. Kato et al., *Appl. Therm. Eng.*, **16**, 852 (1996).
2. J. Ryu et al., *J. Chem. Eng. Jpn.*, **40**, 1281 (2007).
3. J. Ryu et al., *Chem. Lett.*, **37**, 1140 (2008).
4. H. Ishitobi et al., *Appl. Therm. Eng.*, in press.

## A.8 Development of Electron Cyclotron Emission Imaging System on LHD

Shunji TSUJI-IIO

A combined system of Microwave Imaging Reflectometry (MIR) and the Electron Cyclotron Emission Imaging (ECEI) has been developed for Large Helical Device (LHD) at NIFS. Microwave imaging diagnostics has potential to observe fluctuations of electron density and electron temperature profiles in magnetically confined high temperature plasmas. When the plasma density and temperature are sufficiently high, the electron cyclotron emission (ECE) is approximated to be black body radiation in magnetically confined plasmas. The electron temperature profile can be determined by measuring the intensity of each frequency of ECE, since the ECE frequency corresponds to the radial position. By using a 1-D receiving antenna array, 2-D ECE profiles (radial and poloidal directions) can be obtained. The electron temperature is considered to be equal on the same magnetic flux surface so that ECE imaging (ECEI) can be one of the most powerful diagnostics to investigate MHD instabilities.

The developed ECEI system is equipped with the same imaging optics of MIR. Consequently this system enable us to observe both density and temperature fluctuations simultaneously. Our MIR/ECEI system consists of the following three devices; 1) imaging optics, 2) horn-antenna mixer array (HMA), 3) multi-frequency detector. The optical system has three optics, illumination optics for MIR, focusing optics and local oscillator (LO) optics.

Figure 1 shows a block diagram of the ECEI detection system. The ECE signals from plasma are focused on a HMA with focusing optics. In HMA, each antenna element receives both ECE signals and LO signal, and mixer unit generates IF signals. The frequency spectrum of IF signal is detected with a multi-frequency detector. The central frequencies are set from 2 GHz to 9 GHz with 1-GHz steps. The designed bandwidth of each channel is 500 MHz. Figure 2 shows the observation area of this system in the case of  $B_{ax} = 2.1$  T,  $R_{ax} = 3.6$  m magnetic configuration. Sight lines are determined by the optic system while the radial channels are determined by the ECE frequency corresponding to the magnetic field strength.

An example of ECEI signals is shown in Fig. 3. Fig. 3(a) indicates two ECE signals observed by different antenna channels at the same frequency. Fig. 3(b) shows ECE spectrum of the “pol\_2ch, 104 GHz” signal. During 7.2 s to 7.7 s, fluctuations around 2 kHz were observed.

For the next experimental campaign, we plan to change the observation frequency range. Currently, it is between 97 GHz to 104 GHz. However, this frequency range does not match with normal LHD experimental conditions. The observation range of a new system will be set at frequencies of 68 – 75 GHz. This range overlaps conventional ECE diagnostics installed on LHD.

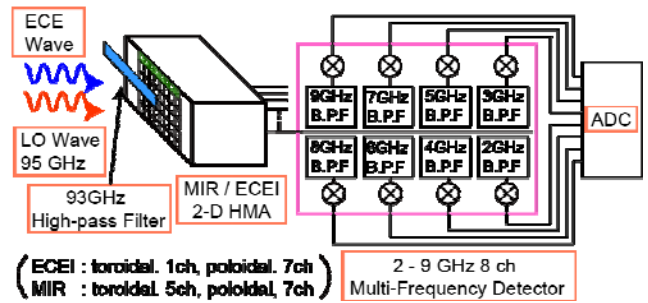


Fig. 1 ECEI detection system. ECE signals are down-converted into 2 - 9 GHz IF signals by LO wave and each HMA element. Multi-frequency detector measures spectrum of IF signals.

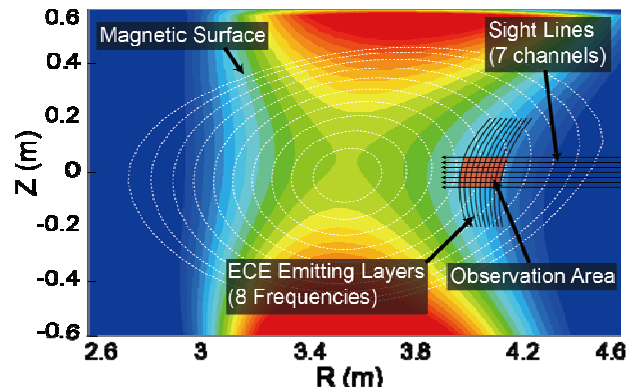


Fig. 2 Observation area of ECE imaging. Color indicates the magnetic field strength of  $B_{ax} = 2.1$  T,  $R_{ax} = 3.6$  m experiment. The observation area is determined by sight lines of antenna elements and magnetic field.

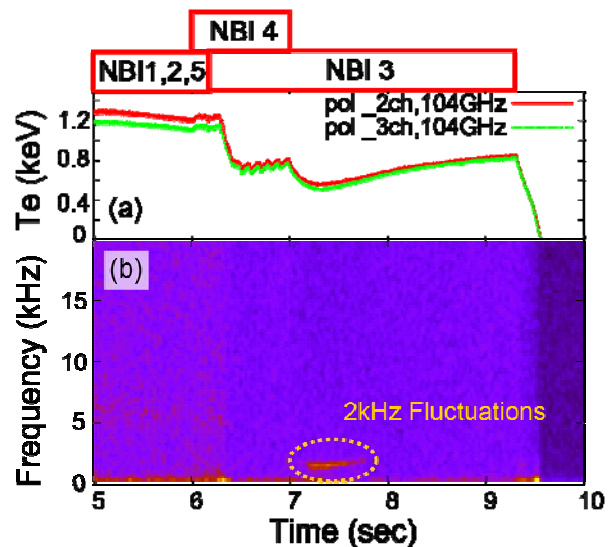


Fig. 3 An example of ECE waveforms and FFT analysis. (a) Waveforms at the same frequency and from poloidally different antenna channels. (b) Spectrum time evolution of pol\_2ch at 104GHz.

## A.9 Development of Fiber-Optic Diagnostic on Vacuum Vessel Current of QUEST

Shunji TSUJI-IIO

We are developing a polarimeter for the measurements of the toroidal currents on the vacuum vessel of QUEST at Kyushu University. We will wind a poloidal loop of an optical fiber around the vacuum vessel as shown in Fig. 1 and measure the toroidal current in the same way as an optical current transformer. The loop must go through the torus center since there is no room between the center stack (CS) coil and the vacuum vessel so that the vacuum-vessel current must be evaluated under significant background signals up to 1.73 MA-turns by the CS-coil current. The Ampere-turns of the CS-coil current will be separately measured with a coil of optical fiber wound at the coil feeder and it will be numerically subtracted from the total Ampere-turns measured with the loop. In order to measure the vacuum current in accuracy of less than 1 kA, the required measurement accuracy is not less than three digits.

The Verdet constant of a flint glass fiber is about six times that of a silica glass fiber and the photo elastic constant of the former is much smaller than that of the latter, which enables us to wind the optical fiber with smaller bending radii. We tested a single-mode flint glass fiber for 1550 nm with a SLD (super-luminescent diode) of wavelength 1545 nm as light source. We adopted the dual photo elastic modulator (HINS Instruments, Inc., PEM-90 I/FS50 and II/FS42) polarimetry. The modulator axes of the two modulators are at 45 degrees with the polarizer passing axis at 22.5 degrees with each modulator. The second harmonic amplitudes of the photodiode output are measured with two lock-in amplifiers. An example result of bench testing of current measurements of a solenoid is shown in Fig. 2. The standard deviation of the measured polarization angle was confirmed to be well below a required accuracy of the Faraday rotation angle measurement of 0.37 degrees.

The QUEST tokamak is normally operated with bake-out temperature of the vacuum vessel at about 100°C. We measured the temperature distribution along the planned route of the loop with thermocouples and found that the integrity of the optical fiber is preserved since the highest temperature does not exceed 50°C. The temperature dependence of the Verdet constant of the flint glass fiber, however, is slightly stronger than that of silica fibers. Figure 3 shows a preliminary evaluation result of the Verdet constant by varying the room temperature. The weak dependence may become a problem to assure the applicability of Ampere's theorem to measure the current. The averaged value agrees with the catalog value when the dependence of inversely proportional to the square of the wavelength is taken into account.

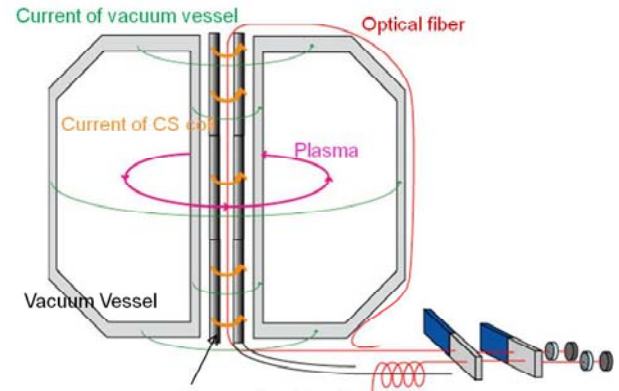


Fig. 1 Schematic illustration of the optical fiber poloidally wound around the vacuum vessel of QUEST. A coil of optical fiber is used to numerically cancel the Ampere-turns of the CS-coil current. Two plates at the bottom right indicate PEMs.

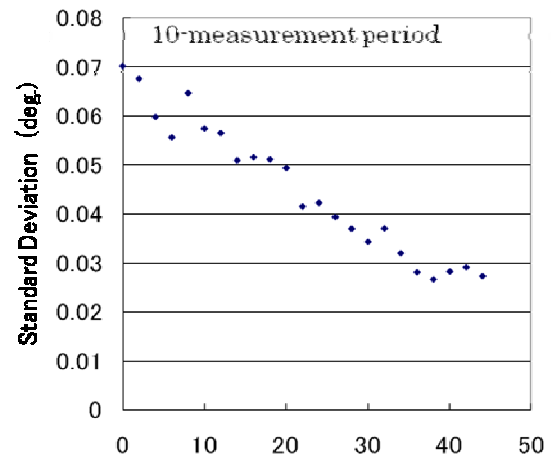


Fig. 2 Polarization angle dependence of the measurement errors with the dual PEM polarimeter.

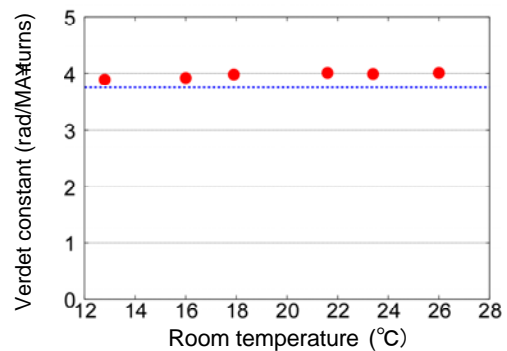


Fig. 3 The Verdet constant of the single-mode flint glass fiber evaluated as a function of the room temperature. The horizontal line indicates the catalog value at 1550 nm.

## A.10 Stress Distribution in Helical Coils with Geodesic Windings based on Virial Theorem

Hiroaki TSUTSUI, Sunji TSUJI-IIO, Ryuichi SHIMADA

### 1 Introduction

A force-balanced coil (FBC) is a multi-pole helical hybrid coil combining toroidal field (TF) coils and a solenoid helically wound on a torus. The combination reduces the net electromagnetic force in the direction of major radius by canceling the centering force due to the TF coil current and the hoop force due to the solenoid current. The FBC concept was extended using the virial theorem which shows that strength of magnetic field is restricted by working stress in the coils and their supporting structure. High-field coils should accordingly have same averaged principal stresses in all directions which is named the virial-limit condition. Recently, we made a model FBC which were neither impregnated with epoxy resin nor reinforced with stainless steel wires. Using acoustic emission measurements, we found that the wires vibrated in response to electromagnetic force changes. Since FBC winding is modulated to reduce the tilting force, the winding is slightly similar to but different from the shortest geodesic trajectory and has no tensile load. In order to reduce the vibration, the geodesic winding is expected to be effective. In this work, we analyze the effect of the winding modulations including the geodesic modulation for the stress distribution of helical windings.

### 2 Toroidally modulated helical coil

#### 2.1 Modulated winding

When a helical coil is modulated in such a way that a magnetic surface coincides with the coil surface, the overturning force generated by electromagnetic forces can be reduced. This magnetic configuration was developed from an axisymmetric surface current model. Poloidal magnetic flux  $\Psi$  at  $\mathbf{x} = (r, z)$  is given by

$$\Psi(\mathbf{x}) = \oint G(\mathbf{x}, \mathbf{x}') j_\phi(\mathbf{x}') ds', \quad (1)$$

where the contour integral is done on the current surface, and  $j_\phi$  is toroidal surface current density, and  $G$  is the Green function expressed by using complete elliptic integral of first kind  $K(k)$  and complete elliptic integral of second kind  $E(k)$  as follows,

$$G(\mathbf{x}, \mathbf{x}') = 2 \frac{\mu_0 \sqrt{rr'}}{k} \left( \frac{1-k^2}{2} K(k) - E(k) \right), \quad (2)$$

$$k \equiv \sqrt{\frac{4rr'}{(r+r')^2 + (z+z')^2}}. \quad (3)$$

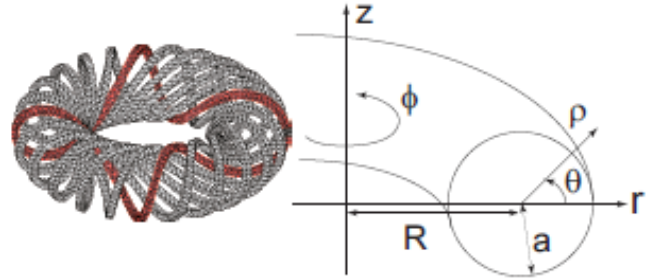


Figure 1: Illustrations of a coil configuration and coordinate systems of cylindrical coordinate  $(r, z, \phi)$  and semi-toroidal coordinate  $(\rho, \phi, \theta)$ , in which  $R$  and  $a$  are major and minor radii of the coil, respectively.

On a magnetic surface, poloidal magnetic flux  $\Psi$  is constant:

$$\Psi(\mathbf{x}) = \Psi_0 = \text{const.} \quad (4)$$

The magnetic surface expressed by (4), in general, intersects the coil surface as shown in Fig. 2(a). The configuration that a magnetic surface coincides with the coil surface can be achieved by distributed toroidal current density  $j_\phi$  as shown in Fig. 2(b). The toroidal surface current density  $j_\phi$  is

$$j_\phi = \frac{I_\phi}{2\pi a} g(\theta), \quad (5)$$

where  $g(\theta)$  is a periodic function satisfying (4) while the poloidal surface current density  $j_\theta$  is

$$j_\theta = \frac{I_\theta}{2\pi r}, \quad (6)$$

where  $r$  is

$$r = R + a \cos \theta, \quad (7)$$

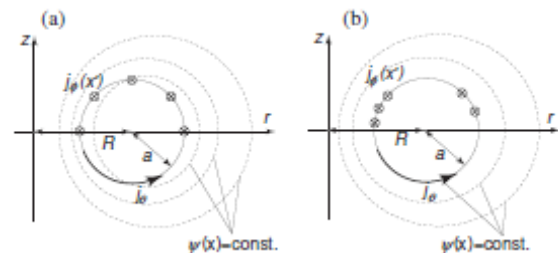


Figure 2: Illustrations of coil current distribution depicted by solid line and magnetic surfaces indicated by dotted lines under the condition that magnetic surfaces intersect coil surface (a), and a magnetic surface coincides with the coil surface (b).

as shown in Fig.1. The current path on the torus is determined by current density components,  $j_\phi$  and  $j_\theta$  as shown by

$$\frac{d\phi}{d\theta} = \frac{aj_\phi}{rj_\theta} = \frac{1}{N}g(\theta), \quad (8)$$

Where

$$N = \frac{I_\theta}{I_\phi}, \quad (9)$$

is the ratio of toroidal current  $I_\theta$  and poloidal current  $I_\phi$ , and called the pitch number of a helical coil. Note that the modulation is determined only by toroidal current distribution, and independent of poloidal current density as shown in (5) and (8).

In general, coils of this modulated winding cannot be under tension because it is not a geodesic. It is, hence, difficult that the coil trajectory with this winding is fixed on a toroidal winding frame.

## 2.2 Geodesic winding

The geodesic on a toroidal surface with a major radius  $R$  and a minor radius  $a$  is determined by a variation problem of

$$\delta S = 0, \quad (10)$$

$$S \equiv \oint ds, \quad (11)$$

$$ds^2 = a^2 d\theta^2 + r^2 d\phi^2, \quad (12)$$

where  $s$  is a length of a coil orbit. When we define the Lagrangian  $L$ ,

$$L(\phi, \frac{d\phi}{d\theta}) \equiv \sqrt{a^2 + r^2 \left(\frac{d\phi}{d\theta}\right)^2}, \quad (13)$$

$$S = \oint L d\theta, \quad (14)$$

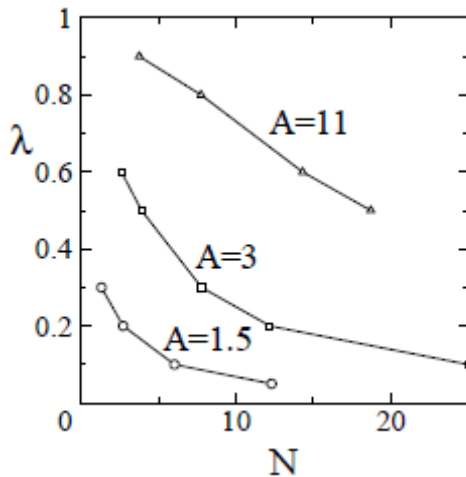


Figure 3: Relations of a non-dimensional integration constant  $\lambda$  and the pitch number  $N$  for aspect ratios  $A = 1.5, 3, 11$ .

the Euler-Lagrange equation is

$$\frac{d}{d\theta} \frac{\partial L}{\partial \dot{\phi}} = \frac{d}{d\theta} \left( \frac{r^2 \frac{d\phi}{d\theta}}{\sqrt{a^2 + r^2 \left(\frac{d\phi}{d\theta}\right)^2}} \right) = 0, \quad (15)$$

where  $\dot{\phi} \equiv \frac{d\phi}{d\theta}$ . The solution of (15) is

$$\frac{d\phi}{d\theta} = \frac{a}{r} \frac{1}{\sqrt{\frac{r^2}{R^2 \lambda^2} - 1}}. \quad (16)$$

Here  $\lambda$  is a non-dimensional integration constant related with the pitch number  $N$ , and has a range of

$$0 < \lambda < 1 - \frac{1}{A}, \quad (17)$$

where  $A = R/a$  is the aspect ratio of the torus. The pitch number  $N$  is obtained from (16) as follows:

$$\frac{1}{N} = \oint \frac{d\phi}{d\theta} d\theta = \oint \frac{a}{r} \frac{d\theta}{\sqrt{\frac{r^2}{R^2 \lambda^2} - 1}}, \quad (18)$$

as shown in Fig.3. Note that the geodesic winding (16) is related with both toroidal and poloidal current distributions, while the modulated winding (8) is determined only by a toroidal current distribution  $j_\phi \propto g(\theta)$ .

Since the solution (16) shows that the geodesic winding has a nearly horizontal direction around the inner region ( $\theta \sim \pi$ ) of the torus, the coil with a tension has a possibility of a detached orbit. In order to investigate the possibility, we obtain the curvature  $\kappa$  as follows:

$$\kappa = \left| \frac{d\mathbf{t}}{ds} \right| = \left| \frac{a - r \left(\frac{d\phi}{d\theta}\right)^2}{a^2 + r^2 \left(\frac{d\phi}{d\theta}\right)^2} \right|, \quad (19)$$

where  $\mathbf{t}$  is a tangential unit vector of the coil orbit. Using the curvature, the detached condition is represented by the condition whether the equation of  $\kappa = 0$  has a solution or not. Thus the detached condition is

$$\frac{d\phi}{d\theta} > \sqrt{\frac{a}{r}} \Big|_{\theta=\pi} = \frac{1}{\sqrt{A-1}}. \quad (20)$$

In the geodesic winding (16), therefore, the detached condition is represented by

$$\left(1 - \frac{1}{A}\right)^{\frac{3}{2}} < \lambda < 1 - \frac{1}{A}. \quad (21)$$

As is shown in Fig. 4, the virial-limit condition with  $A > 2.5$  satisfies the attached condition, in which the coil can be wound under the tension.

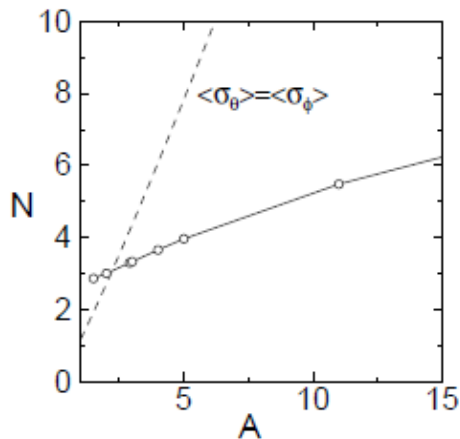


Figure 4: A solid line is the lower limits of the coil pitch number  $N$  in the attached condition against the aspect ratio  $A = R/a$ . A dashed line shows the virial limit condition.

### 3 Comparison of windings

As was mentioned above, the conventional modulated winding and the geodesic winding are quite different mathematically. In order to show their differences, their orbits are computed and depicted in Fig.5. The red lines are trajectories of the modulated winding, while the blue ones are those of the geodesic winding. Although their orbit representations (8), (16) are quite different, they are nearly overlapped. This shows that our modulated winding is practically geodesic.

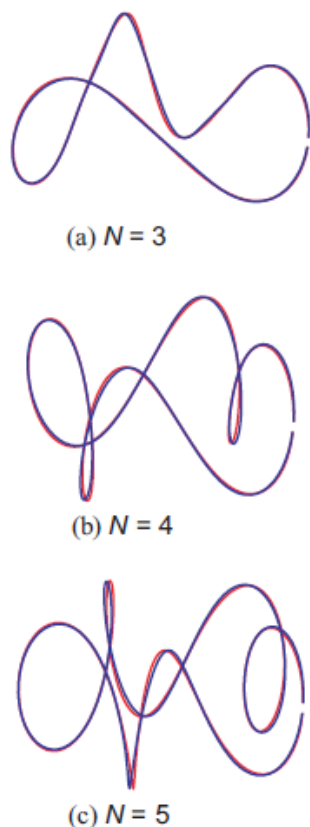


Figure 5: A comparison of trajectories of modulated (red line) and geodesic (blue line) windings for  $N = 3, 4, 5$  and  $A = 2.9$ .

### 4 Conclusion

We compared the conventional modulated helical winding, in which the coil surface coincides with the magnetic surface, with the geodesic winding, in which the coil is manufactured with a tension. At first, the analytic representation of the geodesic on a torus was obtained. The geodesic winding is related with both poloidal and toroidal current distribution, while the conventional modulated winding is related to toroidal current distribution only. Although two modulations are substantially different to each other, the trajectories base on these modulations are numerically overlapped, and our conventional modulated winding is practically geodesic.

Although the modulated winding without tension is unstable to the displacement on the torus, the geodesic winding, which numerically agrees with the modulated winding, under the tension is expected to be mechanically stable and easy to be manufactured.

## A.11 Cold Arc-Jet Plasma Flowing along Weak Mirror or Cusp Magnetic Field

Hiroshi AKATSUKA, Atsushi NEZU and Haruaki MATSUURA

Plasmas are frequently applied to modern industrial technology, and some of their applications accompany external magnetic field, such as thrusters for astronautic applications or thermonuclear fusion reactors for future energy sources. It should be also added that the fundamental physics in space or interplanetary region requires the knowledge of interactions between plasmas and magnetic field. From these points of view, a large number of studies have been reported relevant to the effect of non-uniform magnetic field on the plasma parameters. To understand fundamentals of these phenomena, we are studying characteristics of arc-plasmas flowing along various configurations of magnetic field [1 – 3].

In this study, we applied a rarefied gas wind tunnel as a plasma expansion chamber with its steady-state pumping rate 16,000 l/sec. Experimental set-up consists of an arc-plasma generator, six hollow electromagnets to generate stationary magnetic field, 3-dimensional traversing mechanism that can be manipulated from the atmospheric pressure side, and vacuum system to pump out the wind tunnel. We adopted 4-tip Mach probe to understand the flowing velocity of the plasma jet as well as its flowing direction. One of the tips is also applied as a Langmuir probe to understand the space potential, electron temperature and density. Further account of the experimental setup is described elsewhere [1 – 3].

In the present experimental study, we examined the effects of mirror and cusp magnetic fields on helium arc-jet flow. First, concerning the mirror magnetic field, the vector diagram of the ion flow and the magnetic field is shown in Fig. 1. It is found that in the upstream region, the ion flows to more outer side than the direction of the magnetic field, whereas the direction of ion flow gradually comes close to that of the magnetic field as the plasma moved to the downstream direction. This behavior can be attributed to the difference in the Hall parameters of electrons and ions. That is, the ion hall-parameter  $h_i = 7.1 \times 10^{-2}$ , while the electron hall-parameter  $h_e = 5.2 \times 10^2$  at the position  $(r, z) = (60, 60)$  [mm]. We found that  $h_e = 10^4 h_i$  throughout the present mirror field experiments. This indicates that the electrons are fully magnetized, while the ions are not magnetized. This means that the electrons flow almost along the magnetic field, while the ions obey the electric field that is determined by the electrons flow. Therefore, some kind of flowing-lag must be constructed in the flow-pattern, which is obviously observed in Fig. 1. In the meanwhile, Fig. 2 shows the equipotential contour of the plasma flowing along the mirror magnetic field. We found that the high-potential region exists at the region of  $r = 10 - 30$  mm and  $z = 30 - 60$  mm, which corresponds to the position where ions don't flow along the magnetic field. It

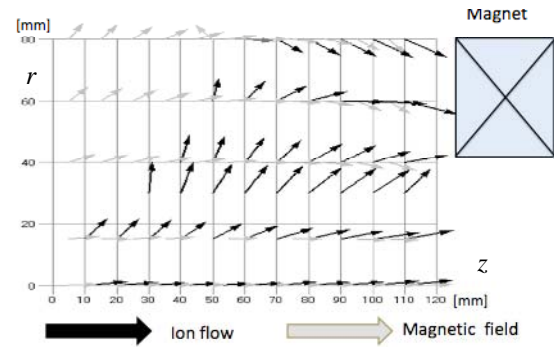


Fig. 1. The vector diagrams of the direction of ion flow and that of the magnetic lines of force for the mirror magnetic field.

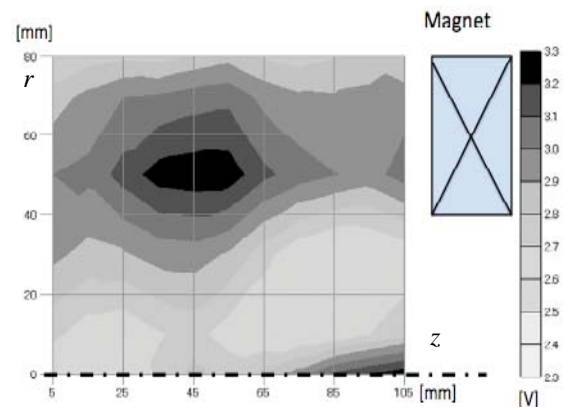


Fig. 2. The equipotential contour of the plasma space potential in the mirror magnetic field.

is considered that the difference in the flowing direction of electron and ions makes the high-potential region in the foregoing domain. Unfortunately, the ion velocity in the mirror field is subsonic in the entire measurement region.

Second, concerning the experiments of the cusp magnetic field, vector diagram of the ion flow and the magnetic field is shown in Fig. 3. We found supersonic ion-flow at  $z = 20 - 30$  [mm], whose maximum Mach number is 1.5. We also visually found a spherical dark region at around  $z = 30$  mm, which is considered to be a shock wave region. This suggestion is also supported by the vector diagram of ion velocity, Fig. 3, which also includes that of magnetic field. The plasma flow becomes subsonic at this area. We confirmed a sudden decrease in the electron temperature and density, which will be discussed later.

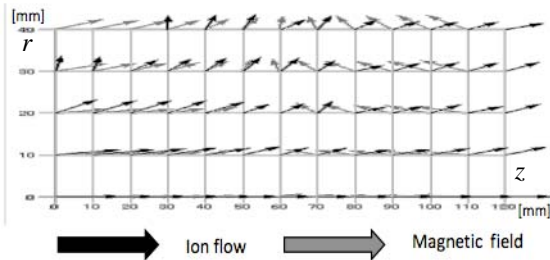


Fig. 3. The vector diagrams of the direction of ion flow and that of the magnetic lines of force for the cusp magnetic field.

Figure 3 indicates that the direction of the ion flow agrees with that of the magnetic field at  $z = 0 - 60$  [mm] and  $r \leq 10$  [mm]. We also understand that ions tend to flow toward outer region at  $r \geq 20$  [mm], which is also due to the difference in the behavior of magnetized electrons and not-magnetized ions. Figure 4 shows the equipotential contour for the plasmas flowing the cusp magnetic field, where the separatrix is situated at  $z = 60$  [mm]. It is found that the space potential rises at near-axis region of the separatrix. Electrons are fully magnetized in the upstream region  $z \leq 30$  mm, and consequently, they tend to flow outward on the separatrix plane. On the other hand, ions flow rather straight due to their inertia even near the separatrix. This causes the increase in the space potential near the separatrix. After crossing the separatrix, the space potential drastically decreases as much as 1 V. On the separatrix, of course, the electrons become unmagnetized locally, and after that, they again become magnetized. The electrons tend to gather onto the axis at  $z \geq 80$  [mm], and consequently, it is considered that the space potential again drops.

Figure 5 and 6 show the contours of density and temperature of the arc-jet under cusp magnetic field, respectively. On the axis, we find a large density drop at  $z = 30$  [mm], which is considered to be due to some kind of shock phenomenon. It is also found that the plasma basically flows along the magnetic field. Meanwhile, we found temperature increase at  $z = 40 - 60$  [mm] on the axis, which is also considered to be attributed to a shock phenomenon, and an energy conversion from the kinetic energy to thermal energy [4].

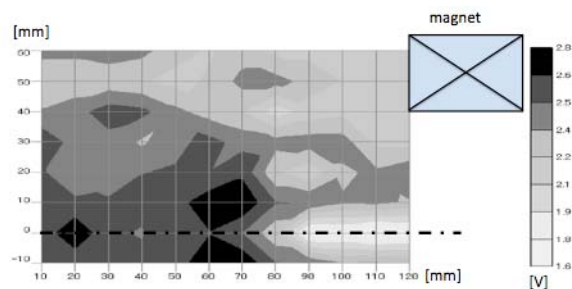


Fig. 4. The equipotential contour of the plasma space potential in the mirror magnetic field.

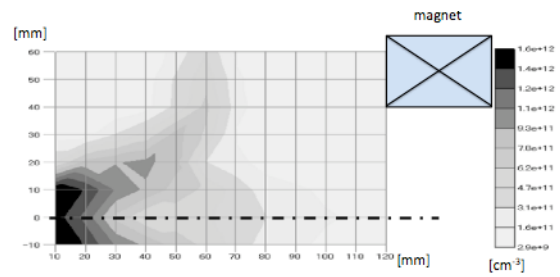


Fig. 5. The contour drawing of the plasma density in the cusp magnetic field.

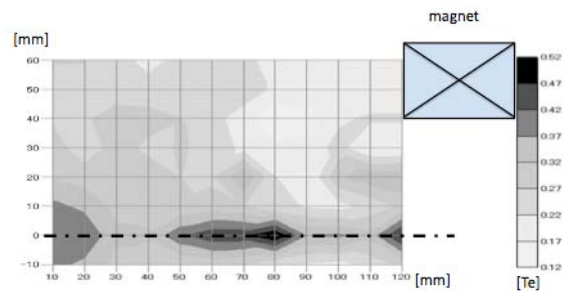


Fig. 6. The contour drawing of the electron temperature in the cusp magnetic field.

- [1] K. Yoshida, T. Shibata, A. Nezu, H. Matsuura and H. Akatsuka, *IEEE Trans. Plasma Sci.*, **37**, [8] pp. 1414 – 1418 (2009).
- [2] K. Yoshida, T. Shibata, A. Nezu, H. Matsuura and H. Akatsuka, *J. Plasma Fusion Res. Ser.*, **8**, pp. 923 – 927 (2009).
- [3] Y. Nagahara, H. Ichii, K. Yoshida, A. Nezu and H. Akatsuka, *The papers of Technical Meeting on Plasma Sciences and Technology IEE Japan*, PST-10-45, pp. 23 – 27 (2010).
- [4] K. Tajima, A. Nezu, H. Matsuura and H. Akatsuka, *The Papers of Joint Technical Meeting on Plasma Sciences and Technology and Pulsed Power Technology, IEE Japan*, PST-10-104, pp. 59 – 64 (2010).

## A.12 Discussion on the Collisional Radiative Model Based on Ordinary Differential Equations

Hiroshi AKATSUKA

We often apply optical emission spectroscopy (OES) measurement to examine plasmas. Line intensities of the plasmas indicate number densities of upper states of the transition  $N_p$  ( $p = 1, 2, \dots, M$  in the ascending order of energy;  $p = 0$  as a ground state), which are theoretically described by collisional-radiative (CR) model as functions of electron temperature  $T_e$  and density  $N_e$ . From the mathematical point of view, the governing equations of the CR model are categorized as first-order nonhomogeneous linear ordinary differential equations (ODE) with constant coefficients, where unknown functions are number densities of excited states  $N_p$ :

$$\frac{d\mathbf{N}}{dt} = \mathbf{a}\mathbf{N} + \boldsymbol{\delta}, \quad (1)$$

where bold fonts denote vectors,

$$\mathbf{N} = \begin{pmatrix} N_1 \\ N_2 \\ \vdots \\ N_M \end{pmatrix}, \quad \boldsymbol{\delta} = \begin{pmatrix} \delta_1 \\ \delta_2 \\ \vdots \\ \delta_M \end{pmatrix}, \quad (2)$$

$$\delta_i = \alpha_i N_e^3 + \beta_i N_e^2 + C_{0i} N_e N_0. \quad (3)$$

$$a_{ji} = \begin{cases} N_e C_{ji} & \text{for } j < i, \\ N_e C_{ji} + A_{ji} & \text{for } j > i, \end{cases} \quad (4)$$

$$\begin{cases} -N_e \left( S_i + \sum_{l=0, \neq i}^M C_{il} \right) - \sum_{l=0}^{i-1} A_{il} & \text{for } j = i. \end{cases} \quad (5)$$

Symbols used above are as conventions in this field. The solution to Eq. (1) is given by the sum of the general solution of the related homogeneous equation and anyone of the particular solutions to Eq. (1). One of the simplest particular solutions to Eq. (1) is the steady-state solution,

$$\begin{aligned} \bar{\mathbf{N}} &= -\mathbf{a}^{-1} \boldsymbol{\delta} = -\mathbf{a}^{-1} \boldsymbol{\delta}_{\text{rec}} - \mathbf{a}^{-1} \boldsymbol{\delta}_{\text{ion}} \\ &= -(\alpha N_e^3 + \beta N_e^2) - C_{0i} N_e N_0. \end{aligned} \quad (7)$$

Up to now, almost all the discussions on CR model seem to have been concentrated on the steady-state solution, Eq. (7). However, this is valid only when the excited species reaches the steady state after relaxation time has passed. If we treat the transient response, we must discuss time-dependent solutions to Eq. (1). For this purpose, we must examine the eigenvalues  $\lambda_i$ . The general solutions to the associate homogeneous ODE is given as

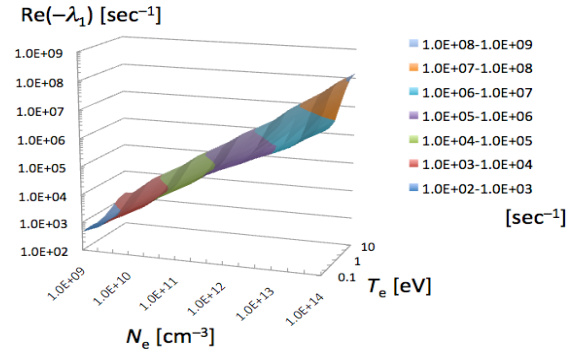


Fig. 1. Dependence of the real part of the first eigenvalue  $\lambda_1$  on  $T_e$  and  $N_e$  for Ar plasma with  $P = 1$  Torr and  $T_g = 500$  K.

$$\mathbf{N}(t) = \sum_{i=0}^M C_i \exp(\lambda_i t) \boldsymbol{\xi}_i, \quad (8)$$

where  $\boldsymbol{\xi}_i$  is the  $i$ -th eigenvector corresponding to the eigenvalue  $\lambda_i$  and  $C_i$  are arbitrary constants. Degeneracy in matrix  $\mathbf{a}$  is not essential, since we can prove that the real part of any eigenvalue is negative, and that the system is exponentially stable by Gershgorin's theorem [1].

We number the eigenvalues as  $|\text{Re}(\lambda_1)| \leq |\text{Re}(\lambda_2)| \leq \dots$ . Figure 1 shows the dependence of the absolute value of the real part  $|\text{Re}(\lambda_1)|$  as function of  $T_e$  and  $N_e$  of Ar plasma [2], where the discharge pressure is 1 Torr and the gas temperature is 500 K with Maxwellian EEDF. It is found that  $|\text{Re}(\lambda_1)|$  is approximately proportional to the electron density  $N_e$ . Since it is found that  $|\text{Re}(\lambda_1)|^{-1}$  becomes several tens of microsecond for  $N_e \sim 10^{11} \text{ cm}^{-3}$ , we should be very careful about the treatment of the excited states as steady-state. However, these time constants are not practically in problem in the OES measurement of the plasmas, where we often apply 4p or 5p levels. We should examine excited states with shorter time constants of pulse-like discharge.

[1] H. Akatsuka, *The papers of Joint Technical Meeting on Plasma Sciences and Technology and Pulsed Power Technology, IEEJ, PST-10-80/PPT-10-124*, pp. 67 – 72 (2010).

[2] H. Akatsuka, *Phys. Plasmas*, **16**, 043502 (2009).

## B.1 Fabrication and Properties of Core-Shell Type SiC/SiO<sub>2</sub> Nanowires Formed by Low-Cost and Catalysis-Free Technique

Toyohiko YANO, Wasana KHONGWONG and Katsumi YOSHIDA

A worth challenge in study on synthesis of SiC nanowires is to seek a low-cost and an un-complex production method for synthesis a large amount of SiC nanowires. In this study, the simple and inexpensive production route to fabricate nanowires through the reaction of cheap Si powder and CH<sub>4</sub> gas in a tube furnace, using separate and continuous heating process, was reported. This method, thermal evaporation, can produce SiC crystalline core/SiO<sub>2</sub> low crystallinity shell composite nanowires at a processing temperature of 1350°C without metal catalysis. The results show that both of separate heating process (performed with Si powders of 5 μm in average particle size) and continuous heating process, (performed with Si powder of 74 μm in average particle size) could obtain SiC/SiO<sub>2</sub> core-shell nanowires. The typical synthesized nanowires owned with approximately 80 nm in diameter and 0.5-2 mm in length, respectively. Photoluminescence of synthesized nanowires showed two broad photo-luminescence peaks located around 405 nm and 470 nm under 260 nm UV excitation at room temperature [1].

### 1. Introduction

During the fast development of nanotechnology in the past decade, SiC nanowires or nanocables have attracted considerable attention among many novel one-dimension nanomaterials since they are found to have various special properties and potential application. SiC nanowires, as a wide bandgap semiconductor (2.3-3.2 eV), with high thermal conductivity (300-500 Wm<sup>-1</sup>K<sup>-1</sup>), high electron saturation velocity (2.0 × 10<sup>5</sup> ms<sup>-1</sup>) and high resistant to chemical corrosion, show potential for application under a range of harsh conditions including high-temperature, high power and high frequency. Moreover, high strength, low density, high stiffness and high temperature stability combined with a high aspect ratio make 3C-SiC nanowires very effective reinforcement for various composites. The strength of SiC nanowire has been found to approach the theoretical strength and is substantially larger than that found in bulk SiC. The morphology of nanomaterials is known to have influence on their properties. In comparison with the whiskers, SiC nanowires have a larger aspect ratio and better elastic modulus and strength. Therefore, SiC nanowires should be more suitable to be used as the reinforcing materials for ceramics than SiC whiskers.

SiO<sub>2</sub> is an insulator and SiO<sub>2</sub> nanotubes have been demonstrated to be highly valuable in bioanalysis, bioseparation, and optics. SiC/SiO<sub>2</sub> nanowires, with crystalline SiC core and amorphous SiO<sub>2</sub> shell, are ideal semiconductor-insulator heterostructures in radial direction, and are expected to have excellent properties of both SiC

nanowires and SiO<sub>2</sub> nanotubes. In addition, SiC nanowires can emit blue-green light, so they would have great potential as light-emitting devices as well. Therefore, a lot of efforts have been made to synthesize SiC nanowires.

In our previous works [2-4], a relatively large amount of SiC/SiO<sub>2</sub> core-shell nanowires can be produced via reaction of evaporated Si, SiO gas and CH<sub>4</sub> gas without metal catalysis, and effect of process parameters on amount of products was clarified. Here, not only synthesis of SiC/SiO<sub>2</sub> nanowires using oxidized Si powder or ground Si ingot as raw powders through separate and continuous processes, but also optical properties of as-grown products were investigated.

### 2. Experimental Procedures

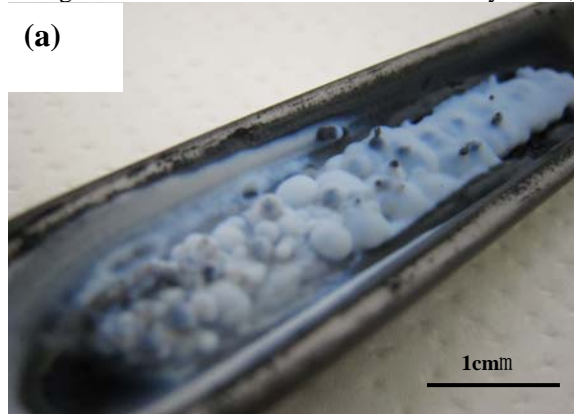
#### 2.1 Fabrication of SiC/SiO<sub>2</sub> Core-Shell Nanowires

The fabrication of SiC/SiO<sub>2</sub> core-shell nanowires was similar to that of our previous work[2,3]. Briefly, SM (silicon powder; average particle size ≈ 5 μm) was oxidized for 1 h in air at 800°C before put in a mullite boat which was then covered with an alumina fiber sheet (Nextel™ Woven Fabric 610 Style). The whole set was carefully pushed into the middle of a tube furnace. Before heating, the tube furnace was evacuated to a pressure below 1.33 Pa using a rotary pump, then the ultra high purity Ar gas (purity: 99.9995%) was released into the furnace at a flow rate of 0.6 dm<sup>3</sup>/min to reduce the oxygen to a negligible level. The furnace was initially raised to 1200°C at a heating rate of 10°C/min and then continued to heat to a peak temperature (1350°C) with heating rate of 5°C/min. At 1350°C, H<sub>2</sub> gas (purity: 99.999%) at a flow rate of 20 sccm (1 sccm = 1.667 × 10<sup>-8</sup> m<sup>3</sup>/s) was fed for 2 min before flowing of CH<sub>4</sub> gas at a flow rate of 10 sccm. CH<sub>4</sub> gas was fed for initial 30 min of keeping at 1350°C. The reaction was kept at the target temperature for 1 h. Synthesis process as mentioned above was named as separate heating process or H1, i.e., oxidation of raw powder and nanowires synthesis were separately conducted. The obtained products synthesized via this process was coded as SM/O8-H1.

To reduce cost, SG (silicon ingot; dark gray, 99% nominal purity) and continuous heating process (H2) instead of SM and H1 were used to prepare nanowires. H2 is continuous heating process, i.e., multi-step heating for oxidation at 800°C and reaction at 1350°C continuously in the same furnace. The Si ingot was ground and then sieved with a sieve (74 μm) before used as a precursor (names as SGG). The obtained products synthesized using SGG through H2 was coded as SGG08-H2.

The as-grown nanowires were characterized by XRD,

FE-  
SE  
M,



TEM and FT-IR.

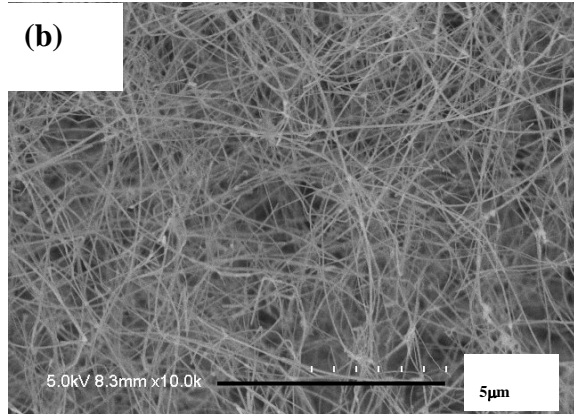


Fig. 1 (a) Photograph of as-grown product in a mullite boat from SM/O8-H1, (b) FE-SEM image of wool-like product from SM/O8-H1.

## 2.2 Photoluminescence Measurement

The synthesized SiC/SiO<sub>2</sub> core-shell nanowires from SM/O8-H1 specimen was used as representative one to measure the optical property. Photoluminescence (PL) of SiC nanowires was measured by a fluorescence spectrophotometer using 260 nm excitation light from a xenon lamp at room temperature.

## 3. Results and Discussion

### 3.1. Characterization of nanowires

After reaction, larger quantity of white-blue wool-like products was obtained on SM/O8-H1 surface (Fig. 1(a)) than that on SGG08-H2 surface. SGG08-H2 was a trial to prepare with the low-priced Si powder. Although the wool-like products from SGG08-H2 was less than the wool-like products from SM/O8-H1, this way is one alternative process to synthesize wool-like products with cheaper raw material and shorter time to production.

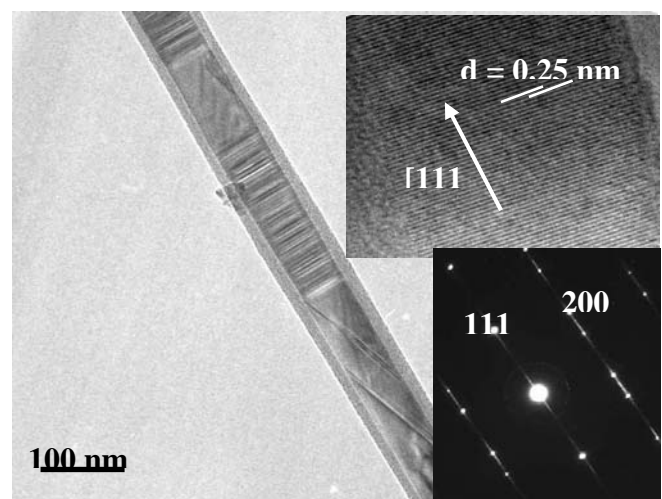
XRD patterns of as-grown products both prepared from SM and SGG confirmed that crystalline phase of all the deposition products was  $\beta$ -SiC. There exist four main strong peaks which can be attributed to the (111), (200), (220) and (311) planes of the cubic type SiC phase. These  $2\theta$  or  $d$  values are almost identical with the known values for  $\beta$ -SiC.

The typical FE-SEM images of nanowires prepared from SM/O8-H1 specimen was shown in Fig. 1 (b). Both the wool-like products from SM/O8-H1 and SGG08-H2 specimens composed of a large amount of straight, curved, tangled, randomly distributed nanowires. Length of the nanowires synthesized from oxidized SM at 800°C was too long to be measured under FE-SEM, and it is estimated to be 1 to 2 mm from the height of the product grown on SM raw powder surface. Whereas the length of the nanowires from SGG08-H2 specimen was about 0.5 mm.

TEM observation confirmed that a structure of as-grown nanowires both from SM/O8-H1 and SGG08-H2

specimens was core-shell structure and the surface was very smooth. The diameter of core of nanowires was ranging from 20 to 80 nm, and it was wrapped with a uniform layer shell with a thickness of 10-20 nm. To obtain more details about the structure and crystallinity of synthesized nanowires, selected-area electron diffraction (SAD) methods were conducted and the results are shown in Fig. 2. The SAD pattern showed that the crystalline SiC core had stacking faults and twins. High-magnification image of SiC nanowire indicated that fringe of 0.25 nm-repeat corresponding to the  $d$ -spacing of the (111) plane. The growth direction of the nanowire was [111] of  $\beta$ -SiC, as same as indicated previously [2,3]. Generally, it is accepted that  $\beta$ -SiC nanowires can grow easily in the [111] direction because the {111} surface have the lowest surface energy among the SiC surfaces and to decrease the formation energy, and hence stacking faults can be inserted easily in the (111) plane.

FT-IR spectrum of the composite (core/shell) nanowires obtained from SM/O8-H1 specimen. Two absorption bands from Si-O stretching vibration at around 1102 and 466 cm<sup>-1</sup>, transversal optic (TO) mode of Si-C



vibration at around  $804\text{ cm}^{-1}$  and a shoulder which was marked by a small circle at around  $860\text{--}950\text{ cm}^{-1}$  corresponding to the longitudinal optic (LO) mode of Si-C vibration were observed. The result is just in agreement with the previous reports. Together with the XRD and

Fig. 2 TEM image of typical nanowires from SGG08-H2 specimen. The upper right inset is a high magnification image of nanowire (The [111]-growth direction is indicated by an arrow).

TEM analyses, it is believed that the outer shell is consisted from low crystallinity or amorphous  $\text{SiO}_2$ .

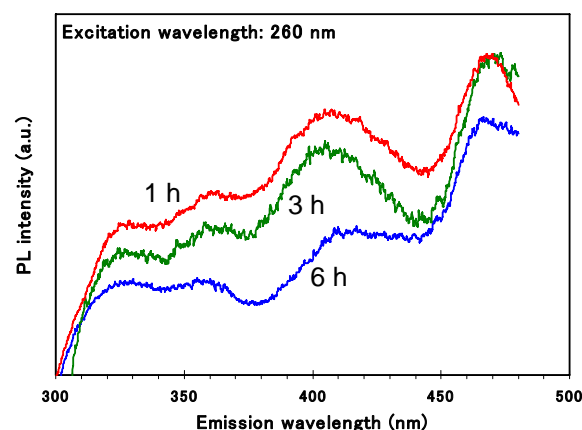
In the growth process of the composite nanowires, the reaction is seemingly involved with  $\text{SiO}$  vapor phase. As the temperature increases,  $\text{SiO}$  vapor is generated by the reaction of  $\text{SiO}_2$  thin layer on the surface of Si and evaporated Si. Dense  $\text{SiO}$  smoke is deposited first near Si powder surface. Subsequently, when the furnace is heated up till close to the melting point of Si ( $1414\text{ }^\circ\text{C}$ ), evaporation of Si accelerated. The main reaction of SiC nucleation might be  $\text{SiO (v)} + \text{Si (v)} + 3\text{CH}_4 = 2\text{SiC (s)} + \text{C (s)} + \text{H}_2\text{O (v)} + 5\text{H}_2$ . The clusters of SiC nuclei assembled to form nanowire. The nanowires in a preferred orientation grow fast as more  $\text{SiO}$  vapor and  $\text{CH}_4$  gas co-exist in the system. These mechanisms were proposed as oxide-assisted growth for the nanowires growth directly from  $\text{SiO}$  powder- $\text{CH}_4$  system by Yao et al.[5]. Subsequently, side surface of the synthesized SiC nanowires is gradually oxidized to form amorphous  $\text{SiO}_2$  outer shell by  $\text{H}_2\text{O}$  vapor, which is a by-product of the formation reaction of SiC nanowires.

### 3.2 Photoluminescence property of synthesized SiC/SiO<sub>2</sub> nanowires

Fig. 3 shows PL spectrum of SiC/SiO<sub>2</sub> core-shell nanowires synthesized at  $1350\text{ }^\circ\text{C}$  for 1, 3 and 6 h using oxidized Si raw material under 260 nm excitation light at room temperature. Two wide bands of the emission peaks centered about 405 and 470 nm were observed. Chiu et al. [6] have studied the room-temperature PL emission spectrum of the SiCNWs under 250 nm light excitation, and two apparent PL bands were reported to be located at about 390 and 470 nm. These were almost same emission peaks with the present experiment. Moreover, the synthesized nanowires at longer soaking time (3 and 6 h) were measured to compare the emission peaks. Two main board peaks still located at about 405 and 470 nm both from spectrum of specimen synthesized for 3 and 6 h. However, peak at about 405 nm of specimen synthesized for 6 h show very low intensity. The emission peak centered at about 405 nm is attributed to the oxygen discrepancy in the  $\text{SiO}_x$  amorphous shell layer. The  $\text{SiO}_2$  outer layer of nanowires synthesized for 6 h was very thin, resulted in lower PL intensity. Disappearance of  $\text{SiO}_2$  layer might be caused from reaction of created- $\text{SiO}_2$  outer layer and Si vapor, because nanowire formation reaction is stopped due to the termination of  $\text{CH}_4$  supply. Therefore, intensity of peak at 405 nm of nanowires synthesized for 6 h was very low. The blue emission band centered at about

470 nm originating from the SiCNWs is similar to those reported in other studies. Compared to SiC bulk materials, the emission wavelength for SiCNWs was blue-shifted (from 539 to 470 nm). This might have resulted from the effect of quantum confinement by size reduction or the concentrations of native defects in the SiCNWs.

Many researches have been conducted on the photoluminescence property of SiC nanowires. Those Fig. 3 PL spectrum of SiC/SiO<sub>2</sub> core-shell nanowires synthesized at



1350°C for different soaking time of 1, 3 and 6 h using Si raw powder pre-oxidized at 800°C.

results indicated that SiC nanowires may be applied as a good light emitting material, since they can emit stable and high-intensity blue-green or violet-blue or red light. Due to its blue-green emission property in this study, present SiC/SiO<sub>2</sub> nanowires may have an application in blue-green light-emitting diodes (LEDs), and in display devices especially for the environment of high temperature.

### 4. Conclusions

The following conclusions were obtained base on the experimental results of this research:

- (1) The simple production process and using the low-cost raw material, such as the continuous heating pattern for reaction of coarse silicon powder, make the present approach attractive and outstanding to synthesize SiC/SiO<sub>2</sub> core-shell nanowires. The synthesized nanowires from coarse silicon powder as raw powder under continuous heating pattern possessed core diameter approximately 20-80 nm with wrapped-SiO<sub>2</sub> outer layer of 10-20 nm in thickness. Length of nanowires was up to 0.5-1 mm.
- (2) Two broad photoluminescence peaks located around 405 nm and 470 nm under 260 nm light excitation at room temperature were confirmed.
- (3) The reaction is seemingly involved with  $\text{SiO}$  vapor phase. Oxide-assisted growth without metal catalysis is considered for the nanowire growth process.

### References

- [1]W. Khongwong, K. Yoshida and T. Yano, *Nanostructured Materials*

- and Nanotechnology IV*, American Ceramic Society, 51-62 (2010).
- [2]W. Khongwong, M. Imai, K. Yoshida, and T. Yano, *J. Ceram. Soc. Jpn.*, **117**, 194-197 (2009).
- [3]W. Khongwong, M. Imai, K. Yoshida, and T. Yano, *J. Ceram. Soc. Jpn.*, **117**, 439-444 (2009).
- [4]W. Khongwong, K. Yoshida and T. Yano, *Mater. Sci. Engineering B*, **173**, 117-121 (2010).
- [5]Y. Yao, S.T. Lee, and F.H. Li, Direct synthesis of 2H-SiC nanowhiskers, *Chem. Phys. Lett.*, **381**, 628-633 (2003).
- [6]S.C. Chiu and Y.Y. Li, *J. Cryst. Growth*, **311**, 1036-1041 (2009).

## B.2 Modeling and Material Design for Improvement of the Thermal Conductivity of Two-Dimensional SiC Fiber-Reinforced SiC Composites

Katsumi YOSHIDA and Toyohiko YANO

### Introduction

Continuous SiC fiber-reinforced SiC composites (SiC<sub>f</sub>/SiC) are expected to be used as components for gas turbine, spacecrafts and future fusion nuclear reactors. In the future fusion power reactor, the reactor concepts based on the use of SiC<sub>f</sub>/SiC composite have been designed by JAEA, ARIES-team and CEA (TAURO). For these applications, SiC<sub>f</sub>/SiC composites with higher thermal conductivity are needed in addition to higher mechanical strength and fracture toughness. Thermal conductivity of the SiC<sub>f</sub>/SiC composite would depend on not only the thermal conductivity of each component such as SiC matrix and SiC fibers but also microstructure of the composite. Polycrystalline SiC fiber (TyrannoSA) cloth with high thermal conductivity has been commercially produced by Ube Industries, Japan. Present authors have improved the thermal conductivity of SiC matrix by the microstructural control using coarse SiC grains[1]. In addition, the authors have developed a novel process of SiC<sub>f</sub>/SiC composite based on microstructure control using sheet stacking, hot-pressing and electrophoretic deposition methods[1-5]. In this study, we focused on microstructure control of the composite using our fabrication process and the simple model of thermal conductivity of composite, and improvement of its thermal conductivity was investigated.

### Experimental Procedures

Submicron-sized  $\alpha$ -SiC powder (average particle size; 0.40  $\mu\text{m}$ , Showa Denko, Japan) containing 20 wt% coarse  $\alpha$ -SiC powder (average particle size; 2-3  $\mu\text{m}$ , Kojundo Chemical Laboratory, Japan) was used as the raw materials. Al<sub>2</sub>O<sub>3</sub>-Y<sub>2</sub>O<sub>3</sub>-CaO system was used as the sintering additives of SiC, and the amount of sintering additives was 20 wt% in total. Green sheet of SiC with sintering additives was prepared by laboratory-scale tape casting equipment (DP-150, Tsugawa Seiki, Japan). Two-dimensionally plain-woven SiC fiber cloth (Tyranno SA, Ube Industries, Japan) was used as the reinforcement. Carbon coating on SiC fibers was formed by electrophoretic deposition (EPD) method reported in our previous paper[4]. SiC matrix between each filament was formed by EPD process using SiC powder suspension or polycarbosilane (PCS, Nippon Carbon, Japan) impregnation. These SiC cloths and SiC green sheets were stacked alternately, and then heat-treated at 300°C in air. The compact was hot-pressed at 1750°C for 1 h in Ar flow under a uniaxial pressure of 40 MPa. The composites using the SiC cloth treated by EPD and PCS were presented as EPD-composite and PCS-composite, respectively. For comparison, the composite was fabricated by hot-pressing using untreated TyrannoSA fiber cloth and SiC green sheet (Untreated composite). Thermal

conductivity of the composite was measured perpendicular to the cloth layers at room temperature by laser-flash method. Microstructure of the composite was observed by scanning electron microscope (SEM).

### Results and Discussion

Monolithic  $\alpha$ -SiC containing 20 wt% coarse  $\alpha$ -SiC grains and Al<sub>2</sub>O<sub>3</sub>-Y<sub>2</sub>O<sub>3</sub>-CaO sintering additives was hot-pressed under the same condition as the SiC<sub>f</sub>/SiC composite described above, and its thermal conductivity was 54 W/m•K at room temperature. Thermal conductivity of monolithic submicron-sized  $\alpha$ -SiC ceramics was 47 W/m•K. From this result, the addition of coarse  $\alpha$ -SiC grains to submicron-sized  $\alpha$ -SiC, i.e. microstructural control of SiC matrix, was effective to increase the thermal conductivity of SiC matrix. Fiber volume fraction, bulk density, open porosity and thermal conductivity of the SiC<sub>f</sub>/SiC composites are shown in Table 1. The thermal conductivity of PCS-composite was 18 W/m•K. This value was higher than that of the composite fabricated in our previous study[1], but a significant increase in thermal conductivity was not achieved. On the other hand, the thermal conductivity of EPD-composite and Untreated composite was 45 W/m•K and 56 W/m•K, respectively, and these values were much higher than that of the composite reported in our previous paper and PCS-composite. Figure 1(a) shows the schematic illustration of a rule of mixtures in multilayered structures. Thermal conductivity of the multilayered structures in the directions parallel ( $\kappa_{c1}$ , parallel model) and perpendicular ( $\kappa_{c2}$ , series model) to the layer, i.e. fiber cloth alignment, can be simply given by

$$\kappa_{c1} = \kappa_f V_f + \kappa_m V_m \quad (1)$$

$$1/\kappa_{c2} = V_f/\kappa_f + V_m/\kappa_m \quad (2)$$

where  $\kappa_m$  is the thermal conductivity of the matrix,  $\kappa_f$  the thermal conductivity of the matrix,  $V_m$  volume fraction of matrix,  $V_f$  volume fraction of fibers. Assuming that the  $\kappa_f$  of Tyranno SA is 60 W/m•K and the  $\kappa_m$  is 30, 54 and 60

Table 1 Fiber volume fraction ( $V_f$ ), bulk density (B.D.), open porosity (O.P.) and thermal conductivity ( $\kappa$ ) of the SiC<sub>f</sub>/SiC composites fabricated in this study.

Sample	$V_f$ (vol%)	B.D. (g/cm <sup>3</sup> )	O.P. (%)	$\kappa$ (W/m•K)
(a) EPD-composite	41.9	3.12	1.43	44.5
(b) PCS-composite	38.4	2.97	1.06	18.3
(c) Untreated-composite	50.9	3.14	1.36	56.1

W/m•K (54 W/m•K and 60 W/m•K is corresponding to the value of SiC matrix and the value of Tyranno SA fibers, respectively), the thermal conductivities of the composite calculated by Eq.(1) and Eq.(2) as a function of fiber volume fraction are shown in Fig.1(b). Untreated composite had a multilayered structure consisting of polycrystalline SiC fiber cloths and SiC matrices derived from SiC sheet, and its thermal conductivity well agreed with the ideal thermal conductivity calculated by series model using  $\kappa_m$  (54 W/m•K) in Fig.1(b). In the case of PCS-composite, the SiC matrix formed in SiC fiber cloths was derived from PCS, and this matrix shows lower thermal conductivity due to its low crystallinity. PCS-impregnated SiC fiber cloths would act as the layer with low thermal conductivity since the low thermal conductivity of PCS-derived SiC matrix would be dominant to that of the cloth layers. As a result, the thermal conductivity of PCS-composite would be very low. EPD-composite had a thermal conductivity of 45W/m•K, and this value was slightly lower than the value calculated by series model. This difference in thermal conductivity would be caused by the interfacial condition between SiC matrix and fibers. From these results, higher thermal conductivity of SiC<sub>f</sub>/SiC composite was successfully achieved by microstructural control, and the thermal conductivity of the SiC<sub>f</sub>/SiC composite will approach the value of untreated composite in maximum by the optimization of EPD process for the fabrication of SiC<sub>f</sub>/SiC composite.

## Summary

We focused on microstructure control of the composite using our fabrication process and the simple model of thermal conductivity of composite, and improvement of its thermal conductivity was investigated. Untreated composite had a multilayered structure consisting of polycrystalline SiC fiber cloths and SiC matrices and its thermal conductivity well agreed with the ideal thermal conductivity calculated by series model. In the case of PCS-composite, PCS-impregnated fiber cloths would act as the layer with low thermal conductivity since the low thermal conductivity of PCS-derived SiC matrix would be dominant to that of the cloth layers. The SiC<sub>f</sub>/SiC composite fabricated by electrophoretic deposition and sheet stacking method showed high thermal conductivity of 45 W/m•K.

## References

- [1] K. Yoshida, M. Imai and T. Yano, *High Temperature Ceramic Matrix Composites*, 381-387(2001).
- [2] K. Yoshida, Budiyanto, M. Imai and T. Yano, *J. Nucl. Mater.*, **258-263**, 1960- 1965(1998).
- [3] K. Yoshida, M. Imai and T. Yano, *Compos. Sci. Technol.*, **61**, 1323-1329(2001).
- [4] K. Yoshida, K. Matsukawa, T. Yano, *J. Nucl. Mater.*, **386-388** (2009) 643-646.
- [5] K. Yoshida, *J. Ceram. Soc. Japan*, **118**, 82-90 (2010).

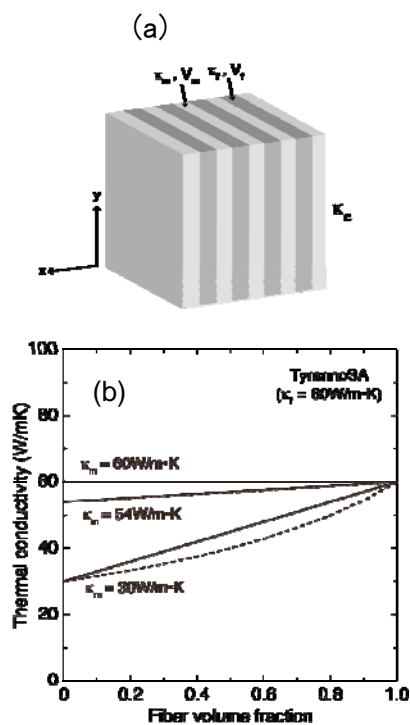


Fig.1 (a) Schematic illustration of a rule of mixture in multilayered structures. (b)Relation between fiber volume fraction and thermal conductivity of the multilayered structure calculated by Eqs.(1)(Straight line) and (2) (broken line)

## B.3 Computational Analyses of $^{238}\text{U}$ Samples Irradiated in the Experimental Fast Reactor JOYO

Tomooki SHIBA, Masaki SAITO and Hiroshi SAGARA\*

### INTRODUCTION

This report deals with the computational analyses of the U samples irradiated in the Experimental Fast Reactor Joyo to examine the transmutation performance of pure isotopes in fast neutron environment during the irradiation, and deals with the comparison with the experimental result to verify the prediction method used by PPP project<sup>[1]</sup>. Subsequently, as a next step of PPP project, the irradiation behavior of RepU-Am pellet loaded in Joyo core was predicted.

### COMPUTATIONAL METHOD AND RESULTS

As irradiated sample materials,  $^{238}\text{U}$  metallic powder was encapsulated in vanadium capsules. The samples were irradiated from the 30th cycle started on 3/21/1997 to the 33rd cycle ended on 8/31/1999, and radio-chemical analyses were conducted in June, 2008. In this study, numerical analyses of irradiated U samples were performed by ORIGEN2.2<sup>[2]</sup> referring the irradiation and cooling history of JOYO, with effective one-group neutron flux and cross section data produced from three-dimensional transport calculation by MCNP4C<sup>[3]</sup> based on the cross-section library JENDL3.3. The detailed irradiation conditions are referred to at Ohnishi *et al.*<sup>[4]</sup>.

Figure 1 shows Pu production in the vanadium capsules with the sample positions. The plutonium contents in the lower region tend to be higher than in the upper region because JOYO has a bigger reflector region in the lower area compared to the upper region. Therefore, the neutron spectra in lower region, e.g. at -627mm, are well moderated. Since neutron capture cross-section of  $^{238}\text{U}$  is very high in epi-thermal spectrum, neutron capture reaction of  $^{238}\text{U}$  is accelerated and the most  $^{239}\text{Pu}$  is generated at -627mm.

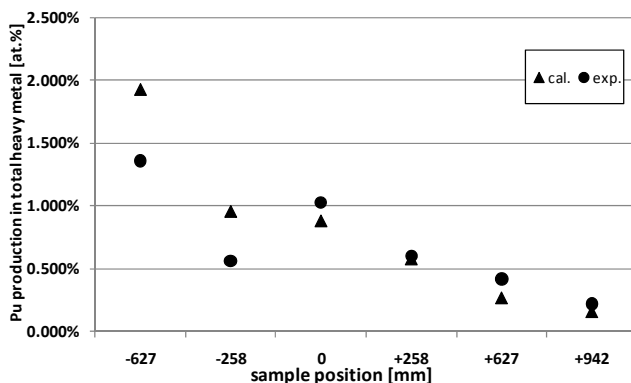


Fig. 1 Pu Production with Sample Positions

### EVALUATION OF PLUTONIUM DENATURING

Owing to the preceding papers<sup>[5]</sup> and the previous section of this report, the transmutation behaviors of Am and U pure metal materials came out; the dependence of epi-thermal neutron ratio is accentuated especially in moderator area. Since the nuclear transmutation from  $^{238}\text{U}$  to  $^{239}\text{Pu}$  is accelerated in moderated neutron area, high self shielding effect will occur and a large distribution of generated Pu isotopes will be apparent. Since there is a high self-shielding effect with moderated neutron spectra, it is predicted that there is a radial distribution of isotopic compositions of  $^{238}\text{Pu}$  and  $^{239}\text{Pu}$  inside the pellet, especially at the region close to the moderator. That indicates that around peripheral area of pellets Pu with high isotopic composition of  $^{239}\text{Pu}$  exists and if only the peripheral area is reprocessed e.g. as the pellets are dissolved for a short time, the resultant Pu has high ratio of  $^{239}\text{Pu}$ .

For analyzing the phenomena and as feasibility study of PPP pellet as well, we investigated Rep-U pellets including some percentage of  $^{241}\text{Am}$  as PPP pellets.

Figure 2 shows the radial distribution of the isotopic composition of  $^{238}\text{Pu}$  inside the pellets irradiated at -627mm. It is noticeable that the isotopic composition of  $^{238}\text{Pu}$  tends to decrease exceedingly towards exterior. This is caused by the strong self shielding effect at the irradiated position.

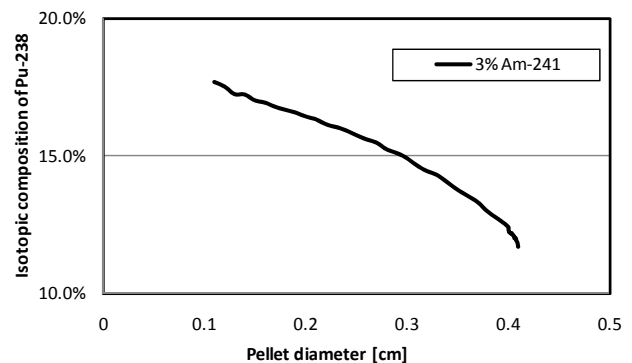


Fig. 2 Radial Distribution of Isotopic Composition of  $^{238}\text{Pu}$

### REFERENCES

1. M. Saito: *Int J Nucl Energy Sci and Technol.*, Vol. 1, No 2&3(2005).
2. A. G. Croff: Origen2: A Versatile Computer Code for Calculating the Nuclide Compositions and Characteristics of Nuclear Materials; *Nucl. Technol.*, vol. 62, p. 335-352 (1983).
3. "MCNP4C," CCC0700, RSICC (2000).
4. T. Ohnishi *et al.*, to be submitted.
5. H. Sagara *et al.*, *Trans. Ame. Nucl. Soc.*, Vol 101, P. 765, (2009).

## B.4 Systematic Measurement of keV-Neutron Capture Cross Sections and Capture Gamma-Ray Spectra of Pd Isotopes

Masayuki IGASHIRA, Kazushi TERADA and Tatsuya KATABUCHI

### 1. Introduction

Nuclear waste includes long-lived fission products (LLFPs). Currently, the deep geological disposal of nuclear waste is the national policy in Japan. However, it needs the long-term management that prevents the public from suffering radiological hazard due to LLFPs. Thus, the nuclear transmutation of LLFPs into stable or short-lived nuclides is an attractive option to decrease the hazard.

The neutron capture cross sections of LLFPs are important physical quantities for the research and development of nuclear transmutation systems, because the performance of system using neutron capture reaction depends on these quantities directly.

The nuclide  $^{107}\text{Pd}$  is one of the most important LLFPs. However, there is only one experimental data of its neutron capture cross section at the thermal neutron energy.

On the other hand, keV-neutron capture cross sections of stable Pd isotopes are also important for design of  $^{107}\text{Pd}$  transmutation system because stable Pd isotopes are inherently contained in  $^{107}\text{Pd}$  batch in reprocessing unless isotope separation is performed.

Our research group started a project of systematic measurement of the keV-neutron capture cross sections and capture gamma-ray spectra of  $^{107}\text{Pd}$  and stable Pd isotopes in 2010. We finished the measurement of  $^{105}\text{Pd}$  at incident neutron energies below 100 keV in 2010. We present the experimental results in this report.

### 2. Experiments

The detail of experimental procedure has been given in Ref. [1]. Only brief description is given here.

The capture cross section and capture gamma-ray spectrum of  $^{105}\text{Pd}$  were measured at incident neutron energies below 100 keV, using the 3 MV Pelletron accelerator of the Research Laboratory for Nuclear Reactors at the Tokyo Institute of Technology. An experimental arrangement is shown in Fig.1.

Pulsed neutrons were produced by the  $^7\text{Li}(p,n)^7\text{Be}$  reaction with a pulsed proton beam (1.5 ns width, 4 MHz repetition rate) from the accelerator. The incident neutron spectrum on a capture sample was measured by a Time of Flight (TOF) technique with a  $^6\text{Li}$ -glass scintillation detector (5 mm diam.  $\times$  5 mm thick).

The  $^{105}\text{Pd}$  sample was highly isotopically enriched metal (98.4% enrichment), and its net weight was about 0.5 g. A gold sample was used as a standard sample of capture cross section. The distance between the neutron source and the sample was 12 cm.

Capture gamma rays emitted from the sample were detected with a large anti-Compton NaI(Tl) spectrometer by means of a TOF method. The main NaI(Tl) detector of the spectrometer had a diameter of 15.2 cm and a length of 30.5 cm, and was centered in an annular NaI(Tl) detector (33.0 cm OD  $\times$  35.6 cm length) for Compton suppression. The detectors were shielded with a combination of various materials: borated paraffin, borated polyethylene, Cd,  $^6\text{LiH}$  and potassium free lead [2]. Capture gamma rays were observed at an angle of  $125^\circ$  with respect to the proton beam direction. The pulse height (PH) and TOF of signals from the spectrometer were sequentially recorded in a list-mode data format and then, were analyzed offline.

The runs for the  $^{105}\text{Pd}$ ,  $^{197}\text{Au}$  and blank were repeated cyclically, thereby for changes in experimental conditions such as the incident neutron spectrum averaging out.

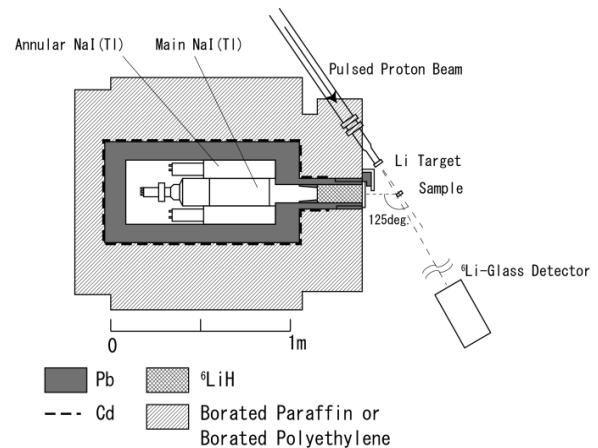


Fig.1 Experimental setup for capture cross section measurements of  $^{105}\text{Pd}$ .

### 3. Data Processing

In order to obtain the capture yields of the  $^{105}\text{Pd}$  and  $^{197}\text{Au}$  samples, a pulse-height weighting technique [3] was applied to the net capture gamma-ray PH spectra. The evaluated data of the  $^{197}\text{Au}$  capture cross section from ENDF/B-VII.0 [4] was used as standard cross section.

Corrections for the neutron self-shielding and multiple-scattering in the sample were made by a Monte-Carlo method [5]. Moreover, other corrections were made for the gamma-ray scattering and absorption in the sample.

The capture gamma-ray spectra were derived by unfolding the net capture gamma-ray PH spectra with the response matrix of the gamma-ray spectrometer. Unfolding process was done by using a computer code, FERDOR [6].

#### 4. Results and Discussion

The derived capture cross section of  $^{105}\text{Pd}$  is shown in Figs. 2. The evaluated data of JENDL-4 [7] and ENDF/B-VII.0 [8] are shown for comparison. The evaluated cross section data shown in Fig. 2 are averaged over the same energy bins as the present data.

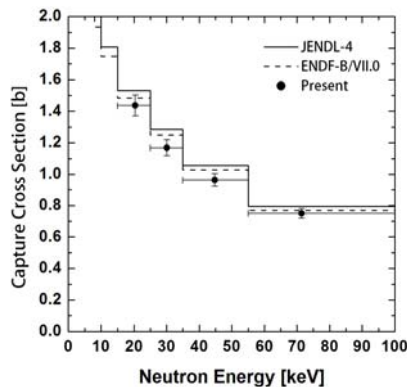


Fig. 2 Neutron capture cross section of  $^{105}\text{Pd}$ .

In the evaluations of both JENDL-4 and ENDF-B/VII, the capture cross section of  $^{105}\text{Pd}$  was calculated from statistical model. These evaluations overestimate the capture cross section by about 5 - 10% from the present results.

The measured capture  $\gamma$ -ray spectrum of  $^{105}\text{Pd}$  is shown in Figs. 3. Known discrete levels of the residual nucleus  $^{106}\text{Pd}$  are shown as bars in the same energy scale as emitted  $\gamma$ -rays. The primary transitions from the capture state to low-lying states were clearly observed. Cascade transitions among low-lying states were also observed around 1 MeV.

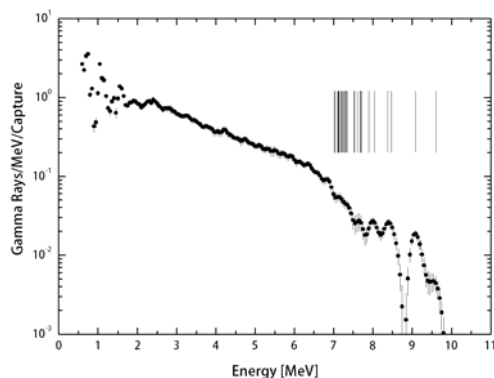


Fig. 3 Neutron capture gamma ray spectrum of  $^{105}\text{Pd}$ .

#### 5. Conclusions

We have measured the neutron capture cross section and capture gamma-ray spectrum of  $^{105}\text{Pd}$  at incident neutron energies below 100 keV to provide nuclear data relevant to the study on the transmutation of  $^{107}\text{Pd}$  and to obtain important physical quantities such as gamma-ray strength function and nuclear level density, which are useful for the theoretical calculation of capture cross section.

#### References

- [1] S. Mizuno *et al.*, *J. Nucl. Sci. Technol.*, **36**, 493 (1999).
- [2] M. Igashira, H. Kitazawa and N. Yamamuro, *Nucl. Instrum. Methods*, **A245**, 432 (1986).
- [3] R.L. Macklin and J.H. Gibbons, *Phys. Rev.*, **159**, 1007 (1967).
- [4] ENDF/B-VII.0 data file for  $^{197}\text{Au}$  (MAT=7925), evaluated by P. G. Young (2006).
- [5] K. Senoo *et al.*, *Nucl. Instrum. Methods*, **A339**, 556 (1994).
- [6] H. Kendrick and S.M. Sperling, *Gulf Radiation Technology*, **GA-9882** (1970).
- [7] K. Shibata, O. Iwamoto, T. Nakagawa *et al.*, *J. Nucl. Sci. Technol.*, **48**, 1 (2011).
- [8] M. B. Chadwick, P. Oblozinsky, M. Herman *et al.*, (CSEWG collaboration) *Nucl. Data Sheets*, **102**, 2931 (2006).

## B.5 Separation of Am(III) from Eu(III) using Polymer gels Cross-Linked with TPEN Analogs

Takeshi OGATA and Kenji TAKESHITA

*N,N,N',N'*-tetrakis(2-pyridylmethyl)ethylenediamine (TPEN) is one of the podand-type ligands with six nitrogen-donors and recognize the slight difference in the softness between minor actinide(MA) and lanthanide.<sup>[1]-[9]</sup> We have tried to synthesize a novel extraction chromatographic agent, which exploit such feature of TPEN. The use of a polymer gel as a support of the extractant can be expected to keep the flexibility of extractant and suppress the effluence of the extractant.<sup>[10]-[16]</sup>

*N,N,N',N'*-tetrakis[4-(prop-2-en-1-yloxy)pyridin-2-ylmethyl]ethylenediamine (TPPEN, **Fig. 1**) which is a TPEN analog introducing polymerizable group to pyridine rings was used as a cross-linker of acrylic monomers. We have synthesized polymer gels from various acrylic monomers, such as *N*-isopropylacrylamide (NIPA), acrylic acid (AAc), methyl methacrylate (MMA), and *N,N*-dimethylacrylamide (DMAAm).

These gels were prepared by free radical polymerization under nitrogen atmosphere. TPPEN and each acrylic monomer were dissolved in *N,N*-dimethylformamide (DMF). After addition of azobisisobutyronitrile (AIBN) as an initiator, the solution was transferred to a test tube containing glass capillaries of 20  $\mu$ L. The polymerization was carried out at 333 K for 18 hours. After gelation, the cylindrical gels were taken out of the capillaries and washed thoroughly with distilled water to remove the residual chemicals. Water contents of the gels,  $u$ , and swelling degrees of the gels,  $r_s$ , were calculated from Eqs. (1) and (2), respectively.

$$u = \frac{W_{\text{wet}} - W_{\text{dry}}}{W_{\text{wet}}} \times 100 \quad (1)$$

$$r_s = d/d_0 \quad (2)$$

where  $W_{\text{wet}}$  is the weight of gels on the wet basis at 298 K,  $W_{\text{dry}}$  is the dry weight of gels,  $d$  is the diameter of gels at 298 K and pH 5, and  $d_0$  is the inside diameter of the glass capillary ( $= 0.92$  mm).

We synthesized four kinds of the acrylic polymer gels cross-linking by TPPEN, of which the photographs are shown in **Fig. 2** and water contents of the gels,  $u$ , and swelling degrees of the gels,  $r_s$ , at pH 5 and 25°C are listed in **Table 1**. Both the NIPA- and the DMAAm-TPPEN gel were swollen at room temperature, whereas the volume change of the AAc- and the MMA-TPPEN gel were not observed.

The adsorption tests of  $^{241}\text{Am(III)}$  and  $^{152}\text{Eu(III)}$  by these gels were carried out. The distribution ratios,  $K_d$ , of Am(III) and Eu(III) and the separation factors of Am(III) over Eu(III),  $SF_{\text{Am/Eu}}$ , for the gels are plotted against the  $\text{pH}_{\text{eq}}$  of the solutions and shown in **Fig. 3**. In the pH range of 4.5 to 6.0, the NIPA- and the DMAAm-TPPEN gel had the high  $SF_{\text{Am/Eu}}$  value, which were evaluated to be 26 and 18, respectively. These  $SF_{\text{Am/Eu}}$  values are sufficient for the chromatographic separation of MA. On the other hand, the adsorption amount of Am(III) for AAc-TPPEN gel was higher than those for NIPA- and DMAAm-TPPEN gel in the pH range below 3. The separation of Am from Eu, however, was not observed for AAc-TPPEN gel, because of the ionic exchange effect of acrylic acid. Both the adsorption amount of Am(III) and the  $SF_{\text{Am/Eu}}$  value for MMA-TPPEN gel were lower than those for NIPA- and DMAAm-TPPEN gel. These results indicate that the swollen gels, such as the NIPA- and the DMAAm-TPPEN gel are suitable for Am/Eu separation.

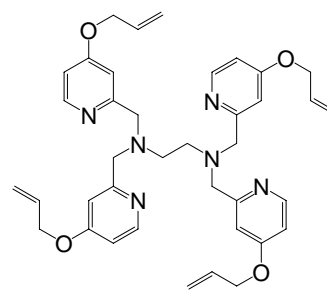


**Figure 1:** Chemical structures of cross-linkers for synthesis of gels; *N,N,N',N'*-tetrakis[4-(prop-2-en-1-yloxy)pyridin-2-ylmethyl]ethylenediamine (TPPEN).



(a) NIPA-TPPEN gel (b) AAc-TPPEN gel (c) MMA-TPPEN gel (d) DMAAm-TPPEN gel

**Figure 2:** The photographs of the acrylic polymer gel cross-linking by TPPEN: (a) NIPA-TPPEN gel; (b) AAc-TPPEN gel; (c) MMA-TPPEN gel; (d) DMAAm-TPPEN gel.

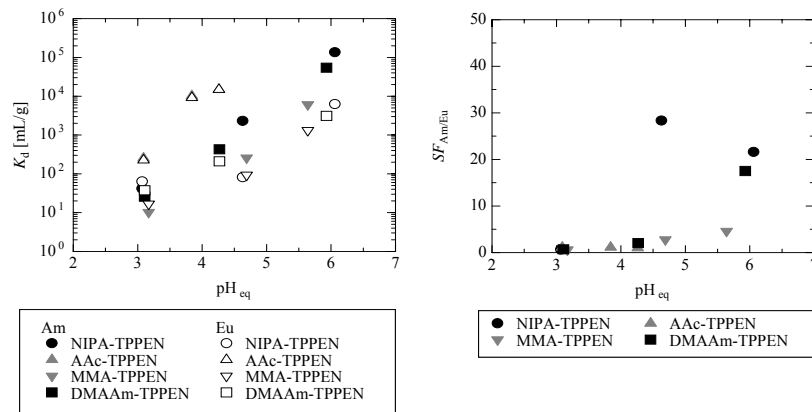


**Figure 3:** Equilibrium pH dependence of the distribution ratios of Am(III) and Eu(III) and the separation factors of Am(III) over Eu(III) for the gels.

**Table 1:** Properties of the acrylic polymer gels cross-linking by PPEN.

Sample	$W_{\text{wet}}$ [mg]	$W_{\text{dry}}$ [mg]	$u$ [%]	$r_s$
NIPA-TPPEN gel	61.75	8.68	85.9	1.66
AAc-TPPEN gel	16.80	10.35	38.4	0.99
MMA-TPPEN gel	20.89	10.66	49.0	1.02
DMAAm-TPPEN gel	221.94	8.65	96.1	3.15

## ACKNOWLEDGEMENTS

This research has been performed with supports from the Development of Innovative Nuclear Technologies Project organized by the Ministry of Education, Culture, Sports, Science and Technology of Japan.

## REFERENCES

- [1] Watanabe, M., Mirvaliev, R., Tachimori, S., Takeshita, K., Nakano, Y., Morikawa, K., and Mori, R.; "Separation of americium(III) from lanthanide by encapsulating hexadentate-ligand." *Chem. Lett.*, **31**, 1230–1231 (2002).
- [2] Mirvaliev, R., Watanabe, M., Matsumura, T., Tachimori, S., and Takeshita, K.; "Selective separation of Am(III) from Ln(III) with a novel synergistic extraction system, *N,N,N',N'*-tetrakis(2-methylpyridyl)ethylenediamine (TPEN) and carboxylic acid in 1-octanol." *J. Nucl. Sci. Technol.*, **41**, 1122–1124 (2004).
- [3] Watanabe, M., Mirvaliev, R., Tachimori, S., Takeshita, K., Nakano, Y., Morikawa, K., Chikazawa, T., and Mori, R.; "Selective extraction of americium(III) over macroscopic concentration of lanthanides(III) by synergistic system of TPEN and D2EHPA in 1-octanol." *Solvent Extr. Ion Exch.*, **22**, 377–390 (2004).
- [4] Matsumura, T. and Takeshita, K.; "Extraction separation of Am(III) and Eu(III) with TPEN isomers and decanoic acid." ACS Symposium Series, 933, 261–273 (2006).
- [5] Matsumura, T. and Takeshita, K.; "Extraction behavior of Am(III) from Eu(III) with hydrophobic derivatives of *N,N,N',N'*-tetrakis(2-methylpyridyl)ethylenediamine (TPEN)." *J. Nucl. Sci. Technol.*, **43**, 824–827 (2006).
- [6] Matsumura, T. and Takeshita, K.; "Extraction separation of trivalent minor actinides from lanthanides with hydrophobic derivatives of TPEN." *Prog. Nucl. Energy*, **50**, 470–475 (2008).
- [7] Fugate, G. A., Takeshita, K., and Matsumura, T.; "Separation of americium(III) and lanthanide(III) ions using TPEN analogs." *Sep. Sci. Technol.*, **43**, 2619–2629 (2008).
- [8] Matsumura, T., Inaba, Y., Mori, A., and Takeshita, K.; aration with a New Ligand, *N,N,N',N'*-tetrakis((4-butoxypyridin-2-yl)methyl)ethylenediamine (TBPEN), a Hydrophobic Derivative of TPEN." *J. Nucl. Sci. Technol.*, **47**, 123–126 (2010).
- [9] Kida, T., Inaba, Y., Watanabe, W., Nakajima, Y., Fukuoka, S., Takeshita, K., Mori, A.; "Extraction of  $\text{Cd}^{2+}$  and  $\text{Am}^{3+}$  Ions into Organic and Fluorous Solvents with a TPEN Chelating Agent bearing a Fluoroalkyl Substituent." *Chem. Lett.*, **39**, 774–776 (2010).
- [10] Takeshita, K., Tanaka, M., and Nakano, Y.; "Extraction of Cd(II) from aqueous nitrate solution by thermosensitive gel crosslinked with 2,6-di(3-vinylbenzyl-1,2,4-triazol-5-yl)pyridine (BTP)." *Solvent Extr. Ion Exch.*, **20**, 139–150 (2002).
- [11] Takeshita, K., Tanaka, M., Nakano, Y., and Seida, Y.; "Thermal-swing extraction of Cd(II) by thermosensitive gel crosslinked with nitrogen-donor ligands." *J. Chem. Eng. Jpn.* **36**, 1253–1258 (2003).
- [12] Takeshita, K., Ishida, K., Nakano, Y., and Matsumura, T.; "Thermal-swing Extraction of Cadmium(II) by Thermosensitive Polymer Gel Crosslinked with Encapsulating Hexadentate Ligand." *Chem. Lett.*, **36**, 1032–1033 (2007).
- [13] Takeshita, K., Matsumura, T., and Nakano, Y.; "Separation of Americium(III) and Europium(III) by thermal-swing extraction using thermosensitive polymer gel." *Prog. Nucl. Energy*, **50**, 466–469 (2008).
- [14] Fukuoka, S., Kida, T., Nakajima, Y., Tsumagari, T., Watanabe, W., Inaba, Y., Mori, A., Matsumura, T., Nakano, Y., and Takeshita, K.; "Thermo-responsive extraction of cadmium(II) ion with TPEN-NIPA gel. Effect of the number of polymerizable double bond toward gel formation and the extracting behavior." *Tetrahedron*, **66**, 1721–1727 (2010).
- [15] Maekawa, T., Kida, T., Miyazaki, Y., Watanabe, W., Inaba, Y., Takeshita, K., and Mori, A.; "Temperature-Dependent Change of Extraction Performance of Soft Cadmium(II) Ion with TPEN-NIPA Gel. Studies on the Effect of the Ethylenediamine Skeleton." *Bull. Chem. Soc. Japan*, **84**, 122–124 (2011).
- [16] Inaba, Y., Tsumagari, T., Kida, T., Watanabe, W., Nakajima, Y., Fukuoka, S., Mori, A., Matsumura, T., Nakano, Y., and Takeshita, K.; "Thermoresponsive extraction of cadmium(II) ions by poly(TPEN-NIPA) gels. Effect of chain length and branched spacer structure on gel formation and extraction behavior." *Polym. J.*, **43**, 630–634 (2011).



## B.6 Thermo-Responsive Extraction of Cadmium(II) Ion with Poly(TPEN-NIPA) Gel

Yusuke INABA, Atsunori MORI and Kenji TAKESHITA

A polymer gel composed of poly(*N*-isopropyl acrylamide) (NIPA), which reversibly switch swelling and shrinking corresponding to a temperature change, is intriguing as a thermo-responsive functional materials.<sup>1-4</sup> We have recently shown that poly(TPEN-NIPA) gel effectively extract soft metal ions such as Cd<sup>II</sup> and its extraction behaviors are thermally dependent in various pH regions. It was shown to extract Cd<sup>II</sup> at lower temperature, while little extraction has been observed at the elevated temperatures.<sup>5-8</sup> TPEN, *N,N,N',N'*-(tetrakis-2-pyridylmethyl)ethylenediamine, is recognized as a hexadentate ligand with six nitrogen donors and has been shown to chelate a variety of soft metal ions such as Hg, Cd, Au and Pd.<sup>9-13</sup> It was also shown to be effective for chelation of *f*-block metals; the separation of minor actinides from high level radioactive waste (HLW) is a pressing issue.<sup>14-23</sup> Thereby TPEN derivatives have been employed as an extracting agent for variety of metal ions in organic solvents. On the other hand, it is possible to extract metal ions in aqueous solutions without organic solvent if the TPEN moiety is incorporated into a polymer gel. Since poly-NIPA (*N*-isopropyl acrylamide) gel is shown to swell at low temperature in water and shrink at temperatures higher than the lower critical solution temperature,<sup>1</sup> this thermo-responsive swelling/shrinking can be applied for the corresponding conformational change of TPEN that induces temperature dependent change of extraction behaviors when the TPEN moiety such as **1a** is employed as a cross linker in the poly-NIPA gel.

Herein, we report synthesis of several TPEN derivatives bearing four polymerizable double bond in the substituent on the pyridine ring with different methylene spacer length and branched structure and studies on the temperature-dependent extraction behaviors of cadmium ion with poly(TPEN-NIPA) gels of the different spacer structure.

### Results and discussion

The synthetic pathway of TPEN derivatives with different side-chain length (**1a-c**) and branched structure (**1d**) was summarized in Scheme 1.

TPEN derivatives, thus obtained, were subjected to the radical copolymerization leading to poly(TPEN-NIPA) gel (Scheme 2). The reaction was performed with *N*-isopropyl acrylamide (NIPA) and TPEN derivatives **1a-d** (2.5 mol%) in the presence of AIBN as a radical initiator in DMF.

With these poly(TPEN-NIPA) gels extraction studies were carried out using cadmium(II) ion. Temperature-dependent extraction behaviors were examined in the swollen state (5 °C) and the shrinking state (45 °C) at the

pH values of ca. 2.0 and 6.5, respectively. A 1 mM solution of Cd(NO<sub>3</sub>)<sub>2</sub> was prepared and the pH value was controlled to 1.9 and 5.3 (at 5 °C), 2.0 and 5.9 (45 °C) respectively, by the addition of NH<sub>4</sub>NO<sub>3</sub>. Extraction was performed by the addition of dried poly(TPEN-NIPA) gel to 0.2 mL of 1 mM solution of Cd(NO<sub>3</sub>)<sub>2</sub>. The amount of Cd<sup>II</sup> ion incorporated into the gel was estimated by ICP-AES analysis of the remaining amount of cadmium ion. Figure 1 summarizes the results.

As reported previously, **C3** extracted cadmium ion efficiently at 5 °C ( $7.91 \times 10^{-2}$  mmol-Cd/g-dry gel) when the extraction was carried out at pH = 6.5, while at 45 °C hardly extracted Cd<sup>II</sup> ( $0.08 \times 10^{-2}$ ). Such behaviors were also observed at pH = ca. 2 although the extraction performance was slightly lower ( $3.20 \times 10^{-2}$  at 5 °C,  $1.07 \times 10^{-2}$  at 45 °C). **C4** was found to show slightly superior performance to **C3** in both the amount of extraction and the thermo-responsive difference (at pH = ca. 2,  $4.64 \times 10^{-2}$  at 5 °C,  $0.48 \times 10^{-2}$  at 45 °C). Such a better performance would be due to the homologation of the side chain, which improved hydrophobicity of the TPEN moiety.<sup>16</sup> **C10** also showed improved performance in extraction at the pH values of both ca. 2 and 4.5 at 5 °C ( $5.50 \times 10^{-2}$ ,  $9.13 \times 10^{-2}$ ). This would also be due to the improved hydrophobicity of long methylene chains. However, extraction in the shrinking state at 45 °C unexpectedly improved leading to the inferior thermo-responsive change at the pH of 2 and 4.5 ( $1.64 \times 10^{-2}$ ,  $4.62 \times 10^{-2}$ ). Poly(TPEN-NIPA) gel bearing a branched structure was found to show remarkable extraction in swelling state and thermo-responsive change at pH = 6.5 to observe the highest extraction at 5 °C and little extraction at 45 °C. Worthy of note, in addition, is the remarkably high extraction at pH of 2 at 5 °C ( $6.40 \times 10^{-2}$ ) and its thermo-responsive change was also excellent ( $6.40 \times 10^{-2}$  to  $0.26 \times 10^{-2}$ ). This would be due to the formation of stiff gel as well as the improved hydrophobicity.

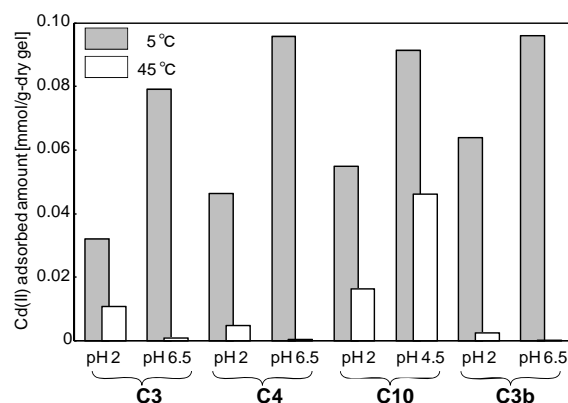
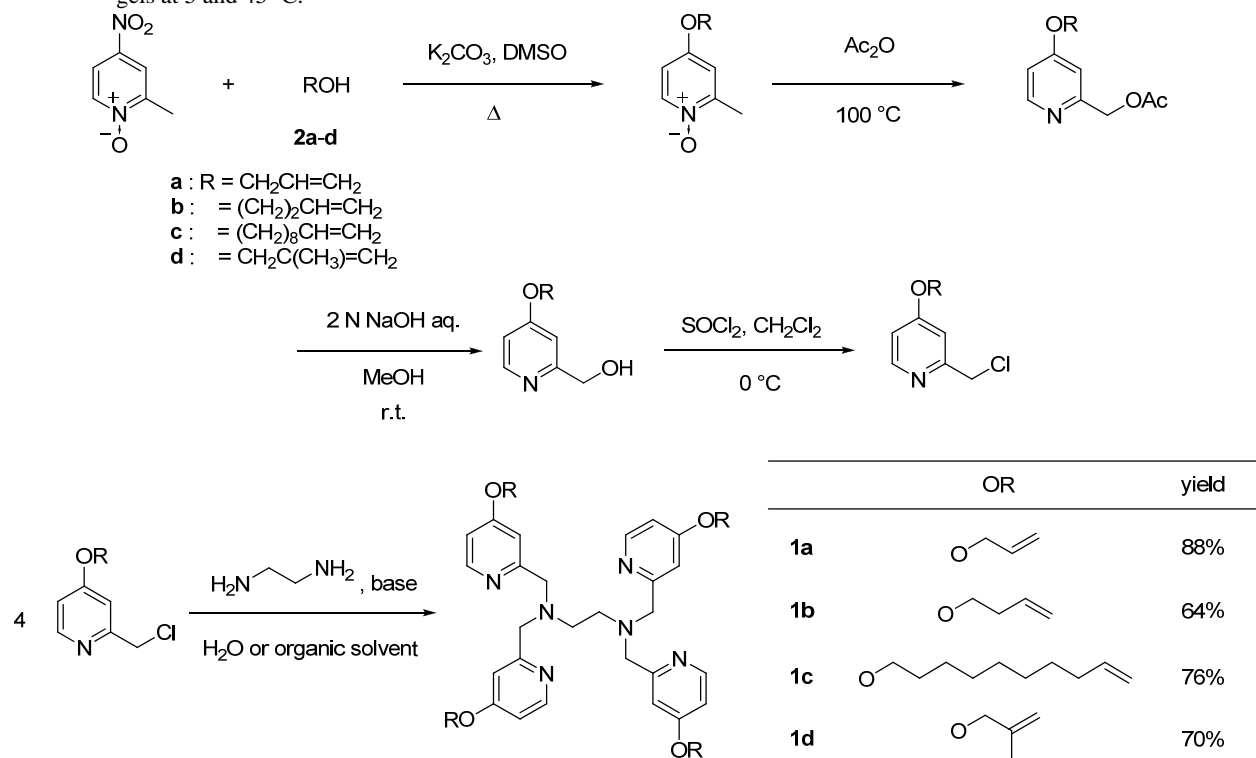
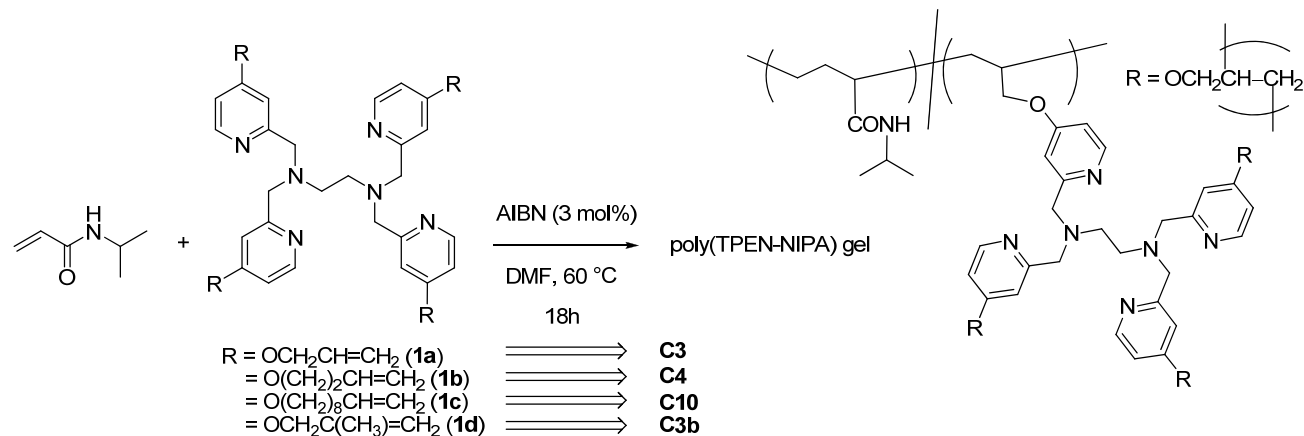


**Figure 1.** Thermo-responsive extraction of poly(TPEN-NIPA) gels at 5 and 45 °C.



**Scheme 1.** Synthesis of TPEN derivatives.



**Scheme 2.** Synthesis of poly(TPEN-NIPA)gel.

## Conclusion

In summary, we have synthesized TPEN derivatives bearing different side-chains involving the chain length and the branched structures. The prepared derivatives were subjected to the formation of poly(TPEN-NIPA) gels. The temperature-dependent change of extraction behaviors of cadmium(II) ion with poly(TPEN-NIPA) gels were highly influenced to the side-chain structures. The excellent thermo-responsive change particularly under highly acidic conditions such as pH=ca. 2 would be potentially practical

for the chromatographic separation of metal ions, namely thermal swing chromatography, which would be applied for the separation of minor actinides from high level radioactive wastes (HLW). The high performance of TPEN-NIPA gel **C3b** is remarkably noteworthy.

## References and notes.

1. Tanaka, T., Nishio, I., Sun, S.-T., Ueno-Nishio, S. Collapse of gels in an electric field. *Science* **218**, 467-469 (1982).

2. Tokuyama, H., Kanehara, A. Temperature swing adsorption of gold(III) ions on poly(*N*-isopropylacrylamide) gel. *React. Funct. Polym.* **67**, 136-143 (2007).
3. Kohri, M., Sato, K., Ide, K., Inoue, Y., Okouchi, H. Solid phase extraction for the speciation of organotin compounds in shellfish samples. *Anal. Sci.* **1997**, *13*, 141-143.
4. Takeshita, K., Tanaka, M., Nakano, Y., Seida, Y. Thermal-swing extraction of Cd(II) by thermosensitive gel crosslinked with nitrogen-donor ligands. *J. Chem. Eng. Jpn.* **36**, 1253-1258.
5. Takeshita, K., Matsumura, T., Nakano, Y. Separation of Americium(III) and Europium(III) by thermal-swing extraction using thermosensitive polymer gel. *Prog. Nucl. Energy.* **50**, 466-469 (2008).
6. Takeshita, K., Ishida, K., Nakano, Y., Matsumura, T. Thermal-swing extraction of cadmium(II) by thermosensitive polymer gel crosslinked with encapsulating hexadentate ligand. *Chem. Lett.* **36**, 1032-1033 (2007).
7. Fukuoka, S., Kida, T., Nakajima, Y., Watanabe, W., Tsumagari, T., Inaba, Y., Mori, A., Matsumura, T., Nakano, Y., Takeshita, K. Thermo-responsive extraction of cadmium(II) ion with TPEN-NIPA gel. Effect of the number of polymerizable double bond toward gel formation and the extracting behavior. *Tetrahedron*, **66**, 1721-1727 (2010).
8. Maekawa, T., Kida, T., Miyazaki, Y., Watanabe, W., Inaba, Y., Takeshita, K., Mori, A. Temperature-dependent change of extraction performance of soft Cadmium(II) ion with TPEN-NIPA gel. Studies on the effect of the ethylenediamine skeleton. *Bull. Chem. Soc. Japan*. **84**, 122-124 (2011).
9. Jensen, M. P., Morss, L. R., Beitz, J. V., Ensor, D. D. Aqueous complexation of trivalent lanthanide and actinide cations by *N,N,N',N'*-tetrakis(2-pyridylmethyl)ethylenediamine. *J. Alloys. Compd.* **303-304**, 137-141 (2000).
10. Cukrowski, I., Cukrowska, E., Hancock, R. D., Anderegg, G. The effect of chelate ring size on metal ion size-based selectivity in polyamine ligands containing pyridyl and saturated nitrogen donor groups. *Anal. Chim. Acta* **312**, 307-321 (1995).
11. Hirayama, N., Iimuro, S., Kubono, K., Kokusen, H., Honjo, T. Formation of dinuclear copper(II) complex with *N,N,N',N'*-tetrakis(2-pyridylmethyl)-1,2-ethanediamine in aqueous solution. *Talanta* **43**, 621-626 (1996).
12. Watanabe, M., Mirvaliev, R., Tachimori, S., Takeshita, K., Nakano, Y., Morikawa, K., Mori, R. Separation of americium(III) from lanthanide by encapsulating hexadentate-ligand. *Chem. Lett.* **31**, 1230-1231 (2002).
13. Mirvaliev, R., Watanabe, M., Matsumura, T., Tachimori, S., Takeshita, K. Selective separation of Am(III) from Ln(III) with a novel synergistic extraction system, *N,N,N',N'*-tetrakis(2-methylpyridyl)ethylenediamine (TPEN) and carboxylic acid in 1-octanol. *J. Nucl. Sci. Technol.* **41**, 1122-1124 (2004).
14. Kolarik, Z. *Chem. Rev.* Complexation and separation of lanthanides(III) and actinides(III) by heterocyclic N-donors in solutions. **108**, 4208-4252 and references therein.
15. Blindauer, C. A., Razi, M. T., Parsons, S., Sadler, P. J. Metal complexes of *N,N,N',N'*-tetrakis(2-pyridylmethyl)ethylenediamine (TPEN): Variable coordination numbers and geometries. *Polyhedron* **25**, 513-520 (2006).
16. Ogata, T., Takeshita, K.; Fugate, G. A.; Mori, A. Extraction of soft metals from acidic media with nitrogen-donor ligand TPEN and its analogs. *Sep. Sci. Technol.* **43**, 2630-2640 (2008).
17. Ogata, T., Takeshita, K., Tsuda, K., Mori A. Solvent extraction of perhenate ions with podand-type nitrogen donor ligands. *Sep. Purif. Technol.* **68**, 288-290.
18. Shimojo, K., Naganawa, H., Noro, J., Kubota, F., Goto, M. Extraction behavior and separation of lanthanides with a diglycol amic acid derivative and a nitrogen-donor ligand. *Anal. Sci.* **23**, 1427-1430 (2007).
19. Mikata, Y., Yamanaka, A., Yamashita, A., Yano, S. Isoquinoline-based TQEN family as TPEN-derived fluorescent zinc sensors. *Inorg. Chem.* **47**, 7295-7301 (2008).
20. Heitzmann, M., Bravard, F., Gateau, C., Boubals, N., Berthon, C., Pecaut, J., Charbonnel, M. C., Delangle, P. Comparison of two tetrapodal N,O ligands: Impact of the softness of the heterocyclic N-donors pyridine and pyrazine on the selectivity for Am(III) over Eu(III). *Inorg. Chem.* **48**, 246-256 (2009).
21. Ekberg, C., Fermvik, A., Retegan, T., Skarnemark, G., Foreman, M. R. S., Hudson, M. J., Englund, S., Nilsson, M. An overview and historical look back at the solvent extraction using nitrogen donor ligands to extract and separate An(III) from Ln(III). *Radiochimica Acta*, **96**, 225-233 (2008).
22. Takeshita, K., Watanabe, K., Nakano, Y., Watanabe, M. Solvent extraction separation of Cd(II) and Zn(II) with the organophosphorus extractant D2EHPA and the aqueous nitrogen-donor ligand TPEN. *Hydrometallurgy* **70**, 63-71 (2003).
23. Takeshita, K., Watanabe, K., Nakano, Y., Watanabe, M. Extraction of Cd(II) and Zn(II) with dialkylthiophosphinic acid and hexadentate nitrogen-donor ligand. *Chem. Lett.* **32**, 96-97(2003).

## B.7 Nuclear Rare Metals, as “Kopernikanische Wendung“

Masaki OZAWA and Tatsuya SUZUKI

A hydrometallurgical separation technologies by novel solvent extraction (SX), ion exchange chromatography (IXC) and electrolytic extraction techniques are reviewed as separation tools for light PGM (Ru, Rh, Pd), Tc and *f*-elements in high level liquid wastes of the nuclear fuel cycle. The IXC process utilizing a tertiary pyridine resin (TPR) provides a very high degree of separation of the *f*-elements in spent nuclear fuel and the recovery of pure Am and Cm products. The catalytic electrolytic extraction (CEE) process utilizing Pd<sub>adatom</sub> or Rh<sub>adatom</sub> can effectively separate platinum group metals (PGM), Tc and Re by means of controlled under potential deposition (UPD). Some of the basic work on the hydrometallurgical separation of the elements of interest has been carried out through the strategic *Advanced (Adv.-) ORIENT Cycle* research in Japan. The *Adv.-ORIENT Cycle* process cannot only improve the radioactive waste problem, but can also provide useful rare metals to leading industries as from this secondary resource.

### 1. Introduction

Resources of natural energy (oil, gas, <sup>235</sup>U) and most of rare metals will run out within 200 years. In particular at fiscal year 2004, the R (resource) / P (production) ratio (year) for oil was 41 years, 67 years for natural gas, 192 years for coal for and 85 years for uranium. Despite the rather long R/P ratio of ca.150 years for the platinum group metals (PGM), the current price increases for Ru, Rh, and Pd in the market have been significant, and it should be noted that the production of PGM is limited to mainly those two countries namely South Africa (75 %) and Russia (17 %) in the year 2008[1]. On the other hand, the R/P ratio for rare earths is not so limiting, but 93 % of rare earth production is monopolized by one country, China. In this context, nuclear fission is said to be able to counter such a natural energy crisis issue if <sup>238</sup>U (<sup>239</sup>Pu) can be utilized in fast breeder reactors (FBR) in future.

Fission reaction of <sup>235</sup>U and <sup>239</sup>Pu currently is creating more than 40 elements and 400 nuclides as fission products (FP) in the spent fuel, while generating enormous amounts of energy, approximately two million times greater than that from chemical reaction per gram of fuel. Among them, 31 elements are categorized as rare metals, and particularly Zr, Mo, Ru, Pd, Cs, Ce, Nd are highly enriched in FBR spent fuel. Because of their individual radiochemical properties, these should be recognized as not only the radioactive wastes but a second source of nuclear rare metals (NRM). Separation and utilization (stock-pile) technologies should be at once developed for the next generation, and hence in the nuclear fuel cycle, a policy change such as *Kopernikanische Wendung* (Copernican Revolution) is necessarily. This paper will review the state of the art of the hydrometallurgical, e.g.,

solvent extraction (SX), ion exchange chromatography (IXC) and electrolytic extraction (EE), technologies for the separation and recovery of NRM as well as actinides present in the radioactive wastes.

### 2. Rare Metals in the Nuclear Fuel Cycle

Typical yields for Pd, Ru, Rh (light PGMs) and Tc will reach to around 11kg, 13kg, 4kg and 3kg, respectively per metric ton of the reference FBR spent fuel (150 GWd/t, cooled for 5 years). The quantity of NRM is shown in Figure 1. Since such yields are proportional to the degree of burn-up, those in common light water reactors (LWR) will be approximately one third of FBR. It is notable that, Mo and some heavy lanthanides (Ln) (Dy, Er, Yb) are already non-radioactive and non-exothermic on reprocessing after 5 years cooling. Also, Nd and La are no longer radioactive beyond the natural one's level. Furthermore, after cooling for more than 50 years in a stock-pile, the specific radioactivity of Ru, In, some of Ln like Pr, Gd and Tb will be less than 0.1 Bq/g. The quality (isotopic composition) of some of NRM is shown in Figure 2. The radiochemical properties are summarized as follows [2],

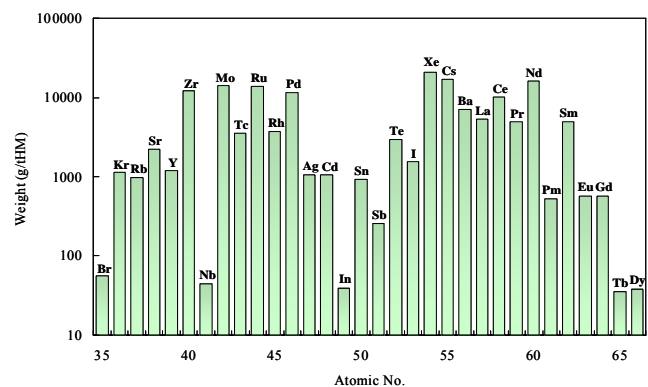


Figure 1 Typical yields for Pd, Ru, Rh (light PGM) and Tc in the reference FBR spent fuel (150 GWd/t, cooled for 5 years)

- After 40 years in a FP stock-pile the radioactivity of Ru will decrease to be below the exemption level (BSS\*) of <sup>106</sup>Ru. Its isotopic abundance will become to stable Ru (<sup>99</sup>Ru, <sup>100</sup>Ru, <sup>101</sup>Ru, <sup>102</sup>Ru, <sup>104</sup>Ru) and <sup>106</sup>Pd only. \*Note BSS; International Basic Safety Standards for Protection against Ionizing Radiation and for the Safety of Radiation Sources, Safety Series No.115, IAEA, Vienna (1996).
- After 80 years in a FP stockpile the radioactivity of Rh will decrease to below the exemption level (NRPB\*) of <sup>102</sup>Rh. Its isotopic abundance will become stable at <sup>103</sup>Rh and <sup>102</sup>Ru. \*Note NRPB; National Radiological Protection Board-R306 (1999).

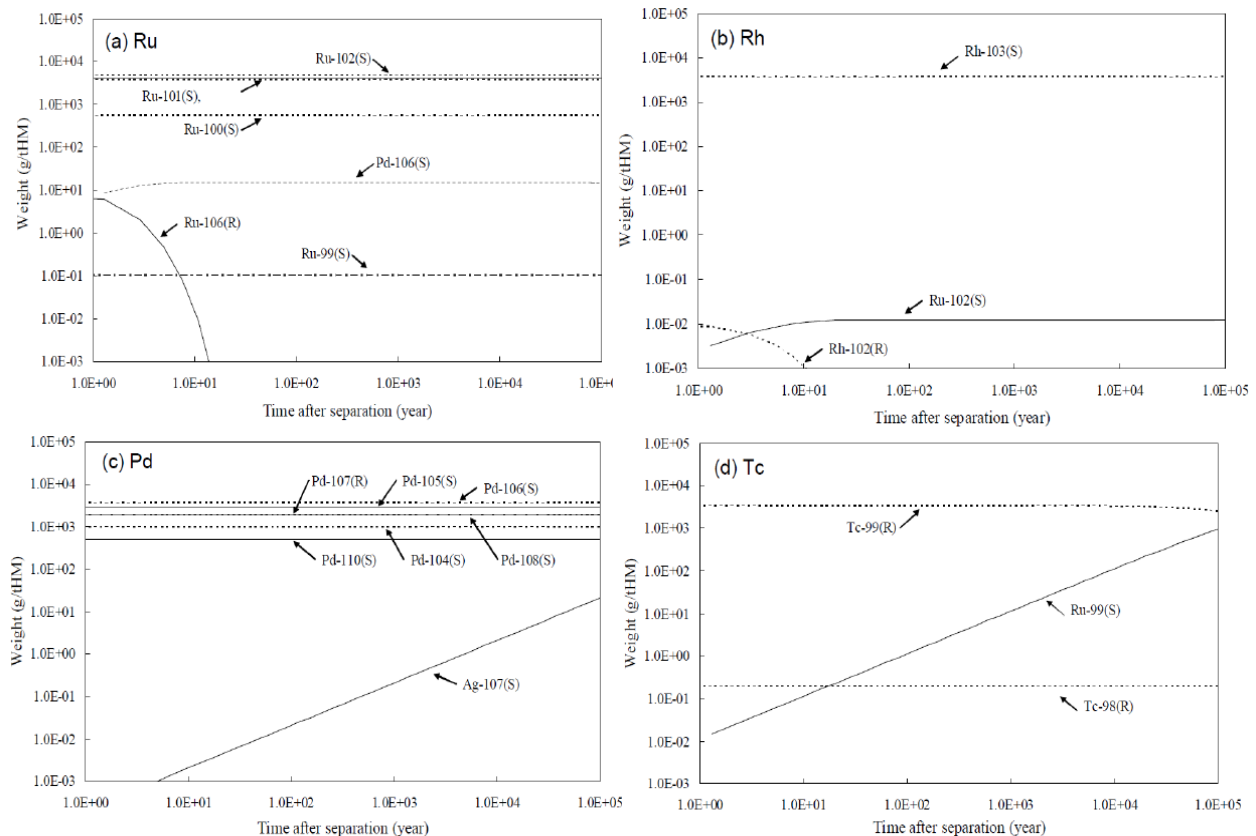


Figure 2 Time dependence of isotopic abundance of fission products, PMGs and Tc, after the separation (for a fast reactor, 150,000MWd/t, cooled for 5 years)

- (c) Only  $^{107}\text{Pd}$  only is radioactive (long-lived) in isotopic abundance in FP Pd. Its ratio is ca.16 wt %, and  $^{107}\text{Ag}$  will be gradually generated. The radio toxicity of FP Pd is very low, just ca. 30 times as high as  $^{107}\text{Pd}$ 's BSS level ( $10^3$  Bq/g).
- (d)  $^{99}\text{Tc}$  is the only major radioactive (long-lived) nuclide in isotopic abundance of FP Tc. Stable  $^{99}\text{Ru}$  will be gradually generated.

From close investigation, a possible "exit strategy" can be drawn up for individual NRM with regard to utilization. Namely, (i) Material/Chemical use; **Ru, Rh, Pd, Mo, Ln (La, Nd, Dy, etc)** and **Tc**. It is particularly noted that the isotopic abundance of Mo in stable FP will be composed of mainly higher order nuclides like  $^{97}\text{Mo}$  (22.1 wt %) and  $^{98}\text{Mo}$  (26.8 wt %). Such abundances might be advantageous for the production of  $^{99}\text{Mo}$  and  $^{99\text{m}}\text{Tc}$ . (ii) Radiochemical use;  $^{137}\text{Cs}$  (e.g., radiation source as an alternative to  $^{60}\text{Co}$ ),  $^{90}\text{Sr}$ ,  $^{238}\text{Pu}$ ,  $^{241}\text{Am}$  and  $^{242,244}\text{Cm}$ , (iii) Additional nuclear fuel;  $^{237}\text{Np}$ ,  $^{241}\text{Am}$  and **Cm** (as  $^{238,240}\text{Pu}$ , by  $\alpha$  decay of  $^{242,244}\text{Cm}$ ), (iv) Sale of stable isotopes on the market;  $^{99}\text{Ru}$ ,  $^{102}\text{Ru}$ ,  $^{103}\text{Rh}$ ,  $^{106}\text{Pd}$  and  $^{107}\text{Ag}$ . These stable nuclides will be obtained after long-term stock-piling of FP Ru, Rh, Pd and Tc.  $^{100}\text{Ru}$  can be also obtained as a transmutation product of  $^{99}\text{Tc}$ . The exit strategy for PGM will depend on the ability to cool for several decades.

Prior to the industrial utilization of NRM, a radiochemically precise separation of them and the actinides in the spent fuel is required. Such separation technologies should be integrated to be well compatible with each other in the fuel cycle where the reprocessing function must also be changed to meet environment-friendly requirements.

### 3. Separation of Minor Actinides

In the past three decades, partitioning and transmutation (P&T) of long-lived nuclides has been studied world-wide with the objective of creating an environmentally friendly nuclear fuel cycle. Figure 3 shows historical view on radiochemical separation relating to P&T technology in Japan. In this context, the TRUEX (TRansUranium EXtraction) solvent extraction process, using a bifunctional extractant OÖD[IB]CMPO (n-octyl(phenyl)-N,N-diisobutylcarbamoylmethylphosphine oxide) with TBP in n-dodecane as the solvent, was successfully found to be a vital method for recycling trivalent actinides (An(III)) from high level liquid wastes (HLW) of spent fuel reprocessing [3]. The separation of trivalent actinides and lanthanides from HLW was investigated by not only CMPO but also malonamide in the European framework projects [4]. These extractants are in the development stage for practical use. The process flow-sheets using these extractants have been successfully tested. One of the topical technological issues was inter-group separation of trivalent Ln (III) from

An(III) for efficient actinide recycling into the FBR, as these are reviewed in other papers [5].

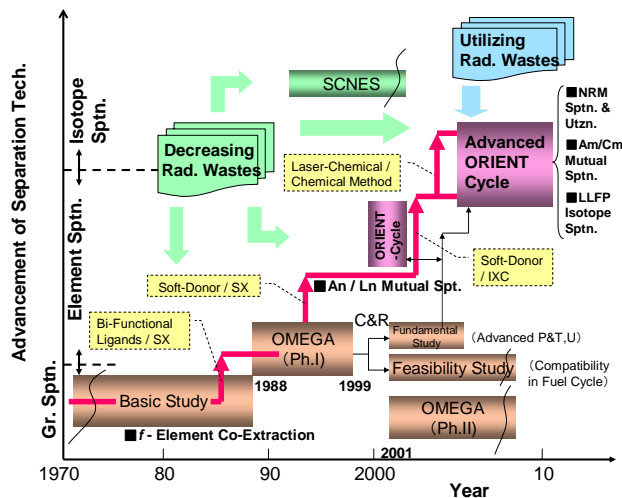


Figure 3 historical view on radiochemical separation relating to P&T technology in Japan

As mentioned above, tri-valent An (III) existing in spent nuclear fuels, have been treated as high level wastes in the nuclear cycle. At present, transmutation of MA like An (III) by fast neutrons with an Accelerator Driven System (ADS) and/or a FBR has been studied. These transmutation technologies use a neutron source. Therefore, if a burnable poison like Ln is present in this target, the transmutation efficiency of Am (III) and Cm (III) is decreased. In order to achieve a high transmutation efficiency of Am (III) and Cm (III), separation of An (III) from Ln (III) is therefore very important. On the other hand, the 5f-electrons on An (III) are of a largely relativistic, itinerant nature, providing a degree of covalency, which makes the behavior of An (III) ions slightly softer than Ln (III) ions. Consequently, most separations of An (III) from Ln (III) were achieved with ligands using soft donors like sulfur (S) or nitrogen (N) atoms. For this purpose, new MA/Ln separation ligands were developed in several countries. For instance, the purified bis(2,4,4-trimethylpentyl) di-thio phosphinic acid (CYANEX 301) gave a high separation factor; SF [Am (III) / Eu (III)] = 4900 [6,7]. Process flowsheets were developed and tested in China with real HLW and the radiolysis of CYANEX 301 was also investigated [8].

In the meantime, the simultaneous recovering of all of the actinides with one type of solvent, bifunctional organophosphorus extractants dissolved in highly polar fluorinated diluents, was studied. 0.4M OÖD[iB]CMPO with 30% TBP dissolved in metanitrobenzotrifluoride (Fluoropole-732) was found to achieve total extraction of all of the f-elements from the dissolver solution of spent nuclear fuel without splitting a third phases [9]. This new solvent system was named the ORGA process (\*abbreviation of **O**rganophosphoryl-fluoropole solvent for **R**ecovery of **G**roup of **A**ctinides) [10].

## 5. A New Back-end Fuel Cycle Concept (Adv.-ORIENT Cycle)

Aiming at simultaneous realization of the utilization of elements/nucleides and ultimate minimization of radioactive wastes, a new fuel cycle concept, **Adv.-ORIENT (Advanced Optimization by Recycling Instructive Elements) Cycle** [2, 11, 12, 13], is proposed under the following strategies as shown in Figure 4 ;

- 1/ *Trinitarian* research on separation, transmutation and utilization (S&T, U) of nucleides and elements, based on FBR fuel cycle.
- 2/ Significant reduction of radioactive wastes and eventual ecological risks: Within a few hundred years, achieve a radiotoxic inventory decrease to the level of natural U tons corresponding to one ton of vitrified HLW.
- 3/ Cascade separation of all actinides, NRM, Cs and Sr by a multi-functional and compact reprocessing process and plant.
- 4/ Challenge on isotope separation of long lived radio nuclide  $^{135}\text{Cs}$  from FP Cs for advanced transmutation.
- 5/ Accept and separate natural radioactive materials (U, Th) to burn, on demand of the RE industry.

The most important policy change is that NRM shall not be just the waste constituents but be the main product in the fuel cycle. Actinides will no longer be the products, but will just be the material burned in the reactors. To realize this concept at both scientific and industrial levels, several separation tactics are proposed as follows;

- 1/ Higher purity of NRM for utilization, while lower decontaminated actinides are permitted for burning in FBR. Separation factors of 90-99.9 % will be chosen for the individual impact of radio nucleides.
- 2/ Adopt *soft* hydrometallurgical separation processes with *salt-free* reagents to reduce the secondary radioactive wastes. Ultimately, low greenhouse gas emission technology is required.
- 3/ A high degree of separation of all actinides into 3-4 groups, U, Pu/U/Np, Am and Cm, directly from the spent fuel by an IXC (Ion Exchange Chromatography) method.
- 4/ As non-SX methods, CEE (Catalytic Electrolytic Extraction[14]) and adsorptive separation methods for NRM are chosen to alleviate the radiation effect. Solid state will be preferable as the end product for utilization and/or stockpiling.
- 5/ HCl media is allowed in combination with  $\text{HNO}_3$  media to improve the separability.
- 6/ Identification of anti-corrosive materials in both conc. HCl and  $\text{HNO}_3$  are indispensable from an industrialization point of view. Verification of thermo- and radio-chemical stability of the novel IX resin is also required.
- 7/ Preliminary separation of actinides from the NRM is advantageous because Zr, Mo, Pd,  $^{99}\text{Tc}$ ,  $^{106}\text{Ru}$  and  $^{125}\text{Sb}$ , etc will disturb the operation of both reprocessing and vitrification of HLW.

The time to reduce the radio-toxicity Sv (Sievert) of 1 ton of vitrified HLLW below the level of equivalent tons of natural raw uranium is one of the indexes for environmental impact. In the *Adv.-ORIENT Cycle*, by putting the separation factors at 99.9 % for all actinides, 99 % for  $^{137}\text{Cs}$ ,  $^{90}\text{Sr}$  and the other NRM, and 90 % for Ln, such a period can dramatically be reduced to around 10<sup>2</sup> years.

## 6. Conclusion

The isotopic composition and radiochemical properties of nuclear rare metals have been reviewed. Hydrometallurgical separation technologies using solvent extraction (SX), ion exchange chromatography (IXC) and catalytic electrolytic extraction (CEE) techniques were developed as vital separation tools for light PGM (Ru, Rh, Pd), Tc and *f*-elements present in high level liquid wastes of the nuclear fuel cycle. The IXC process utilizing a tertiary pyridine resin (TPR) gives a high separation of the *f*-elements in spent nuclear fuel and produce pure Am and Cm products. The CEE process utilizing Pd<sub>adatom</sub> or Rh<sub>adatom</sub> can effectively separate PGM, Tc and Re by utilizing under potential deposition (UPD) phenomena.

## REFERENCES

- [1] P. Wager, D. J. Lang and A. Stamp, *R'09 Twin World Congress -Resource Management and Technology for Material and Energy Efficiency-*, Davos, Switzerland, September 14-16(2009).
- [2] M. Ozawa, S. Koyama, R. Fujita and Y. Fujii, *Proc.14<sup>th</sup> International Conference on Emerging Nuclear Energy Systems (ICENES 2009)*, pp.85(2009).
- [3] E.P. Horwitz and D.G. Kalina, *Solvent Extraction and Ion Exchange*, **2**, 179 (1984)
- [4] C. Madic, M.J. Hudson, J.O. Liljenzin, J.P. Glantz, R. Nannicini, A. Facehini, Z. Kolarik and R. Odoj, *Progress in Nuclear Energy*, **40**, 523 (2002)
- [5] Y. Sasaki, S. Suzuki and M. Ozawa, *Fine Chemical*, **38**, 47 (2009).(in Japanese)
- [6] Y. Zhu, *Radiochim. Acta*, **68**, 95 (2005).
- [7] Y. Zhu, J. Chen and R. Jiao, *Solvent Extraction Ion Exchange*, **140**, 61 (1996).
- [8] J. Chen, Y. Zhu and R. Jiao, *Nuclear Technology*, **122**, 64 (1998).
- [9] M. Ozawa, T. Iwai, V. Babain and A. Shadrin, *Solvent Extraction*, **1**, 623 (2008).
- [10] M. Ozawa, V.A. Babain, A. Shadrin, S. Strelkov, *Global 2007 Advanced Nuclear Fuels Cycles and Systems*, CD-ROM, September 9-13, Boise, Idaho, USA(2007).
- [11] M. Ozawa, T. Suzuki, S. Koyama, I. Yamagishi, R. Fujita, K. Okada, K. Tatenuma, H. Mimura and Y. Fujii, *Proc.Global 2009 (CD)*, pp.1117-1126, Paris, France, 6<sup>th</sup> -11<sup>th</sup> September(2009).
- [12] M. Ozawa, S. Koyama, T. Suzuki and Y. Fujii, *Journal of Nuclear and Radiochemical Science*, **6**, 275 (2005).
- [13] M. Ozawa, T. Suzuki, S. Koyama, H. Akatsuka, H. Mimura and Y. Fujii, *Progress in Nuclear Energy*, **50**, 476, ELSEVIER(2008).
- [14] M. Ozawa, M. Ishida and Y. Sano, *Radiochemistry*, **45**, 225 from *Radiokhimiya*, **45**, 205 (2003).

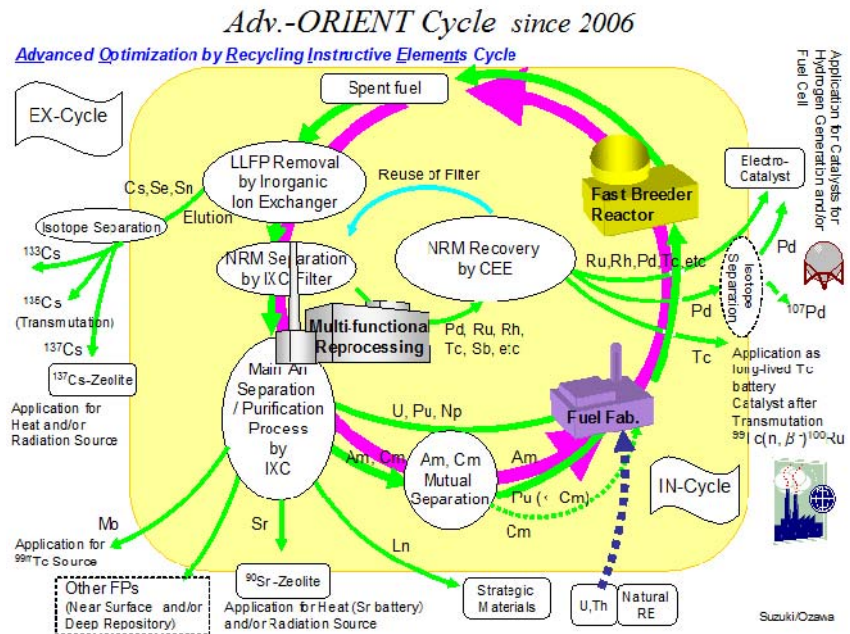


Figure 4 *Adv.-ORIENT Cycle Concept*

Some of the basic work on hydrometallurgical separation of concerned elements is being progressed in the frame of strategic *Advanced (Adv.-) ORIENT Cycle* research program in Japan. The *Adv.-ORIENT Cycle* process can not only improve the rad. waste problem, but also offer useful rare metals to leading industries from this secondary resource.

## B.8 Relativistic Density-Functional Study of the Alloying Behavior of Transition Metal into $\gamma$ -type Solid Uranium

Jun ONOE, Masayoshi KURIHARA, Masaru HIRATA and Chikashi SUZUKI

### 1. Introduction

Uranium alloys have been extensively investigated as fuels for next-generation nuclear reactors. Such alloys include low  $^{235}\text{U}$ -enriched fuels used in research reactors, such as  $\text{U}_3\text{Si}_2$ -aluminum (Al) dispersion fuel [1] and 10-wt% molybdenum (Mo) dispersed in an Al matrix [2, 3]. Zirconium based U-Pu alloy is a promising fuel for advanced fast reactors [4].

Solid uranium has  $\alpha$  (orthorhombic)-,  $\beta$  (tetragonal)- and  $\gamma$  (body centered cubic)- phases: which phase is present depends on the ambient temperature [5]. The  $\alpha$ - and  $\beta$ -U phases form solid solutions with other metallic elements to a limited extent [5], whereas the  $\gamma$ -U phase readily forms solid solutions with other elements [5]. In addition, the  $\alpha$ -U phase forms many intermetallic compounds with other metallic elements [6]. Accordingly, several  $\alpha$ - and/or  $\gamma$ -U/transition metal (TM) alloys have been used in research nuclear reactors [7]. To produce advanced nuclear fuels, it is critical to understand the dissolution process of TM atoms into  $\gamma$ -U in terms of the constitutional diagram. Recently, some groups have theoretically studied the thermodynamic properties of U/TM alloys. Landa *et al.* studied the phase equilibria of U-Zr alloys, using the scalar-relativistic (i.e., without spin-orbit coupling) Green's function technique based on the Korringa-Kohn-Rostoker method [8]. They obtained good agreement between theoretical and experimental results for the ground-state properties of the  $\gamma$ - (bcc) and  $\delta$ - (C32) phases of U-Zr alloys. Li *et al.* obtained the thermodynamic assessments of the Th-U and Th-Zr binary alloys and the Th-U-Zr ternary alloy, using the CALPHAD (Calculation of Phase Diagrams) method based on experimental data that included the phase equilibria and thermodynamic properties of the alloys [9]. They found good agreement between the calculated phase equilibria and experimental data. Ab-initio calculations based on density-functional theory have also been used to examine the thermodynamic properties of U-Al systems [10, 11]. To understand the dissolution of elements in solid U, in addition to obtaining the phase diagram or phase equilibria, it is also necessary to determine which electronic terms contribute to the thermodynamic properties of U alloys by employing density-functional theory in combination with experimental results.

We have previously investigated the alloying behavior of 3d-, 4d- and 5d-TMs in  $\gamma$ -U, using the discrete-variational Dirac-Fock-Slater (DV-DFS) molecular orbital (MO) method [12, 13] taking into account fully relativistic effects including spin-orbit coupling. We found that, with the exception of Ta and W,

the maximum solid solubility (MSS) of TMs in  $\gamma$ -U was exponentially proportional to both the d-orbital energy of the TM (Md) and the orbital overlap population (OOP) between the TM d and U 6d atomic orbitals. The reason for this relation is not currently understood.

The aim of the present report is to clarify the reason of the exponential dependences of Md and OOP on the MSS [14]. The MSS strongly depends on the thermodynamic equilibrium constant ( $K$ ) that varies exponentially on the difference between the Gibbs free energies before and after substituting TM elements in  $\gamma$ -U. We discuss the dependence of the MSS on the Md and the OOP from a thermodynamic perspective.

### 2. Computational details

The DV-DFS MO method [15-17] is a powerful tool for studying the electronic structures of molecules containing heavy elements such as uranium [18-22]. The one-electron molecular Hamiltonian ( $H$ ) in the DV-DFS MO method is written as

$$H = c\alpha P + \beta mc^2 + V(r) \quad (1)$$

Here,  $c$  is the velocity of light,  $P$  is the momentum operator,  $m$  is the rest mass of an electron,  $\alpha$  and  $\beta$  are Dirac matrices, and  $V(r)$  is the sum of Coulomb and exchange-correlation potentials. The MOs were obtained by taking a linear combination of atomic orbitals (AOs). Details of the DV-DFS MO method used in the present study are described elsewhere [15, 23].

The basis functions, which are numerical solutions of the atomic DFS equations in an atomic-like potential, were obtained in the initial stage of iterations using a self-consistent procedure [24]. Thus, each basis function corresponds to an atomic orbital. The atomic-like potentials used for generating the basis functions were derived from the spherical average of the molecular charge density around nuclei obtained by adding a well potential (5.0 au in radius and -0.5 au in depth) for each atom. One-center (atomic) charges were estimated by Mulliken population analysis [25] in the self-consistent charge method [26] based on the self-consistent field approximation. All the DV-DFS MO calculations were performed with a Slater exchange parameter of 0.7 and with 18,000 DV sample points. The basis functions used were 1s-7p AOs for uranium, 1s-4s AOs for 3d TMs, 1s-5s AOs for 4d TMs, and 1s-6s AOs for 5d TMs. All the calculations were performed self-consistently until the difference between the orbital populations before and after every iteration became less than 0.01.

Morinaga *et al.* have demonstrated that the parameter Md is important when considering the alloying behaviors

of metal alloys [27-31]. Md is defined to be a weighted average of the  $d_{3/2}$  and  $d_{5/2}$  orbital energies of the TM. The Md of the TM in  $\gamma$ -U/TM alloys and the U 6d orbital energy of U(1) (see Fig. 1) were evaluated by taking a weighted average of the  $d_{3/2}$  and  $d_{5/2}$  orbitals. The Md value was shifted relative to the Fermi level ( $E_F$ ) of  $\gamma$ -U, which was used as a reference [27, 28].

Since the bond overlap population (Bo) and the orbital overlap population (OOP) respectively express the covalent bonding and interaction strengths between AOs, they have been often used to determine the contributions of individual AOs to covalent bonding [32]. We employed Mulliken population analysis to estimate the Bo and the OOP [25]. The Bo,  $P_B(k,l)$ , for a specific pair of atoms  $k$  and  $l$  in a polyatomic molecule is defined as

$$P_B(k,l) = \sum_{(i)} \sum_{(r,s)} 2N_{(i)} C_{ir}^k C_{is}^l \langle \phi_r^k | \phi_s^l \rangle \quad (2),$$

where  $N_{(i)}$  denotes the number of the electrons that occupy the  $i$ th MO and  $C_{ir}^k$  and  $C_{is}^l$  respectively represent the coefficients of the normalized AOs,  $\phi_r^k$  and  $\phi_s^l$ , in the linear combination of AOs for the  $i$ th MO. In a similar manner, the OOP,  $P_O(k,r,l,s)$ , for the  $\phi_r^k$  and  $\phi_s^l$  AOs is also defined as

$$P_O(k,r,l,s) = \sum_{(i)} 2N_{(i)} C_{ir}^k C_{is}^l \langle \phi_r^k | \phi_s^l \rangle \quad (3).$$

As described above, each basis function used in the present method corresponds to a specific AO, so that Eqs. (2) and (3) enable us to discuss the roles of individual AOs in the electronic structures and chemical bonding of molecules and condensed matters.

Figure 1 shows a schematic representation of a model cluster for discussing the alloying behavior of TM atoms in  $\gamma$ -U.

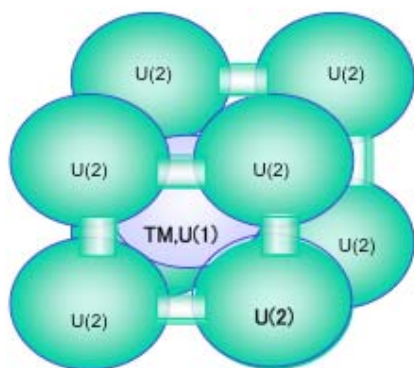


Fig. 1. Schematic representation of a cluster model for  $\gamma$ -U/TM alloys in which the central U atom is replaced by a TM atom in the unit cell of  $\gamma$ -U.

The central uranium atom [U(1)] is substituted by a TM atom. We used this model cluster for the following three reasons; (1) a similar small cluster consisting of nine U

atoms reproduced the photoelectron spectra of solid  $\alpha$ -phase U well [22]; (2) a similar small cluster consisting of one C and eight U atoms reproduced the photoelectron spectra of solid UC reasonably well [21]; (3) Morinaga *et al.* predicted the functional properties of metal alloys using such a small model cluster [31]. In addition, since the electrons in metal alloys are not significantly polarized like ionic bonded crystals, it is not necessary to consider point charges surrounding the present model cluster.

To determine the differences in the electronic structures of the  $\gamma$ -U/TM alloys, the MO energy level structures and the chemical bonding of the  $\gamma$ -U/TM alloys were examined [13]. In the present study, lattice relaxation caused by the substitution of a TM atom was ignored because the values of Md and the OOP were not expected to be significantly affected by lattice relaxation [27-29]. The lattice constant of the model cluster was taken from the experimental value of 6.659 au for  $\gamma$ -U crystal [33].

### 3. Results and Discussion

Figure 2 shows a plot of the MSS as a function of the energy difference ( $\alpha_U - \alpha_{TM}$ ) between the U6d and TMd AOs for  $\gamma$ -U/TM alloys. The energy difference ( $\alpha_U - \alpha_{TM}$ ) is used to discuss charge transfer between U and TM atoms: it is an important parameter for quantum design of metal alloys [31]. Figure 2 shows that the MSS exhibits an inverse exponential dependence on ( $\alpha_U - \alpha_{TM}$ ), so that a smaller value of ( $\alpha_U - \alpha_{TM}$ ) provides a larger MSS. Since the energy difference between the d orbitals is related to the magnitude of charge transfer between them, Figure 2 implies that a smaller charge transfer between TM and U atoms gives rise to a larger MSS for  $\gamma$ -U/TM alloys.

Figure 3 shows the correlation between the Bo and the MSS for  $\gamma$ -U/TM alloys (top), along with Fig. 7 of Ref. 10 showing the correlation between the TM d/U 6d OOP and the MSS (bottom). Although the Bo is thought to be a good parameter for predicting the physicochemical properties of metal alloys [27-31], the top of Fig. 3 indicates that there is a poor correlation between the Bo and the MSS. On the other hand, the bottom of Fig. 3 demonstrates the exponential dependence of the MSS on the OOP for all  $\gamma$ -U/TM alloys except those containing Ta and W. Thus, increasing the OOP increases the MSS of  $\gamma$ -U/TM alloys.

Figures 2 and 3 reveal that the parameters describing the correlation between the TM d and U 6d AOs play an important role in determining the magnitude of the MSS of  $\gamma$ -U/TM alloys. In other words, the orbital interaction between the TM d and U 6d AOs is a key parameter for estimating the MSS. We next discuss the physical effect of TM d/U 6d orbital interactions on the MSS.

Figure 4 shows a schematic illustration depicting the relationship between the orbital interactions between the U 6d and TM d AOs based on the simple Hückel approximation [34] and the MSS.

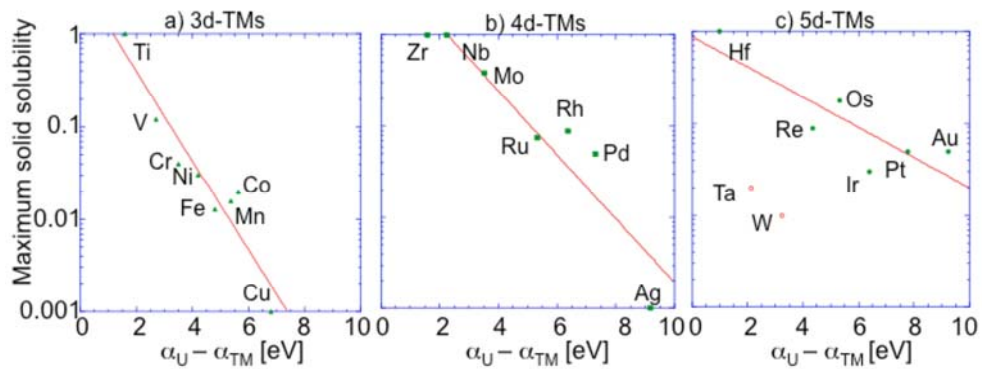


Fig. 2. Plot of the MSS as a function of the energy difference ( $\alpha_U - \alpha_{TM}$ ) between the U 6d and TM d AOs.

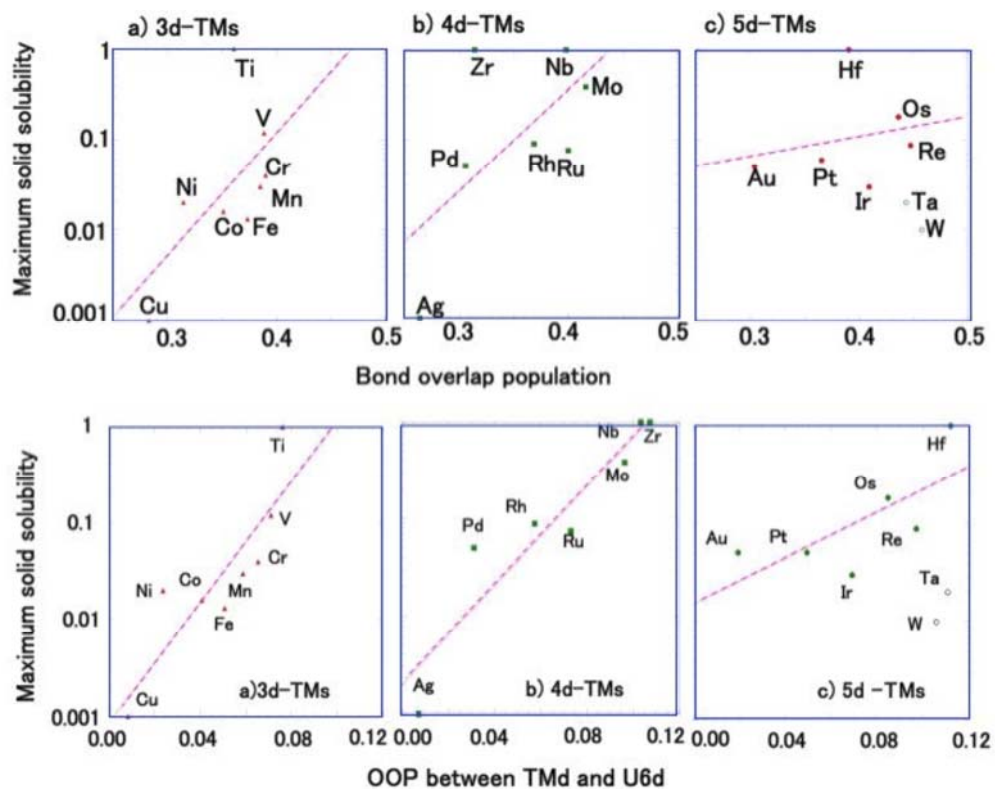


Fig. 3. Plot of the MSS as a function of the Bo (top) and the U 6d – TM d OOP (bottom: taken from Fig. 7 of Ref. 10).

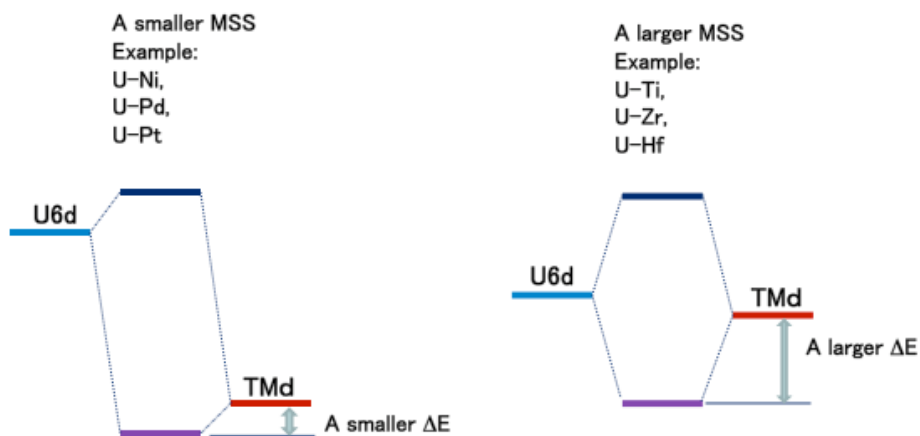


Fig. 4. Schematic illustration of the correlation between the MSS, the stabilization energy ( $\Delta E$ ), and the U 6d – TM d orbital energy difference ( $\alpha_U - \alpha_{TM}$ ).

Using this approximation, the stabilization energy ( $\Delta E$ ) generated by the orbital interactions between the TM d and U 6d AOs can be expressed as

$$\Delta E = \frac{1}{2} \left[ \sqrt{(\alpha_U - \alpha_{TM})^2 + 4\beta^2} - (\alpha_U - \alpha_{TM}) \right] \quad (\alpha_U > \alpha_{TM}) \quad (4).$$

Here,  $\alpha_U$  and  $\alpha_{TM}$  respectively denote the energies of the U 6d and TM d AOs;  $\alpha_U$  is always greater than  $\alpha_{TM}$  (see Fig. 4 of Ref. 12).  $\beta$  expresses the resonance integral between them, which is proportional to the overlap integral (S) between the AOs and to the OOP. To discuss the correlation between  $\Delta E$  and Md/OOP more clearly, we

introduce the variables  $t = \frac{(\alpha_U - \alpha_{TM})}{2|\beta|}$  and

$F(t) = \sqrt{t^2 - 1} - t$  into Eq. (4).  $\Delta E$  can then be rewritten as:

$$\Delta E = F(t) \cdot |\beta| \quad (5).$$

By considering the ranges of the two quantities on the right-hand side of Eq. (5) (i.e.,  $t \geq 0$  and  $0 < F(t) \leq 1$ ), we obtain

$$0 < \Delta E \leq |\beta| \quad (6).$$

Accordingly,  $\Delta E$  is a maximum ( $= |\beta|$ ) when  $F(t)$  is unity at  $t = 0$ . Thus,  $\Delta E$  is maximized when  $\alpha_U = \alpha_{TM}$ . Conversely,  $\Delta E$  becomes very small when the energy difference ( $\alpha_U - \alpha_{TM}$ ) is much larger than unity ( $\gg 1$ ). Consequently, a larger MSS for  $\gamma$ -U/TM alloys is obtained for a lower value of ( $\alpha_U - \alpha_{TM}$ ) (corresponding to a larger  $\Delta E$ ), whereas a smaller MSS is obtained for a larger value of ( $\alpha_U - \alpha_{TM}$ ) (corresponding to a smaller  $\Delta E$ ). This tendency can explain the results shown in Fig. 2. As Eq. (5) shows,  $\Delta E$  also depends on  $|\beta|$ , which is proportional to the overlap integral S. Because the OOP increases with increasing S,  $\Delta E$  also increases with increasing OOP. This tendency can also explain the result of Fig. 3 (bottom). Consequently, it can be concluded that the magnitude of  $\Delta E$  generated by the interactions between TM d and U 6d AOs plays a key role in determining the magnitude of the MSS.

Why does the MSS vary exponentially with the Md [or ( $\alpha_U - \alpha_{TM}$ )] and the OOP? We employed the present model cluster (see Fig. 1) as the basis for forming  $\gamma$ -U/TM alloys by substituting the central U atom with a TM atom. The following equilibrium has been considered using this model cluster



where, TM denotes a TM atom in the TM phase, whereas  $U_9/U_8TM$  and U respectively denote a model cluster and an atom in the  $\gamma$ -U phase. When the equilibrium constant ( $K$ ) of Eq. (7) increases, the concentration of  $U_8TM$  increases, thus increasing the MSS. On the other hand,

when  $K$  decreases, the  $U_8TM$  concentration decreases, thus reducing the MSS. Consequently, the MSS is proportional to  $K$ . The MSS and  $K$  can then be written as

$$MSS \propto K = Ae^{-\frac{\Delta G}{RT}} \quad (8).$$

Here, A is a constant,  $\Delta G$  denotes the Gibbs free energy difference before and after the substitution,  $R$  is the gas constant, and  $T$  is the absolute temperature. Since the lattice relaxation on substitution is negligible, the entropy is constant ( $\Delta S = 0$ ) in the present substitution model. Thus,  $\Delta G$  is equal to the enthalpy difference ( $\Delta H$ ) before and after the substitution. Accordingly, Eq. (8) can be expressed as

$$MSS \propto K = Ae^{-\frac{\Delta G}{RT}} = Ae^{-\frac{\Delta H}{RT}} \quad (9).$$

Since  $\Delta H$  includes  $\Delta E$  due to the TMd-U6d orbital interactions, the following relationship is obtained

$$MSS \propto K = Ae^{-\frac{\Delta H}{RT}} \propto e^{-\frac{\Delta E}{RT}} \quad (10).$$

As mentioned above,  $\Delta E$  is proportional to both ( $\alpha_U - \alpha_{TM}$ ) and S. Consequently, the MSS depends exponentially on both Md and the OOP.

Using Md and the OOP as parameters for determining the MSS, we examined the OOP-Md plot for  $\gamma$ -U/TM alloys. Figure 5 shows the correlation map between the two parameters.

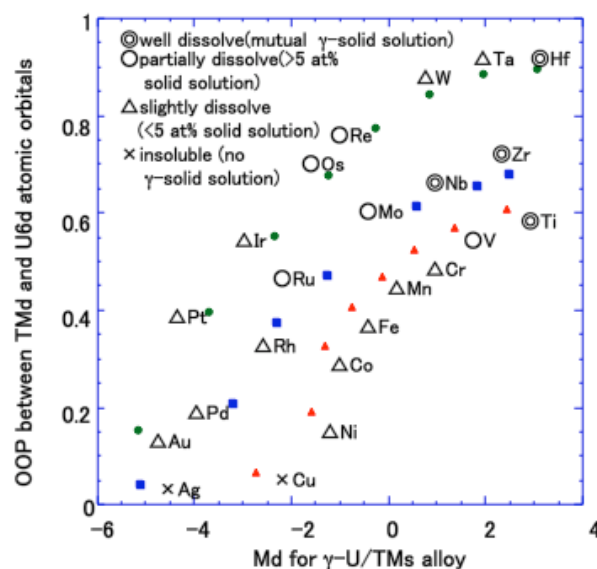


Fig. 5. OOP-Md plot for  $\gamma$ -U/TM alloys.

Interestingly,  $\gamma$ -U/TM alloys with a lower MSS appear in the lower left of the OOP-Md map, whereas those with a higher MSS appear in the upper right. Thus, the map obtained using the OOP and Md is useful for designing  $\gamma$ -U/TM alloys. We believe that the present map can be used for other alloy systems besides the present alloy system.

#### 4. Summary

We performed the relativistic DFT calculations for  $\gamma$ -UTM alloys. Md and the OOP (U 6d–TM d) exhibited good correlations with the MSS for  $\gamma$ -U/TM alloys. The magnitude of the MSS was explained based on the stabilization energy ( $\Delta E$ ) caused by U6d–TMd orbital interactions for  $\gamma$ -U/TM alloys. The exponential dependence of the MSS on Md and the OOP was explained in terms of the equilibrium constant obtained using a substitution cluster model for  $\gamma$ -U/TM alloys. The OOP–Md plot is a good map for determining the MSS magnitude of  $\gamma$ -U/TM alloys. We believe that it can be used for other alloy systems besides the present alloy system.

#### References

- [1] K.-H. Kim, J.-M. Park, C.-K. Kim, G.L. Hofman and K.-W. Paik, *J. Nucl. Mater.* **270**, 315 (1999).
- [2] K.-H. Kim, J.-H. Park, G.L. Hofman and M.K. Meyer, *Nucl. Eng. Design* **211**, 229 (2002).
- [3] M.K. Meyer, G.L. Hofman, S.L. Clark, T.C. Wiencek, J.L. Snelgrove, R.V. Strain and K.-H. Kim, *J. Nucl. Mater.* **304**, 221 (2002).
- [4] W. Chernock and K.E. Horton, *IAEA TECDOC-791*, 68 (1994).
- [5] P. Chiotti, V.V. Akhachinskij and I. Ansara, “*The Chemical Thermodynamics of Actinide Elements and Compounds*”, Part 5, IAEA, Vienna (1981).
- [6] A.R. Kaufman, “*Nuclear Reactor Fuel Elements*”, Interscience, Butterworth (1962).
- [7] R.W. Buzzard, Progress Report-Alloying Theory, *National Bureau of Standard Report*, 4032 (1955).
- [8] A. Landa, P. Soderlind and P.E.A. Turchi, *J. Alloys Compd.* **478**, 103 (2009).
- [9] Z.S. Li, X.J. Liu and C.P. Wang, *J. Alloys Compd.* **476**, 193 (2009).
- [10] P.R. Alonso, J.R. Fernandez, P.H. Gargano and G.H. Rubiolo, *Physica B* **404**, 2851 (2009).
- [11] D. Sedmidubsky, R.J.M. Konings and P. Soucek, *J. Nucl. Mater.* **397**, 1 (2010).
- [12] M. Kurihara, M. Hirata, J. Onoe and H. Nakamatsu, *Prog. Nucl. Ener.* **50**, 549 (2008).
- [13] M. Kurihara, M. Hirata, R. Sekine, J. Onoe and H. Nakamatsu, *J. Nucl. Mater.* **326**, 75 (2004).
- [14] M. Kurihara, J. Onoe, M. Hirata, and C. Suzuki, *J. Alloys Compd.* **509**, 1152 (2011).
- [15] A. Rosen and D. E. Ellis, *J. Chem. Phys.* **62**, 3039 (1975).
- [16] H. Adachi, A. Rosen, and D. E. Ellis, *Mol. Phys.* **33**, 199 (1977).
- [17] H. Nakamatsu, H. Adachi and T. Mukoyama, *Bull. Inst. Chem. Res., Kyoto Univ.* **68**, 304 (1991).
- [18] M. Hirata, H. Monjyushiro, R. Sekine, J. Onoe, H. Nakamatsu, T. Mukoyama, H. Adachi and K. Takeuchi, *J. Electron Spectrosc. Relat. Phenom.* **83**, 59 (1997).
- [19] J. Onoe, K. Takeuchi, H. Nakamatsu, T. Mukoyama, R. Sekine and H. Adachi, *J. Electron Spectrosc. Relat. Phenom.* **60**, 29 (1992).
- [20] J. Onoe, K. Takeuchi, H. Nakamatsu, T. Mukoyama, R. Sekine and H. Adachi, *J. Electron Spectrosc. Relat. Phenom.* **70**, 89 (1994).
- [21] M. Kurihara, M. Hirata, R. Sekine, J. Onoe, H. Nakamatsu, T. Mukoyama and H. Adachi, *J. Alloys Compd.* **283**, 128 (1999).
- [22] M. Kurihara, M. Hirata, R. Sekine, J. Onoe, H. Nakamatsu, T. Mukoyama and H. Adachi, *J. Nucl. Mater.* **281**, 140 (2000).
- [23] J. Onoe, K. Takeuchi, H. Nakamatsu, T. Mukoyama, R. Sekine, B. J. Kim and H. Adachi, *J. Chem. Phys.* **99**, 6810 (1993).
- [24] H. Adachi, M. Tsukada and C. Satoko, *J. Phys. Soc. Jpn.* **45**, 875 (1977).
- [25] R. S. Mulliken, *J. Chem. Phys.* **23**, 1833 (1955); **23**, 1841 (1955); **23**, 2338 (1955); **23**, 2348 (1955).
- [26] A. Rosen, D. E. Ellis, H. Adachi and F. W. Averil, *J. Chem. Phys.* **65**, 3629 (1976).
- [27] M. Morinaga, N. Yukawa and H. Adachi, *J. Phys. Soc. Jpn.* **53**, 653 (1984).
- [28] M. Morinaga, N. Yukawa and H. Adachi, *J. Phys. F. Met. Phys.* **15**, 1071 (1985).
- [29] M. Morinaga, N. Yukawa, H. Ezaki and H. Adachi, *Phil. Mag.* **51**, 223 (1985); **51**, 247 (1985).
- [30] M. Moringa, S. Nasu, H. Adachi, J. Saito and N. Yukawa, *J. Phys. Cond. Mater.* **3**, 6817 (1991).
- [31] M. Morinaga, Y. Murata and H. Yukawa, “*Hartree-Fock-Slater Method for Materials Science: The DV-X $\alpha$  Method for Design and Characterization of Materials*” (H. Adachi, T. Mukoyama, J. Kawai, eds.), Springer Series in Materials Science, vol. 84, 23 (2005).
- [32] J. Onoe, *J. Phys. Soc. Jpn.* **66**, 2326 (1997).
- [33] W. B. Pearson, “*A Handbook of Lattice Spacings and Structure of Metals and Alloys*” (Vol. 2), Pergamon Press (1967).
- [34] E. Hückel, *Z. F. Phys.* **70**, 204 (1931).

## B.9 Molecular Mechanisms of DNA Double-Strand Break Repair And Its Potentiality toward Cancer Radiotherapy

Yoshihisa MATSUMOTO, Radhika Pankaj KAMDAR and Mukesh Kumar SHARMA

### 1. Introduction

DNA double-strand breaks (DSBs) are considered most critical lesion among those generated by ionizing radiation [1]. DSB are caused also by radiomimetic drugs, or spontaneously, by oxidative stresses or replication errors. Eukaryotic cells have evolved two major pathways to repair DNA DSBs: non-homologous end-joining (NHEJ) and homologous recombination (HR). NHEJ is a reaction to heal DSB by joining most adjacent DSBs with minimal modifications (Fig.1). One of the key players in NHEJ, especially in vertebrates, is DNA-dependent protein kinase (DNA-PK), composed of the catalytic subunit (DNA-PKcs) and heterodimeric Ku protein (Ku86 and Ku70). Because of its striking property to be activated upon binding to the ends of double-stranded DNA, DNA-PK is thought to act as the sensor to recognize DSBs, initiating NHEJ and, possibly, other DNA damage responses. Another core component of NHEJ pathway is the complex of XRCC4 and DNA ligase IV, which is thought to join the DSBs finally. Recently, a new essential factor of NHEJ, named XLF or Cernunnos, which is associated with XRCC4-DNA ligase IV complex, was identified. Our research has sought to clarify the detailed molecular mechanism of NHEJ, especially spatiotemporal regulation of NHEJ machinery, and to explore potential applicability in cancer diagnosis and therapeutics.

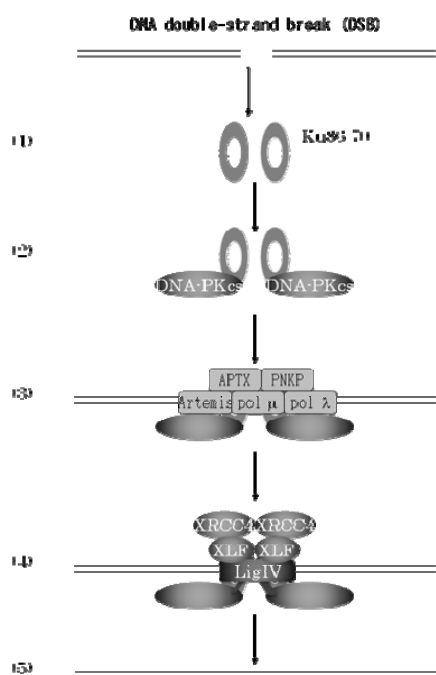


Fig.1 DNA double-strand break repair through non-homologous end-joining.

### 2. Recruitment of XRCC4-DNA ligase IV complex to DSB

There are several lines of evidence *in vitro* indicating that DNA-PKcs and/or Ku directly associate with XRCC4-DNA ligase IV and facilitate its recruitment to DNA ends. However, it remains to be clarified how these proteins are recruited to DSB sites and assembled into repair machinery, especially in living cells [1].

Many proteins in the homologous recombination pathway, *e.g.*, Nbs1-Mre11-Rad50, BRCA1 and Rad51, exhibit local accumulation after DSB induction, forming microscopically visible structures, termed ionizing radiation-induced foci (IRIF) [2]. Such change in the localization of HR proteins has been observed also in partial volume irradiation and laser micro-irradiation experiments. As the distribution of these proteins after irradiation, at least partially, overlapped with irradiated area or DSBs, visualized by DNA end labeling or immunofluorescence analysis of  $\gamma$ -H2AX, these phenomena are believed to reflect the accumulation of these proteins around DSB sites. In the case of NHEJ proteins, however, IRIF has been observed only for autophosphorylated form of DNA-PKcs. The failure or difficulty to detect IRIF of NHEJ proteins might be attributable to several reasons, which are not mutually exclusive: (i) only a very small number of molecules might be recruited to each DSB and, thereby, do not appear as foci. (ii) NHEJ proteins, especially Ku and DNA-PKcs, are abundant. Therefore, even if some NHEJ molecules really moved to DSB sites, their overall distribution would not change to a discernable extent. (iii) As NHEJ is a very rapid reaction, healing most of DSBs within minutes after irradiation, the association of NHEJ enzymes with DSB might be very transient and, thereby, difficult to be captured. Recently, several studies using laser micro-irradiation demonstrated the accumulation of NHEJ molecules in irradiated area but local dose may be high.

Another approach to examine the association of DNA repair proteins with damaged DNA is sequential extraction with increasing concentration of detergent or salt. This approach has been used to demonstrate the recruitment and retention of ATM and Nbs1/Mre11/Rad50 complex to DSB site. Using this approach, we detected and analyzed the association of XRCC4 with chromatin DNA, which was induced by ionizing irradiation [3]. A subpopulation of XRCC4 changed into a form that is resistant to the extraction with 0.5 % Nonidet P-40-containing buffer after irradiation. This form of XRCC4 was liberated by micrococcal nuclease treatment, indicating that it had been tethered to chromatin DNA. This chromatin-recruitment

of XRCC4 could be seen immediately (<0.1 hr) after irradiation and remained up to 4 hr after 20 Gy irradiation. It was seen even after irradiation of small doses, *i.e.*, 2 Gy, but the residence of XRCC4 on chromatin was very transient after 2 Gy irradiation, returning to near normal level in 0.2 - 0.5 hr after irradiation. The chromatin-bound XRCC4 represented only ~1 % of total XRCC4 molecules even after 20 Gy irradiation and the quantitative analysis using purified protein as the reference suggested that only a few XRCC4-DNA ligase IV complexes were recruited to each DNA end. The present study would provide us with useful experimental tools and important insights to understand the DNA repair process through NHEJ pathway. We could further show that the chromatin-recruitment of XRCC4 was not attenuated by wortmannin, an inhibitor of DNA-PK, or siRNA-mediated knockdown of the DNA-PK catalytic subunit (DNA-PKcs), indicating that this process does not require DNA-PKcs [3].

### 3. Role of protein phosphorylation by DNA-PK in NHEJ

DNA-PK can phosphorylate *in vitro* a number of proteins and there are lines of evidence indicating the requirement for the kinase activity of DNA-PKcs in its NHEJ function. Catalytically inactive form of DNA-PKcs can restore at most partial NHEJ activity to DNA-PKcs deficient cells. It has remained to be elucidated which protein, and for what reason, should be phosphorylated by DNA-PK. We have identified four phosphorylation sites in XRCC4 and two phosphorylation sites in XLF *in vitro* and verified *in vivo* phosphorylation using phosphorylation specific antibodies against these new sites (manuscript in preparation). By the use of these phosphorylation specific antibodies, we have also observed that these phosphorylation sites in XRCC4 are found to be phosphorylated in living cells in response to ionizing radiation. These phosphorylation sites in the XRCC4 are also biologically important in the process of DNA repair, we have mutated these phosphorylation sites into alanine and found that three of these phosphorylation sites might be important for DNA repair function, as loss of them lead to elevated radiosensitivity with deficient DNA repair capability. Altogether, these results would indicate that XRCC4 phosphorylation by DNA-PK is an essential event in NHEJ repair pathway of DNA double strand break.

### 4. DNA-PK activity and cancer prognosis

In collaboration with Dr. Koichi Sakata, Dr. Masanori Someya and their colleagues at Department of Radiology, Sapporo Medical University, we have pursued relationship of DNA-PK with radiosensitivity and cancer susceptibility [4]. In 2006, we found that DNA-PK activity in peripheral blood lymphocytes (PBLs) of cervical cancer or breast cancer patients are significantly lower than that of healthy volunteers [5]. We further found that DNA-PK activity correlated with protein and mRNA expression level of DNA-PKcs, Ku86 and Ku70, which are

coordinately regulated. Through cDNA array analyses, we found that E2F might underlie this coordinated regulation of DNA-PK components [6]. From these observations, we inferred that measurement of DNA-PK activity would be useful in screening individuals with high cancer risks, who may be subjected to further, in-depth examinations. From a follow-up study, we found that cancer patients with lower DNA-PK activity exhibited higher distant metastasis rate and poorer prognosis [7]. These results suggested that measurement of DNA-PK activity would serve as a marker to predict the prognosis of cancer.

### Acknowledgements

We thank Dr. Koki Sato (Kinki University) for generous permission to use cell line and Mr. Isao Yoda (Tokyo Institute of Technology) and Dr. Atsushi Enomoto (University of Tokyo) for assistance in irradiation. We also appreciate the assistance and cooperation of laboratory members. MKS accomplished this work as a JSPS (Japan Society for the Promotion of Sciences) Postdoctoral Fellow. This study is supported by Grant-in-Aid for Scientific Research from JSPS and MEXT.

### References

- [1] Matsumoto, Y. Biological defense mechanisms against DNA double-strand breaks and their possible medical applications. *J. Surface Sci. Soc. Jpn.*, **32**, 569-574 (2011).
- [2] Kamdar, R.P. and Matsumoto, Y. DNA double-strand break repair through non-homologous end-joining: recruitment and assembly of the players. In *DNA Repair, Book 4*, InTech, in press (2011).
- [3] Kamdar, R.P. and Matsumoto, Y. Radiation-induced XRCC4 Association with Chromatin DNA Analyzed by Biochemical Fractionation. *J. Radiat. Res.*, **51**, 303-313 (2010).
- [4] Sakata, K., Someya, M., Matsumoto, Y., and Hareyama, M. Ability to repair DNA double-strand breaks related to cancer susceptibility and radiosensitivity. *Radiat. Med.* **25**, 433-438 (2007).
- [5] Someya, M., Sakata, K., Matsumoto, Y., Yamamoto, H., Monobe, M., Ikeda, H., Ando, K., Hosoi, Y., Suzuki, N. and Hareyama, M. The association of DNA-dependent protein kinase activity with chromosomal instability and risk of cancer. *Carcinogenesis*, **27**, 117-122 (2006).
- [6] Sakata, K., Yamamoto, H., Matsumoto, Y., Someya, M. and Hareyama, M. cDNA analysis of gene expression associated with DNA-dependent protein kinase activity. *Int. J. Oncol.*, **30**, 413-420 (2007).
- [7] Someya, M., Sakata, K., Matsumoto, Y., Kamdar, R.P., Kai, M., Toyota, M. and Hareyama, M. The association of DNA-dependent protein kinase activity of peripheral blood lymphocytes with prognosis of cancer. *Brit. J. Cancer*, **104**, 1724-1729 (2011)

## B.10 Local Structural Analyses of Molten Thorium Fluoride in Mono - and Divalent Cationic Fluorides

Haruaki MATSUURA, Atsushi NEZU and Hiroshi AKATSUKA

Thorium has been recently focused by the environmental problem on extracting rare earths from ores, such as monazite. Actually thorium can be utilized for nuclear fertile material, thus the electrochemical process is one of promising techniques of separation from rare earth elements. To investigate the relationship between electrochemical behaviour and physico - chemical properties of thorium is important for process design, but structural information of the related materials is still limited. Thus, EXAFS analysis of molten thorium fluoride in mono- and divalent cationic fluoride mixtures have been systematically carried out to elucidate the variation of local structure of thorium cation in various melts.

$\text{ThF}_4$  was synthesized by the fluorination of  $\text{ThO}_2$  with fluorine gas. The samples with monovalent and divalent cationic fluorides containing  $\text{ThF}_4$  were obtained by melting the mixtures in a glassy carbon crucible. The samples for EXAFS measurements were prepared as pressed pellets with boron nitride powder in an argon circulated glove box. These pellets were sanded with two pyrolytic boron nitride plates, tightly bound by bolts and nuts and thoroughly installed in boron nitride (HIP grade) cylindrical cell which can be tightly closed by screwed covers [1]. These sample units were set in the center of an electric furnace which was filled with helium gas under ca 30 kPa, and heated up to certain temperatures to obtain EXAFS spectra. Thorium  $L_{III}$  edge spectra of transmission mode have been collected at BL27B, photon factory, KEK using a double crystals monochromator of Si 111 plane. In some cases, anharmonic oscillation effect in the spectra at high temperature could not be ignored, thus the structural parameters including cumulants were obtained by the curve fitting analysis.

Molecular dynamics simulation of the related ternary systems was also carried out by using the polarisable ionic model [2]. The temperature equilibrated systems of ca. 500 atoms in each box were obtained by the NPT ensemble. To focus on the stability of the local coordination, the cage correlation function, which shows the portion of the number of anions going out from the 1<sup>st</sup> coordination sphere was derived.

The structural parameters obtained by the curve fitting analysis of EXAFS spectra of  $x\text{ThF}_4 - (1-x)\text{MF}$  ( $M = \text{Li}$  and  $\text{Na}$ ,  $0 < x < 1$ ) are shown in Fig. 1. With decreasing the concentration of  $\text{ThF}_4$ , coordination number tends to decrease upto ca. 7 in both systems. This tendency of coordination number of local structure depending on the concentration of  $\text{ThF}_4$  has been also confirmed by NMR and Raman spectroscopic studies in  $\text{ThF}_4$  mixtures as well as  $\text{ZrF}_4$  mixtures which can be sometimes used as a simulant of  $\text{ThF}_4$  [2]. The most striking feature can be

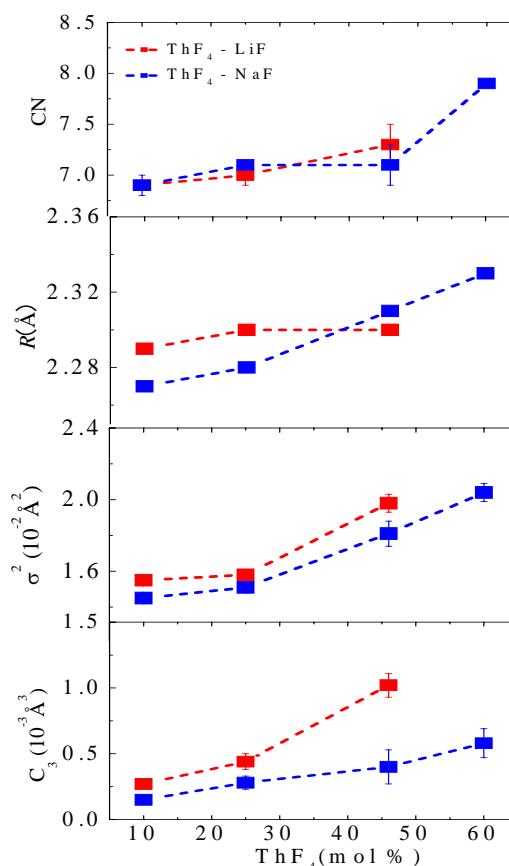


Fig. 1 Structural parameters obtained by EXAFS of molten  $x\text{ThF}_4 - (1-x)\text{MF}$  ( $M = \text{Li}$  and  $\text{Na}$ ,  $0 < x < 1$ ) mixtures, from the top, coordination number, inter-ionic distance, Debye-Waller factor and  $C_3$  cumulant.

found in the tendency of  $\sigma$  and  $C_3$  cumulant. With decreasing the concentration of  $\text{ThF}_4$ , both  $\sigma$  and  $C_3$  decrease, and the values in  $\text{ThF}_4\text{-NaF}$  system are smaller than those in  $\text{ThF}_4\text{-LiF}$  system in general. These features have been also confirmed in the mixture systems including  $\text{TbF}_3$  [3].

To confirm these structural variations extracted from EXAFS, the molecular dynamics simulation of molten  $x\text{ThF}_4 - (1-x)\text{LiF}$  have been also carried out. The time dependence of cage correlation functions of 1<sup>st</sup>  $\text{Th}^{4+}$ -F shell was derived. With decreasing the concentration of  $\text{ThF}_4$ , the structure of 1<sup>st</sup> coordination shell keeps much longer. According to the results by the MD, the 1<sup>st</sup> coordination structure becomes much stabilised with decreasing the concentration of  $\text{ThF}_4$ .

To explain the local structural variation of these mixtures, two factors can be proposed, (1) the balance of coulombic interactions between cation and anion, and (2) number density of fluoride ion. From the first point, as shown in EXAFS results,  $\text{Na}^+$  makes the local structure stabilised around  $\text{Th}^{4+}$  much than  $\text{Li}^+$  does. Since the ionic radius of  $\text{Na}^+$  (0.99 Å) is larger than that of  $\text{Li}^+$  (0.59 Å), thus  $\text{Li}^+$  can approach much closer to the fluorides coordinated around  $\text{Th}^{4+}$ . This leads to large exchange rate of the fluoride around  $\text{Th}^{4+}$  coordination sphere when  $\text{Li}^+$  adds to the mixtures. From the second point, with decreasing the concentration of  $\text{ThF}_4$ , number density decreases. It means that smaller number density results in the smaller exchange rate of fluoride around  $\text{Th}^{4+}$ , that is, the local structure around  $\text{Th}^{4+}$  becomes much stabilised. It has been well known that multivalent cationic chloride melts take network like structure in the pure compounds, and these network like structure is broken with increasing alkali cations [4]. This typical feature is also exactly confirmed in this system.

On the contrary to the relatively simple tendency of the local structure around  $\text{Th}^{4+}$  in monovalent cationic fluoride mixtures, the additional effect of divalent cation is slightly complicated. The  $\text{CaF}_2$  concentration dependence of local structural parameters derived from EXAFS of the constant concentration of  $x_{\text{ThF}_4} = 0.25$  are shown in Fig. 2. Although inter-ionic distance is independent from the concentration of  $\text{CaF}_2$ , coordination number, Debye-Waller factor and  $C_3$  cumulant parameter increase once until the concentration of  $x_{\text{CaF}_2} = 0.17$ , but these values decrease with increasing at  $x_{\text{CaF}_2} > 0.17$ . The local structure of thorium cation has been un - stabilized until certain concentration of calcium fluoride and then going to be stabilized by further addition of calcium fluoride.

To confirm the complicated tendency, the MD simulation of molten  $0.25\text{ThF}_4\text{-LiF-CaF}_2$  has also been performed. The complicated feature depending on the concentration of  $\text{CaF}_2$  is also identified in the cage correlation functions. The diminishing rate of the function is once getting larger, but going back to smaller. This tendency is quite consistent to that derived from the structural parameters obtained by EXAFS.

To explain the complicated feature of mixing by  $\text{CaF}_2$ , (a) balance of coulombic interaction and (b) number density of fluoride are to be discussed again. The ionic radius of  $\text{Ca}^{2+}$  (1.00 Å) is very close to  $\text{Na}^+$  (0.99 Å), thus coulombic interaction between  $\text{Ca}^{2+}$  and  $\text{F}^-$  is even much stronger than that between  $\text{Na}^+$  and  $\text{F}^-$  due to their cationic valences. However, the effect of  $\text{CaF}_2$  on the 'stability of local structure' is not monotonously changed. In the case of mixtures with  $\text{CaF}_2$ , the number density of fluoride affects much to the local structure. In the case of molten  $\text{ThF}_4\text{-LiF-CaF}_2$  system, the number density of fluoride is almost constant until  $x_{\text{CaF}_2} = 0.5$ , thus  $\text{CaF}_2$  acts 'fluoride donor' when the concentration of  $\text{CaF}_2$  is relatively small. When the concentration of  $\text{CaF}_2$  is getting larger, the number density of fluoride decreases, thus the local structure tends to be stabilised. The sensitivity of number density to the local structure in the case of the mixtures

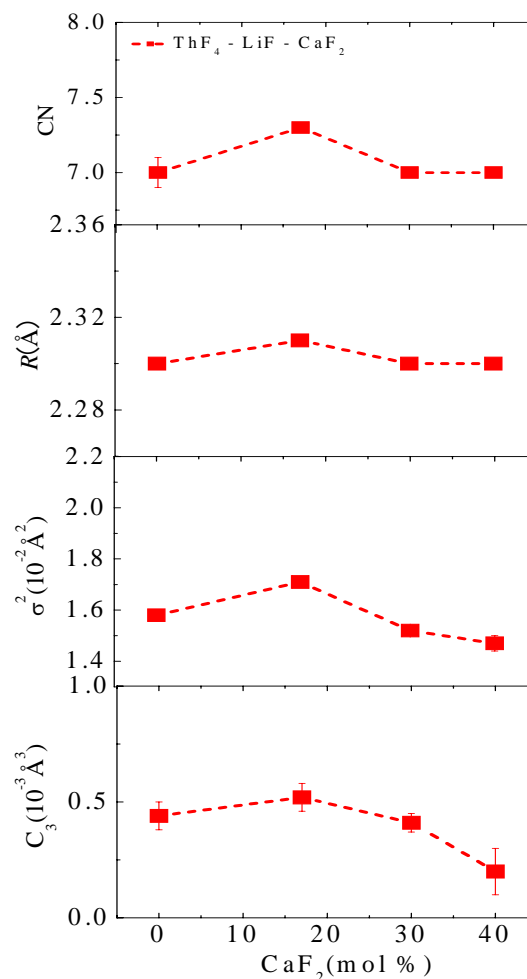


Fig. 2 Structural parameters obtained by EXAFS of molten  $0.25\text{ThF}_4-(0.75-x)\text{LiF}-x\text{CaF}_2$  mixtures ( $0 < x < 1$ ), from the top, coordination number, inter-ionic distance, Debye-Waller factor and  $C_3$  cumulant.

with  $\text{CaF}_2$  is reasonable, since coulombic interaction between multivalent cations and  $\text{F}^-$  is much strongly influenced than that between alkali cations and  $\text{F}^-$ . These facts imply that, for dynamic properties, even relatively small variation of number density of fluoride (it is equivalent to average distance among fluorides) can overcome the balance of coulombic interaction from microscopic point of view.

This study was done by a collaboration research with Prof. N. Sato, Tohoku University and Dr. C. Bessada, CEMHTI, CNRS, France. The authors thank to Drs. Y. Okamoto, H. Shiwaku, T. Yaita, JAEA for valuable discussions.

#### References

- [1] C. Bessada, et al, *Nucl. Sci. NEA/NSC/DOC* **15** (2009) 117.
- [2] O. Pauvert, et al, *J. Phys. Chem. B*, **114** (2010) 6472.
- [3] M. Numakura, *Doctor Thesis*, Tokyo Institute of Technology (2011).
- [4] R. Takagi, et al, *J. Phys. Condens. Matter*. **11** (1999) 645.

## B.11 Electrochemical Behaviour of Light Lanthanides in Molten Chlorides with Fluorides

Haruaki MATSUURA, Atsushi NEZU and Hiroshi AKATSUKA

Neodymium magnet has the strongest magnetism among the magnets currently industrialized, thus it has been used for motors in hybrid cars, electric vehicles, wind farms and medical instruments. However, over 97 % of the first resource of rare earths including neodymium are now produced in China. If the demand of the electric vehicles and wind farms rapidly increases in the world, there is special concern about the lacking of rare earth resource. Therefore, we have focused on Ni-MH batteries as a secondary resource of rare earths, and investigated applicability of molten salt electrolysis to separate neodymium. In this study, the electrochemical behaviour of lanthanum, cerium and neodymium in molten LiCl – KCl eutectic coexisting various amount of LiF using tungsten and nickel electrodes was examined to find out the better electrochemical condition for separation of neodymium.

All the electrochemical studies using molten salts have been performed in an electric furnace which is built in an argon circulated glove box by an electrochemical analyser which is connected to the electrodes via a hermetic feedthrough in the side wall of the glove box. Cyclic voltammograms and differential pulsed voltammograms have been measured by using the electrodes as follows: working electrodes: tungsten or nickel electrode, counter electrode: glassy carbon, and reference electrode: Ag in LiCl-KCl eutectic + AgCl (1mol%), respectively. Molten LiCl-KCl eutectic and low carbon steel was chosen as an electrolyte and a container, respectively. Cationic source of rare earths were introduced by the addition of anhydrous chlorides to be the concentration of 0.5 wt% in the electrolytes. To observe the fluoride addition effect, various amount of LiCl-KCl-LiF (LiCl-KCl eutectic: LiF = 1:1 equimolar ratio) was added to be the relative concentration of 5, 8 and 10 times to the concentration of rare earths. All measurements have been performed at 823 K.

Cyclic voltammograms of LiCl-KCl eutectic + NdCl<sub>3</sub> (0.5wt%) with various concentrations of LiF by using tungsten electrode are shown in Fig. 1(a). It is known that neodymium are electro-reduced through divalent state, and the potential gap between the one to Nd<sup>2+</sup> and the one to

Nd<sup>0</sup> is ca. 0.12V. By the confirmation of differential pulsed voltammetry, the potential gap is ca. 0.08V. It means that the small peaks appeared at ca. -2.30V correspond to the potential of reduction to Nd<sup>2+</sup> and the peak appeared at -2.38V corresponds to the potential of reduction to Nd metal. In the neodymium case, with increasing LiF concentration, the peaks of reduction become identified, but the potential of these peaks are shifted negatively.

Cyclic voltammograms of LiCl-KCl eutectic + NdCl<sub>3</sub> (0.5wt%) with various concentrations of LiF by using nickel electrode are shown in Fig. 1(b). Rare earth metals are known to form alloys with nickel, the electro-reduction related to alloy formation can be identified from -1.75V. However, the beginning potentials of alloy formation seem to be mostly independent from the concentration of LiF. Compared to the case of using tungsten electrode, electro-reduction begins at more positive potential by using nickel electrode, but the effect of LiF could not be well appeared. When rare earths are electro-reduced by alloy formation with nickel, the effect of alloy formation tends to overcome the effect of variation of species in the electrolyte.

To expect the enhancement of electric density and modification of coordination structure around rare earths, fluoride additional effect of electrochemical behaviour of rare earth cations in LiCl-KCl eutectic were examined. By using tungsten electrode, it was confirmed that with increasing the amount of LiF, the electro-reduction peaks of each rare earth were more clarified in general, which would lead to the allowance of larger current density at the electrolysis. On the contrary to the results of using tungsten electrode for working, the major effect of fluoride addition on the potential of electro-reduction of rare earths could not be identified, since all rare earths examined were formed to alloys with nickel. It is conjectured that the variation of local coordination in the melts were not so much effective in the case of reaction of alloy formation. However, to co-extract rare earths effectively from the melt bath, nickel electrode is much suitable than tungsten.

\*This study is granted by the Shinsei Foundation.

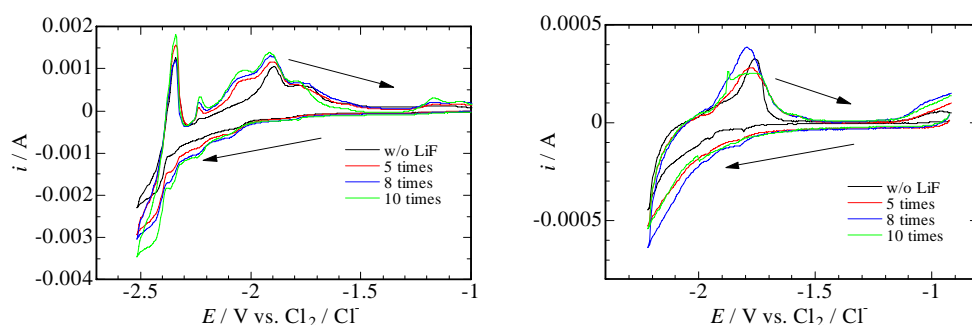


Fig. 1  
Cyclic voltammograms of molten LiCl – KCl – NdCl<sub>3</sub> (0.5 wt%) – LiF (0, 5, 8 and 10 times mole of NdCl<sub>3</sub>) at 823 K by using tungsten (a), and nickel (b) working electrode.

## B.12 Nanospace Confinement Effects on Capillary Evaporation Phenomena of Water

Takehiko TSUKAHARA

The extended-nano spaces (10-100 nm scale) have been paid much attention for not only implementing novel micro and nanofluidics devices but also characterizing physicochemical properties of liquid-phase molecular cluster [1, 2]. Previously, we found that the capillary condensation of water occurred in the extended-nano spaces [3]. However, it is quite unclear about size-confinement mechanisms of the vapor-liquid phase transition phenomena. Herein, we construct a novel experimental system, which can be strictly controlled equilibrium vapor pressures and temperatures in extended-nano spaces, and clarify size-confinement and solvent effects for capillary evaporation phenomena.

Figure 1 shows a schematic diagram of vapor-liquid phase transition measurement apparatus equipped with micro and extended-nano channels on a chip. The saturated vapor (19.8 mmHg) could be formed by pressurizing air into sample solution contained in vials. The temperatures in a vial and a chip were controlled within an accuracy of  $\pm 0.01$  °C, and the humidity of vapor in the channels was confirmed by the hydrometer, where was established at the outlet side of the microchannel (200  $\mu\text{m}$ ). At first, the water was poured into micro and extended-nano channels (120 – 500 nm) by pressure-driven flows. And then, the saturated water vapor filling in vials was delivered to the microchannel, the water could be remained in only extended-nano spaces. After that, we examined time courses of capillary evaporation for water in the extended-nano spaces at 22.0 – 22.2 °C.

The water was found to be evaporated in microchannels at 22.0 °C, while did not evaporate in extended-nano spaces. When the temperature arrived at 22.2 °C, the water in 120 nm spaces evaporated gradually with the elapse of time as shown in Figure 2. Moreover, we examined the size-dependence of the vapor pressures of water, and found that the experimental vapor pressure values of water in extended-nano spaces are lower than the values calculated from a model based on Kelvin's equation, which explains vapor-liquid equilibrium point briefly. The results indicate that the temperatures for phase transition of the confined water were different from bulk water.

We succeeded to clarify that the vapor pressure of polar solvents could be reduced by space size-confinement by using vapor-liquid phase transition measurement apparatus equipped with micro and extended-nano channels on a chip. These techniques and findings have potential for realizing nanofluidic heat exchanger, which is a cooling device with no electric power.

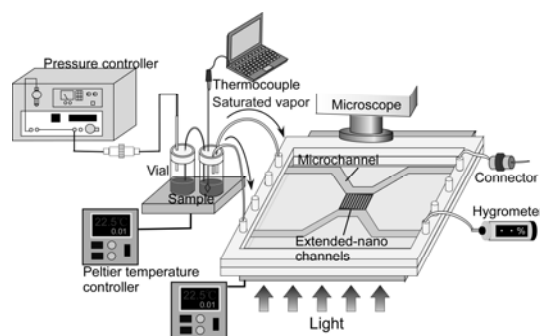


**Figure 1.** Schematic illustration of the fabricated apparatus for examining gas-liquid phase transition phenomena in extended-nano spaces on a chip.

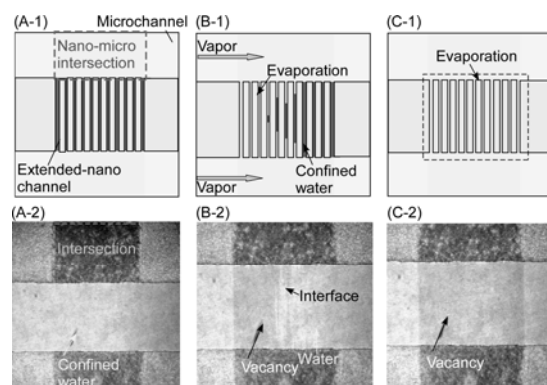


**Figure 2.** Time courses of capillary evaporation of water in 120 nm extended-nano spaces. (A-1) A picture of the initial condition of water in extended-nano channels at 22.0 °C. In only extended-nano channels, the water was filled. (A-2) A microscope image of A-1. (B-1) A picture of the state of vapor-water confined in extended-nano channels at 16 sec after reaching 22.2 °C. (B-2) A microscope image of B-1. (C-1) A picture at 24 sec after reaching 22.2 °C. (C-2) A microscope image of C-1. After 32 sec later, all confined water could be evaporated.

### References

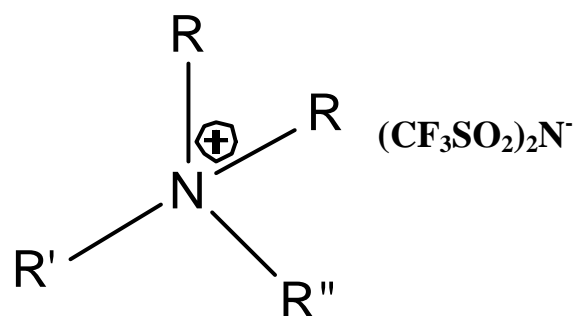
- [1] T. Tsukahara, et al., *Angew. Chem. Int. Ed.*, **46**, 1180 (2007).
- [2] T. Tsukahara, et al., *J. Phys. Chem. B*, **113**, 10808 (2009).
- [3] T. Tsukahara, et al., *Chem. Soc. Rev.*, **39**, 1000 (2010).

### B.13 Application of Novel Ionic Liquids to the Extraction of Uranium(VI) from Nitric Acid Medium and a Study on the Chemical Form of the Uranyl Complexes Extracted

Thomas James BELL and Yasuhisa IKEDA

The current commercial process for recovering actinides, such as U and Pu, from spent nuclear fuels consists of dissolving the spent fuels in an aqueous nitric acid solution followed by selective extraction using a 30% solution of tri-n-butyl phosphate (TBP) in kerosene. Hydrophobic ammonium based ionic liquids (HAILs) are expected to have the potential to act as superior solvents to kerosene, because they show high stability to radiolysis, can help reduce the risk of criticality occurring and are non-volatile and non-flammable. They are also prepared and purified more simply than many other types of ionic liquids. Following the preparation of some novel HAILs of the form  $[R_2NR'R''] [Tf_2N]$  [ $Tf_2N = (CF_3SO_2)_2N$ ] (see Figure 1) *via* the metathesis reaction, the extraction behavior of uranyl species from the aqueous nitric acid solution to the ionic liquid phase was examined to determine the optimum extraction conditions.

The concentrations of uranyl species in the aqueous phase were analyzed by Inductively Coupled Plasma (ICP) and the distribution ratios ( $D$ ) were calculated. Based on the results obtained some HAILs show considerable promise as potential substitutes for kerosene. Examination of the extracted uranyl complexes indicates that the chemical form in the ionic liquid phase varies depending on the ionic liquid used and in some cases is different to those extracted into dodecane (as a proxy for kerosene).



$R = CH_3, C_2H_5$

$R' = CH_3, C_2H_5, CH_2(CH_2)_{14}CH_3,$   
 $(CH_2)_2O(CH_2)_2OC_6H_5C(CH_3)_2-$   
 $CH_2C(CH_3)_3$

$R'' = C_3H_7, CH_2CH_2Cl, CH_2C_6H_5, CH_2-$   
 $C_6H_5NO_2$

Fig. 1. Hydrophobic ammonium based ionic liquids

## B.14 Crystal Structure of $\text{UO}_2(\text{NO}_3)_2(\text{DMPU})_2$ (DMPU = 1,3-dimethyl-3,4,5,6-tetrahydro-2(1H)-pyrimidinone)

Tomoya SUZUKI, Takeshi KAWASAKI, and Yasuhisa IKEDA

Crystal structures of various uranyl(VI) nitrate complexes with neutral unidentate ligands (L) have been reported. The uranyl(VI) nitrate complexes normally have a conformation of  $\text{UO}_2(\text{NO}_3)_2(\text{L})_2$  [1-9]. The  $\text{UO}_2(\text{NO}_3)_2(\text{L})_2$  complexes exhibit hexagonal bipyramidal geometry, in which the  $\text{U}^{\text{VI}}$  atom is coordinated by two oxo ligands in the axial positions, and four oxygen atoms from two bidentate nitrate ions and two donating atoms from two L in the equatorial plane. These ligands are located in the *trans* arrangement. Recently, we have reported that *N*-cyclohexyl-2-pyrrolidone (NCP) can precipitate uranyl(VI) ion selectively in nitric acid aqueous solution and that the precipitate has an above molecular structure of the formula of  $\text{UO}_2(\text{NO}_3)_2(\text{NCP})_2$  [4,5]. Similarly, we have also studied other *N*-alkyl-2-pyrrolidone (NRP)[4-6,9], and 1,3-dimethylimidazolidone (DMI) [6].

We report the synthesis and crystal characterization of the new uranyl(VI) complex,  $\text{UO}_2(\text{NO}_3)_2(\text{DMPU})_2$ , **I** (DMPU = 3,4,5,6-tetrahydro-1,3-dimethyl-2(1H)-pyrimidinone).

The complex **I** crystallized in the centrosymmetric space group *P*-1. The molecular structure of **I** is shown in Fig. 1. U1 is located on a vertex of the unit-cell and has the hexagonal bipyramidal coordination geometry. The two O atoms (O1) occupy the axial position of U1, and two carbonyl oxygen atoms (O2) from the two unidentate dmpu and four oxygen atoms (two O3 and two O4) from the two bidentate nitrates are situated in *trans* positions in the equatorial plane of U1 (Fig. 1). The bond lengths of  $\text{U}=\text{O}_{\text{uranyl}}$  (U1-O1),  $\text{U}-\text{O}_{\text{carbo}}$  (U1-O2) and  $\text{U}-\text{O}_{\text{nitro}}$  (U1-O3 and U1-O4) are 1.774, 2.363, and 2.549 and 2.526 Å, respectively. The bond angle around carbonyl oxygen (U1-O2- C1) is 139.91°. These structural features are similar to those of uranyl(VI) nitrate complexes with pyrrolidone derivatives (NRPs)[4-6,9] and 2-imidazolidone type ligands (1,3-dibutylimidazolidone (DBI) and DMI) [6]. The  $\text{U}-\text{O}_{\text{carbo}}$  bond length of **I** is slightly shorter than those of uranyl(VI) nitrate complex with NHP (2.414 Å)[9], *N*-cyclohexylmethyl-2-pyrrolidone (2.383 Å)[6], 1-ethylpropyl-2-pyrrolidone (2.372 Å) [9], *N*-neopentyl-2-pyrrolidone (2.382, 2.389 Å) [9], and NRPs having alkyl chains of carbon number 2 ~ 4 (about 2.37 ~ 2.4 Å) [5,6,9]. On the other hand, The  $\text{U}-\text{O}_{\text{carbo}}$  bond of **I** is slightly longer than those of uranyl(VI) nitrate complexes with urea (2.341, 2.348 Å) [1], DBI (2.345 Å)[3], and NCP (2.348 Å) [4,5].

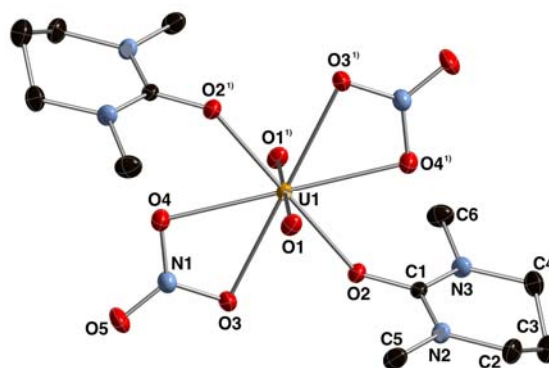


Fig. 1 Molecular view of **I** with 30 % thermal ellipsoids. Hydrogen atoms are omitted for clarity.

### References

- [1] N.W. Alcock, T.J. Kemp, J. Leciejewicz, and Z. Trazaska-Durski, *Acta Cryst.*, **C46**, 981 (1990).
- [2] Z. Cao, H. Wang, J. Gu, L. Zhu, and K. Yu, *Acta Cryst.*, **C49**, 1942 (1993).
- [3] Z. Cao, T. Qi, L. Zhu, D.-C. Zhang, R. Zhou, and K.-B. Yu, (1999). *Acta Cryst.*, **C55**, 1270 (1999).
- [4] T.R. Varga, A.C. Bényei, Z. Fazekas, H. Tomiyasu, and Y. Ikeda, *Inorg. Chim. Acta*, **342**, 291 (2003).
- [5] Y. Ikeda, E. Wada, M. Harada, T. Chikazawa, T. Kikuchi, H. Mineo, Y. Morita, M. Nogami, and K. Suzuki, *J. Alloys Compd.*, **374**, 420 (2004).
- [6] C. Villiers, P. Thuéry, and M. Ephritikhine, *Polyhedron*, **23**, 1613 (2004).
- [7] N. Koshino, M. Harada, M. Nogami, Y. Morita, T. Kikuchi, and Y. Ikeda, *Inorg. Chim. Acta*, **358**, 1857 (2005).
- [8] S. Kannan, S.B. Deb, J.S. Gamare, and M.G.B. Drew, *Polyhedron*, **27**, 2557 (2008).
- [9] K. Takao, K. Noda, Y. Morita, K. Nishimura, and Y. Ikeda, *Cryst. Growth Des.*, **8**, 2364 (2008).

## B.15 Flow Visualization in Centrifugal Extractor using Taylor-Couette Vortex Flow

Hiroshige KIKURA and Kenji TAKESHITA

A new type of centrifugal extractor, which uses Taylor-Couette vortex flow with liquid-liquid two phase counter flow, has been developed by Takeshita et al. [1]. This is expected to be a compact, high speed, high extraction efficiency device for chemical separation / purification in analytical chemistry and nuclide separation.

For obtaining the information about optimum extractor design and operation conditions, it is necessary to study the dynamic flow characteristics of Taylor-Couette vortex flow formed in the extractor. For this purpose, the authors proposed the experimental investigation of flow characteristics in the centrifugal extractor by use of visualization measurement techniques of ultrasound (UVP: Ultrasonic Velocity Profiler) and optical image.

The schematic diagram of the experimental apparatus is shown in Fig.1. The apparatus consists of two concentric cylinders made of transparent acrylic material. The outer cylinder is fixed, and the inner cylinder is rotated with the stepping motor located on the upper lid. The height of the cylinders is  $H_c = 0.145$  m, the outer radius of the inner cylinder is  $R_i = 0.068$  m, and the inner radius of the outer cylinder is  $R_o = 0.075$  m. They are positioned vertically and the space between the two cylinders is filled with working fluid. The upper position of the inner cylinder is covered by the settler part (its height is 0.017 m) : this settler cover height  $H_s$  is 0.128 m from the bottom of cylinders. The inlet and outlet flow rates are adjusted by a syringe pump and by a tubing pump. However, only outlet flow of organic phase flows as over-flow from the outlet pipe. In this experiment, Density of aqueous phase and organic phase are  $\rho_{aqueous} = 998$  kg/m<sup>3</sup>,  $\rho_{organic} = 742$  kg/m<sup>3</sup> (at 296.65 K), and kinematic viscosity of aqueous phase and organic phase are  $\nu_{aqueous} = 9.50 \times 10^{-7}$  m<sup>2</sup>/s,  $\nu_{organic} = 1.82 \times 10^{-6}$  m<sup>2</sup>/s (at 296.65 K).

We investigated the flow patterns of dispersed phase in Taylor-Couette vortex flow with counter flow (two directional, aqueous / organic two phase) by dyeing the dispersed phase. The examples of visualization results by dyeing method are shown in Fig.2(a). The measurement example by ultrasound method is shown in Fig.2(b) with use of organic phase liquid drops as ultrasonic reflectors. Flow rate of through-flow of aqueous phase and organic phase is same,  $Q_{th} = 1.7 \times 10^{-7}$  m<sup>3</sup>/s, i.e., Reynolds number of through-flow,  $Re_{th-aqueous} = 0.4$  (aqueous phase),  $Re_{th-organic} = 0.2$  (organic phase). In this UVP measured plot, horizontal axis  $T_n$  is nondimensionalized time.  $T_{ac}$  is acceleration time of inner cylinder's rotation ( $T_{ac} = 1$  s in this experiment). Vertical axis is nondimensionalized height  $H_n$ . Contour color means nondimensionalized velocity  $V_n$ . Measurement velocity range  $V_{max}$  is  $\pm 0.04$  m/s. As rotational Reynolds number  $Re$  increased, bubbly flow

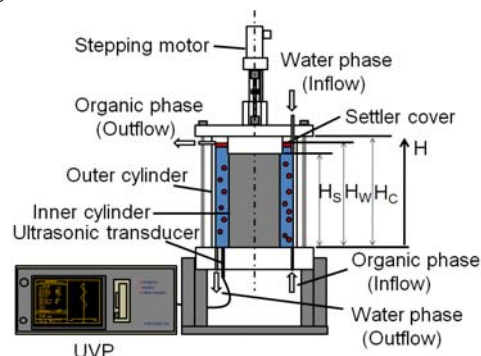
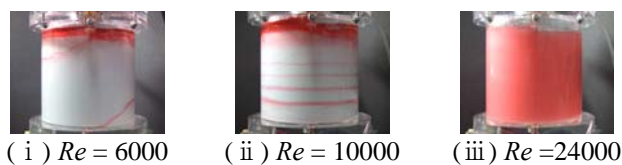
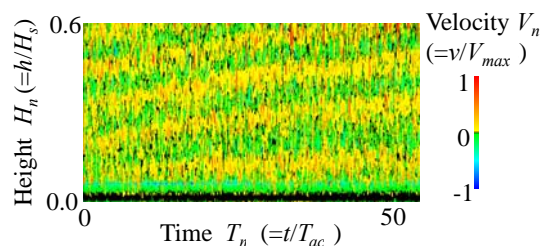


Fig. 1 Schematic diagram of experimental apparatus



(a) By dyeing method ( $Re = 6000 \sim 24000$ )



(b) By ultrasound method ( $Re = 6000$ )

Fig.2 Example of visualization results by dyeing method and ultrasound method ( $Q_{th} = 1.7 \times 10^{-7}$  m<sup>3</sup>/s)

of organic phase, changed to spiral flow, ( i )  $Re = 6000$ , and, to ring flow, ( ii )  $Re = 10000$ , and, at last, turned into (pseudo) perfect emulsion state, ( iii )  $Re = 24000$ .

In conclusion, the author showed the applicability of measurement methods using ultrasound and optical images, and clarified the flow characteristics in the centrifugal extractor using Taylor-Couette vortex flow [2][3].

### References

- [1] K. Takeshita: Development of Liquid-liquid Countercurrent Centrifugal Extractor with Taylor-Couette Flow, *Japanese Journal of multiphase flow*, **24**, 267-274 (2010).
- [2] H. Takahashi, H. Kikura, K. Takeshita and M. Aritomi: UVP Measurement of Taylor-Couette Vortex Flow with Through-Flow, *Transactions of the japan society of mechanical engineers, Series B*, **77**, 1006-1010 (2011).
- [3] H. Takahashi, H. Kikura, K. Takeshita and M. Aritomi: Characteristics of Taylor-Couette Vortex Flow with Counter Flow, *Journal of the Japanese Society for Experimental Mechanics*, **11**, SS168-SS173 (2011).

## B.16 Numerical Analyses on Joule-Heated Glass Furnace for Disposal of High-Level Radioactive Waste

Nobuyoshi TSUZUKI and Hiroshige KIKURA

Nuclear power plants or other facilities of nuclear fuel cycle produce high-level radioactive wastes. The High-level radioactive waste is reprocessed into waste liquid, and the waste liquid is mixed into molten glass in a Joule-heated glass furnace to make vitrified waste. In the glass furnace, glass (and radioactive waste) is heated by electrical current, Joule-heated, where three kinds of field – flow field, electrical field and magnetic field – arise and interfere one another. Thus, very complicated flow behavior is produced in the Joule-heated glass furnace. When the flow behavior is analyzed, the effect of magnetic field is usually thought as negligible. Hence, Laplace's equation presents the distribution of electric field, and an approximate solution can be achieved. However, it is not an accurate solution since the effect of magnetic field is ignored; thus, coupled analyses including magnetic field effect are expected for explanation of flow behavior in the glass furnace. Accordingly, numerical calculations for confirmation of magnetic field effect are executed to contribute development of an analytic code for Joule-heated glass furnace.

The shape of glass furnace is simulated by a cubic cavity in these calculations to simplify the various problems in glass furnace. Dimensions of the model are calculated from the public data of TVF [1] (Figure 1), the test-type glass furnace developed for making the vitrified waste. The cavity consists of two electrode plates on facing sides and constant temperature wall on the top working as a heat sink (Figure 2). Other planes are considered as adiabatic.

In order to solve the couple analysis including the three field (flow field, electrical field and magnetic field), GSMAC-FEM [2] is utilized because only edge finite element method (edge-FEM) can examine coupled analyses with magnetic field. Magnetic permeability of molten glass is difficult to measure because of its high temperature ( $\approx 1200^{\circ}\text{C}$ ) and mixed radioactive waste including platinum group metal particles. Thus, magnetic permeability of working fluid in this study is set as relatively high value as relative magnetic permeability to the air,  $\mu_r$ , equals 10. And the result is compared with that where the effect of magnetic permeability is excluded.

As a result, downflows are occurred from the top surface of the cavity where magnetic permeability effect is excluded. Experimental result with low magnetic permeability fluid, water, with different size cavity verified the result. However, a large upflow appears in the center of cavity in the high magnetic permeability condition (Figure 3). The upflow is maintained through this calculation time, 2000 sec.

Consequently, numerical analyses show that magnetic field affect the flow behavior in the case that working fluid has high magnetic permeability. Unstable downflows occur where magnetic permeability effect is excluded, however, a stable large upflow occurs where the effect of relatively high magnetic permeability is included. The result of high magnetic permeability case suggests that the flow behavior may be stabilized if the magnetic permeability of molten glass is high.

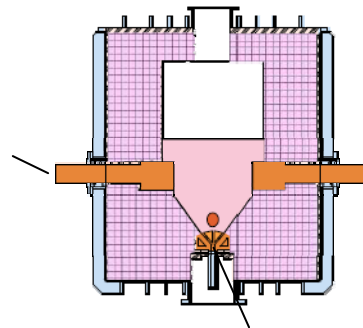


Figure 1 Joule-heated glass furnace (TVF type).

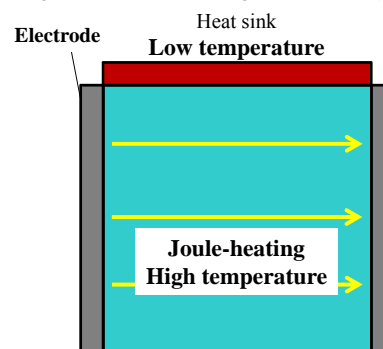


Figure 2 Schematic diagram of the cubic cavity model.

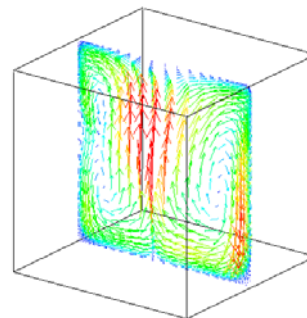


Figure 3 Velocity vectors in the center of cavity at  $t = 2000$  sec for  $\mu_r = 10$ .

### References

- [1] JAEA, Thermal hydraulic analysis using experimental data of TVF cold test, JNC TN8410 98-008 (1998) [in Japanese].

[2] T. Tanahashi: GSMAC-FEM, IPC (1991) [in Japanese].

## C.1 Study on Concept of Innovative Nuclear Reactors and Nuclear Safety

Toru OBARA

Study on innovative nuclear reactors and nuclear safety has been performed. It was intending to give concepts of nuclear reactors for various demands and solutions in nuclear safety. The major topics were about small and simple pebble reactor, equilibrium burn-up analysis in pebble bed reactors, neutron spectrum shift in high temperature gas reactor, small reactor for semiconductor production, reactor pumped laser, and transient analysis in criticality accidents.

### 1. Design study of small simplified pebble bed reactor

In the *Peu à Peu* fuel loading concept, the reactor operation starts with the core cavity partially filled with the fuel elements, and new elements are little by little (*Peu à Peu*) loaded for compensation of the burnup. Neutronic and steady state thermal hydraulic analysis were performed for a reference design of the small simplified Pebble Bed Reactor. Neutronic analysis of the 110 MWth simplified pebble bed reactor design was also performed [1][2][3].

### 2. Development of burn-up analysis code for equilibrium condition in pebble bed reactors

Burn-up analysis of equilibrium condition in pebble bed reactors is essential to discuss the performance, but no computer code is available for the purpose. In the study, development of equilibrium burn-up analysis code for OTTO cycle in Pebble Bed Reactors was performed [4].

### 3. Improvement of burn-up performance in HTGR by neutron spectrum shift

Using the method of shifting neutron spectrum is one accomplishment to achieve the fuel utilization for the block-type HTGR by extending the core life on a single-batch mode operation. Excess neutrons generated in the reactor core can be absorbed by fertile material and converted into fissile material, instead of absorbed in poison material. In this work, changing in the M/F ratio was performed to study its impacts on the burnup performance by the neutron spectrum shifting concept in order to improve the productive use of neutron and prolong the fuel life cycle [5].

### 4. Design study of small reactor for semiconductor production

A small reactor design for NTD Si was proposed in the previous work using shorter PWR fuel assembly. But commercially available conventional PWR fuel assembly has certain standard height. Instead of shorter fuel assembly, the direct use of standard PWR fuel assembly is much better option for new reactor design because there is no need to make a new fabrication process for the fuel assembly; also new fabrication process requires a long

time to be approved. In this work, a small reactor design for NTD Si was proposed using full length of conventional PWR fuel assembly [6][7].

### 5. Kinetic Analysis of Coupled Pulse Reactor for NPL Experiment

A coupled pulse reactor consisting of fast pulse cores made of a uranium alloy and a subcritical thermal laser module comprising laser cell tubes and moderator is one of the most promising designs for nuclear pumped laser (NPL) experiments. In this study, the possibility was shown to perform NPL experiments using the pulse reactor concept with low-enriched uranium by performing kinetic analysis of the prompt supercritical condition [8].

### 6. Transient analysis in super-critical condition of fuel solution tanks

In criticality accidents, the released energy can be higher if several fuel solution tanks exist around the critical tank, because of the neutron coupling between the tanks.

In this study, analyses were performed whether any difference in the transient phenomena would exist if neutron coupling between the fuel solution tanks in several-tank systems were taken into consideration by using originally developed method [9].

### REFERENCES

1. Dwi Irwanto, Toru Obara, et al., *Trans. Am. Nucl. Soc.*, **103**, 791 (2010).
2. Dwi Irwanto, Toru Obara, *2011 AESJ Annual Meeting*, I34 (2011).
3. Dwi Irwanto and Toru Obara, *2010 AESJ Fall Meeting*, Q22 (2010).
4. Topan Setiadi, Toru Obara, *2011 AESJ Annual Meeting*, G20 (2011).
5. Piyatida Trinuruk, Toru Obara, *2011 AESJ Annual Meeting*, G19 (2011).
6. Munkhbat Byambajav, Toru Obara, *Trans. Am. Nucl. Soc.*, **103**, 756 (2010).
7. Munkhbat Byambajav, Toru Obara, *2011 AESJ Annual Meeting*, G27 (2011).
8. Toru Obara and Hiroki Takezawa, *Trans. Am. Nucl. Soc.*, **103**, 775 (2010).
9. Haruka Kikuchi, Toru Obara, *2011 AESJ Annual Meeting*, I46 (2011).

## C.2 Development of Methodology for Plutonium Categorization (IV) - Effect of Compression on Rossi-alpha-

Yoshiki KIMURA, Masaki SAITO and Hiroshi SAGARA\*

### INTRODUCTION

To evaluate the proliferation resistance of Pu, a function “*Attractiveness (ATTR)*” was proposed as a ratio of the characteristic of potential explosive energy to technical difficulty converting to nuclear explosive devices (NEDs)<sup>[1,2,3]</sup>. The characteristic of potential explosive energy was defined by rossi-alpha, the ratio of supercriticality to prompt neutron lifetime. The technical difficulty was assumed as functions of specific decay heat (DH, [W/kg]), spontaneous fission neutron rate (SN, [n/g/s])<sup>[1,2,3]</sup>, and radiation dose rate (RD, [Sv/hr/kg]) was recently introduced as a new factor<sup>[4]</sup>. The high DH and RD make Pu handling and NED manufacturing technically difficult, and the high SN enhances the probability of pre-detonation. The current function of *ATTR* was proposed as<sup>[4]</sup>

$$ATTR = \frac{\frac{\alpha_{\infty}}{\alpha_{\infty}^{239}}}{\frac{DH}{DH^{238}} + \frac{SN}{SN^{238}} + \frac{RD}{RD^{238}}} \quad (1).$$

The rossi-alpha and all technical difficulty factors are normalized to their reference values in Pu isotopes.

### EFFECT OF COMPRESSION ON ROSSI-ALPHA

In Eq.(1), the numerator, rossi-alpha in infinite condition ( $\alpha$ -infinity,  $\alpha_{\infty}$ ), characterizes the power excursion of Pu. In actual NEDs, the Pu-cores would be compressed to make them supercritical state.

Figure 1 shows the effect of compression (initial density: 15.8 [g/cc]) on the  $\alpha$ -infinity of Pu isotopes which is the recalculation of the results in earlier study<sup>[5]</sup>. Supercriticality and prompt neutron lifetime in infinite mass Pu were estimated using MCNP4C code<sup>[6]</sup> with infinite cell geometry and neutron cross-section library FSXLIB-J33<sup>[7]</sup>. The values of  $\alpha$ -infinity at normal density are varied in Pu isotopes and they are changing in proportion to the compression ratio with different rates of increasing. This increasing rate also can be considered as the meaningful feature to characterize the explosive energy.

In the present paper, the increasing rate of  $\alpha$ -infinity was introduced to the function of *ATTR*. The characteristic of potential explosive energy was defined by the product of  $\alpha$ -infinity and its increasing rate. Based on the one-group theory, the  $\alpha$ -infinity is proportional to the compression ratio.

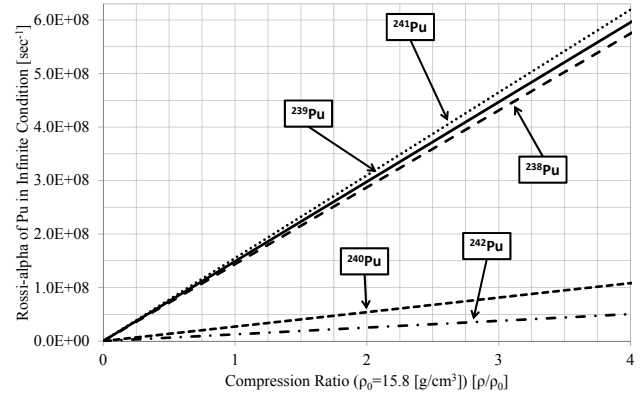


Fig.1 Effect of compression on  $\alpha$ -infinity (recalculating the results in Ref. [5])

$$\alpha(\infty, \rho/\rho_0) = \alpha(\infty, 1) \times \frac{\rho}{\rho_0} \quad (2).$$

It can be also confirmed in Fig.1. Therefore, the characteristic of potential explosive energy with consideration of the effect of compression was defined by  $\alpha$ -infinity squared;

$$\alpha(\infty, 1) \times \frac{d}{d(\rho/\rho_0)} \alpha(\infty, \rho/\rho_0) = \alpha^2(\infty, 1) \quad (3).$$

The function of *ATTR* was improved as below,

$$ATTR = \frac{\left( \frac{\alpha_{\infty}}{\alpha_{\infty}^{239}} \right)^n}{\frac{DH}{DH^{238}} + \frac{SN}{SN^{238}} + \frac{RD}{RD^{238}}} \quad (4).$$

In Eq.(4),  $n=1$  characterizes the power excursion of Pu and  $n=2$  includes the effect of compression on rossi-alpha.

### EVALUATION OF PLUTONIUM DENATURING

Figure 2 shows the *ATTR* of Pu normalized by that of  $^{239}\text{Pu}$  as a function of the doping rate of Pu isotopes to pure  $^{239}\text{Pu}$  ( $n=1\&2$ ). It also shows the example of Pu categorization<sup>[9-12]</sup>.

In both cases, *ATTR* of Pu decrease dramatically by even-mass-number Pu isotopes doping, because the technical difficulties converting to NEDs are enhanced. As the number of  $n$  in Eq.(4), *Attractiveness* of Pu decreases more dramatically by  $^{240}\text{Pu}$  and  $^{242}\text{Pu}$  with high doping rate. This is because the  $\alpha$ -infinity of pure  $^{240}\text{Pu}$  and  $^{242}\text{Pu}$  isotope are comparatively lower than that of  $^{239}\text{Pu}$ .

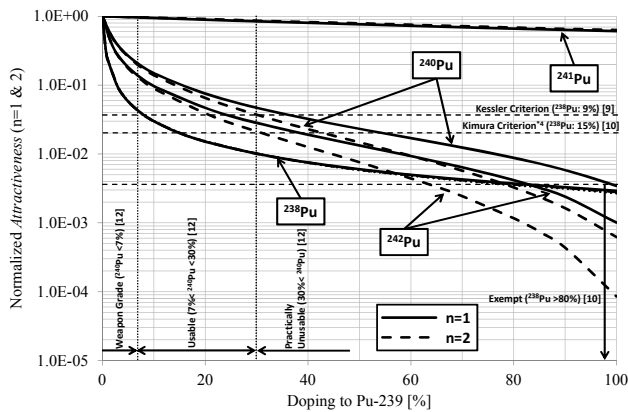


Fig.2 Normalized Attractiveness of denatured Pu ( $n=1$  and  $2$ )

In both cases, *ATTR* of Pu decrease dramatically by even-mass-number Pu isotopes doping, because the technical difficulties converting to NEDs are enhanced. As the number of  $n$  in Eq.(4), *Attractiveness* of Pu decreases more dramatically by  $^{240}\text{Pu}$  and  $^{242}\text{Pu}$  with high doping rate. This is because the  $\alpha$ -infinity of pure  $^{240}\text{Pu}$  and  $^{242}\text{Pu}$  isotope are comparatively lower than that of  $^{239}\text{Pu}$ .

## REFERENCES

1. M. Saito *et al.*, *ANS TRANSACTIONS*, **96** (2007).
2. M. Saito *et al.*, *ANS TRANSACTIONS*, **98** (2008).
3. M. Saito, *Proc. Global09*, Paris, Sep. 6-11, (2009).
4. Y. Kimura *et al.*, *ANS TRANSACTIONS*, **103** (2010).
5. M. Saito *et al.*, to be submitted.
6. "MCNP4C," CCC0700, RSICC (2000).
7. JAERI-DATA/CODE 2003-011, JAERI (2003).
8. J. C. Mark, *Science & Global Security*, **4**, 111 (1995).
9. G. Kessler, *Nucl. Sci. Eng.*, **155**, 53-73 (2007).
10. Y. Kimura, *J. Nucl. Sci. Technol.*, **48**, 5 (2011).
11. IAEA, INFCIRC/153 (1972).
12. B. Pellaud, *J.Nucl.Mat.Management*, **31**, 30 (2002).

### C.3 Burn-up Characteristic of Am-fueled Space Reactor with Reflector Thickness

Masanori NAKAMURA, Masaki SAITO and Hiroshi SAGARA

#### INTRODUCTION

In the future human activities in space will need much electric power for long time. However, it is difficult to satisfy these demands by solar energy and battery such as fuel cell because the low solar power density and very severe mass restriction by the ability of rocket performance. Space nuclear reactor is a very attractive answer to solve above problem. Furthermore, long-life is an essential element. Space reactor is very attractive in its utilization for the human activities in the space. And human activity in the Moon and Mars requires large electric power for the long time in the future. Many concepts have been suggested to satisfy these contradicted conditions. Highly enriched uranium fuel concept is suggested mainly. However, U enriched over 20% is defined as a significant quantity in military utilization by IAEA<sup>[1]</sup>. Because minor actinide (MA) of spent fuel in LWR has large neutron capture cross section, loading MA can enable long life core both thermal and fast reactor<sup>[2]</sup>. Though neutron spectrum of this study is fast, it has used not sodium but lithium<sup>[3]</sup>. It enables high efficiency of electricity conversion because of high boiling point and specific heat. Because gravity and air utilization in space is negligible or small, removal heat of convection and conductivity is not effective. Am nitride is used because Am is very stable to nitride chemically. Main isotope of Am is <sup>241</sup>Am and <sup>243</sup>Am in spent LWR fuel. Transmutation procedure of <sup>238</sup>Pu from <sup>241</sup>Am sustains long-life core in fast spectrum.

#### METHODOLOGY

Computer codes, SLAROM<sup>[4]</sup>, JOINT and CITATION<sup>[5]</sup> and cross section library, JFS-3-J-3.2R, which is based on Japanese Evaluated Nuclear Data Library JENDL3.2, are used in the present calculation. The SLAROM input consists only of the PREP block to obtain 70-group effective cross sections of each material region by homogeneous cell calculation. JOINT is used to convert 70-group effective cross section data sets from the SLAROM output to the CITATION input. The nuclear characteristics are investigated using a calculation of two-dimensional RZ diffusion theory with depletion chain by CITATION. In this calculation, each zone has uniform nuclide number densities with 176 zones and the same set of microscopic cross sections.

#### RESULTS AND DISCUSSIONS

Burn-up characteristic of AmN fuel is shown in Fig.1. In cases A and C, the axial reflector thickness was fixed to 15 cm and the radial reflector thickness was increased (9, 19, and 29 cm). The radial thickness was fixed (29 cm) and the axial thickness was increased (20, 25, and 30 cm) in cases D to F. Compared with cases A and F (comparison with minimum and maximum volume of reflector), the initial keff of case F compared to case A increases by only 1% from 1.00 to 1.01. However, burn-up time increases from about 100 years to 170 years largely because transmutation from <sup>241</sup>Am to <sup>238</sup>Pu near reflector is promoted by increase of the reflector thickness and fission of <sup>238</sup>Pu contributes to burn-up.

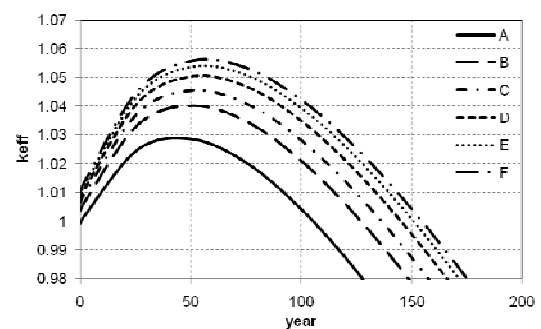


Fig.1 Time Variation in Multiplication Factor with Reflector Thickness

#### REFERENCES

1. IAEA Safeguards Glossary 2001 Edition, IAEA, 2001
2. M. Saito: Multi-Component Self-Consistent Nuclear Energy System for Sustainable Growth; *Progress in Nuclear Energy*, Vol. 40, No.3-4, 2002.
3. M. Kambe *et al.*: Innovative Fast Breeder Reactor Concept 'RAPID' for Improvement of Reactor Performance and Proliferation Resistance; Vol.170, Issues 1-3, *Nuclear Engineering and Design*, 1997.
4. M. Nakagawa *et al.*: SLAROM: A Code for Cell Homogenization Calculation of Fast Reactor; JAERI 1294, *Japan Atomic Energy Research Institute*, 1984.
5. T. B. Fowler *et al.*: Nuclear Reactor Core Analysis Code: CITATION; *Oak Ridge National Laboratory report*, ORNL-TM-2496, Rev2, USA, 1971.

## C.4 Effect of Inner Axial Blanket with Minor Actinides on Extension of Core Life-time of Large-scale Fast Breeder Reactor

Erina HAMASE, Masaki SAITO, Hiroshi SAGARA\*, and Chi Young HAN

### INTRODUCTION

Minor actinides (MAs) discharged from the nuclear reactor spent fuel entail a significantly long-term radiological issue in geological repository. However, the attractive characteristics of MAs as a burnable poison and a fertile material have been proposed for the protected plutonium (Pu) production<sup>1,2</sup>. It was also reported that if MAs were doped into the inner radial blanket at the center of a large-scale fast breeder reactor (FBR) core, the core life-time could be extended by shifting the main fission reaction zone from the active core to the inner radial blanket with burnup because  $^{238}\text{Pu}$  transmuted from MAs can work as a fissile nuclide on fast neutron spectrum<sup>3</sup>. In this study, the effect of an inner axial blanket, which is introduced axially at the center of the FBR, and its MA doping was investigated for the extension of core life-time. Metal fuel as well as MOX fuel was evaluated for a longer core life-time.

### METHODOLOGY

A code system of SLAROM<sup>4</sup>, JOINT, and CITATION<sup>5</sup> was used with the cross section library of JFS-3-J-3.2R<sup>6</sup>. 70-group effective cross sections were prepared by homogeneous cell calculation using SLAROM and converted into the CITATION data format. Core calculation was performed by CITATION based on an R-Z diffusion model.

Six different cores were modeled depending on fuel and inner axial blanket materials based on a large-scale sodium-cooled FBR<sup>7</sup>. Figure 1 shows the R-Z models used for the core calculation. Two cores without inner axial blanket were evaluated as a reference core; REF-MOX and REF-Metal cores. MOX fuels of 18.3 and 20.9 wt% Pu enrichments were loaded in the inner and outer core regions of REF-MOX core, respectively. Metal fuels in the form of U-Pu-10%Zr with 13.1 and 15.0 wt% Pu enrichments were loaded in the regions of REF-Metal core. Pu inventories of both reference cores were set to be 6,747 and 7,340 kg for the inner and outer cores. The outer axial and radial blankets consist of depleted uranium (DU) oxide (in REF-MOX core) or metal uranium (in REF-Metal core). In the four cases with the inner axial blanket (CASE A to D), the inner axial blanket consisting of DU is arranged at the axial core mid-plane as shown in the right-hand side of Fig. 1. Since the Pu inventories were also maintained in CASE A to D, the Pu enrichment was increased to 27.8 and 31.8 wt% in CASE A and B (MOX fuel) and 20.1 and 22.9wt% in CASE C and D (metal fuel). Furthermore, 40 and 28.5 wt% of MAs, equivalent to 9,857 kg heavy metal, were doped into the inner axial blanket in CASE B and D.

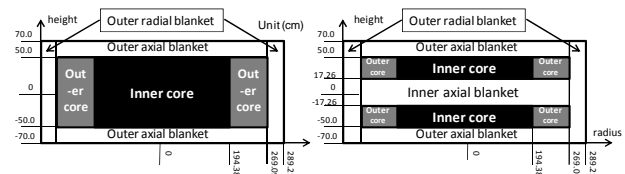


Fig. 1 Core layout of REF-MOX and REF-Metal (left) and CASE A to D (right)

### RESULTS AND DISCUSSIONS

Figure 2 shows the time variations in multiplication factor ( $k_{\text{eff}}$ ) for REF-MOX, REF-Metal, and CASE A to D. It was found that the initial excess reactivity in CASE A to D was smaller than those in REF-MOX and REF-Metal because the absorption of  $^{238}\text{U}$  and MAs in the inner axial blanket of CASE A to D highly contributed to it from the beginning of cycle. CASE A and C give maximum available cycle lengths smaller than REF-MOX and REF-Metal. However, it shows that the maximum available cycle lengths of CASE B and D are significantly extended with keeping the reactivity swing small.

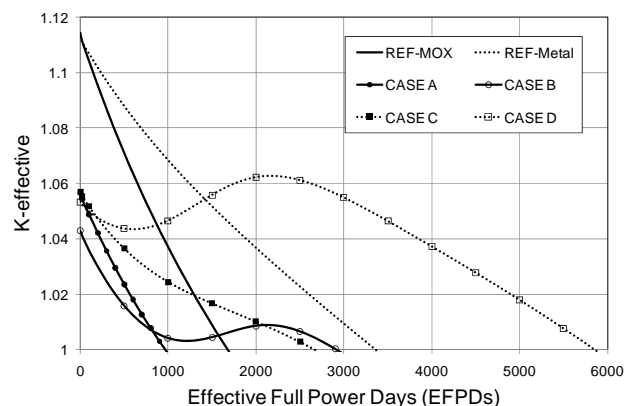


Fig. 2 Effect of inner axial blanket and doping MA on reactivity

In order to investigate the effect of  $^{238}\text{U}$  and MAs as a fertile material in the inner axial blanket, the distribution of neutron flux at different reactor operation times in CASE A and B is examined as shown in Fig. 3. In CASE A, the neutron flux in the inner axial blanket relatively slightly builds up. On the other hand, in CASE B, it shows that the main fission reaction zone is shifted from the active core to the inner axial blanket. It is because  $^{238}\text{Pu}$  transmuted from MAs in the inner axial blanket plays a role as a fissile nuclide in fast neutron spectrum in the same way as the previous study on the inner radial blanket<sup>3</sup>. It was also found that the inner axial blanket with

\*Current organization: Japan Atomic Energy Agency

MAs gave a high feasibility of core life-time extension as well as smaller reactivity swing. In addition, it was confirmed that the metal fuel led to a longer cycle length than oxide fuel.

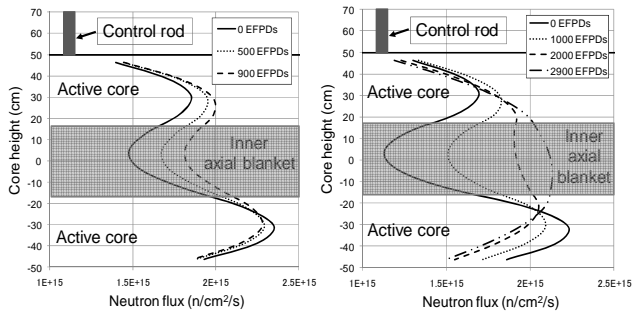


Fig. 3 Neutron flux distribution during irradiation in CASE A (left) and CASE B (right)

## REFERENCES

1. M. Saito, *Prog. Nucl. Energy*, **40**[3-4], 365-374 (2002).
2. M. Saito, *Int. J. Nucl. Sci. Tec.* **1**[23], 127-138 (2005).
3. E. Hamase *et al.*, *Ann. Nucl. Energy*, **38**[7], 1496-1504 (2011)
4. M. Nakagawa and K. Tsuchihashi, JAERI 1294, Japan Atomic Energy Research Institute, (1984).
5. T. B. Fowler *et al.*: Oak Ridge National Laboratory Report, ORNL-TM-2496, Rev2, USA, (1971).
6. G. Chiba *et al.*, *J. Nuc. Sci. Technol.*, **1**[4], 335-340 (2002).
7. M. Naganuma *et al.*, JNC TN9400 2005-051, (2005), [in Japanese].

## C.5 Evaluation of Fukushima Dai-ichi Nuclear Power Plant Accident

Kazumi KITAYAMA, Takao ISHIZUKA, Nobuyoshi TSUZUKI,  
Hiroshige KIKURA and Masanori ARITOMI

A huge earthquake, lately referred as *Higashi-Nihon Dai-Shinsai*, occurred at approximately 100 km east off the coast of Tohoku area at 14:46 on 11<sup>th</sup>, Mar, 2011. Magnitude of the earthquake was 9.0, the 4<sup>th</sup> biggest earthquake of the world in the past. People, buildings, and other facilities were damaged especially in Tohoku area by the earthquake and following tsunami. Many nuclear plants were also attacked by them.

The plant status of Fukushima Dai-ichi nuclear power station (1-F) at unit #1–#3 was in operation, and status at unit #4–#6 was in refueling when the earthquake occurred. The earthquake discharged external power source from the station, and the following tsunami crushed heat sink for removing residual heat. Unit #5-6 of 1-F were not severely troubled because an air-cooled diesel power generator for unit #5–6 could keep working. Otherwise, unit #1–#4 lost all electricity and heat sink. Fuel rods of unit #4 were moved to Spent Fuel Pool because of exchanging shroud in the Reactor Pressure Vessel (RPV), and core cooling for unit #4 was not necessary. Thus, the most important thing for unit #1–3 at that time was coolant injection for cooling the reactor core. Unfortunately, reactor fuel of the unit #1–3 is estimated presently melting, and explosions occurred at reactor buildings of each unit by hydrogen gas. Some radioactive materials blew out from the plant and it cause evacuation near the 1-F for a long time.

Unit #1 of 1-F is a BWR-3 reactor (**Figure 1**). It has some core cooling facilities, which are Isolation Condenser (IC), High Pressure Coolant Injection system (HPCI), and so on. Tokyo Electric Power Company (TEPCO) decided soon after the earthquake that IC could apply for regulation of the pressure of RPV, and that HPCI should be applied when the level of coolant water went down. Accordingly, IC was applied four times before tsunami, and left for about 2 and half hours after tsunami. HPCI which can supply coolant water continuously to the reactor core was not applied. Applying IC only several times was not enough for residual heat removing as a result, and the steam from boiling coolant water went out from RPV through safety relief valve. Thus, the reactor core overheated and reaction between zircalloy and heated steam produced hydrogen gas, which caused explosion at unit #1. The explosion occurred at 15:36 12<sup>th</sup>, Mar, almost 1 day after the earthquake. The explosion also damaged fire pumps or other apparatus of other unit #2–4, and it made harder to inject the coolant water to reactor core of other units.

Unit #2 and #3 (and unit #4 and #5 also) are BWR-4 reactors. A BWR-4 type reactor has Reactor Core Isolation Cooling system (RCIC) instead of IC of BWR-3, and it has

HPCI for injection at small sized piping rupture as well as BWR-3. After the earthquake, RCIC was started manually by workers of TEPCO at both units (#2 and #3). RCIC stopped several times by the alarm of L-8 (coolant water level high), and restarted manually each time. RCIC injected cool water to reactor core for about 20 hours at unit #3, and about 70 hours at unit #2. At unit #3, HPCI automatically followed when RCIC expired and it worked for 14 hours. Thus, continuous coolant injection was maintained by RCIC and HPCI for 70 hours at unit #2, and for 34 hours at unit #3. Nevertheless, coolant injection using fire protection line delayed 6 and half hours after expiration of RCIC at unit #2, and 7 hours after expiration of HPCI at unit #3. These long time deficiencies of coolant injection could cause overheated reactor fuel and production of hydrogen gas which exploded at 6:10 on 15<sup>th</sup>, Mar at unit #2, and at 11:01 on 14<sup>th</sup>, Mar at unit #3.

If injection of coolant water to reactor core executed continuously, the fuel might not melt and explosion might not occur. It means application of HPCI instead of IC at unit #1, and water injection (which includes sea water) through fire protection line soon after expiration of HPCI or RCIC at each unit. It is also remarkable that explosion at unit #1 interfered the effort of water injection for unit #2 and #3. If the explosion of unit #1 were interrupted, unit #2 and #3 could be calmed down at high probability.

The evaluation of this accident induced analysis on Accident Management of nuclear plants for deficiency of all electricity and heat sinks. Some proposal were made for increase of reactor safety by the countermeasures such as diversification of power source, reinforcement of fire protection line, increment of fresh water amount in the power stations, and so on. A management method to terminate the accident without core-melt will be possible by these countermeasures even when all electricity and heat sinks were lost, and BWR power plants can be operated safely when this method is confirmed available.

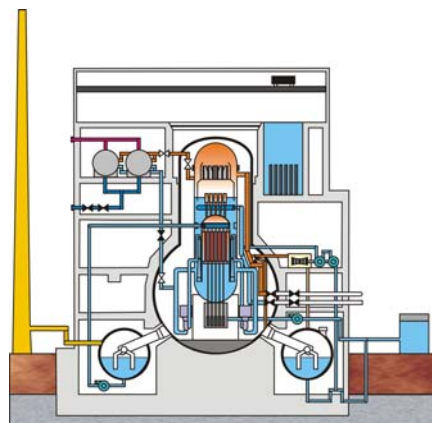


**Figure 1** Schematic diagram of unit #1 at 1-F.

## C.6 Legal Framework to Maintain Expertise in Nuclear Regulatory Body in Japan

Tetsuo SAWADA and Toshio MORIMOTO\*

In the reflection of the Fukushima NPP accident on March 11 in 2011, a number of proposals have been released concerning what the new organization of a nuclear regulatory body ought to be with high level of expertise. In this study, we consider a proper constitution of the body from the viewpoint of legal framework in which we can resolve various safety issues for realizing sustainable and vigorous development of the nuclear energy business. The consideration is focused on the authority, personnel matters, budget, information gathering with keeping the body's independency.

1. **Expertise of the top-management personnel of the new regulatory body**  
The assign procedure of the top manager, or commissioner of the regulatory authority that will be newly established in April 2012, i.e., new authority, will be usually provided by the law to establish new regulatory body. The top personnel of regulatory bodies such as USNRC, French ASN, and Finnish STUK is a expert of nuclear regulation. And the term of office is fixed so that it will not be affected by the political situation. The term is rather long, for instance, five years for USNRC. Therefore, the commissioner of the new body should be an expert of the nuclear regulation, and not just a politician. For keeping the political neutrality and steady administration, the commissioner must be appointed by the cabinet under the consent of the Diet. At the same time, it is appropriate to appoint a number of committee members by the law that prescribes the establishment of new regulatory body.
2. **Adoption of nuclear experts**  
The new regulatory body must be an "extra-ministerial bureau" which is based on the cabinet Office Organization Act 49 or Organization Act 3, so that it is authorized to have the right of adoption. In order that the new body is independent from the Ministry of Economy, Trade and Industry (METI) and controls other nuclear related business such as the regulation of research reactors that are out of the range of METI, it must be established as the extra-ministerial bureau of the Cabinet Office or other Ministry than METI. Therefore the Act must prescribe it. In addition, if it is an urgent task to adopt nuclear experts from private sectors, we can make use of the application of the 1-24 Rule of the National Personnel Authority or the Special Act for Employment of Fixed Term Civil Servant.
3. **Upbringing and application of personnel of the new body**  
It is most important that the commissioner and/or the committee must keep the right to adopt the personnel so that the staff members can have enough opportunity to show flexibly what they can do in any situation. Usually the right of adoption is prescribed by the rule for the organization, i.e., the government ordinance. Therefore, it is crucial to do so when the government ordinance is enacted for the new body.
4. **Safety Goal**  
The essential prerequisite of the safety regulation is prescribed as "there is no hindrance to protect against disasters" by The Law on the Regulation of Nuclear Source Material, Nuclear Fuel Material and Reactors. We need to define the safety goal by which we can materialize the essential prerequisite. The safety goal should be defined as a guideline or standard, thereby the people can understand the essence of safety regulation as well as stabilizing the regulation efforts. Furthermore, following the Ministry of the Environment Act, we should vest the right to enact rules such as guidelines in the new organization by the new organization act.
5. **Systematic dealing with novel safety issues and consideration for controversial opinions**  
In the new body, we must have a systematic method to handle novel safety issues. The related procedure must be prescribed by internal regulations. This is the case of USNRC. The enactment of rules such as standards will be processed involving jurists from its early stage. For the regulation policy of NRC, internal controversial opinions are adopted and examined. Such a procedure is prescribed in the internal documents. The regulation policy for the novel safety issues should be defined smoothly by considering various opinions. Therefore, we are convinced that the establishment of related internal regulations is crucially important for the new body.
6. **Summary**  
In this study, we have examined on trial what is prerequisite in laws and regulations for adopting nuclear experts of safety regulation, fostering them as well as making maximum use of their expertise. We, nuclear engineers and professionals, are not familiar with the law and rules that manage administrative organizations. However, we think that it is more preferable for establishing a new body with high level of expertise so that engineers and professionals are interested in the issues and participate in the dialogues.

## C.7 New Public Commons and Network of Nuclear Site Regions for the Post-Fukushima Accident Re-vitalization

Tetsuo SAWADA

Due to the Fukushima NPP accidents on 11 March 2011, we have deadly lost the regional ties among local people, electricity consumers, and people involved in the nuclear research, development and businesses. Now we need the method to reconstruct the ties and further the activation of locals in accordance to the concept of “New Public Commons [1].” And it is the most important key to recover the people’s confidence for the nuclear business and promote the new siting and replacement of nuclear power stations. More than forty years have past since the earliest stage of invitation of nuclear power stations to regional areas in Japan. For this period, the efforts for the development of regional industries and the improvement of regional life obtained a level of results. However, now a new turn is required in the regional development, as the perception of wealthy has been gradually changed. The primary objective of this study is to make a network among regional areas where nuclear power stations and related facilities are located. It should further the understanding for nuclear energy, stimulate the “emergence” through the cooperative works among regional areas. As a result, such efforts will enhance the Social Responsibility of conducts related to the nuclear energy. i.e., Nuclear SR (NSR) [2]. The basic frame of the NSR should be re-estimated in the reflection of 3.11 Fukushima NPP accidents.

### 1. Introduction

In November 2008, the 13<sup>th</sup> International Maximarathon [3] was held between Kyoto city and Takahama town in Wakasa bay. Through this meeting, it has been envisioned and shared that regional nuclear towns have common characteristic issues concerning the development of the local life. The issues are: (1) they avoid depopulation but it seems superficial, (2) the development of regional areas still closely subsidized by the government, (3) the understanding of nuclear energy by local peoples is not well improved, (4) there may be a twisted situation in the region, (5) they have little cooperation with other nuclear power siting regions, (6) the implication of nuclear energy is misunderstood by the people of consumer area such as large cities.

For the first step, we have established an opportunity where we can cooperatively create something that will assist the regional developments which meet the wish and desire of local peoples. Various partners can change information, know-how, knowledge and experience which will stimulate new activity for the creation leading to emergence. Here the emergence is the way of complex systems and patterns arise out of a multiplicity of relatively simple interactions. Through the emergence, a situation of creation of new values may occur among individuals who

do not have actual relationships until then.

### 2. Practice

The major components of the 13<sup>th</sup> Maximarathon were as follows: (1) a long-distance relay race from Kyoto to Wakasa Takahama town (about 100 km), (2) the runners’ relay of a message baton that prays for the peaceful use of nuclear energy, (3) social gatherings at several regions such as Kyoto, Takahama and other towns where the relay passed, (4) visiting of local schools and goodwill exchange with pupils and students.

The results of this event were: (1) we had opportunity for effective exploration of mutual understanding of local people, workers and scientists related to nuclear business, and people of consumer city; (2) within a sports event, various people with little opportunity to meet in daily life got a chance to fraternize; (3) the pupils and students had a chance to share the message for future as well as to release message to the world.

### 3. A platform: Tour de Atom

According to the above-mentioned successful fruits, we have received a lot of expectation to promote a new platform for the interchange opportunity leading to emergence. As a result, we have originated “Tour de Atom.” This platform will make a harmonization among regions, other various partners beyond generations. Then it can make networks in a region, among the regions, between regional area and city through Japan. This network should be shared with the concerned people in the world. The 1<sup>st</sup> Tour de Atom was held at Wakasa Bay area in 2009 which started Takahama town and reached to Tsuruga city, with engaging rural towns in between them. In Wakasa Bay area, we have 15 nuclear power stations including Monju fast reactor. In the 1<sup>st</sup> Tour de Atom, about 60 runners relayed a message of “萬物生光輝”, that is a calligraphy by former Prime Minister Yasuhiro Nakasone, for the peaceful use of nuclear energy as well as a video message that was planned and made by students of Takahama junior high school. Then Tour de Atom 1.5 was held between Tsuruga and Fukui city in June 2010, when Conference of Energy Ministers of APEC was being held. Succeedingly, the 2<sup>nd</sup> Tour de Atom [4] was held from Fukui city to Shika town in Ishikawa prefecture in October 2010. In Shika town, Hokuriku electric power company has two nuclear power stations. In 2011, after the Fukushima NPP accidents, we have decided to invite the 16<sup>th</sup> International MaxiMarathon to Miyagi and Fukushima prefectures, i.e., Sendai-Minamisouma-Iitate-Fukushima, that will be combined with the 3<sup>rd</sup> Tour de Atom.

#### 4. What is prerequisite for the re-vitalization of locals in the shadow of Fukushima NPP accidents

We need following points to be considered in the frame of recovering confidence and proceeding toward re-vitalization from Fukushima NPP accidents:

- 1) further investigation for what had happened in the early stage, e.g., for about one week, of the accidents, which will lead to identify real cause and consequence of them,
- 2) the reexamination of accident management system,
- 3) the reality of the evacuation immediately after the disaster, say, during the initial several days, which will be make use of reforming the evacuation system and procedure including the reexamination of nuclear off-site centers,
- 4) the verification of national risk management system, especially for NPP terrorism, and
- 5) the removal of radioactive contamination to the lands and the relief aid to the people exposed to the radiation.

#### 5. Summary

We had realized that there was irrecoverable inconsistency between the then Kan Administration and the bodies that promote nuclear energy policy and regulate nuclear safety. It has invited people's suspicion for both the politicians and nuclear experts. It has also lead to the prevailing excess anxiety over the radiation exposures and diseases caused by them. For recovering from the current situation to future progress of nuclear energy and radiation applications, we must do all the possible measures within our hands. Now it's time to show our wisdom with bravery.

#### References:

- [1] Declaration of "New Public Commons". June 4, 2010.  
<http://www5.cao.go.jp/entaku/en/pdf/declaration-english.pdf>
- [2] T. Sawada, et al, Nuclear corporate social responsibility: an approach toward a roadmap for gaining social confidence, *Int. J of NGEE*, vol. 1, Nos. 3 (2007)
- [3] The 13th Maximarathon in Japan from the JAIF TV.  
<http://www.youtube.com/watch?v=h9PrOSFI4yo> ((c) Japan Atomic Industry Forum)
- [4] The 2<sup>nd</sup> Tour de Atom;  
<http://www.jaif.or.jp/ja/jaiftv/index.html> ((c) Japan Atomic Industry Forum)

## C.8 Conceptual Study of Liquid Lithium Target System for Boron Neutron Capture Therapy (BNCT)

Minoru TAKAHASHI, Tooru KOBAYASHI, Shoji UCHIDA and Migguan ZHANG

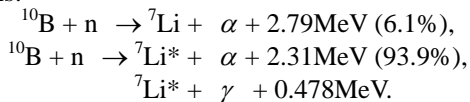
### 1. Introduction

The combination of a lithium target with a proton beam accelerator is the candidate neutron source for the boron neutron capture therapy (BNCT). The most important advantage is that the compact system can be easily facilitated adjacent to a hospital. The problems of the accelerator-driven system using solid lithium target are the damage of the target by the proton beam and the low heat removability for beam energy-deposited target. If a flowing liquid lithium target is used, it is expected that the both problems can be solved. Therefore, a liquid lithium target system has been proposed in the present study.

### 2. Flowing Liquid Lithium Target System

#### 2.1. Neutron source for boron neutron capture therapy

The boron neutron capture therapy is based on the reactions:



The neutrons are produced by the reaction  ${}^7\text{Li}(p,n){}^7\text{Be}$  using proton accelerators. There are two types of neutron sources, i. e., neutrons produced by protons with the energy of 2.5 MeV are moderated and collimated; and low energy-neutrons produced by low energy-protons of around 1.9 MeV are directly used. Both of the neutron sources driven by the accelerator need a lithium target.

#### 2.2. Deposited heat in lithium jet and temperature rise

The energy of the proton beam is deposited in the lithium target, and converted to heat. In case of the use of neutron moderator and a collimator, the proton energy of 2.5 MeV and the beam current of 20 mA correspond to the total heat generation of 50 kW. Practical proton beam conditions of the proton energy of 2.0 MeV and the beam current of 10 mA without neutron moderator and a collimator correspond to the total heat generation rate of about 20 kW, and the average heat generation rate per unit area of about  $q''=28 \text{ MW/m}^2$ . It is assumed that the proton beam intensity is radially in the Gaussian profile with the diameter of 30 mm ( $3\sigma=99.7\%$ ). For both cases, the distributions of the calculated heat generation rate per unit volume in the lithium target film are calculated as shown Fig. 1. It is found that all the energy is deposited within the distances of 0.16 mm and 0.25 mm from the surface of the lithium target in cases of 2.0 MeV and 2.5 MeV, respectively.

The high density of heat deposition in the lithium jet may causes vaporization from the lithium jet surface or boiling/cavitation inside the lithium jet if the lithium jet velocity is low. The lithium vapor affects the accelerator,

and the boiling/cavitation bubble makes the proton beam pass through the lithium jet heating and melting a solid back-wall. Therefore, it is necessary to design the lithium target to avoid the vaporization and boiling. In order to avoid them, the temperature on the lithium jet surface and inside must be kept lower than its saturation temperature. If the pressure in the accelerator tube  $P$  is  $1 \times 10^{-3} \text{ Pa}$ , the lithium temperature must be kept lower than  $342^\circ \text{ C}$ .

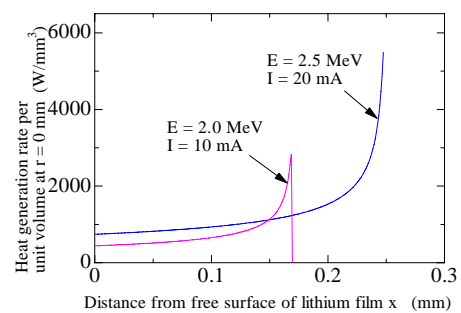


Fig.1 Calculated distribution of heat generation rate per unit volume in a lithium target film in case of beam diameter of 30mm

The deposited heat increases the lithium temperature. Temperature profile in a lithium plane jet at the velocity of 30 m/s for the proton beam conditions of 2.0 MeV, 10 mA and 30 mm in diameter was calculated numerically. In the calculation, the energy conservation equation was solved using the finite-difference method with the assumption of a uniform velocity profile in the cross section of the jet and a laminar flow. Fig.2 shows the calculated temperature profile in vertical plane with hot spot. It is found that the hot spot appeared 11 mm downstream from the beam

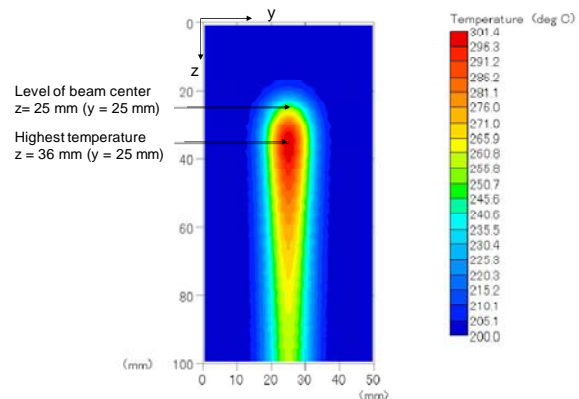


Fig.2 Temperature profile in vertical plane with hot spot in lithium plane jet for proton beam of 2.0 MeV and 10 mA

line, and the hot spot temperature is 301 °C which is less than the saturation temperature of 342 °C. Fig. 3 shows the calculated temperature profiles in the beam center line:  $y = 25$  mm,  $z = 25$  mm; and in the line with the hot spot:  $y = 25$  mm,  $z = 36$  mm. It is found that the maximum temperature in the beam center line is less than 260 °C and position of the hot spot exists at the free surface of the jet.

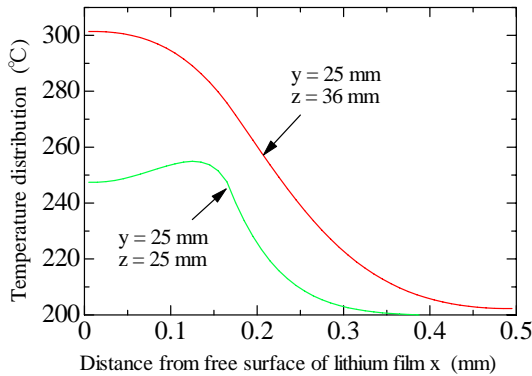


Fig.3 Temperature profile in lithium plane jet for proton beam of 2.0 MeV and 10 mA

## 2.2. Conceptual design of target system

Based on the consideration in the preceding section, the conditions of the lithium jet for the proton beam target are chosen as listed in Table 1.

Table 1 Conditions for lithium target

Proton beam	Diameter (mm)	30
Li target	Width (mm)	50
	Length (mm)	50
	Thickness (mm)	0.5
Li plane jet	Velocity (m/s)	30
	Temperature (°C)	200
	Flow rate (L/min)	45
Accelerator	Pressure (Pa)	$10^{-3}$

Fig. 4 shows the flow diagram of the lithium target system. The lithium main loop consists of the electromagnetic pump (EMP), the electromagnetic flow meter (EMF), the lithium cooler, the target assembly and the quench tank. The major part of pressure losses in the loop is the form loss for flow acceleration in the nozzle, i. e., the dynamic pressure,  $\rho v_z^2 / 2 = 225$  kPa. The level of lithium in the quench tank should be high enough to avoid cavitation in the EMP. It is expected to decrease the level for a compact lithium target system by improving the EMP with a gradient magnetic field so that it can be operated with lower inlet head. The system is equipped with a bypass loop with the EMF and the cold trap for removal of O, C, H and N in the lithium. The lithium cooler and the cold trap are cooled by heat transfer media (diethylbiphenyl) or Ar gas. All the lithium system is

confined in a containment vessel which is filled with Ar gas for fire measure at lithium leak accident.

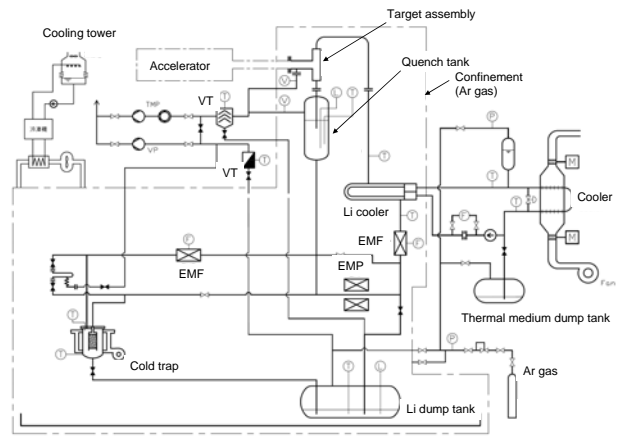


Fig. 4 Flow diagram of lithium target system

Fig. 5 shows the layout of the lithium target system. The sizes of the components and piping lengths are determined by hydrodynamic design. A total friction pressure loss along the loop is estimated to be approximately 7 kPa in case of 1B piping (O.D. 34.0 mm, I. D. 27.8 mm), where the velocity in the pipe is 1.3 m/s. The lithium target system is compact enough for set-up adjacent to hospitals.

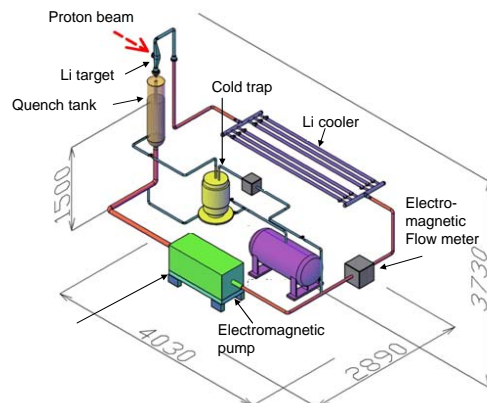


Fig. 5 Layout of lithium target system

## 4. Conclusions

The concept of the liquid lithium target system for the boron neutron capture therapy has been formulated.

## Reference

M. Takahashi, T. Kobayashi, M. Nakatsuka, T. Ardiansyah, M. Kulhanek, A. Vojacek, V. Dostal, S. Uchida, M. Zhang: Study on Liquid Lithium Target System for Boron Neutron Capture Therapy (BNCT); *The 18th Int. Conf. on Nucl. Eng. (ICONE18)*, May 17-21, 2010, Xi'an, China, ICONE18-29516.

## C.9 Hydrodynamic Study on Flowing Liquid Water and Lithium Target for Boron Neutron Capture Therapy (BNCT)

Minoru TAKAHASHI, Tooru KOBAYASHI, Masashi NAKATSUKA,  
Teddy ARDIANSYAH, Martine KULHANEK, Ales VOJACEK, and Vaclav DOSTAL

### 1. Introduction

The combination of a flowing liquid lithium target with a proton beam accelerator is the candidate neutron source for the boron neutron capture therapy (BNCT) that has various advantages compared with a solid target and/or the thermal neutron source of nuclear reactors. In the present study, lithium and water flow loops are designed and fabricated for development of nozzles that provide a stable lithium plane jet for the target. A water flow test is conducted to select a suitable nozzle for liquid lithium target.

### 2. Lithium Jet Experiment

A stable target of the lithium jet should be formed without break-up. It is necessary to demonstrate that a stable plane jet is realized well experimentally. Several candidate of plane jet nozzles developed through water test will be tested for the demonstration. A lithium flow loop is designed and fabricated. The specifications of the lithium loop are as follows: max. temperature 300 °C and max. flow rate 40 L/min. Fig. 1 shows the layout of the lithium flow loop. The test section and the quench tank are located at high level to avoid cavitation in the electromagnetic pump (EMP) under vacuum condition in the test section.

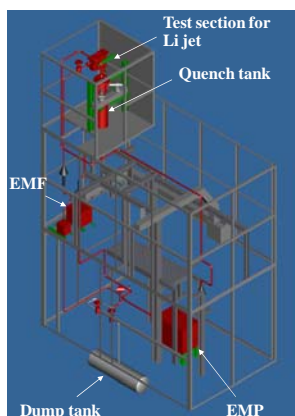


Fig. 1 Layout of lithium flow loop

### 3. Experimental Procedure of Water Jet Flow

In order to develop nozzles which can make a thin plane jet at the velocity of 30 m/s, nozzles with various inner geometries were tested in a water flow loop. Three types of straight rectangular nozzles with the width of 60 mm and the gap of 0.2, 0.5 and 1.0 mm were tested in a rectangular test section (72 x 22 mm<sup>2</sup>). The 0.5 mm-gap nozzles are 10 mm (=10D<sub>e</sub>), 40 mm (=40D<sub>e</sub>) and 70 mm (=70D<sub>e</sub>) in length, where D<sub>e</sub> is the hydraulic diameter. The jet surface was observed by being illuminated with the strobe scope (Fig. 2).

### 4. Experimental result of Water Jet

Fig. 3 shows the surface condition of the water plane jet from the nozzle with a gap of 0.5mm and a length of 70 mm at velocity of 22 m/s. It is found that the jet was stable without entrainment, although the surface was wavy. From the result of the water flow test, it is concluded that a stable 0.5 mm-thick plane jet can be formed using a long nozzle at the outlet of which the flow is fully developed.

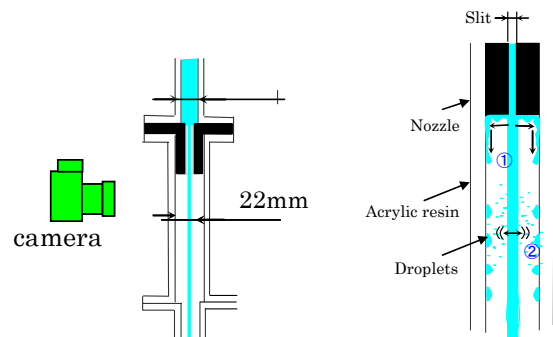


Fig. 2 Entrainment of droplets from water plan jets

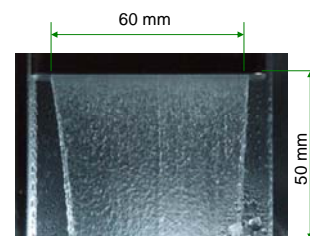


Fig. 3 Surfaces of water plane jet from nozzle with a gap of 0.5mm and a length of 70 mm at velocity of 22 m/s.

### 5. Conclusion

A lithium flow loop was designed and fabricated for development of lithium jet nozzles that could form a stable lithium plane jet. A water flow loop was designed and fabricated for development of lithium jet test nozzles. It was found that a stable plane water jet was formed by using a nozzle with the gap of 0.5mm and the length of 70mm. It was concluded that a fully developed flow without inlet disturbances at the outlet of the nozzle is required for the stability of the high velocity plane jet.

### Reference

M. Takahashi, T. Kobayashi, M. Nakatsuka, T. Ardiansyah, M. Kulhanek, A. Vojacek, V. Dostal, S. Uchida, , M. Zhang: Study on Liquid Lithium Target System for Boron Neutron Capture Therapy (BNCT); *The 18th Int. Conf. on Nucl.Eng. (ICONE18)*, May 17-21, 2010, Xi'an, China, ICONE18-29516

### III. Co-operative Researches

#### III.1 Co-operative Researches within Tokyo Institute of Technology

Under the generic proposition: "The Release and Utilization of Energies existing in Atoms, Molecules and Nuclei" which has been hoisted since the reorganization of RLNR, we advertise for collaborations with any department and laboratory within Tokyo Institute of Technology in order to develop researches for the improvement of energy utilization with safety, mass transmutation by nuclear reactions with high efficiency, and construction of energy system concept with high societal acceptability. The RLNR will promote these collaborations by offering the organizations, facilities, equipments and space as the research base for research project teams and research groups crossing over within Tokyo Tech. We are going to adopt unique and innovative themes which make maximum use of the activities of this research laboratory.

- Heavy-Ion Inertial Fusion and High Energy-Density Physics Driven by Heavy-Ion Beams  
Interdisciplinary Graduate School of Science and Engineering
- CO<sub>2</sub> electrolysis cell for carbon recycling energy system  
Fusion joint research, Multidisciplinary Education and Research Center for Energy Science Tokyo Institute of Technology Global COE Program
- Feasibility study for carbon recycling energy system  
Fusion joint research, Multidisciplinary Education and Research Center for Energy Science, Tokyo Institute of Technology Global COE Program
- Building study of active carbon recycling energy system  
Tokyo Tech AES Center, 2010.
- Feasibility study for carbon recycling energy system  
Fusion joint research, Multidisciplinary Education and Research Center for Energy Science, Tokyo Institute of Technology Global COE Program

#### III.2 Co-operative Researches with Outside of Tokyo Institute of Technology

- Fundamental Study of Thermo-Hydraulic Instability on Reduced-Moderation Natural Circulation BWR Concept (Clarification of Condensation Phenomena under Non-Condensable Gas)  
Japan Atomic Power Co.
- Study on Technical Standards for Safety Transportation of Decommissioned Wastes of Nuclear Power Plant  
Nuclear Fuel Transport Co., Ltd.
- Development of Measurement Instrument of Void Fraction in Steam Generator  
IHI Corporation
- Fundamental Study on Advanced Turbid Water Treatment  
NPO. Saiseisya
- Two-Phase Flow Dynamics for Future Light Water Reactor Development  
Korea Atomic Energy Research Institute, Korea
- Experimental and Analytical Studies on Multi-Dimensional Two-Phase Flow  
PSF Zittau, Germany
- Advanced Fluid Dynamics and Developed of Measurement Technique  
Chulalongkorn University, Thailand
- Thermal Hydraulics for Advanced Water Cooling Reactors  
Bhabha Atomic Research Center, India
- Future Light Water Reactor Development  
Chulalongkorn University, Thailand
- Research and Development of High Performance Ceramics  
Chiba Institute of Technology, Tokai University
- Establishment of Fabrication Process of Silicon-Containing Ceramics for Inert Matrix of TRU Elements  
Japan Atomic Energy Agency
- Study on Novel Process of SiC/SiC Composite by Electrophoretic Deposition Method :  
Japan Aerospace Exploration Agency (JAXA)
- Study on the Improvement of Irradiation Resistance of Ceramics by Their Orientation Control :  
National Institute for Materials Science (NIMS)

- Evaluation of Sinterability and Properties of SiC Ceramics using Al<sub>4</sub>SiC<sub>4</sub> as Sintering Additives : National Institute for Materials Science (NIMS)
- Studies on Separation of Uranium Species Using Polyvinylpolypyrrolidone  
Japan Atomic Energy Agency and Tokai University
- A Study of Extraction Behavior of ReO<sub>4</sub><sup>-</sup> by Using Monoamide Compounds  
Japan Atomic Energy Agency
- A Study on Partitioning of Lanthanoid and Actinoid Species  
Japan Atomic Energy Agency
- A Study on Separation of Uranyl Species Using Alginate Acid  
Prof. R.M. Hassan, Assiut University, Egypt
- A Study on Electron Transfer Reaction between Uranyl(V) and Uranyl(VI) Carbonate Complexes  
Professor I. Grenthe, Royal Institute of Technology, Sweden
- A Study on Electrochemical Reactions of Uranyl Species in Choline Based Ionic Liquids  
Professor A.P. Abbott, University of Leicester, U.K.
- Studies on Structures of Uranyl Complexes in Ionic Liquids  
Dr. C. Hennig, Forschungszentrum Rossendorf, Germany
- Studies on Electrochemical Reactions of Uranyl(VI) Species in Ionic Liquids  
Japan Atomic Energy Agency
- Neutron Capture Cross Section Measurement n\_TOF Collaboration
- Development of a new gamma-ray detector for keV-neutron capture experiment  
Osaka University, Japan Atomic Energy Agency
- Study on keV-Neutron Capture Cross Sections of Fe isotopes  
Dong-A University, Kyungpook National University
- Study on Glass Vitrification Process  
Japan Nuclear Fuel Limited.
- Study on Extraction Chromatographic Process using Multidentate Encapsulating Ligands for Recovery of Minor Actinides  
Japan Science and Technology Agency
- Development of Continuous Optimal-response Extraction Process of Precious Metals  
Japan Science and Technology Agency
- Study on Recovery of Platinum Group Metals from High-level Liquid Wastes  
Tokyo Electric Power Company, Incorporated
- Preparation and utilization of Tc and Re complex using novel ligands, mino-bis-diacetamides  
Japan Atomic Energy Agency, Ibaraki University, Tohoku University
- Basic Characteristics for PEN Film Surface Modification Using Atmospheric-Pressure Nonequilibrium Microwave Plasma Jet  
University of Miyazaki, ADTEC Plasma Technology Co. Ltd., JEOL Ltd. Japan, Kagawa University.
- Surface Modification of Silicon Wafer by Low-Pressure High-Frequency Plasma Chemical Vapor Deposition Method  
Minami-Kyushu Junior College, King Mongkut's University of Technology Thonburi, University of Miyazaki, Kagawa University, Hiroshima National College of Maritime Technology, ADTEC Plasma Technology Co. Ltd., Miyazaki Technical High School
- Optical Emission Spectroscopy Measurement of High-Frequency Low-Pressure at Plasma-Enhanced Chemical Vapor Deposition  
University of Miyazaki, Osaka University
- Development of Liquid Lithium Target for Neutron Production in Neutron Irradiation System for Neutron Capture Therapy based on by Accelerators  
Kyoto University
- Development of Low-Load Wood Drying System using Heat Pump, Practical Technical Project to Promote the Development of New Agriculture Policy  
Ministry of Agriculture, Forestry and Fisheries, #2008-2034, 2008-2010
- Chemical heat pump for waste heat recovery from iron making process, Environmentally Friendly Steel Process Technology  
NEDO commissioned project, 2010
- Study on low-carbon and carbon recycling iron-making system using ACRES  
Sumitomo Metal Ind., 2010
- Material Development of Chemical Heat Storage for Effective Use of Industrial Waste Heat

- Industrial Technology Research Grant Program from New Energy and Industrial Technology Development Organization (NEDO) of Japan, #08B33005c, 2008-2010  
Japan Atomic Energy Agency
- In situ high-resolution photoelectron spectroscopic study of 1D peanut-shaped C<sub>60</sub> polymers  
UVSOR Facility, Institute for Molecular Science
- DFT study of low-dimensional peanut-shaped C<sub>60</sub> polymers  
Yokohama National University
- Photodynamic properties of nanomaterials  
Department of Applied Physics, Hokkaido University
- Riemannian geometrical effects on physical properties of 1D uneven peanut-shaped C<sub>60</sub> polymer  
Department of Applied Physics, Hokkaido University,  
Department of Physics, Nara Women's University
- Fabrication of AZO transparent electrodes for Organic Photovoltaic cells  
Department of Electronic Engineering and Applied Physics, Osaka City University
- Application of 1D uneven peanut-shaped C<sub>60</sub> polymer to a detector for THz wave spectroscopy  
Department of Electronic Engineering and Applied Physics, Osaka City University
- A Study of Surface and Interfaces of Organic Photovoltaic Cells”  
J-Power Co. Ltd
- Survey on the Trend in Scientific Research on Zoology and Related Field  
Survey on the Trend in Scientific Research  
Japan Society for the Promotion of Sciences, Japan
- Analyses of the Repair of DNA Double-Strand Breaks Generated by Low Dose/Low Dose Rate Radiation  
Central Research Institute of Electric Power Industries
- Study on Electron density fluctuations by Microwave Imaging Reflectometry  
National Institute for Fusion Science
- Development of ECE imaging system by the use of 1-D horn antenna array  
National Institute for Fusion Science
- Development of Fiber-Optic Diagnostic on Vacuum Vessel Current of QUEST  
Research Institute for Applied Mechanics, Kyushu University
- Separation and recovery of molybdenum in spent fuel by ion exchange technique  
Japan Atomic Energy Agency
- Basic study on solidification of low-level radioactive liquid waste  
Japan Atomic Energy Agency
- Study on ion exchange behavior of actinides, VII group elements and fission products  
Japan Atomic Energy Agency
- Characterization of structure and physico-chemical properties of molten rare-earth metal halides  
Japan Atomic Energy Agency
- Innovative characterization of materials under severe condition  
(Conditions Extrêmes et Matériaux : Haute Température et Irradiation)  
Centre National de la Recherche Scientifique
- Structure and physico-chemical properties of thorium fluoride mixtures  
Institute of Multidisciplinary Research for Advanced Materials, Tohoku University (Network Joint Research Center for Materials and Devices)
- Pyro-reprocessing of rare earth elements from Ni-MH battery  
The Shinsei Foundation
- Experimental investigation of positional stabilization of torus plasma with helical coils  
National Institute for Fusion Science
- Gyrokinetic simulation study on turbulence in finite beta plasmas  
National Institute for Fusion Science
- Characteristics of MHD equilibrium, stability and transport in high-beta plasmas  
National Institute for Fusion Science
- Effects of MHD Disruption on Plasma Confinement  
Japan Atomic Energy Agency

### III.3 Themes Supported by Grants-in-Aid for Scientific Research of the Ministry of Education, Culture, Sports, Science and Technology

- Material Development of Porous Ceramics for Diesel Particulate Filter Based on In-Situ Crystal Growth and Orientation : Grant-in-Aid for Young Scientists (B)
- Systematic Study on Neutron Capture Reaction Cross Sections for the Technological Development of Nuclear Transmutation of Long-Lived Nuclear Waste.
- Development of Liquid-liquid Counter-current Centrifugal Extractor for Nuclide Separation
- Angiocinematography Using Particle-Induced Dual-Wavelength Pulsed-X-rays for Minimization of Dosages of Contrast-Medium and Radiation
- Development of a Variable-Energy, Variable-Intensity, On/Off-switchable Gamma-Ray Needle-Source for Brachytherapy
- High-Efficient High-Temperature Process by Hybrid Method using Chemical Heat Storage
- Development of new quantum electronic science in Riemannian geometric space
- New Strategy for the Prediction and Control of Radiosensitivity Based on the Life Cycle and Homeostasis of DNA Double-Strand Breaks Enzymes
- Development of A Novel Nanofluidic-based Separation System for Rare-Earth Elements  
Japan Society for the Promotion of Science, Funding Program for Next Generation World-Leading Researchers (NEXT Program)
- Development of Ion Transport Method in Extended-Nano Space for Photo Fuel Cell  
Core Research for Evolutional Science and Technology (CREST), Japan Science and Technology Agency
- Hydrothermal Synthesis Process of Metal Oxidized Nanomaterials using Supercritical Water  
Preceding Basic Engineering Research Program, Japan Atomic Energy Agency
- NMR Studies on Water and Radionuclides Confined in Bentonite Clay under High-Temperature and -Pressure Conditions  
Japan Society for the Promotion of Science, Grant-in-Aid for Young Scientists B
- NMR Studies on Molecular Structures and Dynamics of Liquid-Phase Cluster Molecules in Soft Material Interfaces

Japan Society for the Promotion of Science, Grant-in-Aid for Scientific Research on Innovative Areas

- Investigation of Biophysical Chemistry in Extended-Nano regions using Nuclear Magnetic Resonance Method  
Mizuho Foundation for the Promotion of Sciences, Engineering research aid projects

#### IV. List of Publications

Yasushi Muto, Shintaro Ishiyama, Yasuyoshi Kato, Takao Ishiduka and Masanori Aritomi: Application of Supercritical CO<sub>2</sub> Gas Turbine for the Fossil Fired Thermal Plant; *Journal of Energy and Power Engineering*, **4**, No. 1, pp. 6-10 (2010).

Noriyuki Watanabe, Se-Young Chun, Masanori Aritomi and Hiroshige Kikura: Experimental Study on Heat Transfer Characteristics of Vertical 5\*5 Heated Rod Bundles around Critical Pressure with R-134a; *Journal of Nuclear Science and Technology*, **48**, No. 1, pp. 135-144 (2011).

Masanori Aritomi, Takao Ishiduka, Yasushi Muto. and Nobuyoshi Tsuzuki: Performance Test Results of a Supercritical CO<sub>2</sub> Compressor Used in a New Gas Turbine Generating System; *Journal of Power and Energy Systems*, **5**, No. 1, pp.45-59 (2011).

Atushi Ui, Shigeo Ebata, Fumio Kasahara, Tsunakiyo Iribe, Hiroshige Kikura and Masanori Aritomi: Study on Solid-Liquid Two-Phase Flow on PWR Sump Clogging Issue; *Journal of Nuclear Science and Technology*, **47**, No. 9, pp. 820-828 (2010).

Masanori Aritomi, Takao Ishiduka, Yasushi Muto and Nobuyuki Tsuzuki: Performance Test Results of the Supercritical CO<sub>2</sub> Compressor for a New Gas Turbine Generating System; *The 18th International Conference on Nuclear Engineering (ICONE18)*, ICONE18-29371, Xi'an, China (2010).

Masanori Aritomi: Asbestos harmless mobile Treatment Systems on Pulling Down Sites; *Proceedings of 24<sup>th</sup> National Congress for Environmental Studies*, Tokyo, Japan, pp.129-134, (2010-4-15~16), in Japanese.

Motoaki Utamura, Masanori Aritomi, Kei Yamamoto and Hiroshi Hasuike: Preliminary Test result of a Closed Cycle Gas Turbine with Supercritical CO<sub>2</sub> as Working Fluid; *The 15<sup>th</sup> National Symposium on Power and Energy System, (SPES 2010)*, Tokyo, Japan, CD-ROM, pp. 197-198, (2010-6-21~22), in Japanese.

Masanori Aritomi, Toshinori Takata, and Takayuki Morii: Effective technology of Preventive Measures Against Piping Damage on Stream Lines in Nuclear Power Plants; *The 15<sup>th</sup> National Symposium Power and Energy Systems (SPES 2010)*, Tokyo, Japan, pp.83-86, (2010-6-21~22), in Japanese.

Masanori Aritomi, Junko Takanashi, Shigeki Hosobuchi, Noriko Hasegawa: Development of Water System for Cutting Asphalt Road (III); *Mechanical Engineering Congress, 2010 Japan (MECJ-10)*, pp. 149-150, Nagoya Institute of Technology, Japan, (2010-9-5~8).

Masanori Aritomi, Junko Takanashi, Shigeki Hosobuchi and Noriko Hasegawa: Development of Simplified Treatment of System of Turbid Water in Disaster Area; *Mechanical Engineering Congress, 2010 Japan (MECJ-10)*, pp. 147-148, Nagoya Institute of Technology, Japan, (2010-9-5~8).

T. Yano, J. Yamane, K. Yoshida, S. Miwa and M. Ohsaka: Low Temperature Liquid-Phase-Assisted Sintering of Si<sub>3</sub>N<sub>4</sub> Ceramics as an Inert Matrix for Confinement of Minor Actinides; *ACTINIDES 2009, IOP Conf. Series: Mater. Sci. Engineer*, **9**, 012024 (2010). Doi: 10.1088/1757-899x/9/1/012024.

H. Yokota, M. Yoshida, H. Ishibashi, T. Yano, H. Yamamoto and S. Kikkawa: Concentration Effect of Cerium in (Y<sub>0.9-x</sub>Gd<sub>0.1</sub>Ce<sub>x</sub>)<sub>2</sub>SiO<sub>5</sub> Blue Phosphor; *J. Alloys and Compounds*, **495**, 162-166 (2010). Doi: 10.1016/j.alocom2010.01.112.

S. Miwa, M. Osaka, T. Ukai and T. Yano: Densification of Inert Matrix Fuels Using Naturally-Occurring Material as a Sintering Additive; *Proc. MRS* (printed).

S. Miwa, M. Osaka, Y. Akutsu, T. Yano, K. Kurosaki, S. Yamanaka, S. Takano and Y. Yamane: Inert Matrix Fuel Concept for the Rapid Incineration of Minor Actinides Harmonious with a Fast Reactor Cycle System; *Proc. International Conference on Fast Reactors and Related Fuel Cycles*, (printed).

W. Khongwong, K. Yoshida and T. Yano: Simple Approach to Fabricate SiC-SiO<sub>2</sub> Composite Nanowires and Their Oxidation Resistance; *Mater. Sci. Engineering B*, **173**, 117-121 (2010).

W. Khongwong, K. Yoshida and T. Yano: Fabrication and Properties of Core/Shell Type SiC-SiO<sub>2</sub> Nanowires through Low-Cost Production; *Nanostructured Materials and Nanotechnology IV*, American Ceramic Society, 51-62 (2010).

T. Yano: Application of Ceramics for Components of Fission and Fusion Nuclear Reactors; Present Status and Challenge ; *Text of the 42<sup>nd</sup> Seminar on Engineering Ceramics*, pp.37-46 (2010).

K. Yoshida: Development of Silicon Carbide Fiber-Reinforced Silicon Carbide Matrix Composites with High Performance Based on Interfacial and Microstructure Control; *J. Ceram. Soc. Japan*, **118** [2], 82-90 (2010).

K. Yoshida: Improvement of Sinterability and Mechanical Properties of β-Tricalcium Phosphate; *J. Soc. Inorg. Mater., Japan (Muki-Materiaru)*, **17** [346], 188-195 (2010).

K. Yoshida, H. Hyuga, N. Kondo and H. Kita: Synthesis of Precursor for Fibrous Mullite Powder by Alkoxide

- Hydrolysis Method; *Mater. Sci. Eng. B*, **173**, 66-71 (2010).
- N. Matsumoto, K. Yoshida, K. Hashimoto and Y. Toda: Dissolution Mechanisms of  $\beta$ -Tricalcium Phosphate Doped with Monovalent Metal Ions; *J. Ceram. Soc. Japan*, **118** [6], 451-457 (2010).
- N. Matsumoto, A. Yokokawa, K. Ohashi, K. Yoshida, K. Hashimoto and Y. Toda: Mechanical Properties of  $\square$ -Tricalcium Phosphate Ceramics Doped with Vanadate Ions; *Phosphorous Research Bulletin*, **24**, 73-78 (2010).
- N. Matsumoto, K. Yoshida, K. Hashimoto and Y. Toda: Preparation of Beta-Tricalcium Phosphate Powder Substituted with Na/Mg Ions by Polymerized Complex Method; *J. Am. Ceram. Soc.*, **93** [11], 3663-3670 (2010).
- K. Yoshida, A. Kawasumi, K. Hashimoto, Y. Toda, M. Imai and T. Yano: Fabrication of Three-Dimensional  $\text{Al}_2\text{O}_3/\text{YAG}$  Composites Using Porous  $\text{Al}_2\text{O}_3$  Ceramics Prepared by  $\alpha$ - $\text{Al}_2\text{O}_3$  Powder and Their Mechanical Properties; *High Temperature Ceramic Materials and Composites (Proc. 7<sup>th</sup> International Conference on High Temperature Ceramic Matrix Composites (HT-CMC7))*, pp. 492-497 (2010).
- K. Yoshida, A. Kawasumi, K. Hashimoto, Y. Toda, M. Imai and T. Yano: Fabrication and Mechanical Properties of Three-Dimensional  $\text{Al}_2\text{O}_3/\text{YAG}$  Composite Using Hollow Spherical  $\text{Al}_2\text{O}_3$  Powder Prepared by Spray Pyrolysis Method; *High Temperature Ceramic Materials and Composites (Proc. 7<sup>th</sup> International Conference on High Temperature Ceramic Matrix Composites (HT-CMC7))*, pp. 485-491 (2010).
- W. Khongwong, K. Yoshida and T. Yano: Fabrication of Core-Shell Type  $\text{SiC}/\text{SiO}_2$  Nanowires through Low-Cost Production Technique; *Abst. The 34<sup>th</sup> International Conference and Exposition on Advanced Ceramics and Composites*, Daytona Beach, Florida, USA, S7-P135 (2010) p.100.
- K. Yoshida, C. C. See and T. Yano: Fabrication of Porous Silicon Carbide using in-situ Crystal Growth; *Abst. The 34<sup>th</sup> International Conference and Exposition on Advanced Ceramics and Composites*, Daytona Beach, Florida, USA, S9-P058 (2010) p.58.
- S. C. Chet, K. Yoshida, M. Imai and T. Yano: Fabrication and Properties of Porous Silicon Carbide Ceramics based on Control of Grain Growth; *Abst. Ann. Meeting of Ceram. Soc. Jpn.*, 2010, 3C04, pp.273. (2010).
- S. Miwa, M. Osaka, T. Usuki and T. Yano: Densification of Nuclear Fuel Pellets Using Asbestos Waste as a Sintering Additives; *Abst. Ann. Meeting of Ceram. Soc. Jpn.*, 2010, 3I24, pp.313. (2010).
- M. Osaka, S. Miwa, K. Kurosaki, S. Yamanaka, M. Uno, Y. Yamane, H. Mimura and T. Yano: Fundamental Study of Inert Matrix Fuels Adaptable to a Fast Reactor Cycle System, (1) Concept"; *Abst. 2010 Ann. Meetings of the Atom. Energy Soc. Jpn.*, L28, pp.560 (2010).
- T. Yano, K. Yoshida, M. Imai, S. Miwa and M. Osaka: Fundamental Study of Inert Matrix Fuels Adaptable to a Fast Reactor Cycle System, (2)  $\text{Si}_3\text{N}_4$  Based Fuels; *Abst. 2010 Ann. Meeting of the Atom. Energy Soc. Jpn.*, L29, pp.561 (2010).
- T. Usuki, K. Yoshida, M. Imai, T. Yano, S. Miwa and M. Osaka: Sintering and Characterization of Silicon Nitride Ceramics as Inert Matrix with Magnesium Silicates; *Abst. 2010 Ann. Meeting of the Atom. Energy Soc. Jpn.*, L31, pp.562 (2010).
- K. Yoshida, Y. Sekimoto, K. Katayama, W. Thanakorn, M. Imai and T. Yano: Change in Thermal Conductivity of Silicon Nitride Ceramics by Thermal Treatment; *Abst. 124 Committee of JSPS 134 Meeting*, pp.83-84. (2010).
- T. Yano, K. Yoshida, W. Khongwong:  $\text{SiC}/\text{SiO}_2$  Core-Shell Nanowires Synthesized by Thermal Evaporation Method Using Raw Powders; *Abst. 3<sup>rd</sup> International Symposium on SiAlONs and Non-Oxides (ISSNOX3)*, pp.29. (2010).
- K. Yoshida, H. Katsumata, M. Imai and T. Yano: The Effect of BN Particle Size on Mechanical Properties and Machinability of  $\text{SiC}/\text{BN}$  Composites; *Fourth International Conference on Science and Technology of Advanced Ceramics (STAC-4)*, PP-69. (2010).
- K. Yoshida and T. Yano: Contribution of Ceramic Materials for Electric Power Generation System; *Fourth International Conference on Science and Technology of Advanced Ceramics (STAC-4)*, 2a-B01. (2010).
- K. Yoshida, A. Kawasumi, K. Hashimoto, Y. Toda, M. Imai and T. Yano: Fabrication of Three-Dimensional  $\text{Al}_2\text{O}_3/\text{YAG}$  Composites Using Porous  $\text{Al}_2\text{O}_3$  Ceramics Prepared by  $\alpha$ - $\text{Al}_2\text{O}_3$  Powder and Their Mechanical Properties; *7<sup>th</sup> International Conference on High Temperature Ceramic Matrix Composites (HT-CMC7)*, HT-CMC7-PS-264, pp.114-115(2010).
- K. Yoshida, A. Kawasumi, K. Hashimoto, Y. Toda, M. Imai and T. Yano: Fabrication and Mechanical Properties of Three-Dimensional  $\text{Al}_2\text{O}_3/\text{YAG}$  Composite Using Hollow Spherical  $\text{Al}_2\text{O}_3$  Powder prepared by Spray Pyrolysis Method; *7<sup>th</sup> International Conference on High Temperature Ceramic Matrix Composites (HT-CMC7)*, HT-CMC7-40b-263, p.114 (2010).
- M. Osaka, S. Miwa, K. Tanaka, K. Ikeda, H. Mimura, T. Usuki and T. Yano: Reformation of Hazardous Wastes into Useful Supporting Materials for Fast Reactor Fuels; *The Third International Symposium on Innovative Nuclear Energy Systems-Innovative Nuclear Technologies for Low-Carbon Society-(INES-3)*, 1B-23, pp.58. (2010).

- S. Miwa, M. Osaka, T. Usuki and T. Yano: Densification of Inert Fuels Using the Waste of Asbestos as a Sintering Additive; *The Third International Symposium on Innovative Nuclear Energy Systems–Innovative Nuclear Technologies for Low-Carbon Society– (INES-3)*, 1B-22, pp.57. (2010).
- Y. Futamura, M. Imai, K. Yoshida and T. Yano: Recovery Behavior of Neutron-Irradiation-Induced Damage of AlN by Thermal Annealing; *The Third International Symposium on Innovative Nuclear Energy Systems–Innovative Nuclear Technologies for Low-Carbon Society– (INES-3)*, P-130, pp.154. (2010).
- T. Usuki, K. Yoshida, M. Imai, T. Yano, S. Miwa, M. Osaka: Fabrication and Characterization of Silicon Nitride Based Inert Matrix Fuels; *The Third International Symposium on Innovative Nuclear Energy Systems–Innovative Nuclear Technologies for Low-Carbon Society – (INES-3)*, P-134, pp.158. (2010).
- M. Akiyoshi, H. Tsuchida, T. Yoshiie, X. Qiu, K. Sato and T. Yano: Irradiation Damage in Ceramics Induced by 30MeV Electron Linac; *The Third International Symposium on Innovative Nuclear Energy Systems–Innovative Nuclear Technologies for Low-Carbon Society – (INES-3)*, 1B-25, pp.60. (2010).
- T. Yano and K. Yoshida: Fabrication of SiC Continuous Fiber-Reinforced SiC Composite Using Electrophoretic Deposition and Hot-Pressing; *3<sup>rd</sup> International Congress on Ceramics (ICC3)*, S10-018. (2010).
- K. Yoshida, C.-C. See, M. Imai and T. Yano: Fabrication of Porous Silicon Carbide Ceramics Based on In-Situ Grain Growth; *3<sup>rd</sup> International Congress on Ceramics (ICC3)*, S12-028. (2010).
- T. Yano, Y. Horie, M. Imai and K. Yoshida: Sintering of Silicon Carbide Ceramics with Co-addition of Gadolinium Oxide and Silica and Their Mechanical Properties; *3<sup>rd</sup> International Congress on Ceramics (ICC3)*, S14-P001. (2010).
- K. Yoshida, Y. Sekimoto, K. Katayama, T. Wasanapiarnpong, M. Imai and T. Yano: The Effect of Heat-Treatment on Thermal Conductivity of Silicon Nitride Ceramics; *3<sup>rd</sup> International Congress on Ceramics (ICC3)*, S14-P016. (2010).
- K. Yoshida: Development of Silicon Carbide-Based Materials for Environmental and Energy Application; *The 33<sup>rd</sup> Nano Ceramics Center Seminar (NIMS)*, (2010).
- K. Yoshida: Development of SiC Fiber-reinforced SiC Composites with High Performance Based on Interfacial and Microstructure Control; *Ann. Meeting of The Ceram. Soc. Jpn, 2010*, 2C31A, p.107 (2010).
- K. Ohashi, S. Mitsumori, R. Miyamoto, K. Yoshida, K. Hashimoto and Y. Toda: Cellular Reactivity of Osteoclast-Like Cells on Na<sup>+</sup> Ions Doped  $\beta$ -Tricalcium Phosphate Ceramics; *Ann. Meeting of The Ceram. Soc. Jpn, 2010*, 1E28, p.38 (2010).
- N. Matsumoto, K. Sato, K. Yoshida, K. Hashimoto and Y. Toda: Substitution Model of Silicate Ions in  $\beta$ -Tricalcium Phosphate Structure ; *Ann. Meeting of The Ceram. Soc. Jpn, 2010*, 2E02, p.114 (2010).
- E. Takahashi, N. Matsumoto, K. Yoshida, K. Hashimoto, Y. Toda, S. Udagawa and T. Kanazawa: Fabrication of Sintered Body Consisted of  $\beta$ -Tricalcium Phosphates Doped with Divalent and Trivalent Metal Ions; *120<sup>th</sup> Meeting of the Soc. Inorg. Mater., Japan*, (11), pp.22-23 (2010).
- A. Yokoya, N. Matsumoto, K. Yoshida, K. Hashimoto and Y. Toda, S. Udagawa and T. Kanazawa: Substituted Mechanism of Anion into Crystal Structure of  $\beta$ -Type Tricalcium Phosphate; *120<sup>th</sup> Meeting of the Soc. Inorg. Mater., Japan*, (33), pp.66-67(2010).
- K. Ohashi, R. Miyamoto, H. Shibata, K. Yoshida, K. Hashimoto and T. Kanazawa: Cellular Evaluation of MC3T3-E1 Cells on VO<sub>4</sub><sup>3-</sup> Ions Doped  $\beta$ -Tricalcium Phosphate; *20<sup>th</sup> Meeting of Japanese Assoc. Inorg. Phosphorous Chem.*, P15-Y, pp.78-79(2010).
- A. Ozawa, R. Miyamoto, H. Shibata, K. Yoshida, K. Hashimoto and T. Kanazawa: Inhibitor Test of Osteoclast Cells on Manganese(II) Ion-Doped  $\beta$ -Tricalcium Phosphate Ceramics; *20<sup>th</sup> Meeting of Japanese Assoc. Inorg. Phosphorous Chem.*, P17-Y, pp.82-83 (2010).
- R. Miyamoto, H. Shibata, K. Yoshida and K. Hashimoto: Acceleration of Cell Behavior onto Sodium Ions Doped  $\beta$ -Tricalcium Phosphate; *20<sup>th</sup> Meeting of Japanese Assoc. Inorg. Phosphorous Chem.*, P32-Y, pp.112-113 (2010).
- K. Yoshida, C.-C. See, M. Imai and T. Yano: Fabrication and Evaluation of Porous SiC Ceramics Based on In-Situ Grain Growth; *The 1<sup>st</sup> Ceram. Eng. Workshop*, p.9 (2010).
- R. Miyamoto, K. Ohashi, H. Shibata, K. Yoshida and K. Hashimoto: ST2/C7 Cells Differentiation Ability on  $\beta$ -Tricalcium Phosphate Doped with Various Amount of Sodium Ions; *The 14<sup>th</sup> Symp. Ceram. in Medicine, Biology and Bioceramics*, 12, p.12 (2010).
- S. Hanazawa, A. Ozawa, R. Miyamoto, H. Shibata, K. Yoshida and K. Hashimoto: Evaluation of Osteoclast-Like Cells on Potassium Ion-Doped  $\beta$ -Tricalcium Phosphate Ceramics; *The 14<sup>th</sup> Symp. Ceram. in Medicine, Biology and Bioceramics*, 13, p.13 (2010).

- R. Miyamoto, H. Shibata, K. Yoshida and K. Hashimoto: Relationship between Bone Absorption and Protein Adsorption on  $\beta$ -Tricalcium Phosphate Doped with Sodium Ions; *3<sup>rd</sup> International Congress on Ceramics (ICC3)*, S13-P052 (2010).
- A. Ozawa, R. Miyamoto, H. Shibata, K. Yoshida and K. Hashimoto: Cell Test on  $\beta$ -Tricalcium Phosphate Doped with Manganese (II) Ions; *3<sup>rd</sup> International Congress on Ceramics (ICC3)*, S13-P053 (2010).
- H. Sagara, T. Yamamoto, S. Maeda, S. Koyama and M. Saito: Numerical Analysis of Am Sample Irradiation in Experimental Fast Reactor Joyo; *IOP Conf. Ser.: Mater. Sci. Eng.*, vol. **9**, no.1, 012006, p. 1-8 (2010).
- Go Chiba, Keisuke Okumura, Akito Oizumi and Masaki SAITO: Sensitivity Analysis of Fission Product Concentrations for Light Water Reactor Burned Fuel; *J. Nucl. Sci. Technol.*, Vol. **47**, No. 7, p. 652-660 (2010).
- S. Koyama, M. Osaka, M. Itoh, H. Sagara, M. Saito: Protected Plutonium Production by Transmutation of Minor Actinides for Peace and Sustainable Prosperity - Irradiation Tests of Np and Np-U Samples in the Experimental Fast Reactor JOYO (JAEA) and the Advanced Test Reactor at INL; *J. Nucl. Sci. Technol.*, **47** [8], 1-10 (2010).
- Y. Meiliza, M. Saito and H. Sagara: Denaturing Generated Pu in Fast Breeder Reactor Blanket; *J. Nucl. Sci. Technol.*, **47** [10], 1-14 (2010).
- Y. Kimura, M. Saito and H. Sagara: Development of Methodology for Plutonium Categorization (III) - Effect of Radiation -; *Trans. Am. Nucl. Soc.*, **103** (2010).
- E. Hamase, M. Saito and H. Sagara: Long-life FBR with Inner Blanket by Doping MA; *Trans. Am. Nucl. Soc.*, vol. **103** (2010).
- H. Sagara, S. Koyama, and M. Saito: Irradiation Analysis of U, Am Samples Irradiated in Experimental Fast Reactor "Joyo" for Protected Plutonium Production in Fast Breeder Reactor Blanket; *INES-3*, Oct 31 – Nov. 3 (2010).
- K. Ismailov, M. Saito, H. Sagara and Kenji Nishihara: Transmutation of Minor Actinides in Accelerator Driven System with Uranium Spallation TARGET; *INES-3*, Oct 31- Nov. 3 (2010).
- M. Nogami, Y. Sugiyama, and Y. Ikeda: Adsorptivity of Silica-supported Monoamide Resins to U(IV) in Nitric Acid Media; *J. Radioanal. Nucl. Chem.*, **283**, 177-180 (2010).
- M. Nogami, Y. Sugiyama, T. Kawasaki, M. Harada, Y. Morita, T. Kikuchi, and Y. Ikeda: Adsorptivity of Polyvinylpyrrolidone for Selective Separation of U(VI) from Nitric Acid Media; *J. Radioanal. Nucl. Chem.*, **283**, 541-546 (2010).
- A. Canlier, T. Kawasaki, S. Chowdhury, and Y. Ikeda: Structural Characterization, Electrochemistry, and Spectroelectrochemistry of *trans*-Dioxorhenium(V) Complex with 4-Methoxypyridine,  $[\text{ReO}_2(4\text{-MeOpy})_4]\text{PF}_6$ , and Characterization of  $[\text{ReO}_2(4\text{-MeOpy})_4]^{2+}$  Generated Electrochemically; *Inorg. Chim. Acta*, **364**, 1-7 (2010).
- R.M. Hassan, S.M. Ahmed, A.Fawzy, A.A. Abdel-Kader, Y. Ikeda, and H.D. Takagi: Acid-catalyzed Oxidation of Carboxymethyl Cellulose Polysaccharide by Chromic Acid in Aqueous Perchlorate Solutions. A Kinetics Study; *Cat. Commun.*, **11**, 611-615 (2010).
- K. Takao, M. Kato, S. Takao, A. Nagasawa, G. Bernahard, C. Hennig, and Y. Ikeda: Molecular Structure and Electrochemical Behavior of Uranyl(VI) Complex with Pentadentate Schiff Base Ligand: Prevention of Uranyl(V) Cation-Cation Interaction by Fully Chelating Coordination Sites; *Inorg. Chem.*, **49**, 2349-2359 (2010).
- K. Takao and Y Ikeda:  $\mu\text{-}\eta^2\text{:}\eta^2\text{-Peroxo-bis}[\text{nitratodioxidobis}(\text{pyrrolidine-2-one})\text{uraniu(VI)}]$ ; *Acta Cryst.* **E66**, m539-m540 (2010).
- S.-Y. Kim, K. Takao, Y. Haga, E. Yamamoto, Y. Kaswata, Y. Morita, K. Nishimura, and Y. Ikeda: Molecular and Crystal Structures of Plutonyl(VI) Nitrate Complexes with *N*-Alkylated 2-Pyrrolidone Derivatives: Cocrystallization Potentiality of U(VI) and Pu(VI) for Uniform MOX Fuel Precursor; *Crystal Growth & Design*, **10**, 2033-2036 (2010).
- T. Kawasaki, A. Canlier, S. Chowdhury, and Y. Ikeda: *trans*-Tetrakis- (4-methylpyridine- $\kappa\text{N}$ )dioxidorhenium(V) Hexafluoridophosphate; *Acta Cryst.*, **E66**, m857-m858 (2010).
- R.M. Hassan, A. Alaraifi, A. Fawzy, I.A. Zaafarany, K.S. Khairou, Y. Ikeda, and H.D. Takagi: Acid-catalyzed Oxidation of Some Sulfated Polysaccharides, Kinetics and Mechanism of Oxidation of Kappa-carrageenan by Cerium(IV) in Aqueous Perchlorate Solutions; *J. Mole. Catal. A: Chemical*, **332**, 138-144 (2010).
- P.C. Burns, Y. Ikeda, and K. Czerwinski: Advances in Actinide Solid-state and Coordination Chemistry; *MRS Bull.*, **35**, 868-876 (2010).
- S.-Y. Kim, T. Ogura, Y. Morita, N. Asanuma, and Y. Ikeda: Electrochemical Studies of Uranyl Chloro and Nitrate complexes in 1-Ethyl-3-methylimidazolium Based Ionic Liquids; *2nd International Conference on Asian Nuclear Prospects 2010 (ANUP 2010)*, Mamallapuram, India, October 10-13, 2010.

- M. C. Ali, M. Nogami, T. Kawasaki, Y. Sasaki, and Y. Ikeda: Highly Selective Extraction of  $\text{ReO}_4^-$  in  $\text{HNO}_3$  Solution Using New Extractant, 2,2'-(Methylimino)bis(*N,N*-diethylacetamide); *The Third International Symposium on Innovative Nuclear Energy Systems (INES-3)*, Tokyo Institute of Technology, Japan, October 31-November 3, 2010.
- T. Tsukahara and Y. Ikeda: A Study on Behavior of Metal Ions in Nanospace for Separation of Radionuclides Based on Nanofluidics; *The Third International Symposium on Innovative Nuclear Energy Systems (INES-3)*, Tokyo Institute of Technology, Japan, October 31-November 3, 2010.
- M. Nogami, M. Harada, Y. Sugiyama, T. Kawasaki, Y. Kawata, Y. Morita, T. Kikuchi, and Y. Ikeda: Selectivity and Stability of 1,3-Dimethyl-2-imidazolidone for Precipitation of U(VI) in Nitric Acid Media; *The Third International Symposium on Innovative Nuclear Energy Systems (INES-3)*, Tokyo Institute of Technology, Japan, October 31-November 3, 2010.
- N. Asanuma, Y. Takahashi, and Y. Ikeda: Extraction Mechanisms of Uranyl Ions by 1-Butyl-3-methylimidazolium nonafluorobutanesulfonate Containing *N*-Dodecyl-2-pyrrolidone; *The Third International Symposium on Innovative Nuclear Energy Systems (INES-3)*, Tokyo Institute of Technology, Japan, October 31-November 3, 2010.
- T. Suzuki, M. Nogami, and Y. Ikeda: A Study on Coordination Ability of Urea Derivatives with Highly Selective Precipitation Ability to Uranyl Ions in  $\text{HNO}_3$ ; *The 60<sup>th</sup> Symposium of Coordination Chemistry of Japan* (2010).
- T. Ogura, N. Ohta, Y. Ikeda, Y. S.-Y. Kim, Y. Morita, and K. Takao: A Study on Uranyl(VI) Complexes for Producing Stable Uranyl(V) Complexes in Various Media; *The 60<sup>th</sup> Symposium of Coordination Chemistry of Japan* (2010).
- Y. Tachibana, M. Nogami, Y. Sugiyama, and Y. Ikeda: Kinetic Studies on Decomposition Reactions of Pyrrolidone Derivatives Using Ozone; *The 19<sup>th</sup> Annual Meeting of Japan Ozone Association* (2010).
- Y. Tachibana, M. Nogami, Y. Sugiyama, and Y. Ikeda: Kinetic Studies on Ozone Oxidation of Pyrrolidone Derivatives Using Pd(II) as a Catalyst; *41<sup>st</sup> Annual Meeting of Union of Chemistry-Related Societies in Chubu Area, Japan* (2010).
- Y. Takahashi, N. Asanuma, and Y. Ikeda: A Study on Mechanism of Extraction Reaction of Uranyl Ions Using BMINfO Containing Pyrrolidone Derivatives; *The Annual Meeting of the Atomic Energy Society of Japan* (2010).
- T. Tsukahara and Y. Ikeda, and T. Kitamori: Development of Partitioning Method Using Nano-fluidics; *The Annual Meeting of the Atomic Energy Society of Japan* (2010).
- M. Tokeshi, H. Hotokezaka, M. Harada, Y. Ikeda, T. Tsukahara, Y. Kikutani, T. Kitamori, Y. Morita, and Y. Ban: A Study of Partitioning Method Using Thermal Response Compounds and Microchannel; *The Annual Meeting of the Atomic Energy Society of Japan* (2010).
- M. Harada, M. Nogami, Y. Sugiyama, T. Kawasaki, Y. Ikeda, Y. Morita, and T. Kikuchi: Development of Advanced Reprocessing System Using Precipitants with High Selectivity and Control Ability (18) Examination of Masking Effect; *The Fall Meeting of the Atomic Energy Society of Japan* (2010).
- T. Kawasaki, M. Nogami, Y. Sugiyama, M. Harada, Y. Ikeda, Y. Morita, and T. Kikuchi: Development of Advanced Reprocessing System Using Precipitants with High Selectivity and Control Ability (19) Examination of Recycling Pyrrolidone Derivatives as Precipitant Using Vaporization Method; *The Fall Meeting of the Atomic Energy Society of Japan* (2010).
- M. Nogami, Y. Sugiyama, T. Kawasaki, M. Harada, Y. Ikeda, Y. Kawata, Y. Morita, and T. Kikuchi: Development of Advanced Reprocessing System Using Precipitants with High Selectivity and Control Ability (20) Examination of Decomposition of Residual Pyrrolidone Derivatives with  $\gamma$ -irradiation; *The Fall Meeting of the Atomic Energy Society of Japan* (2010).
- S.-Y. Kim, Y. Morita, Y. Kawata, Y. Ikeda, and T. Kikuchi: Development of Advanced Reprocessing System Using Precipitants with High Selectivity and Control Ability (21) Precipitation Behavior of Pu in U-Pu Co-precipitation Process; *The Fall Meeting of the Atomic Energy Society of Japan* (2010).
- T. Kikuchi, T. Chikazawa, H. Someya, Y. Morita, and Y. Ikeda: Development of Advanced Reprocessing System Using Precipitants with High Selectivity and Control Ability (22) Examination of Precipitation and Fuel Preparation in the Engineering Scale; *The Fall Meeting of the Atomic Energy Society of Japan* (2010).
- Y. Ikeda, M. Nogami, Y. Sugiyama, T. Kawasaki, M. Harada, Y. Morita, and T. Kikuchi: Development of Advanced Reprocessing System Using Precipitants with High Selectivity and Control Ability (23) Overall Evaluation; *The Fall Meeting of the Atomic Energy Society of Japan* (2010).
- S. Goko, A. Kimura, H. Harada, M. Oshima, M. Ohta, K. Furutaka, T. Kin, F. Kitatani, M. Koizumi, S. Nakamura, Y. Toh, M. Igashira, T. Katabuchi, M. Mizumoto, Y. Kiyonagi, K. Kino, M. Furusaka, F. Hiraga, T. Kamiyama, J. Hori, T. Fujii, S. Fukutani, K. Takamiya: Measurement of Neutron

- Capture Cross Section Ratios of  $^{244}\text{Cm}$  Resonances Using NNRI; *Journal of Nuclear Science and Technology*, Vol. **47**, No. 12, pp. 1097–1100 (2010).
- K. Kino, M. Furusaka, F. Hiraga, T. Kamiyama, Y. Kiyanagi, K. Furutaka, S. Goko, H. Harada, M. Harada, T. Kai, A. Kimura, T. Kin, F. Kitatani, M. Koizumi, F. Maekawa, S. Meigo, S. Nakamura, M. Ooi, M. Ohta, M. Oshima, Y. Toh, M. Igashira, T. Katabuchi, M. Mizumoto: Measurement of Energy Spectra and Spatial Distributions of Neutron Beams Provided by the ANNRI Beam Line for Capture Cross-Section Measurements at the J-PARC/MLF; *Nuclear Instruments and Methods in Physics Research A*, Vol. **626-627**, pp. 58-66 (2010).
- T. V. Daniels, W. Arnold, J. M. Cesaratto, T. B. Clegg, A. H. Couture, H. J. Karwowski, T. Katabuchi: Spin-Correlation Coefficients and Phase-Shift Analysis for  $p + ^3\text{He}$  Elastic Scattering; *Physical Review C*, **82**, 034002 (2010).
- S. Kamada, M. Igashira, T. Katabuchi, M. Mizumoto: Measurements of keV-Neutron Capture Cross Sections and Capture Gamma-Ray Spectra of  $^{77}\text{Se}$ ; *Journal of Nuclear Science and Technology*, **47**, No. 7, pp. 634 - 641 (2010).
- J. Hori, M. Ohta, M. Oshima, F. Kitatani, A. Kimura, T. Kin, M. Koizumi, S. Goko, Y. Toh, S. Nakamura, H. Harada, K. Furutaka, M. Igashira, T. Katabuchi, M. Mizumoto, T. Kamiyama, K. Kino, Y. Kiyanagi, F. Hiraga, M. Furusaka: Measurement of Neutron Capture Cross Section of  $^{93}\text{Zr}$  Using a  $4\pi$  Ge Spectrometer at the J-PARC/NNRI; *2010 Fall Meeting of the Atomic Energy Society of Japan*, pp. 481, (2010).
- T. Katabuchi, N. Canh Hai, M. Igashira, S. Kamata, M. Tajika, M. Mizumoto: Measurement of Neutron Capture Cross Section and Capture  $\gamma$ -Ray Spectrum of Sr-88 at 510 keV; *2010 Fall Meeting of the Atomic Energy Society of Japan*, pp. 479 (2010).
- M. Mizumoto, T. Katabuchi, M. Igashira, Y. Kiyanagi: The Characteristic Experiments of Neutron Flux and Neutron and Gamma-Ray Fields with Gamma-Ray Detectors at the BL04 of J-PARC MLF (2); *2010 Fall Meeting of the Atomic Energy Society of Japan*, pp. 480 (2010).
- N. Hayashizaki, T. Hattori, Y. Matsumoto, T. Katabuchi, T. Tsukahara, T. Kobayashi: Development of BNCT Irradiation System using Compact Linac; *2010 Fall Meeting of the Atomic Energy Society of Japan*, pp. 502 (2010).
- A. Kimura, M. Ohta, M. Oshima, F. Kitatani, T. Kin, M. Koizumi, S. Goko, Y. Toh, S. Nakamura, H. Harada, K. Furutaka, M. Igashira, T. Katabuchi, M. Mizumoto, K. Kino, Y. Kiyanagi, J. Hori: Measurements of Neutron-Capture Cross Sections of  $^{244}\text{Cm}$  and  $^{246}\text{Cm}$  using a  $4\pi$  Ge spectrometer at the J-PARC/NNRI; *2010 Fall Meeting of the Atomic Energy Society of Japan*, pp. 482 (2010).
- K. Terada, M. Igashira, T. Katabuchi, T. Matsuhashi: Measurements of keV-Neutron Capture Cross Sections and Capture Gamma-Ray Spectra of  $^{105}\text{Pd}$ ; *2011 Annual Meeting of the Atomic Energy Society of Japan*, pp. 611 (2011).
- T. Katabuchi, M. Mizumoto, M. Igashira, A. Kimura, Y. Toh, S. Nakamura, S. Goko, K. Hara, T. Kin, M. Ohta, F. Kitatani, K. Furutaka, M. Koizumi, K. Hirose, H. Harada, M. Oshima, J. Hori, K. Kino, T. Kamiyama, F. Hiraga, M. Furusaka, Y. Kiyanagi: Measurements of the Neutron Capture Cross Section of Tc-99 Using an Nai(Tl) Detector at J-PARC/ANNRI; *2011 Annual Meeting of the Atomic Energy Society of Japan*, pp. 613 (2011).
- T. Kobayashi, M. Takahashi, M. Aritomi, M. Nakagawa, N. Hayashizaki, T. Katabuchi, G. Bengua, K. Tanaka, T. Hattori, M. Igashira, T. Yamamoto, H. Nakamura: Development of Liquid Lithium Target for Neutron Capture Therapy Using Accelerator —(1) An Outline of the Neutron Producing Target for NCT; *2011 Annual Meeting of the Atomic Energy Society of Japan*, pp. 688 (2011).
- S. Nakamura, M. Ohta, M. Oshima, F. Kitatani, A. Kimura, T. Kin, M. Koizumi, S. Goko, Y. Toh, K. Hara, H. Harada, K. Furutaka, M. Igashira, T. Katabuchi, M. Mizumoto, K. Kino, Y. Kiyanagi, J. Hori, K. Takamiya, S. Fukutani, T. Fujii: Measurement of Neutron-Capture Cross Section of Pd-107 Using ANNRI; *2011 Annual Meeting of the Atomic Energy Society of Japan*, pp. 614 (2011).
- H. Harada, M. Ohta, M. Oshima, F. Kitatani, A. Kimura, T. Kin, M. Koizumi, S. Goko, Y. Toh, S. Nakamura, K. Furutaka, M. Igashira, T. Katabuchi, M. Mizumoto, K. Kino, Y. Kiyanagi, K. Takamiya, S. Fukutani, T. Fujii, J. Hori: Measurement of Neutron-Capture Cross Section of Am-241 Using ANNRI; *2011 Annual Meeting of the Atomic Energy Society of Japan*, pp. 615 (2011).
- T. Kida, Y. Inaba, W. Watanabe, Y. Nakajima, S. Fukuoka, K. Takeshita and A. Mori: Extraction of Cd $^{2+}$  and Am $^{3+}$  Ions into Organic and Fluorous Solvents with a TPEN Chelating Agent bearing a Fluoroalkyl Substituent; *Chem. Lett.* **39**, 774-776 (2010).
- T. Maekawa, T. Kida, Y. Miyazaki, W. Watanabe, Y. Inaba, K. Takeshita and A. Mori: Temperature-Dependent Change of Extraction Performance of Soft Cadmium(II) Ion with TPENNIPA Gel. Studies on the Effect of the Ethylenediamine Skeleton; *Bull. Chem. Soc. Jpn.* **84**, 122–124 (2011).
- K. Takeshita: Development of Liquid-liquid Countercurrent Centrifugal Extractor with Taylor-Couette Flow; *Japanese J. Multiphase Flow*, **24**, 267-274 (2010).

- H. Takahashi, H. Kikura, K. Takeshita and M. Aritomi: UVP Measurement of Taylor-Couette Vortex Flow with Trough-flow; *Transactions of the Japan Society of Mechanical Engineers, Series B*, **77**, 97-101 (2011).
- H. Takahashi, H. Kikura, K. Takeshita and M. Aritomi: Characteristics of Taylor-Couette Vortex Flow with Counter Flow; *Journal of the Japanese Society for Experimental Mechanics*, **11**, Special Issue, SS168-173 (2011).
- Y. Inaba, T. Tsumagari, T. Kida, W. Watanabe, Y. Nakajima, S. Fukuoka, A. Mori, T. Matsumura, Y. Nakano and K. Takeshita: Thermoresponsive Extraction of Cadmium(II) Ions by Poly(TPEN-NIPA) Gels. Effect of Chain Length and Branched Spacer Structure on Gel Formation and Extraction Behavior; *Polym. J.* **43**, 630-634 (2011).
- H. Takahashi, H. Kikura, K. Takeshita and M. Aritomi: Flow Field Measurement of Taylor-Couette Vortex Flow with Axial Flow using UVP; *The 14th International Symposium on Flow Visualization (ISFV14)*, ISFV14-8A-4 (2010).
- H. Takahashi, H. Kikura, K. Takeshita and M. Aritomi: H. Takahashi, H. Kikura, K. Takeshita and M. Aritomi : UVP Measurement of Taylor-Couette Vortex Flow with Axial Flow, *The 15th National Symposium on Power and Energy Systems (SPES 2010) of the Japan Society of Mechanical Engineers*, 127-128 (2010).
- T. Maekawa, T. Kida, Y. Miyazaki, Y. Inaba, K. Takeshita, A. Mori: *The 57th Kobe Polymer Research Symposium*, Pa-22 (2010).
- H. Takahashi, H. Kikura, K. Takeshita and M. Aritomi: Ultrasonic Velocity Profile Measurement of Taylor-Couette Vortex Flow in Centrifuge Extractor; *Annual Meeting 2010 of the Japanese Society for Multiphase Flow*, 302-303 (2010).
- H. Takahashi, H. Kikura, K. Takeshita and M. Aritomi: Visualization and Ultrasonic Measurement of Taylor-Couette Vortex Flow in Centrifugal Extractor; *2010 Annual Conference on Experimental Mechanics*, 17-18 (2010).
- K. Takehista, H. Kinuhata, and R. Makabe: *The 42<sup>nd</sup> Autumn Meeting of the Society of Chemical Engineers*, Japan, S32 (2010).
- K. Takeshita and H. Inazuka: *The 42<sup>nd</sup> Autumn Meeting of the Society of Chemical Engineers*, Japan, D118 (2010).
- K. Takeshita and D. Kuwae: *The 42<sup>nd</sup> Autumn Meeting of the Society of Chemical Engineers*, Japan, S122 (2010).
- T. Ogata, K. Takeshita, Y. Inaba, H. Oaki, and A. Mori: *The 42<sup>nd</sup> Autumn Meeting of the Society of Chemical Engineers*, Japan, D117 (2010).
- K. Takeshita and H. Kinuhata: *Fall Meeting of the Atomic Energy Society of Japan*, A12 (2010).
- S. Suzuki, Y. Okamoto, A. Ikeda, T. Kobayashi, H. Shiwaku, K. Akutsu, T. Yaita, T. Ogata, K. Takeshita, Y. Inaba, H. Oaki, and A. Mori: *Fall Meeting of the Atomic Energy Society of Japan*, A23 (2010).
- T. Ogata, Y. Inaba, H. Oaki, K. Takeshita, A. Mori, T. Yaita, and S. Suzuki: Separation of MA from Ln using Polymer Gels Cross-Linked with TPEN Analogs; *Fall Meeting of the Atomic Energy Society of Japan*, A24 (2010).
- H. Takahashi, H. Kikura, K. Takeshita and M. Aritomi: Flow Characteristics of Taylor Vortices in a New Type Liquid-Liquid Countercurrent Centrifugal Extractor; *The 8th International Topical Meeting on Nuclear Thermal-Hydraulics, Operation and Safety (NUTHOS-8)*, CD-ROM Paper No. N8P0304, Book of Abstract p.44 (2010).
- Y. Inaba, T. Kida, W. Watanabe, A. Mori, T. Matsumura, D. Kuwae, T. Ogata, K. Takeshita: Synthesis and Properties of Hydrophobic TPEN Derivatives for MA/Ln Separation; *The Third International Symposium on Innovative Nuclear Energy Systems (INES-3)*, Paper ID: 124 (2010).
- T. Ogata, K. Takeshita, H. Oaki, Y. Inaba, A. Mori: Separation of Am(III) from Eu(III) using Polymer Gels Cross-Linked with TPEN Analogs; *The Third International Symposium on Innovative Nuclear Energy Systems (INES-3)*, Paper ID: 127 (2010).
- K. Takeshita, H. Rokkaku and H. Kinuhata: Development of Counter-current Centrifugal Extractor with Taylor-Couette Flow for Nuclide Separation; *The Third International Symposium on Innovative Nuclear Energy Systems (INES-3)*, Paper ID: 129 (2010).
- H. Takahashi, H. Kikura, K. Takeshita and M. Aritomi: Characteristics of Taylor Vortex on Counter Flow; *5th International Symposium on Advanced Science and Technology in Experimental Mechanics (5th ISEM'10-Kyoto)*, CD-ROM Paper No. 149, Book of Abstract p.94 (2010).
- T. Maekawa, W. Watanabe, T. Kida, Y. Miyazaki, Y. Inaba, A. Mori, K. Takeshita: Temperature-Dependent Change of Extraction Performance of Soft Cadmium(II) Ion with TPEN-NIPA Gel; *The 2010 International Chemical Congress of Pacific Basin Societies (Pacifichem)*, 1790 (2010).
- H. Takahashi, H. Kikura, K. Takeshita and M. Aritomi: Visualization of Dispersed Phase Flow in Centrifugal Extractor Using Taylor-Couette Vortex Flow; *The 8th ASME-JSME Thermal Engineering Joint Conference*

- (AJTEC2011), CD-ROM Paper No. AJTEC2011-44403 (2011).
- R. Hasu, Y. Inaba, D. Kuwae, A. Mori and K. Takeshita: Separation of Heavy Metals by Hydrophobic TPEN Derivatives; *91st Annual Meeting of The Chemical Society of Japan*, 4D6-03 (2011).
- T. Ogata, K. Takeshita, H. Oaki, Y. Inaba and A. Mori: *The 76<sup>th</sup> Annual Meeting of the Society of Chemical Engineers*, Japan, O204 (2011).
- T. Ogata, K. Takeshita, H. Oaki, Y. Inaba and A. Mori, T. Yaita, and S. Suzuki: Adsorption Property of Am(III) using Polymer Gels Cross-Linked with TPEN Analogs; *Annual Meeting of the Atomic Energy Society of Japan*, D11 (2011).
- Masaki Ozawa, Akira Ohtaki and Toshihide Asakura: Rare Metals in Nuclear Spent Fuels, Their Separation and Utilization. Strategy; *INCS (International Nuclear Chemistry Society) News*, 27th issue, Volume VII, 3, pp.17-26, July (2010).
- Masaki Ozawa: Reprocessing of Radioactive Waste, Toward Recycling of Nuclear Rare Metals; (Invited, Round Table), *International Nuclear Forum "Bulgarian Nuclear Energy-National, Regional and World Energy Safety"* by Bulgarian. Nuclear Forum (bulATOM), Riviera Holiday Club, June 9<sup>th</sup> -11<sup>th</sup> 2010.
- Masaki Ozawa: Advanced ORIENT Cycle for Turning Radioactive Waste into Resource (Invited Lecture), *CIMTEC2010 5<sup>th</sup> Forum on New Materials*, Abstracts, pp.67, Montecatini Terme, Tuscany, Italy, June 13-18, 2010.
- M.Ozawa, S.Koyama, and T.Suzuki: Nuclear Rare Metals and Their Separation in Adv.-ORIENT Cycle Strategy, 2<sup>nd</sup> *International conference on Asian Nuclear Prospects 2010 (ANUP2010)*, Proceedings (CD), FR 4, Mamallapuram, India, October 10-13, 2010.
- Masaki Ozawa: Separation and Utilization of Nuclear Rare Metals and Actinides in Advanced Reprocessing System (Invited Lecture); The 389<sup>th</sup> Xiangshan Science Conference Workshop of Nuclear Fuel Reprocessing, *Proc. Radiochemical Challenges in Nuclear Fuel reprocessing*, pp.27-29, Xiangshan Hotel, Beijing, China, Dec. 22-24, 2010.
- Masaki Ozawa: Chapter 19. Rare Metals in Nuclear Industries; *Rare Metal Binran*, pp.262-273 ISBN 978-4-621-08276-8 MARUZEN, Jan. 30<sup>th</sup> 2011.(in Japanese)
- Masaki Ozawa, Shinichi Suzuki, Kenji Takeshita: Advanced Hydrometallurgical Separation of Actinides and Rare Metals in Nuclear Fuel Cycle; *Solvent Extraction Research and Development, Japan*, Vol. 17, 19-34 (2010).
- Masaki Ozawa: Considering the Utilization of Valuable Rare Metals in Spent Nuclear Fuel; *Energy Review*, 5, pp.42-46 (2010). (in Japanese)
- Masaki Ozawa: Nuclear Fuel Cycle and Resources; *Journal of the Atomic Energy Society of Japan*, Vol.52, 9, pp.48(2010). (in Japanese)
- Masaki Ozawa: Research Strategy of Advanced ORIENT Cycle; *Nuclear Viewpoints*, Vol.56, 10, pp7-11 (2010). (in Japanese)
- Masaki Ozawa, Yuezhou Wei: The 389<sup>th</sup> Xiangshan Science Conference; Radio- chemical Challenges in Nuclear Fuel Reprocessing, *Journal of the Atomic Energy Society of Japan*, Vol.53, 6, pp451-452 (2011). (in Japanese)
- Masaki Ozawa, Tatsuya Suzuki, Yoshihiko Shinoda, Naoyuki Takaki: New Strategy on Rare Earth in Advanced Nuclear Fuel Cycle; *RARE EARTHS* 56, pp.186-187, ISSN0910-2205 Kidorui CODEN:KIDOEP, May 2010. (in Japanese)
- Masaki Ozawa: Advanced ORIENT Cycle; Spinning A Dream Come True; 4<sup>th</sup> Advanced ORIENT Cycle Seminar, Swany Hall, Rokkasho-mura, Jul. 30<sup>th</sup>, 2010. (in Japanese)
- Masaki Ozawa: Rare Metals in High Level Liquid Wastes; Special Committee on Nuclear Fuel Cycle, Rokkasho-mura Village Assembly, Sep. 8<sup>th</sup>.2010. (in Japanese)
- Masaki Ozawa: Advanced ORIENT Cycle – New Resource Strategy and Issues by Forefront Nuclear Science and Technology, *JST Luncheon Seminar*, Ichigaya- office, Tokyo, Jan.17<sup>th</sup> 2011. (in Japanese)
- Masaki Ozawa, Yasuhiko Fujii: Advanced ORIENT Cycle (Phase1) 1) Strategy and Concept; *2010 Fall Meeting of Japan Atomic Energy Society of Japan*, A36, Sep.16<sup>th</sup>, 2010. (in Japanese)
- T. Tada, H. Fukuda, J. Hasegawa and Y. Oguri: Application of a Wavelength Dispersive Particle Induced X-ray Emission System to Chemical Speciation of Phosphorus and Sulfur in Lake Sediment Samples; *Spectrochim. Acta B*, 65, 46 (2010).
- S. Wonglee, T. Tada, H. Fukuda, J. Hasegawa and Y. Oguri: Development of a Target Positioning System Based on a Laser Position Sensor for High-Efficiency Wavelength-Dispersive PIXE Analysis; *Int. J. PIXE*, 20, 1 (2010).
- Y. Oguri and J. Hasegawa: Calculation of Heavy-Ion Stopping Power in Warm Dense High-Z Targets Using Temperature-Dependent Dielectric Response Functions;

- Meeting Abstract of the Physical Society of Japan, **65** [2], Part 2, 118 (2010).
- J. Hasegawa, S. Jaiyen and Y. Oguri: Quality Evaluation of Ion Beams Focused by Tapered Glass Capillaries; *Meeting Abstract of the Physical Society of Japan*, **65** [2], Part 2, 168 (2010).
- Y. Oguri and J. Hasegawa: Calculation of Heavy-Ion Stopping Power in Warm Dense Plutonium Targets for Equation-of-State Studies; *2011 Annual Meeting of the Atomic Energy Society of Japan*, N27, 679 (2011).
- J. Hasegawa and Y. Oguri: Microbeam Analyses Using Glass Capillary Lenses; *2011 Annual Meeting of the Atomic Energy Society of Japan*, N31, 683 (2011).
- S. Thomyasirigul, H. Fukuda, J. Hasegawa and Y. Oguri: Speciation and Determination of Cr(III) and Cr(VI) in Water by Energy-Dispersive PIXE Analysis; *The 12th International Conference on Particle Induced X-ray Emission and its Analytical Applications*, 27 June - 2 July 2010, Guildford, UK, O05 (2010).
- J. Hasegawa, Y. Oguri and S. Jaiyen: Monte-Carlo Simulation of Ion Beam Focusing Using Glancing-Angle Scattering; *The 18th International Symposium on Heavy Ion Inertial Fusion*, 30 August - 3 September 2010, Darmstadt, Germany, MON-0404 (2010).
- J. Hasegawa, S. Jaiyen and Y. Oguri: Development of a Micro-PIXE System Using Tapered Glass Capillary Optics; *The 10th European Conference on Accelerators in Applied Research and Technology*, 13-17 September 2010, Athens, Greece, PII-58 (2010).
- S. Wonglee, T. Tada, H. Fukuda, Jun Hasegawa and Y. Oguri: Chemical Speciation of Chlorine in Particulate Matter by Wavelength-Dispersive PIXE Technique; *The 10th European Conference on Accelerators in Applied Research and Technology*, 13-17 September 2010, Athens, Greece, PII-60 (2010).
- S. Wonglee, H. Fukuda, J. Hasegawa and Y. Oguri: Chemical Speciation of Chlorine in Size-Fractioned Particulate Matter Samples by High-Resolution Measurement of Proton-Induced K-beta X-rays; *The 27th Annual Meeting of the Japan Society for Particle Induced X-ray Emission (PIXE) Research*, 17-19 November 2010, Kyoto, Japan, 29 (2010).
- T. Yuji, T. Urayama, S. Fujii, Y. Iijima, Y. Suzuki, H. Akatsuka: Basic Characteristics for PEN Film Surface Modification Using Atmospheric-Pressure Nonequilibrium Microwave Plasma Jet; *Electronics Communications Jpn.*, **93**, [5], pp. 42 - 49, (2010).
- H. Akatsuka: Optical Emission Spectroscopy Measurement of Processing Plasmas; *IEEEJ Trans. FM*, **130**, [10], 892 - 898 (2010) [in Japanese].
- Y. Ichikawa, T. Sakamoto, A. Nezu, H. Matsuura and H. Akatsuka: Actinometry Measurement of Dissociation Degree of Nitrogen and Oxygen in N<sub>2</sub>-O<sub>2</sub> Microwave Discharge Plasmas; *Jpn. J. Appl. Phys.*, **49**, 106101 (16 pages) (2010).
- H. Akatsuka: Recent Trends of Traditional Optical Emission Spectroscopic Measurement of Non-Equilibrium Plasmas - Atmospheric-Pressure Ar Plasma and Low-Pressure N<sub>2</sub> Plasma -; *IEEEJ Trans. FM*, **131**, [1], 6 - 10 (2011) [in Japanese].
- H. Kataoka, N. Mungkung, T. Yuji, M. Kawano, Y. Kiyota, D. Uesugi, K. Nakabayashi, Y. Suzuki, H. Shibata, N. Kashihara, K. Sakai, T. Bouno, H. Akatsuka: Surface Modification of Silicon Wafer by Low-Pressure High-Frequency Plasma Chemical Vapor Deposition Method; *24th International Symposium on Discharges and Electrical Insulation in Vacuum (ISDEIV)*, IEEE, pp. 505 - 508 (2010).
- H. Akatsuka, K. Kuwano, A. Nezu, H. Matsuura: Measurement of Nitrogen Dissociation Degree of Nitrogen Discharge Plasma by Actinometry Method with Subtraction of First Positive Band Spectrum; 63rd Gaseous Electronics Conference (GEC), *Bull. Am. Phys. Soc.*, **55**, [7], pp. 26 - 27 (2010).
- H. Akatsuka, K. Kuwano, A. Nezu, H. Matsuura: Measurement of Nitrogen Dissociation Degree of Nitrogen Discharge Plasma by Actinometry Method with Subtraction of First Positive Band Spectrum; *Proc. 7th International Conference on Reactive Plasmas (ICRP)*, pp. 59-60 (2010).
- H. Akatsuka, Y. Ichikawa, K. Kuwano, T. Sakamoto, A. Nezu and H. Matsuura: Measurement of Nitrogen Dissociation Degree of Nitrogen Discharge Plasma by Actinometry Method with Subtraction of First Positive Band Spectrum; *The Papers of Technical Meeting on Plasma Science and Technology*, IEEEJ, PST-10-14, pp. 23 - 28 (2010).
- Y. Nagahara, H. Ichii, K. Yoshida, A. Nezu and H. Akatsuka: Effect of Collisions with Neutral Particles on Stall Phenomena of Supersonic Plasma Flow; *The Papers of Technical Meeting on Plasma Science and Technology*, IEEEJ, PST-10-45, pp. 23 - 27 (2010).
- K. Kuwano, A. Nezu, H. Matsuura and H. Akatsuka: Actinometry Measurement of Nitrogen Atom Density with Subtraction of 1PS Band and Effect of Rare-Gas Admixture on the Dissociation Degree of Nitrogen; Extended Abstracts (The 71st Autumn Meeting, 2010); *The Japan Society of Applied Physics*, 08-043 (2010).

- Y. Nagahara, K. Yoshida, A. Nezu and H. Akatsuka: Effect of Collisions of Supersonic Plasma Flow with Neutral Particles on Deceleration into Subsonic Region; *Meeting Abstracts of the Physical Society of Japan*, **65** [2] p.175 (2010).
- K. Kuwano, A. Nezu, H. Matsuura and H. Akatsuka: Actinometry Measurement of Density of Nitrogen Atoms in Nitrogen Plasma and the Effect of Rare-Gas Admixture; *Proc. 27th Annual Meeting, The Japan Society of Plasma Science and Nuclear Fusion Research*, 01p15 (2010).
- H. Akatsuka: Discussion on the Collisional Radiative Model Based on Fundamentals of Linear Ordinary Differential Equations; *The Papers of Joint Technical Meeting on Plasma Science and Technology and Pulsed Power Technology*, IEEJ, PST-10-80/PPT-10-100, pp. 67 - 72 (2010).
- K. Tajima, A. Nezu, H. Matsuura and H. Akatsuka: Experimental Study of Plasma Parameters of Flowing Arc Jet Plasma along Mirror and Cusp Magnetic Fields; *The Papers of Joint Technical Meeting on Plasma Science and Technology and Pulsed Power Technology*, IEEJ, PST-10-104/PPT-10-124, pp. 59 - 64 (2010).
- T. Yuji, Y. Kiyota, M. Kawano, K. Nakabayashi, S. Tashiro, M. Tanaka and H. Akatsuka: Optical Emission Spectroscopy Measurement of High-Frequency Low-Pressure at Plasma-Enhanced Chemical Vapor Deposition; *The 2011 Annual Meeting Record*, IEEJ, p. 241 (2011).
- K. Tajima, A. Nezu, H. Matsuura and H. Akatsuka: Experimental Study of Velocity and Space Potential of Stationary Arc-Jet Flowing in Mirror-Type and Cusp-Type Magnetic Field; *The 2011 Annual Meeting Record*, IEEJ, p. 260 (2011).
- H. Akatsuka: Discussion on Ordinary Differential Equations Required for Analysis of Pulse-like Optical Emission Spectroscopy by Collisional Radiative Model; *Extended Abstracts (The 58th Spring Meeting)*; The Japan Society of Applied Physics and Related Societies, 08-036 (2011).
- Abu Khalid Rivai, Minoru Takahashi: Investigations of a Zirconia Solid Electrolyte Oxygen Sensor in Liquid Lead; *Journal of Nuclear Materials*, Vol.**398** (2010) pp.160 - 164.
- Abu Khalid Rivai, Minoru Takahashi: Corrosion Investigations of Al-Fe-coated Steels, High Cr Steels, Refractory Metals and Ceramics in Lead Alloys at 700°C; *Journal of Nuclear Materials*, Vol.**398** (2010) pp.146 - 152.
- Abu Khalid Rivai, Minoru Takahashi: Corrosion Characteristics of Materials in Pb-Bi under Transient Temperature Conditions; *Journal of Nuclear Materials*, Vol. **398** (2010) pp.139 - 145.
- Minoru Takahashi, Tooru Kobayashi, Masashi Nakatsuka, Teddy Ardiansyah, Martin Kulhanek, Ales Vojacek, Vaclav Dostal, Shoji Uchida and Mingguang Zhang: Study on Liquid Lithium Target System for Boron Neutron Capture Therapy (BNCT); *18th International Conference on Nuclear Engineering (ICONE18)*, May 17-21, 2010, Xi'an, China, ICONE18-29516.
- Minoru Takahashi, Takanori Yumura, Isao Yoda, Rongyuan Sa: Visualization of Bubbles Behavior in Lead-bismuth Eutectic by Gamma-ray; *18th International Conference on Nuclear Engineering (ICONE18)*, May 17-21, 2010, Xi'an, China, ICONE18-29522.
- Teddy Ardiansyah, Minoru Takahashi, Yoshio Yoshizawa, Masamichi Nakagawa, Makoto Asaba, Kuniaki Miura: Numerical Simulation of Cavitation for Comparison of Sodium and Water Flows; *18th International Conference on Nuclear Engineering (ICONE18)*, May 17-21, 2010, Xi'an, China, ICONE18-29659.
- Teddy Ardiansyah, Makoto Asaba, Kuniaki Miura, Minoru Takahashi: Characteristics of Cavitation Erosion Phenomena in Sodium Flow; *18th International Conference on Nuclear Engineering (ICONE18)*, May 17-21, 2010, Xi'an, China, ICONE18-29545.
- Asril Pramutadi Andy Mustari, Minoru Takahashi: Corrosion Properties of Welded Ferritic-Martensitic Steels In Liquid Lead-Bismuth At 600C; *18th International Conference on Nuclear Engineering (ICONE18)*, May 17-21, 2010, Xi'an, China, ICONE18-29927.
- Rongyuan Sa, Minoru Takahashi: Thermal Interaction of Lead-alloy Droplet with Subcooled Water in Pool Water Tank; *Proc. of 18th Int. Conf. on Nucl. Eng. (ICONE18)*, May 17-21, 2010, Xi'an, China, ICONE18-29621.
- Asril Pramutadi Andi Mustaria, Minoru Takahashi: Study on Corrosion of Welded Steel for LBE-Cooled Fast Reactors; *3rd International Symposium on Innovative Nuclear Energy Systems (INES-3)*, October 31 - November 3, 2010, Tokyo Institute of Technology, Japan (2010), P-133.
- Rongyuan Sa, Minoru Takahashi, Kiyofumi Moriyama: Study on Thermal Interactions of Lead Alloy and Water; *3rd International Symposium on Innovative Nuclear Energy Systems (INES-3)*, October 31 - November 3, 2010, Tokyo Institute of Technology, Japan (2010), P-104.
- Minoru Takahashi, Masatoshi Kondo: Corrosion Resistance of Ceramics SiC and Si<sub>3</sub>N<sub>4</sub> in Flowing Lead-bismuth Eutectic; *3rd International Symposium on Innovative Nuclear Energy Systems (INES-3)*, October 31 - November 3, 2010, Tokyo Institute of Technology, Japan (2010), 1B-35.

- Teddy Ardiansyah, Minoru Takahashi: Investigation of Cavitation Phenomena for Innovative Sodium- and Lead-bismuth-cooled Fast Reactors; *3rd International Symposium on Innovative Nuclear Energy Systems (INES-3)*, October 31 - November 3, 2010, Tokyo, Japan (2010), P-132.
- Eriko Yamaki-Irisawa, Shunichi Numata, Minoru Takahashi: Corrosion Behavior of Heat-treated Fe-Al Coated Steel in Lead-bismuth Eutectic under Loading; *3rd International Symposium on Innovative Nuclear Energy Systems (INES-3)*, October 31 - November 3, 2010, Tokyo Institute of Technology, Japan (2010), P-131.
- Teddy Ardiansyah, Makoto Asaba, Kuniaki Miura, Minoru Takahashi: Experimental Study on Cavitation Erosion and Onset Condition in Sodium Flow; *Proceedings of 2nd Multidisciplinary International Student Workshop 2010 (MISW 2010)*, August 5-6, 2010, Tokyo, Japan.
- Rongyuan Sa, Minoru Takahashi: Thermal Interaction of lead and lead-bismuth Droplets with Subcooled Water; *2010 Annual Meeting of Atomic Energy Society of Japan*, Ibaraki March 25-28, 2010, E31.
- Teddy Ardiansyah, Minoru Takahashi, Makoto Asaba, Kuniaki Miura: Study on Sodium Cavitation for Fast Reactors (III) Analysis of Cavitation with FLUENT and Erosion Experiment; *2010 Annual Meeting of Atomic Energy Society of Japan*, Ibaraki, March 25-28, 2010, E28.
- Masamichi Nakagawa, Toru Kobayashi, Minoru Takahashi, Masanori Aritomi: Momentum Defects of Sheet Jets / Film Flows of Liquid Lithium for the Target and Coolant of BNCT using Accelerators; *Meeting of JSME Fluids Engineering Division*, Yonezawa, Oct. 30-31, 2010, O117.
- Yuki Tagawa, Shinsuke Mori, Masaaki Suzuki, Ichiro Yamanaka, Toru Obara, Ryu Junichi, Yukitaka Kato: Synergistic Decomposition of CO<sub>2</sub> by Hybridization of a Dielectric Barrier Discharge Reactor and a Solid Oxide Electrolyser Cell; *KAGAKU KOGAKU RONBUNSHU*, **37** (2), pp. 114-119 (2011).
- Hirokazu Ishitobi, Yoshitomo Sato, Keirei Uruma, Junichi Ryu, and Yukitaka Kato: Dehydration and Hydration Behavior of LiCl-Modified Mg(OH)<sub>2</sub> as a Material for Chemical Heat Pumps; *Proc. of Int'l Symposium on Innovative Materials for Processes in Energy Systems 2010 (IMPRES2010)*, Furama Riverfront Hotel, Singapore, 30 November, 2010.
- Junichi Ryu, Rui Takahashi, Hirokazu Ishitobi, Yoshitomo Sato, Keirei Uruma, Yukitaka Kato: Dehydration and Hydration Behavior of Magnesium-Aluminum Mixed Hydroxide for Chemical Heat Pump; *Proc. of Int'l Symposium on Innovative Materials for Processes in Energy Systems 2010 (IMPRES2010)*, Furama Riverfront Hotel, Singapore, 30 November, 2010.
- Yukitaka Kato, Kanta Inoue, Michito Urasaki, Satoshi Tanaka, Hiroaki Ninomiya, Tomoya Minagawa, Azusa Sakurai and Junichi Ryu: Development of Composite Hydrogen Permeation Membrane Using a Reverse Build-Up Method; *Proc. of Int'l Symposium on Innovative Materials for Processes in Energy Systems 2010 (IMPRES2010)*, Furama Riverfront Hotel, Singapore, 30 November, 2010.
- Yukitaka Kao, Yutaka Ujisawa: Iron Making Process; PCT patent, PCT/JP2011/050400, 13 January, 2011.
- Y. Kato., Y. Yasunaga, T. Kashiwaya edited: Energy beyond '20, Honebuto-no-Energy Road Map 2; Kagaku Kogyo Sha, 2010.
- Y. Kato: Energy beyond '20 Outline; *Kagaku Kogaku*, **75** (3), pp. 110-114 (2011).
- Y. Kato, M. Matsukata: Energy beyond '20 (3) Manufacturing and Energy; *75* (3), pp. 110-114 (2011).
- Andreas Hauer, Stefan Gschwander, Yukitaka Kato, Viktoria Martin, Peter Schossig, Fredrik Setterwall: FINAL REPORT for IEA/ECES Annex 18 on "Transportation of Energy by Utilization of Thermal Energy Storage Technology", IEA, 2010.
- Zamengo Massimiliano, Seon-Tae Kim, Ryu Junichi, Kato Yukitaka: Performances of a MgO-expanded Graphite Packed Bed Reactor of Chemical Heat Pump; *SCEJ 76<sup>nd</sup> Annual Meeting*, J206, Tokyo Univ. A&T, Tokyo, 22-24 March, 2011.
- Kim Seon Tae, Uruma Keirei, Ryu Junichi, Kato Yukitaka: Expanded Graphite Mixture for Packed Bed Reactor of Chemical Heat Pump; *SCEJ 76<sup>nd</sup> Annual Meeting*, J207, Tokyo Univ. A&T, Tokyo, 22-24 March, 2011.
- Dipu Arnoldus, Uruma Keireim, Ryu Junichi, Kato Yukitaka: Reactivity Measurement of High Temperature Electrolysis of Carbon Dioxide; *SCEJ 76<sup>nd</sup> Annual Meeting*, I209, Tokyo Univ. A&T, Tokyo, 22-24 March, 2011.
- Kim Seon Tae, J. Ryu, Y. Kato: Reactivity Enhancement of Chemical Materials for Packed Bed Reactor of Chemical Heat Pump; *SCEJ 42<sup>nd</sup> Autumn Meeting*, C121, Doshisha Univ., 6<sup>th</sup> September, 2010.
- Y. Sato, H. Ishitobi, K. Uruma, J. Ryu, Y. Kato: Application of Magnesium - Transition Metal Hydroxide Composites on Chemical Heat Storage; *SCEJ 42<sup>nd</sup> Autumn Meeting*, C120, Doshisha Univ., 5<sup>th</sup> September, 2010.
- A. Sakurai, K. Inoue, J. Ryu, Y. Kato: An Experimental Study of Making Method of a Composite of Hydrogen Permeable Membrane using Reverse Build-up Method; *SCEJ 42<sup>nd</sup> Autumn Meeting*, C205, Doshisha Univ., 6<sup>th</sup>

September, 2010.

H. Ishitobi, Y. Sato, K. Uruma, J. Ryu, Y. Kato: Repetitive Reaction Durability of Lithium Chloride Modified Magnesium Hydroxide; *SCEJ 42<sup>nd</sup> Autumn Meeting*, C119, Doshisha Univ., 6<sup>th</sup> September, 2010.

Y. Kato: Concept of the Energy Beyond '20; *SCEJ 42<sup>nd</sup> Autumn Meeting*, C207, Doshisha Univ., 6<sup>th</sup> September, 2010.

Y. Kato, Y. Ujisawa: Thermal Feasibility Study on Carbon Recycling Iron Making System; *160th ISIJ Autumn Meeting*, No. 156, 25 September, 2010, Hokkaido Univ.

Y. Kato: Effective Use of Surplus Heat by Chemical Heat Pump using Magnesium; *160th ISIJ Autumn Meeting*, 26 September, 2010, Hokkaido Univ.

J. Ryu, Y. Kato, K. Aika: Ammine Complex of  $\text{CaCl}_2\text{-CaBr}_2$  Mixed Halide as a Material for Hydrogen Storage; *Pacificchem 2010*, 16 December, 2010, Honolulu.

H. Shima, H. Yoshioka and J. Onoe: Curvature Effects on Collective Excitations in Dumbbell-Shaped Hollow Nanotubes; *Physica E*, **42**, 1151-1154 (2010).

A. Takashima, J. Onoe and T. Nishii: In situ Infrared Spectroscopic and Density-Functional Studies on the Cross-Linked Structure of One-Dimensional  $\text{C}_{60}$  Polymer; *J. Appl. Phys.* **108**, 033514 (2010).

J. Onoe, A. Takashima and Y. Toda: Infrared Phonon Anomaly of One-Dimensional Metallic Peanut-Shaped  $\text{C}_{60}$  Polymer; *Appl. Phys. Lett.* **97**, 241911 (2010).

J. Onoe: Exotic-Nanocarbons: Toward the Development of New Riemannian Space Quantum Systems; *Proc. Optical-electronic device committee of the electronic society of Japan*, OQD-10-001 (2010).

J. Onoe: Exotic-Nanocarbons: The Development of New Quantum Electronic Systems in a Curved Space; *SCAT Tech. J.* **66**, 16-32 (2010).

J. Onoe: Riemannian Geometric Effects on the Tomonaga-Luttinger Liquids of One-Dimensional Metallic Exotic Nanocarbons with Positive and Negative Gaussian Curvatures; (invited lecture), Institute "Jozef-Stefan", Department of Complex Matter, Ljubljana (Slovenia), Sept. 17 (2010).

J. Onoe: In situ Infrared Spectroscopic and Density-Functional Studies of the Cross-Linked Structure of One-Dimensional Metallic  $\text{C}_{60}$  Polymer; (invited talk), *6<sup>th</sup> International Conference on DV-X $\alpha$  Method*, Daejeon (Korea), Aug. 4-6 (2010).

J. Onoe: The Crystallization Effects on the External Quantum Efficiency of Organic Photovoltaic Cells with a  $\text{Zn(OEP)/C}_{60}$  Layered Structure; (invited talk), *KRICT workshop on "Recovery of rare metals from useless module of Solar cells and Battery"*, Daejeon (Korea), Dec. 3 (2010).

S. Ryuzaki, T. Kai, and J. Onoe: The Dependence of Open Circuit Voltage on Incident Light Wavelength for Organic Photovoltaic Cells Consisting of Zinc-Porphyrin and Fullerene Films; *4th Asian Consortium on Computational Materials Science-Virtual Organization*, Sendai, Jan. 12-14 (2010).

A. Takashima, T. Nishii, and J. Onoe: Structural Properties of an Electron-Beam Irradiated  $\text{C}_{60}$  Film Studied by Vibrational Spectroscopy and Density-Functional Calculations; *4th Asian Consortium on Computational Materials Science-Virtual Organization*, Sendai, Jan. 12-14 (2010).

T. Kai, S. Ryuzaki, and J. Onoe: An Impedance Spectroscopic Study on the Carrier Dynamics in Zinc-Porphyrin / Fullerene Photovoltaic Cells; *4th Asian Consortium on Computational Materials Science-Virtual Organization*, Sendai, Jan. 12-14 (2010).

J. Onoe, A. Takashima and Y. Toda: In situ Low-Temperature Infrared Spectroscopic Study on Kohn Anomaly of One-Dimensional Metallic Exotic-Nanocarbon; (selected paper), *9th Conference on Solid State Chemistry*, Prague (Czech Republic), Sept. 10-15 (2010).

J. Onoe, M. Hirata and M. Kurihara: Relativistic Density-Functional Study of Nuclear Materials; (selected paper), *3rd International Symposium on Innovative Nuclear Energy Systems (INES-3)*, Tokyo, Oct. 31-Nov.3 (2010).

J. Onoe, S. Ryuzaki and Y. Toda: The Roles of Intra- and Inter-Molecular Excitons on the External Quantum Efficiency of Organic Photovoltaic cells with  $\text{Zn(OEP)/C}_{60}$  Layered Structures; (selected paper), *5th International Conference on Surface, Coatings and Nanostructured Materials*, Reims (France), Oct. 19-21 (2010).

A. Takashima, S. Ono, H. Shima and J. Onoe: Anomalous Increase in the Infrared Peak Intensity of One-Dimensional Metallic Peanut-shaped  $\text{C}_{60}$  Polymer; *5th International Conference on Surface, Coatings and Nanostructured Materials*, Reims (France), Oct. 19-21 (2010).

J. Onoe, A. Takashima and T. Nishii: Riemannian Geometrical Effects on the Electronic Properties of One-Dimensional Metallic  $\text{C}_{60}$  Polymers with a Periodic Peanut-Shaped Unevenness Structure; (Selected paper), *The Fifth General Meeting of ACCMS-VO(Asian Consortium on Computational Materials Science - Virtual*

Organization), Sendai, Dec. 10-12 (2010).

T. Orikoshi, T. Nishii and J. Onoe: Photocurrent Properties of Organic Photovoltaic Cells Laterally Contacted with Metal Electrodes; (Selected paper), *The Fifth General Meeting of ACCMS-VO (Asian Consortium on Computational Materials Science - Virtual Organization)*, Sendai, Dec. 10-12 (2010).

A. Takashima, M. Nishiyama and J. Onoe: Infrared Spectroscopic Study of the Reaction Mechanism of One-Dimensional Metallic Peanut-Shaped C<sub>60</sub> Polymer; *The Fifth General Meeting of ACCMS-VO (Asian Consortium on Computational Materials Science - Virtual Organization)*, Sendai, Dec. 10-12 (2010).

J. Onoe and S. Ryuzaki: An Impedance Spectroscopic Study of the Open-Circuit Voltage of Zn(OEP)/C<sub>60</sub> Layered Photovoltaic Cells; *Hybrid Materials 2011*, Strasbourg (France), March 6-10 (2010).

T. Orikoshi, T. Nishii and J. Onoe: The Photo-Current Characteristics of Multilayered Organic Photovoltaic Cells with Lateral Electrodes; *Hybrid Materials 2011*, Strasbourg (France), March 6-10 (2010).

J. Onoe: Low-Dimensional Exotic-Nanocarbon Fabricated using Photo- and Electron-Beam-Induced Excitation of C<sub>60</sub>; *A workshop on advanced quantum beams and their application to nanomaterials*, Tokyo, Feb. 15 (2010).

S. Ryuzaki, T. Kai and J. Onoe: The Capacitance-Voltage Characteristics and Open-Circuit Voltage of Zn(OEP)/C<sub>60</sub> Layered Photovoltaic Cells; (Selected paper), *57<sup>th</sup> spring meeting of the Applied Physic Society of Japan*, Kanagawa, March 17-20 (2010).

T. Kai, S. Ryuzaki and J. Onoe: Impedance Characteristics of Zn(OEP)/C<sub>60</sub> Layered Photovoltaic Cells; (Selected paper), *57<sup>th</sup> spring meeting of the Applied Physic Society of Japan*, Kanagawa, March 17-20 (2010).

A. Takashima, Y. Toda and J. Onoe: In situ Low-Temperature Infrared Spectra of One-Dimensional Metallic Peanut-Shaped C<sub>60</sub> Polymers; (selected as a B-type oral paper), *90<sup>th</sup> spring meeting of the Chemical Society of Japan*, Osaka, March 26-29 (2010).

J. Onoe, A. Takashima, and Y. Toda: In situ Infrared Spectroscopy of One-Dimensional Metallic Exotic-Nanocarbon at a Low Temperature; (selected paper), *8<sup>th</sup> annual meeting of the Nano-Society*, Okazaki, May 13-15 (2010).

S. Ryuzaki, T. Kai, and J. Onoe: The Origins of the Open-Circuit Voltage for Zinc-Porphyrin/C<sub>60</sub> Hetero-Junction Solar Cells; *8<sup>th</sup> annual meeting of the Nano-Society*, Okazaki, May 13-15 (2010).

S. Ryuzaki, T. Kai, and J. Onoe: The Carrier Mobility of Zn(OEP)/C<sub>60</sub> Hetero-Junction Solar Cells under Photo-Irradiation Studied using in Situ Impedance Spectroscopy; *8<sup>th</sup> annual meeting of the Nano-Society*, Okazaki, May 13-15 (2010).

J. Onoe: External Quantum Efficiency and Open-Circuit Voltage of Zn(OEP)/C<sub>60</sub> Hetero-Junction Solar Cells; (Invited talk), *A workshop on "Current status and perspective of Opto-electronic materials"*, Kagawa Univ., Takamatsu, May 28 (2010).

A. Takashima and J. Onoe: Synthesis and Physical Properties of New Form of Nanocarbon Materials Utilizing Electron-Beam Induced Coalescence between C<sub>60</sub> Molecules; *A workshop on "Current status and perspective of Opto-electronic materials"*, Kagawa Univ., Takamatsu, May 28 (2010).

T. Orikoshi, T. Nishii, and J. Onoe: The Effects of the Number of Layers on the Photo-Current for Organic Solar Cells with Lateral-Type Electrodes; *71<sup>st</sup> fall meeting of the Applied Physics Society of Japan*, Nagasaki, Sept. 14-17 (2010).

T. Orikoshi, T. Nishii, and J. Onoe: The Effects of the Number of Layers on the Photo-Current for Organic Solar Cells with Lateral-Type Electrodes; *39<sup>th</sup> symposium of the Fullerene and Nanotube Society of Japan*, Kyoto, Sept. 5-7 (2010).

J. Onoe:  $\pi$ -Electron Conjugated Nanocarbons – from Low Dimensionality to Topology-; (Invited lecture), *Science of Tokyo Univ.*, Tokyo, June 2 (2010).

J. Onoe: Carbon-Based Nanoscience – Structure, Properties, and Functions –; (Invited talk), *16<sup>th</sup> seminar on photo-science project at Miyazaki Univ.*, Miyazaki, Nov. 19 (2010).

T. Tsuchimoto, K. Sakata, M. Someya, H. Yamamoto, R. Hirayama, Y. Matsumoto, Y. Furusawa and M. Hareyama: Gene Expression Associated with DNA-Dependent Protein Kinase Activity under Normoxia, Hypoxia and Reoxygenation; *J.Radiat.Res.*, **52**, 464-471 (2011).

M. Someya, K. Sakata, Y. Matsumoto, Kamdar, R. P., M. Kai, M. Toyota and M. Hareyama: The Association of DNA-Dependent Protein Kinase Activity of Peripheral Blood Lymphocytes with Prognosis of Cancer; *Brit.J.Cancer*, **104**, 1724-1729 (2011).

M. Takagi, K. Sakata, M. Someya, H. Tauchi, K. Iijima, Y. Matsumoto, T. Torigoe, A. Takahashi, M. Hareyama and M. Fukushima: Gimeracil Sensitizes Cells to Radiation via Inhibition of Homologous Recombination; *Radiother. Oncol.*, **96**, 259-266 (2010).

- Kumar, A., and Y. Matsumoto: Radiation Protection by Herbs and Plants; *Emerging Trends in Zoology*,. Edit. Srivastva, U.C. and Kumar, S., Narendra Publishing House (2011).
- Sharma, M.K., and Y. Matsumoto: DNA-PK Phosphorylation Targets in XRCC4 and XLF Proteins in DNA Double-Strand Break Repair; *Ataxia-Telangiectasia Workshop 2010*, Redondo Beach (Crowne Plaza Hotel), CA, USA, 11-14 April 2010, Poster #168.
- Kamdar, R.P. and Y. Matsumoto: Assembly of Non-Homologous End-Joining Machinery on Radiation-Induced DNA Double-Strand Breaks; *Ataxia-Telangiectasia Workshop 2010*, Redondo Beach (Crowne Plaza Hotel), CA, USA, 11-14 April 2010, Poster #122.
- Y. Matsumoto: XRCC4: a Bona Fide Substrate of DNA-PK in DNA Double-Strand Break Repair; *56th Annual Meeting Radiation Research Society*, Maui (Grand Wailea Resort Hotel and Spa), Hawaii, USA, 25-29 September 2010, Symposium Talk (Invited) S1201.
- Sharma, M.K. and Y. Matsumoto: Identification of DNA-PK Phosphorylation Targets in XRCC4 & XLF Proteins and Their Physiological Significance in the Process of DNA Double-Strand Break Repair; *56th Annual Meeting Radiation Research Society*, Maui (Grand Wailea Resort Hotel and Spa), Hawaii, USA, 25-29 September 2010, Poster Session PS2.36.
- M. Someya, M. Takagi, K. Sakata, H. Tauchi, Y. Matsumoto, M. Hareyama and M. Fukushima: Radiosensitizing Effects of Gimeracil; *56th Annual Meeting Radiation Research Society*, Maui (Grand Wailea Resort Hotel and Spa), Hawaii, USA, 25-29 September 2010, Poster Session PS2.15.
- Y. Matsumoto, Sharma M. K., Kamdar R. P. and Sharma, A: Missing Links in the DNA Double-Strand Break Repair Mechanism and Its Possible Application to Cancer Therapy. International Conference on Radiation Biology: Nanotechnology, Imaging and Stem Cell Research in Radiation Oncology, Chennai (Sri Ramachandra University), India, 15-17 November 2010, Symposium Talk (Invited) S14-IL-86.
- D. Kuwahara, S. Tsuji-Iio, Y. Nagayama, T. Yoshinaga, M. Sugito, Z. Shi, S. Yamaguchi, Y. Kogi, A. Mase: Upgrade of 2-D Antenna Array for Microwave Imaging Reflectometry and ECE Imaging; *J. Plasma Fusion Res. SERIES*, **9**, 125-130 (2010).
- T. Habuchi, H. Tsutsui, S. Tsuji-Iio, R. Shimada: 3-Dimensional Stress Analysis of Virial-Limit Coils; *IEEE Transactions on Applied Supercond.*, **20** [3], 1924-1927 (2010).
- S. Maeyama, A. Ishizawa, T.-H. Watanabe, M. M. Skoric N. Nakajima, S. Tsuji-Iio, and H. Tsutsui: Effects of Time-Varying  $E \times B$  flow on Slab Ion-Temperature-Gradient Turbulence; *Phys. Plasmas*, Vol. **17**, 062305-1-9 (2010).
- T. Akiyama, K. Kawahata, K. Tanaka, T. Tokuzawa, Y. Ito, S. Okajma, K. Nakayama, C.A. Michael, L.N. Vyacheslavov, A. Sanin, S. Tsuji-Iio: Interferometer Systems on LHD; *Fusion Sci. Technol.* **58** [1] 352-363 (2010).
- T. Yoshinaga, Y. Nagayama, D. Kuwahara, H. Tsuchiya, S. Yamaguchi, Y. Kogi, S. Tsuji-Iio, and A. Mase: Simultaneous Projection and Detection System of Four Different Frequencies for Microwave Imaging Reflectometry in Large Helical Device; *Rev. Sci. Instrum.* **81**, 10D915-1-4 (2010).
- D. Kuwahara, S. Tsuji-Iio, Y. Nagayama, T. Yoshinaga, H. Tsuchiya, S. Sugito, S. Yamaguchi, Y. Kogi, K. Akaki, and A. Mase: Development of Electron Cyclotron Emission Imaging System on Large Helical Device; *Rev. Sci. Instrum.* **81**, 10D919-1-3 (2010).
- T. Yoshinaga, Y. Nagayama, D. Kuwahara, H. Tsuchiya, S. Yamaguchi, Y. Kogi, S. Tsuji-Iio, H. Hojo, A. Mase: Optics Design for Microwave Imaging Reflectometry in LHD; *Plasma Fusion Res.* **5**, 030-1-3 (2010).
- D. Kuwahara, S. Tsuji-Iio, Y. Nagayama, T. Yoshinaga, H. Tsuchiya S. Yamaguchi, Y. Kogi, A. Mase: ECE Imaging Diagnostics on LHD; *27th Annual Meeting of the Japan Soc. of Plasma Sci. and Nucl. Fusion Res.*, 01P3, Sapporo, Nov. 30 - Dec. 3, 2010.
- T. Yoshinaga, Y. Nagayama, D. Kuwahara. H. Tsuchiya, S. Yamaguchi, Y. Kogi, S. Tsuji-Iio, A. Mase: Microwave Imaging Reflectometry Diagnostics in LHD; *27th Annual Meeting of the Japan Soc. of Plasma Sci. and Nucl. Fusion Res.*, 01P37, Sapporo, Nov. 30 - Dec. 3, 2010.
- G. Fujii, S. Tsuji-Iio, H. Tsutsui, O. Mitarai, K. Nakamura, M. Hasegawa, H. Zushi, T. Akiyama: Development of Fiber-Optic Diagnostics on Vacuum Vessel Current of QUEST; *27th Annual Meeting of the Japan Soc. of Plasma Sci. and Nucl. Fusion Res.*, 01P51, Sapporo, Nov. 30 - Dec. 3, 2010.
- D. Kuwahara, S. Tsuji-Iio, Y. Nagayama, T. Yoshinaga, H. Tsuchiya, S. Yamaguchi, Y. Kogi and A. Mase: Development of ECE Imaging Diagnostic System on LHD; *20th International Toki Conference*, Toki, Dec. 7-10, 2010.
- T. Habuchi, H. Tsutsui, S. Tsuji-Iio, R. Shimada: Force Balance and Stability of Circular Cross Section Toroidally Helical Coil; *20th International Toki Conference*, Toki, Dec. 7-10, 2010.

- S. Maeyama, A. Ishizawa, T.-H. Watanabe, N. Nakajima, S. Tsuji-Iio, H. Tsutsui: Numerical Methods for Parallel Particle Motions in Gyrokinetic Vlasov Simulation; *20th International Toki Conference*, Toki, Dec. 7-10, 2010.
- T. Habuchi, H. Tsutsui, S. Tsuji-Iio, R. Shimada: Optimization of the Stress Distribution of Helical Coils With a Cable-in-Conduit Configuration; *IEEE Transactions on Applied Superconductivity*, **21**, Issue 5, p. 3494 – 3500.
- T. Dwi Irwanto, Toru Obara, Yukitaka Kato, Ichiro Yamanaka: 2-dimensional Core Temperature Profile During Operation in the Small Simplified Pebble Bed Reactor with PeU a PeU Fuel Loading; *The Third International Symposium on Innovative Nuclear Energy Systems*, 31<sup>st</sup> October – 3<sup>rd</sup> November, 2010, Tokyo Institute of Technology, Japan, P-113, (2010).
- Munkhbat Byambajav, Toru Obara: Design Concept of Small Reactor for Larger Diameter neutron Transmutation Doping using Conventional PWR Fuel Assemblies; *The Third International Symposium on Innovative Nuclear Energy Systems*, 31<sup>st</sup> October – 3<sup>rd</sup> November, 2010, Tokyo Institute of Technology, Japan, P-108, (2010).
- Toru Obara, Yu Yamazawa: Decontamination Efficiency of Metal Mesh Plonium Filter for Lead Alloy Cooled Reactors; *The Third International Symposium on Innovative Nuclear Energy Systems*, 31<sup>st</sup> October – 3<sup>rd</sup> November, 2010, Tokyo Institute of Technology, Japan, 1B-34, (2010).
- Dwi Irwanto and Toru Obara: Burnup Analysis of a PeU a PeU Fuel-loading Scheme in a Pebble Bed Reactor Using the Monte Carlo Method; *Proc. of Joint International Conference on Supercomputing in Nuclear Applications and Monte Carlo 2010(SNA+MC2010)*, October 17-21, 2010, Tokyo, Japan, 10190, (2010).
- Toru OBARA, Hiroki TAKEZAWA: Kinetic Analysis of Weakly Coupled Systems Using Probability Density Function of Coupling Coefficient Obtained by Monte Carlo; *Proc. of Joint International Conference on Supercomputing in Nuclear Applications and Monte Carlo 2010(SNA+MC2010)*, October 17-21, 2010, Tokyo, Japan, 10258, (2010).
- Toru Obara and Hiroki Takezawa: Kinetic Analysis of Coupled Pulse Reactor for NPL Experiment; *Trans. American Nuclear Society*, **103**, 775 (2010).
- Byambajav Munkhbat and Toru Obara: Design Study on Nuclear Reactor for Large Diameter NTD Using PWR Fuel; *Trans. American Nuclear Society*, **103**, 756 (2010).
- Dwi Irwanto, Toru Obara, Yukitaka Kato, and Ichiro Yamanaka: Burnup Characteristics of PeU-a-PeU Fuel Loading Scheme in Small PBR; *Trans. American Nuclear Society*, **103**, 791 (2010).
- Dwi Irwanto, Toru Obara: Design Study of Innovative Simplified Small Pebble Bed Reactor; (3) Analysis of the 110MWt Simplified PBR Design with PeU a PeU fuel loading scheme; *2011 Atomic Energy Society Japan Annual Meeting*, I34 (2011).
- Piyatida Trinuruk, Toru Obara: Effect on Burnup Performance in HTGR by Neutron Spectrum Shift; *2011 Atomic Energy Society Japan Annual Meeting*, I34 (2011).
- Topan Setiadipra, Toru Obara: Development of Equilibrium Burnup Analysis Code for OTTO Cycle in Pebble Bed Reactor; *2011 Atomic Energy Society Japan Annual Meeting*, I34 (2011).
- Byambajav Munkhbat, Toru Obara: Design Study on Small Reactor for Silicon Semiconductor Production using LWR Fuel; (2) Reactor Optimization; *2011 Atomic Energy Society Japan Annual Meeting*, I34 (2011).
- Haruka Kikuchi, Toru Obara: Fundamental Study on Criticality Safety Transient Analysis in Weakly Coupled System; *2011 Atomic Energy Society Japan Annual Meeting*, I46 (2011).
- Dwi Irwanto and Toru Obara: Design Study of Innovative Simplified Small Pebble Bed reactor; (2) Steady State Thermal Hydraulic Analysis of Reference Design; *2010 Atomic Energy Society Japan Fall Meeting*, Q22(2010).
- Yuji Fukuda, Yong-Hong Zhang, Masao Nomura, Tatsuya Suzuki, Yasuhiko Fujii and Takao Oi: Strontium Isotope Effects Observed in Liquid Chromatography with Crown Ether resins; *J. Nucl. Sci. technol.*, **47** (2010) 176-183.
- Xingcheng Ding, Masao Nomura, Tatsuya Suzuki and Yasuhiko Fujii: Chromatographic Zinc Isotope Separation by Chelating Exchange Resin; *Chromatographia*, **71** (2010) 195-199.
- Shin-ichi Koyama, Tatsuya Suzuki, Masaki Ozawa: From Waste to Resource, Nuclear Rare Metals as a Dream of Modern Alchemists; *Energy Conversion and Management*, **51** (2010) 1799-1805.
- Minori Abe, Tatsuya Suzuki, Yasuhiko Fujii, Masahiko Hada, and Kimihiko Hirao: Ligand Effect on Uranium Isotope Fractionations Caused by Nuclear Volume Effects: An ab Initio Relativistic Molecular Orbital Study; *J. Chem. Phys.*, **133**, 044309 (2010) (5 pages).
- Tatsuya Suzuki, Masao Nomura, Yasuhiko Fujii, Atsushi Ikeda-Ohno, Toru Takaoka, and Koichi Oguma: Zinc Isotope Fractionation in Anion Exchange in Hydrochloric Acid Solution; *Journal of Ion Exchange*, **21** (2010) 328-333.
- Y. Fujii, M. Nomura, T. Kaneshiki, Y. Sakuma, T. Suzuki, S. Umehara, T. Kishimoto: Mass Dependence of Calcium

- Isotope Fractionations in Crown-ether Resin Chromatography; *Isotopes in Environmental and Health Studies*, **46** (2010) 233-241.
- Masao Nomura, Toshitaka Kaneshiki, Tatsuya Suzuki, Kazuhiro Otaka, Toshihiko Okazaki, Takashi Hoshi and Yasuhiko Fujii: Separation of Carbon Isotopes by Adsorption Chromatography; *The 5th International Conference on Ion Exchange*, Melbourne, Australia, July 18-21, (2010) 5B-4.
- Tatsuya Suzuki, Masao Nomura, Yasuhiko Fujii, Atsushi Ikeda-Ohno, Toru Takaoka and Koichi Oguma: Zinc Isotope Fractionation in Anion Exchange in Hydrochloric Acid Solution; *The 5th International Conference on Ion Exchange*, Melbourne, Australia, July 18-21, (2010) 2P-36.
- Tatsuya Suzuki, Maiko Tanaka, Yasuyuki Ikeda, Shin-ichi Koyama: Adsorption Behaviors of Trivalent F-Elements on Pyridine Resin in Lithium Chloride Aqueous Solution; *The 6th International Conference on Rare Earth Development and Application*, Beijing, China, August 2-6, (2010) P16.
- T. Suzuki, S. Koyama, M. Ozawa, M. Osaka: Extraction of Valuable elements in Spent Nuclear Fuel by using Pyridine Resin; *The 2nd International Conference on Asian Nuclear Prospects 2010 (ANUP 2010)*, Chennai, India, Oct. 11-13 (2010).
- Tatsuya Suzuki, Maiko Tanaka and Shin-ichi Koyama: Recovery of Minor Actinides from Spent Molten Salt Waste and Decontamination of Molten Salt Waste; *The 3rd International Symposium on Innovative Nuclear Energy Systems*, Tokyo, Japan, Oct.31- Nov.3, (2010) 2C-21.
- Minori Abe, Tatsuya Suzuki, Yasuhiko Fujii, Masahiko Hada: Theoretical Study of Nuclear Volume Effects in Uranium Enrichment; *The 3rd International Symposium on Innovative Nuclear Energy Systems*, Tokyo, Japan, Oct.31- Nov.3, (2010) 2C-23.
- Shin-ichi Koyama, Isao Yamagishi, Tatsuya Suzuki, Hitoshi Mimura, Reiko Fujita, Masaki Ozawa: Current Status and Future Plan of Advanced ORIENT Cycle Strategy; *The 3rd International Symposium on Innovative Nuclear Energy Systems*, Tokyo, Japan, Oct.31- Nov.3, (2010) 2C-24.
- Yoshihiko Sato, Ken Okada, Miyako Akiyoshi, Takehiro Matsunaga, Shin-ichi Koyama, Tatsuya Suzuki, Masaki Ozawa: Thermochemical Safety Evaluation of Tertiary Pyridine Resin for the Application to Multi-Functional Reprocessing Process - Adv.-ORIENT Cycle Development -; *The 3rd International Symposium on Innovative Nuclear Energy Systems*, Tokyo, Japan, Oct.31- Nov.3, (2010) 2C-25.
- Masao Nomura, Toshitaka Kaneshiki, Tatsuya Suzuki, Yasuhiko Fujii, Kazuhiro Otaka, Toshihiko Okazaki and Takashi Hoshi: Carbon Isotope Effect in the Carbon Dioxide Adsorption by the Column Method which Filled up Zeolite; *2010 fall meetings of atomic energy society of Japan*, (2010) p.657.
- Tatsuya Suzuki, Yasuyuki Ikeda, Shin-ichi Koyama, Masahiko Osaka and Masaki Ozawa: Advanced ORIENT Cycle Study (Phase I) 4) Separation Process Flowsheet and Element Distribution; *2010 fall meetings of atomic energy society of Japan*, (2010) p.708.
- Ken Okada, Yoshihiko Sato, Miyako Akiyoshi, Takehiro Matsunaga, Tatsuya Suzuki, Shin-ichi Koyama and Masaki Ozawa: Advanced ORIENT Cycle Study (Phase I) 6) Study on Thermal Stability of Tertiary Pyridine Resin; *2010 fall meetings of atomic energy society of Japan*, (2010) p.710.
- Yoshihiro Okadome, Masayuki Iwata, Katsuhisa Nagayama, Tsuyoshi Arai, Tatsuya Suzuki, Kenichi Horiguchi and Atsushi Sugaya: Study for Separation and Stabilization of Sodium from Low Level Liquid Waste Using Inorganic Ion Exchanger; *2010 fall meetings of atomic energy society of Japan*, (2010) p.752.
- Masayuki Iwata, Yoshihiro Okadome, Tsuyoshi Arai, Katsuhisa Nagayama, Tatsuya Suzuki, Kenichi Horiguchi and Atsushi Sugaya: A Basic Study for Solidification of Low Level Liquid Waste with Iron Phosphate Glass; *2010 fall meetings of atomic energy society of Japan*, (2010) p.753.
- T. Suzuki, Y. Ikeda, M. Honda, N. Asanuma, M. Osaka: Recovery of Molybdenum by using Pyridine Resin from Simulant Irradiated Nuclear Fuel Solution; *2010 annual meeting of the Japan society of nuclear and radiochemical sciences*, (2010) 1P17.
- Masao Nomura, Yiqun Zhang, Tatsuya Suzuki and Yasuhiko Fujii: Lithium Isotope Effect by Ion Exchange Chromatography with Li-6 Enriched Sample Material; *2011 annual meetings of atomic energy society of Japan*, (2011) p.534.
- Fumiaki Kawakami, Moriyasu Tokiwai, Yasuhiko Fujii and Tatsuya Suzuki: Plant Designing of Chemical Uranium Enrichment and Its Characteristics; *2011 annual meetings of atomic energy society of Japan*, (2011) p.535.
- Shin-ichi Koyama, Masaki Ozawa, Yasuhiko Fujii, Kiyoko Kurosawa, Yukio Hanamoto, Katsuyoshi Tatenuma and Tatsuya Suzuki: Metal Corrosion Evaluation in Hydrochloric Acid Media on Tertiary Pyridine-Type Resin Applying to Fuel Reprocessing System (5); *2011 annual meetings of atomic energy society of Japan*, (2011) p.583.
- Tatsuya Suzuki, Toshitaka Kaneshiki, Masao Nomura, Yasuhiko Fujii, Hidekazu Kobayashi, Shigeru Kano and Teruo Yamashita: Development of water absorptive porous glass beads; *Proceedings of Annual / Fall Meetings of*

*Atomic Energy Society of Japan, 2011 annual meetings of atomic energy society of Japan*, (2011) p.604.

M. Numakura, Y. Okamoto, T. Yaita, H. Shiwaku, H. Akatsuka, A. Nezu, K. Tajima, Y. Shimohara, C. Bessada, O. Pauvert, D. Zanghi, P. Chamelot, H. Matsuura: Local Structural Analyses on Molten Terbium Fluoride in Lithium Fluoride and Lithium – Calcium Fluoride Mixtures; *J. Fluor. Chem.* **131**, 1039-1043, (2010).

O. Pauvert, D. Zanghi, M. Salanne, C. Simon, A. Rakhmatullin, H. Matsuura, Y. Okamoto, F. Vivet, C. Bessada: In situ Experimental Evidence for an Nonmonotonous Structural Evolution with Composition in the Molten LiF-ZrF<sub>4</sub> System; *J. Phys. Chem. B*, **114**, 6472-6479, (2010).

Haruaki Matsuura, Masahiko Numakura, Hiroshi Akatsuka, Nobuaki Sato: Structure and Physico-Chemical Properties of Thorium Fluoride Mixtures (1) Synthesis of Thorium - Lithium Fluoride Mixture; *2010 Annual Meeting of the Atomic Energy Society of Japan*, J39, 465, (2010).

Masahiko Numakura, Haruaki Matsuura, Atsushi Nezu, Hiroshi Akatsuka, Nobuaki Sato, Catherine Bessada, Didier Zanghi, Olivier Pauvert, Pierre Chamelot: Structure and Physico-Chemical Properties of Thorium Fluoride Mixtures (2) XAFS Analysis on Molten ThF<sub>4</sub>-LiF; *2010 Annual Meeting of the Atomic Energy Society of Japan*, J40, 466, (2010).

Masahiko Numakura, Haruaki Matsuura, Hiroshi Akatsuka, Atsushi Nezu, Tsuyoshi Yaita, Yoshihiro Okamoto, Hideaki Shiwaku, Catherine Bessada: Structural Analyses on Terbium Fluorides in Molten Alkali and Alkaline Earth Fluorides; *The 27<sup>th</sup> symposium on rare earths*, 1C-05, 86-87, 2010.

Masahiko Numakura, Catherine Bessada, Nobuaki Sato, Hiroshi Akatsuka, Atsushi Nezu, Yasuaki Shimohara, Keisuke Tajima, Hirokazu Kawano, Takeshi Nakahagi, Haruaki Matsuura: Structural Analysis of Molten Terbium Fluoride Mixtures; *The 13<sup>th</sup> XAFS symposium*, 5O-03, 57-58, 2010.

Yasuaki Shimohara, Atsushi Nezu, Masahiko Numakura, Hiroshi Akatsuka, Haruaki Matsuura: Electrochemical Behaviour of Neodymium in Molten LiCl-KCl-LiF; *The 42<sup>nd</sup> symposium on molten salt chemistry*, 1A01, 1-2, 2010.

Masahiko Numakura, Nobuaki Sato, Catherine Bessada, Hiroshi Akatsuka, Atsushi Nezu, Yasuaki Shimohara, Keisuke Tajima, Hirokazu Kawano, Takeshi Nakahagi, Haruaki Matsuura: The variation of Local Structure Around Thorium Fluoride and Terbium Fluoride Melts by Addition of Alkali and Alkaline Fluorides; *The 42<sup>nd</sup> symposium on molten salt chemistry*, 1B10, 43-44, 2010.

Masahiko Numakura, Haruaki Matsuura, Atsushi Nezu, Yasuaki Shimohara, Keisuke Tajima, Hiroshi Akatsuka, Nobuaki Sato, Olivier Pauvert, Didier Zanghi, Pierre Chamelot, Catherine Bessada: Structure and Physico-Chemical Properties of Thorium Fluoride Mixtures (3) XAFS Analyses on Molten Fluoride Mixtures Containing ThF<sub>4</sub>; *2010 Fall Meeting of the Atomic Energy Society of Japan*, B40, 103, (2010).

Masahiko Numakura, Nobuaki Sato, Catherine Bessada, Hiroshi Akatsuka, Pierre Chamelot, Haruaki Matsuura: Structural Investigation on Thorium Fluoride in Molten Alkali-Alkaline Earth Fluoride Mixtures; *NuMat 2010 the Nuclear Materials Conference*, MSNA17, 2010.

Haruaki Matsuura, Atsushi Nezu, Hiroshi Akatsuka: Pyrochemical Reprocessing Based on Co-Electrodeposition Technique – Speciation of Uranyl Ion in Various Molten Salts and In-situ Observation of Electrodeposition Reaction Investigated by X-ray from Synchrotron Source; *The 3<sup>rd</sup> International symposium on Innovative Nuclear Energy Systems*, 1C-12, 68, 2010.

Masahiko Numakura, Hiroshi Akatsuka, Atsushi Nezu, Keisuke Tajima, Yasuaki Shimohara, Haruaki Matsuura: Feasibility Study of Pyrochemical Reprocessing using Molten Lithium- Calcium Fluoride Mixtures in Salt Treatment Process for Molten Salt Reactor; *The 3<sup>rd</sup> International symposium on Innovative Nuclear Energy Systems*, P-125, 149, 2010.

S. Nomura, K. Tsuboi, K. Ito, H. Tsutsui, S. Tsuji-Iio, A. Ninomiya R. Shimada: Acoustic Emission in a Superconducting Force-Balanced Helical Coil; *IEEE Trans. Appl. Supercon.*, Vol **21**, 1636-1639 (2011).

"Simulations", S. Maeyama, A. Ishizawa, T.-H. Watanabe, N. Nakajima, S. Tsuji-Iio, H. Tsutsui: A Numerical Method for Parallel Particle Motions in Gyrokinetic Vlasov ; *Plasma and Fusion Research*, **87**, 359-370 (2011).

Yasuyuki Sakamoto, Kiichi Sato, Mitsuru Abo, Takehiko Tsukahara, Takehiko Kitamori, Keiko Abe, and Etsuro Yoshimura: Cell Culture and Motility Study on a Polymer Surface with a Nanometer-Scaled Stripe Structure; *Biosci. Biotechnol. Biochem.*, **74** (3), 569-572 (2010).

kyojiro Morikawa, Kazuma Mawatari, Masaru Kato, Takehiko Tsukahara, and Takehiko Kitamori: Streaming Potential/Current Measurement Systems for Investigating Liquid Properties Confined in Extended-Nano Space; *Lab on a Chip*, **10** (7), 871 - 875 (2010).

Masaru Kato, Masanori Inaba, Takehiko Tsukahara, Kazuma Mawatari, Akihide Hibara, and Takehiko Kitamori: Femto Liquid Chromatography with Atto-Liter Sample Separation in the Extended Nanospace Channel; *Analytical Chemistry*, **82**, 543 - 547 (2010).

Kazuma Mawatari, Takehiko Tsukahara, Yasuhiko Sugii, Takehiko Kitamori: Extended-nano Fluidic Systems for Analytical and Chemical Technologies; *Nanoscale*, **2**, 1588-1595 (2010).

Takehiko Tsukahara, Kazuma Mawatari, and Takehiko Kitamori: Integrated Extended-nano Chemical Systems on a Chip; *Chemical Society Reviews*, **39**, 1000 - 1013 (2010).